HHS Public Access

Author manuscript

Chem Rev. Author manuscript; available in PMC 2021 September 23.

Published in final edited form as:

Chem Rev. 2020 September 23; 120(18): 9994–10078. doi:10.1021/acs.chemrev.0c00306.

Enzymatic Noncovalent Synthesis

Hongjian He, **Weiyi Tan**, **Jiaqi Guo**, **Meihui Yi**, **Adrianna N. Shy**, **Bing Xu**

Department of Chemistry, Brandeis University, 415 South St., Waltham, MA 02454, USA

Abstract

Enzymatic reactions and noncovalent (i.e., supramolecular) interactions are two fundamental non-genetic attributes of life. Enzymatic noncovalent synthesis (ENS) refers to a process where enzymatic reactions control intermolecular noncovalent interactions for spatial organization of higher-order molecular assemblies that exhibit emergent properties and functions. Like enzymatic covalent synthesis (ECS), in which an enzyme catalyzes the formation of covalent bonds to generate individual molecules, ENS is a unifying theme for understanding the functions, morphologies, and locations of molecular ensembles in cellular environments. This review intends to provide a summary of the works of ENS within the last decade and emphasize ENS for functions. After comparing ECS and ENS, we describe a few representative examples where nature uses ENS, as a rule of life, to create the ensembles of biomacromolecules for emergent properties/functions in a myriad of cellular processes. Then, we focus on ENS of man-made (synthetic) molecules in cell-free conditions, classified by the types of enzymes. After that, we introduce the exploration of ENS of man-made molecules in the context of cells by discussing intercellular, peri/intracellular, and subcellular ENS for cell morphogenesis, molecular imaging, cancer therapy, and other applications. Finally, we provide a perspective on the promises of ENS for developing molecular assemblies/processes for functions. This review aims to be an updated introduction for researchers who are interested in exploring noncovalent synthesis for developing molecular science and technologies to address societal needs.

Graphical Abstract

Correspondence to: Bing Xu.

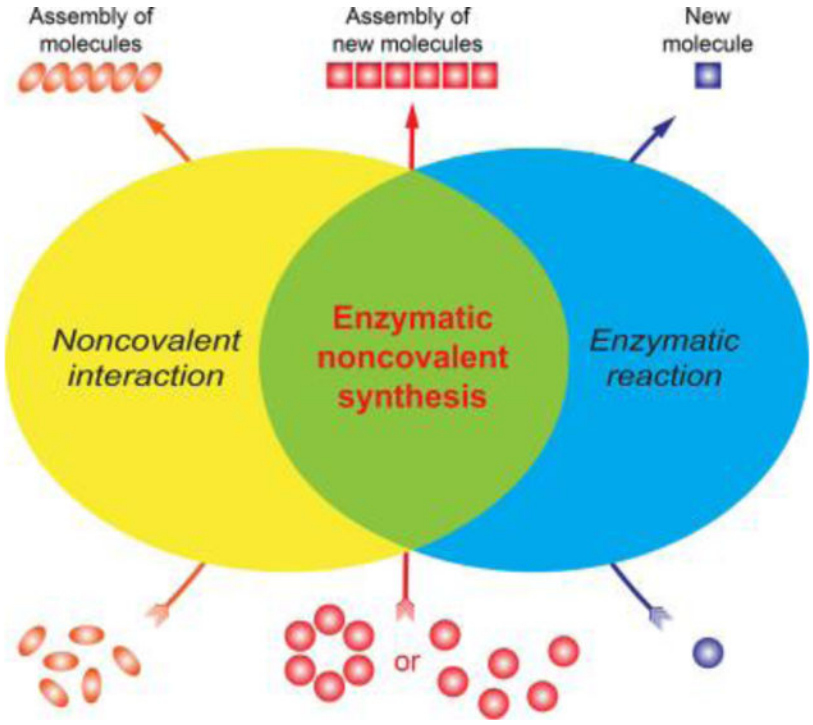

Keywords

Enzyme; noncovalent; self-assembly; imaging; cancer; gel; ensembles; supramolecular; higher-order; emergent; neurodegenerative; amyloids

1. Introduction

1.1. Enzymes and Noncovalent Interactions

Enzymes are biomacromolecules that catalyze chemical reactions to make molecules. Enzymes, being categorized into six types (oxidoreductases,[1] transferases,[2] hydrolases,[3] lyases,[4] isomerases,[5] and ligases[6]), are highly efficient and specific catalysts for a wide range of reactions that maintain the proliferation, differentiation, migration, and metabolism of cells.[7] Thus, while enzymes, being proteins, are a genetic feature of cells, enzymatic reaction is a non-genetic attribute of life. Previously, the study of enzymatic reactions has focused on the formation of covalent bonds to generate individual molecules, which consist of the atoms covalently connected. While strong interactions (i.e., covalent bonds) connect the atoms to make the molecules in cells, the intermolecular interactions (e.g., hydrogen bonding, ionic, and hydrophobic interactions) are ubiquitous, weak, and noncovalent (i.e., supramolecular interactions[8]). Therefore, another fundamental non-genetic attribute of life is noncovalent interactions. These noncovalent interactions between biomolecules are unlikely to be completely random; they must be under certain controls. The dynamic characteristics of cells suggest that such controls have to involve reactions. Unavoidably, most of the reactions must be enzymatic reactions. Therefore, enzymatic reactions also control noncovalent interactions in cells. Thus, we refer the formation of covalent bonds catalyzed

by enzymatic reactions as enzymatic covalent synthesis (ECS) and the formation of noncovalent interactions controlled by enzymatic reactions as enzymatic noncovalent synthesis (ENS). ECS generates individual molecules, and ENS produces ensembles of molecules.

1.2. Enzymatic Covalent Synthesis

The study of enzymes started with the identification and categorization of enzymes more than 70 years ago.[9–10] The emphasis, then, has focused on the mechanisms of enzyme actions.[11–15] With the rapid advance of structural biology, researches over the last forty years have elucidated the structures of many enzymes, especially their active sites.[16–18] Recently, the advance of activity-based probes has provided a powerful tool to understand the functions of enzymes for drug discovery.[19] Since the discovery of enzymes, enzymatic reactions have carried out industrial biotransformation for making fine chemicals.[20] Recently, the design of enzymes by "directed evolution" has achieved exciting success—one can evolve enzymes to carry out new catalytic reactions with high selectivity and efficiency.[21–24] Although the intermolecular interactions between enzymes and their substrates or products are part of the inquiry in understanding the mechanisms of enzyme actions,[11,25] the research activities on enzymes, largely, have focused on enzymatic covalent synthesis (ECS)—that is, enzyme catalyzes the formation of covalent bonds to generate individual molecules.

1.3. Enzymatic Noncovalent Synthesis

Because nearly every major process in a cell is carried out by assemblies of 10 or more protein molecules, Alberts has proposed that a cell is a collection of protein machines.[26] Noncovalent interactions are the forces that hold the protein machines together. Recent advances in cell biology have only reinforced such notion. Increasing numbers of studies have shown that biomacromolecules are able to form higher order assemblies, as functional centers (i.e., signalosomes[27–28]) or as a form of compartmentalization (i.e., membraneless condensates for biochemical reactions[29–34]). These supramolecular assemblies[27] are dynamic, heterogeneous, and play a critical role in cell functions,[35–36] but it is still largely unknown how cells control these assemblies for functions. Enzymatic reactions must be one of the controlling mechanisms of life, and probably the most important "rule of life". Thus, it becomes increasingly necessary to consider and to investigate how enzymatic reactions instruct intermolecular noncovalent interactions to form molecular ensembles for functions. Since the functions of the molecular assemblies usually differ from individual molecules, it is necessary to define enzymatic noncovalent synthesis (ENS)—a process that integrates enzymatic reactions and supramolecular (i.e., noncovalent) interactions for spatial organization of higher-order molecular assemblies to achieve emergent properties or functions. Figure 1 illustrates the relationship among ECS, noncovalent interactions, and ENS. ECS makes one molecule from another by enzyme catalysis; noncovalent interactions results in molecular assemblies from many molecules by self-assembly, but no new molecules are made; ENS converts many molecules (either individually or in ensembles) to assemblies of new molecules by ECS and self-assembly. That is, the target of ECS is one molecule, but the focus of ENS is assemblies of molecules and their emergent properties. By this definition, ENS includes one or more ECS processes, but it has to incorporate

intermolecular noncovalent interactions to result in molecular ensembles that exhibit emergent properties. In other words, ENS enables a coherent outcome of the morphological and functional organization of molecules.

1.4. Scope and Arrangement

As a unifying theme for understanding functions and locations of molecular ensembles in cellular environments, ENS also represents an emerging research area at the interface of physical science (e.g., chemistry,[37] physics,[38] and nanotechnology[39]) and biological sciences (e.g., structural biology,[27] biochemistry,[29] and cell biology[35]). The aim of this review is to examine how enzymatic reactions provide spatiotemporal control of noncovalent (or supramolecular) interactions of both natural and man-made molecules to result in emergent properties or functions of molecular assemblies. To provide a relatively comprehensive summary of the works of ENS within the last decade and to put emphasis particularly on the applications of ENS, we start with discussing a few representative examples to show how nature uses ENS to create biomacromolecules ensembles for a myriad of cellular functions and processes. After introducing these facts to support ENS as a rule of life, we focus on ENS of man-made molecules in cell-free conditions, classified by the type of enzymes. Then, we describe ENS of man-made molecules in the context of cells to illustrate the applications of ENS. We discuss intercellular, peri/intracellular, and subcellular ENS for cell morphogenesis, molecular imaging, cancer therapy, etc. Finally, we provide a perspective on the promises of ENS. We hope that this review will serve as an updated introduction and reference for researchers who are interested in exploring noncovalent synthesis for developing molecular technologies for addressing societal needs at various frontiers.

2. Enzymatic Noncovalent Synthesis in Nature

ENS is an integrated behavior of cells because enzymatic reactions and noncovalent interactions are two fundamental non-genetic attributes of cells that act reciprocally. Several well-known biological facts have revealed that enzymatic reactions control the formation of supramolecular assemblies for functions. For example, enzymatic hydrolysis of GTP drives the dynamic of microtubules,[40] kinases and phosphatases activate inflammasomes,[41–42] proteinases regulate the formation of collagen fibers,[43] and aberrant proteolysis or phosphorylation contributes to forming disease-associated amyloids.[44–45] Because enzymes control dynamic posttranslational modifications (PTMs) of polypeptide chains,[46] and noncovalent interactions drive the formation of the molecular ensembles, cells use ENS as a fundamental biochemical mechanism to control functional assemblies as evidenced by the following representative examples.

2.1. Intracellular ENS

A unique feature of the interiors of all cells is crowding—supramolecular functional structures (Figure 2) like biomacromolecules occupy a significant fraction (typically 20–30%) of the total volume of cells. It has been recognized that biomacromolecular crowding plays a role in all biological processes at the biochemical level,[47–49] and the relevant studies have centered largely on how the crowding (or excluded-volume) promotes colloidal phase

separation[50] or influences the rate of ECS.[51–52] Obviously, crowding is dynamic and associates with noncovalent interactions of the biomacromolecules in the microenvironment. Since local enzymatic reactions change the dynamics of the microenvironment, enzymatic reactions also control biomacromolecular crowding. Such a reciprocal feedback or interdependence between enzymatic reactions and crowding leads to a challenge to parameterize the degree of crowding of the cell interior. Thus, it is necessary to examine enzymatic reactions and noncovalent interactions in a holistic manner. That is, evaluating how enzymatic reactions control noncovalent interactions to lead to emergent properties of molecular ensembles, which is the essence of ENS. The following sections discuss the formation of intracellular supramolecular functional structures from the perspective of ENS. Since it is impossible to numerate all of them, we chose the ensuing representative examples and categorized them following the convention used by the creation of the cell atlas.[53]

Actin Filaments.—The formation of actin filaments is an ultimate example of ENS. As one of the most abundant proteins in eukaryotic cells and existing in both monomeric G-actin (G for globular) and polymeric F-actin (F for filament), actin[54] itself is an enzyme. The substrate of actin is ATP, so actin is an ATPase.[55] ATP hydrolysis on actin is the key reaction for maintaining the actin filaments.[56] As shown in Figure 3, in cells, most of the G-actins bind with ATP, and most of the F-actin subunits contain ADP. ATP-actin attaches to the barbed end of F-actin, and ATP gradually hydrolyzes to become ADP. Overtime, ADP-actin dissociates from the pointed end of the filaments. The ADP-actin monomer then exchanges with ATP to form the ATP-actin, which can attach to the barbed end again. An assembly-disassembly process such as this occurs continuously without the presence of actin binding proteins (ABPs). In the presence of ABPs, actin filaments act as a key component of cytoskeletons (Figure 2) for various cellular functions, such as motility,[57] endocytosis,[58] and mitochondria dynamics.[59–60] The functions of F-actin are the emergent properties of the assemblies of actins, which rely on the enzymatic hydrolysis of ATP, as well as other protein-protein interactions (PPI). Fitting well with the definition of ENS, the formation of F-actin not only underscores the unique advantage of ENS, but also represents a case of self-organization or assembly away from equilibrium. In addition, the formation of actin filaments, of course, changes crowding of the microenvironment for controlling other enzymatic reactions for various functions of proteins in cells. This kind of feedback regulates observable cellular behaviors, such as focal adhesion.[61–62]

Aggresomes.—As the aggregation of misfolded proteins in eukaryotic cells, aggresomes[65] are a consequence of multiple enzymatic reactions and multiple proteins. In essence, the presence of misfolded proteins results in ubiquitination, which involves ubiquitin-activating enzyme (E1), ubiquitin-conjugating enzyme (E2), ubiquitin ligase (E3). When the proteasome is unable to degrade the ubiquitinated proteins, a histone deacetylase (HADC6) further interacts with the ubiquitinated proteins to form the aggresomes.[66] Since the discovery of aggresomes, by Kopito et al., in the study of undegraded cystic fibrosis transmembrane conductance regulator (CFTR),[65] considerable efforts have focused on the misfolded proteins related to neurodegenerative diseases. Several other enzymes, such as parkin and ataxin-3,[67–69] are also implicated in aggresome formation. Generally, aggresome formation is a normal cellular response to a large amount of misfolded proteins. Inhibition or

loss function of proteasome would result in the activation of aggresome pathways because aggresomes, acting as a holding station of potentially cytotoxic protein aggregates, facilitate their eventual clearance from the cell by lysosomes or autophagy. One interesting feature of aggresomes is that they form around the microtubule-organizing center (MTOC) in eukaryotic cells, adjacent to or enveloping the centrosomes of the cell.[70] Though it remains to be determined, it is possible that more enzymes and proteins are involved in the formation of aggresomes, which is an ENS process.

Centrosomes.—Centrosomes are the organelles that serve as the MTOCs in animal cells during mitosis. The key components of centrosomes are centroles, pericentriolar material (PCM), and microtubules (Figure 5A).[71] A centrosome[71–72] may consist of hundreds of proteins as the PCM. Since many of the proteins only transiently associate with centrosomes for signaling functions, it is difficult to define the components of centrosomes precisely. The transient nature of PCM implies that enzymatic reactions control the centrosome scaffolds (or assemblies) at the different phases of mitosis. A study of the expansion of the mitotic PCM around the mother centriole in flies, indeed, supports that ENS is a feature of the dynamics of centrosomes. Such an ENS process involves three key molecules: a kinase, Polo, and two proteins, Spd-2, and Cnn. As shown in Figure 5B,[73] during interphase, Polo is inactive, Spd-2 and Cnn are not phosphorylated, and there is no fibrous-like scaffold. As cells prepare for mitosis, activated Polo phosphorylates Spd-2. Then, the phosphorylated Spd-2 assembles into a fibrous-like scaffold that spreads away from the centriole and recruits Polo and Cnn. After Polo phosphorylates Cnn, then Cnn assembles into a scaffold, which helps to maintain the Spd-2 scaffold and allow it to expand further and thus recruits more Polo and Cnn. This process creates a positive feedback loop. In this relatively complicated ENS process, Polo, as a master regulator and an enzyme, controls the assembly of phosphorylated Spd-2 and phosphorylated Cnn to form the centrosome scaffolds. This perspective from ENS may help to avoid the difficulty in distinguishing solid-like or liquid phase separations[73] in the understanding of centrosomes dynamics.

Cleavage Furrow.—At the end of cell division, a cleavage furrow forms and eventually separates the two daughter cells. The key feature of a cleavage furrow is that the assembly and contraction of actomyosin filaments drive a contractile-ring (Figure 6A).[75] Actin and myosin are ATPases, they catalyze ATP hydrolysis for the formation of actin filament and the movement of myosin. Other enzymatic reactions also control these processes (Figure 6B): GTP-bound RhoA activates two kinases (ROK and CITK) to phosphorylate the myosin's regulatory light-chain (MRLC) to promote the sliding of myosin heads along actin filaments. GTP-bound RhoA also interacts with formin to promote profilin-mediated actin polymerization. In animal cells, RhoA is a small GTPase, which acts as the key regulator for both the assembly and contractions of the actiomyosine filaments. Like other regulators in cells, the level of RhoA-GTP is controlled by other modulators, such as RhoA-GAP and Rho-GEF.[76] Thus, the dynamics of contractile-rings is a fine example of a rather sophisticated ENS process evolved by nature.

Cytoplasmic Bodies.—Cytoplasmic bodies are the collective term for aggregation of biomacromolecules inside the cytoplasm. Cytoplasmic bodies are poorly defined, except for

processing bodies (P-bodies) and stress granules that are known to contain RNA and proteins. Among the cytoplasmic bodies, P-bodies, since its discovery,[77] received more detailed characterization than other cytoplasmic bodies did. P-bodies, consisting of many enzymes and RNA, function as a center for mRNA turnover, such as degradation of unwanted mRNAs, storing mRNA for translation, and aiding in translational repression,[78] though some of these functions remain controversial. With the report of a new method to purify P-bodies,[79] an increased number of proteins in P-bodies have been identified.[80] Although different P-bodies may have different compositions, many essential protein components in P-bodies carry PTM sites (e.g., serine residues for phosphorylation in the enhancer of mRNA-decapping protein 4 (EDC4),[81] cytoplasmic polyadenylation element-binding protein 1 (CPEB1),[82] and eukaryotic translation initiation factor 4E transporter (EIF4ENIF1)[83]), indicating enzymatic control of the assembly and disassembly of P-bodies. Recent reports also suggest that ATPases play a role to maintain P-bodies.[84–85] These observations indicate that enzymatic reactions modulate protein-protein interactions to form P-bodies, which turns out to be true. For example, after the report that JNK kinase phosphorylates DCP1a to control formation of P bodies,[86] a subsequent study shows a new mode for dynamic P-bodies remodeling by combined enzymatic phosphorylation/ubiquitylation events (Figure 7).[87]

Cytosol.—Cytosol contains many biomacromolecules. Although it is believed that the biomacromolecular crowding promotes phase separation and oligomerization of colloidal-like biomacromolecules, the reversible and dynamic nature of the assemblies or liquid-liquid phase separation suggests the involvement of ENS. While it is obvious that ENS controls the formation of actin filaments, microtubules, and intermediate filaments, many other biomacromolecular ensembles resulted from ENS either perform normal cellular functions or cause detrimental diseases. Since it is impossible to enumerate all the assemblies or filaments of proteins in cytosol, we arbitrarily chose inflammasomes, Tau filaments, and apoptosomes as the representative examples. Inflammasomes are supramolecular organization centers (SMOC)[88] for host defense inside cells. The structural determination by Wu et al. has established that three proteins, NLRP3, ASC, and caspase 1, self-assemble to form nucleated filaments as NLRP3 inflammasomes.[89] As shown in Figure 8A, the adaptor protein ASC bridges the sensor proteins (NLRP3) and caspase-1 to form ternary inflammasome complexes. This study has elucidated the noncovalent interactions between NLPR3 and ASC through pyrin domain (PYD) and between ASC and caspase-1 through caspase activation and recruitment domain (CARD) for the formation of the filaments. Recent advances in the study of NLPR3 inflammasome activation have confirmed that enzymatic reactions posttranslationally modify the proteins for initiating the assembly (Figure 8B).[42] These processes, again, involve multiple enzymes and multiple proteins for controlling noncovalent interactions among biomacromolecules, which support ENS as a unifying theme in creating multiple protein complexes or biomacromolecular ensembles to exhibit emergent properties.

A defining feature of many human neurodegenerative diseases is the filamentous assemblies formed by aberrant Tau proteins.[90] Recently, cryo-electron microscopy (cryo-EM) has revealed the structures of tau filament from the brain of an individual with Alzheimer's

disease. Besides the determination of the filament cores that comprise residues 306–378 of tau protein and adopt a combined cross-β/β-helix structure, this work also shows that the paired helical filaments (PHF) and straight filaments (SF) are composed of hyperphosphorylated tau.[91] Although the presence of the hyperphosphorylated tau indicates the involvement of kinases, many kinases can phosphorylate tau proteins.[92] In addition, there are many phosphatases inside cells. Increased numbers of studies indicates that pathogenic tau filaments are resulted from the imbalanced actions of kinases and phosphatases.[93–94] This example highlights the complexity of ENS processes inside cells, which also underscores the importance of ENS in the understanding of pathogenesis of neurodegenerative diseases.

Cell death signaling is an important cytosolic process that utilizes ENS. In other words, ENS, as a multistep process, is an inherent feature of apoptosis. In the intrinsic pathway of apoptosis, enzymatic reaction induces the conformation change of Apaf-1 to allow it to interact with cytochrome c,[95] which results in subsequent self-assembly that forms the apoptosome.[96] The formation of the apoptosome further activates cascade events of cell death. During the extrinsically induced cell death,[97–98] the cell death ligands (e.g., TRAIL, TNF, and CD95L), being resulted from enzymatic reactions,[99–101] interact with the cell death receptors (e.g., TRAIL-R1/R2, TNFR1, and CD95) to initiate the self-assembly of the death receptors to form oligomers. Such oligomerization further triggers the down-stream signaling of apoptosis. These ENS features of apoptosis enable the quantitative aspects of signaling transduction, such as location, duration, thresholds, and amplitude. Such multistep ENS processes, avoiding a simple “on or off” (or “live or dead”) switch, achieve targeting with spatiotemporal precision, thus minimizing side effects. In fact, this insight has provided a blue print for developing ENS for selectively targeting cancer cells.[102]

Endoplasmic Reticulum.—The endoplasmic reticulum (ER) is an organelle in eukaryotic cells. The key feature of ER is an interconnected network of flattened, membrane-enclosed sacs or tube-like structures. There are two types of ER, rough (RER) and smooth (SER). The outer face of RER is the site of protein synthesis. The SER is the place for lipid synthesis. The dynamic feature of ER implicates the need of enzymatic reactions to control the formation of the network of ER, which are the assemblies of proteins and phospholipids. A recent study by Rapoport et al. has shown that the addition of GTP in the mixtures of a GTPase (Sey1P), a curvature stabilizing protein (Yop1p), and liposomes results in a tubular network.[103] Moreover, the same lab also shows that atlastin (ATL),[104] the vertebrate orthologue of Sey1p, forms a GTP-hydrolysis-dependent network on its own (Figure 9). These results show that ENS of a small set of proteins controls the shape of organelles via interacting with lipids.

Endosomes.—Endosomes are the organelles that sort and transport materials to lysosomes for degradation. As a membrane-bound compartment, endosomes form during endocytosis and are composed of lipids, proteins, and cargos. The formation of endosomes is a complicated and transient process, which implicates the involvement of ENS. A recent study[105] of the formation of clathrin-coated pits (CCPs) during clathrin-mediated endocytosis (CME) supports this notion. As shown in Figure 10A–C, during mammalian

CME, a reversible phosphorylation on the μ2 subunit of the main endocytic clathrin adaptor, AP2, is crucial during clathrin-coated pit (CCP) initiation and increases throughout CCP lifetime. Such phosphorylation by AAK1 allows binding endocytic NECAP proteins without significantly altering AP2's cargo affinity. The binding of NECAP recruits SNX9 for the late stages of CCP formation. In another study,[106] AAK1 phosphorylates the μ2 subunit of AP2 to promote CME of LRP6 in WNT signaling (Figure 10D).

Focal Adhesion Sites.—Focal adhesion (FA) is the signaling center for regulating the mechanical interactions between the extracellular matrix (ECM) and intracellular cytoskeletons.[62,107–108] As dynamic assemblies of multiple proteins, FA undergoes enzyme-controlled assembly and disassembly. For example, during the maturation of FA, integrin stimulation results in the accumulation of phosphorylation proteins (Figure 11A), which is controlled by enzymatic phosphorylation.[109] Because one of the most common interaction domains in FA proteins is SH2 (a tyrosine phosphate binding domain), kinases phosphorylate tyrosines, switch on SH2-mediated interactions, and promote FA assembly. In the reverse process, phosphatases remove the phosphates from tyrosine residues, turn off the SH2-mediated interaction, and lead to FA disassembly. Among these enzymes, a key member for the assembly and disassembly of FA is focal adhesion kinase (FAK), which undergoes integrin-induced autophosphorylation of FAK or phosphorylation by Src family kinases. Carragher[110] reported that Src-dependent FAK phosphorylation controls the assembly of a calpain 2/FAK/Src/p42ERK complex, calpain activation, and proteolysis of FAK (Figure 11B), which are critical for adhesion dynamics and cell survival. The studies of FA also highlight the critical role of enzymatic reactions in forming the noncovalent and functional multiple protein assemblies.

Golgi Apparatus.—The Golgi apparatus (or Golgi complex) is a stack of flattened membrane-enclosed disks known as cisternae (Figure 12A). Golgi, being dynamically regulated during cell cycles in mammalian cells, acts as the site for posttranslational modifications of proteins (e.g., glycosylation), protein sorting, and protein trafficking (e.g., secretion).[111] The stack has two sides. The cis face is near the ER, and the other side is trans face. Many enzymes locate and distribute in the Golgi complex, and these enzymes are responsible for the modification of many cellular and secretory proteins, such glycosyltransferases, trimming enzymes, sugar transporters, or enzymes involved in other posttranslational modifications. The dynamic nature of Golgi implicates that proteins mediate the stacking of Golgi cisternae. Barr et al. has identified the proteins involved in the stacking of Golgi cisternae.[112] One of the proteins is Golgi reassembly stacking protein with the size of 65 kDa (GRASP65). Enzymatic controlled assembly of GRASP65 is responsible for the stacking and unstacking of the Golgi cisternae (Figure 12B). During interphase, PP2A catalytically dephosphorylates phospho-GRASP65 to generate GRASP65, which oligomerizes to connect the adjacent cisternae to form Golgi stacks. During mitosis, CDK1 and PLK1 phosphorylate multiple sites on GRASP65, resulting in the disassembly of GRASP65 oligomers to homodimers and the subsequent Golgi stack disassembly. This process (Figure 12B) is also a fine example of ENS evolved by nature for controlling the dynamics of subcellular organization.

Intermediate Filaments.—Intermediate filaments (IFs)[114] are one of the three major types of cytoskeletons. Resulting from the assembly of IF proteins, such as lamins, keratins, vimentin, desmin, neurofilaments and glial fibrillary acidic protein, IFs have diameters around 10 nm, which is smaller than microtubules (24 nm), but bigger than actin filaments (7 nm). IFs provide mechanical support to cells, participate in cell adhesion, facilitate intracellular communication, and maintain tissue integrity in cell-specific fashion.[115] Since multiple types of PTMs, including phosphorylation, glycosylation, sumoylation, acetylation, and prenylation, regulate the functions of IFs,[116] the formation of IFs unavoidably is controlled by enzymatic reactions. For example, Fields et al. suggested that protein phosphatase 1 (PP1) dephosphorylates lamin B for the nuclear lamin reassembly at the completion of mitosis.[117] Broday et al. reported that reversible sumoylation of the cytoplasmic intermediate filament (cIF) protein named IFB-1 in *C. elegans* regulates cIF assembly by maintaining a cytoplasmic pool of nonpolymerized IFB-1.[118] A recent report by Boyce and co-workers suggests that site-specific glycosylation of a serine residue in the "head" domain of vimentin promotes the intermolecular interactions of vimentin molecules to favor dimerization.[119] This model suggested by Boyce agrees with the unique kinetic of IFs of vimentin, which are resulted from both lateral association and elongation (Figure 13), and indicates ENS in the formation of IFs.

Lipid Droplets.—Largely located in the adipose tissues, lipid droplets are lipid-rich cellular organelles for the storage and hydrolysis of neutral lipids, as well as a reservoir for cholesterol and acyl-glycerols. Although lipid droplets were considered just as fat depots initially, the discovery of the proteins in the coat of lipid droplets reveal that they are highly dynamic organelles and play a very important role in inflammatory responses, obesity, cancer, and atherosclerosis. The sizes of lipid droplets range from 20–40 nm to 100 μm. Generally, a phospholipid monolayer surrounds a neutral lipid core (mainly triacylglycerols (TAGs) and cholesteryl esters) to constitute the lipid droplets, which are decorated by a number of proteins involved in the regulation of lipid metabolism (Figure 14A).[121] Although the exact mechanism of formation of lipid droplets remains to be elucidated, increasing numbers of studies suggested that enzymatic reactions control biogenesis of lipid droplets.[122] The most widely accepted model for lipid droplet formation comprises several discrete steps: nucleation, growth, and budding (Figure 14B).[122] Several enzymes are involved in this process. For example, DGAT produces neutral lipids for the growth of lipid droplets,[123] atlastin for ER shaping,[104] and FITM transfers phosphate-containing headgroups between lipids or in exchange for water.[124] In this case, multiple enzymatic reactions cooperatively lead to the biogenesis of lipid droplets, and likely more molecular details will emerge, such as the recent structure characterization of the seipin oligomers (Figure 14C).[125]

Lysosomes.—Lysosomes are spherical, membrane-bound organelles for biomolecular degradation. A lysosome contains more than 60 different enzymes and has over 50 membrane proteins. In addition to receiving their substrates through endocytosis, phagocytosis, or autophagy, lysosomes play roles in other physiological processes, including cholesterol homeostasis, plasma membrane repair, bone and tissue remodeling, pathogen defense, cell death and cell signaling (Figure 15A).[127] To perform such a diverse range of functions, lysosomes must be dynamic and able to form higher-order assemblies that carry

out different functions. For example, damaged lysosomes may cause unwanted cell death, so cells have evolved mechanisms for lysosome repair. A recent study suggested that components of the endosomal sorting complex required for transport (ESCRT)-I, ESCRT-II, and ESCRT-III are recruited for lysosome repair.[128] Among them, ESCRT-III is the most prominent one because it plays a role in all ESCRT mediated processes.[129] The higher-order assemblies formed by ESCRT-III proteins are long filaments. The recruitment of ESCRT-III proteins can start with the formation of ESCRT-I, and Pkh1/2 kinase phosphorylates Vps27 to regulate ESCRT-I recruitment.[130] This mechanism likely involves multiple ENS processes. In a recent study related to lysosome functions, Zoncu et al. reported that Rag GTPase controls the capture of nutrient-induced mTORC1 to the lysosome. As shown in Figure 15B, in the absence of amino acid, Rag heterodimers bind to the Ragulator on the lysosomal surface. In the presence of amino acid, the Rags switch to the active nucleotide state to destabilize the Rag interaction with Ragulator. Then, mTORC1 and Rag GTPases undergo spatial cycling, which regulates the mTORC1 activated by Rheb at the lysosomal surface.[131] This observation, again, confirms that nature ubiquitously uses enzymatic reactions control the assembly and disassembly of higher-order protein structures.

Microtubules.—In nature, an enzyme-regulated molecular assembly can play critical roles in many cell processes. The self-organization of tubulins to form microtubules is an example. As the name suggests, microtubules are hollow filaments made of tubulins in all eukaryotic cells. With the diameter of about 25 nm (Figure 16A) and as one type of cytoskeletons, microtubules not only support motility, but also are essential to many cellular functions. Like actins, tubulin itself is an enzyme, a GTPase. The hydrolysis of GTP to GDP catalyzed by tubulin maintains the unique asymmetric growth of microtubules (Figure 16B). All these dynamic behaviors depend on the assembly of microtubules, which, like the formation of actin filaments, is a representative example of an enzymatically controlled dynamic process. That is, microtubules grow (rescue state) and shrink (catastrophe state) at their ends. As a GTPase, β-tubulin binds and hydrolyzes GTP, which provides a conformational switch that helps to drive assembly and disassembly states of the microtubules. Such dynamic states depend on the local concentration of soluble dimers at the microtubule plus end. At low concentrations of tubulin, microtubules shrink, and vice versa.[133] Such asymmetric growth interacts with many microtubule-associated proteins (MAPs) to generate movements (Figure 16C). Microtubules also facilitate movement by acting as tracks to pull cargo for intracellular transportation. A recent study[134] of microtubules by cryo-EM not only provides useful insights into their dynamics, interactions with cellular components, and contributions to cellular functions, but also confirms enzymatic control in these assemblies.

Microtubule Ends.—The GTPase activity of β-tubulin, which hydrolyzes GTP to GDP, drives the dynamic instability of microtubules, such as transitions between catastrophe and rescue phases. As shown in Figure 16B, the growth and shrinkage of microtubules are asymmetric and occur at the plus end of microtubules. Since microtubule ends play important roles in cellular functions, considerable amount of research efforts have focused on the elucidation of the molecular details of microtubule ends. Although these studies have revealed that the ends of microtubules are structurally heterogeneous, there still are quite a

few unknowns. For example, while microtubules are cylindrical, the ends of microtubule cap during assembly are uneven. This observation excludes the possibility that the ends of microtubule correspond to a single position or tubulin structure. A recent study suggested that curvatures of protofilaments on growing and shrinking microtubules are similar.[135] The tips of the protofilament are curved, indicating that the bent GTP-tubulin in solution has to be straightened to be incorporated into the microtubule wall. But it remains a challenge to elucidate how it happens from structural analysis alone. It is not unreasonable to speculate that the dynamics of other biochemical states of tubulins may provide clues, such as enzymatic reaction controlled PTM of tubulins.[136]

Microtubule Organizating Centers (MTOCs).—In eukaryotic cells, microtubules emerge from MTOCs. There are several types of MTOCs, such as centrosomes, basal bodies, and spindle pole bodies. In an earlier section we already introduced centrosomes in the context of ENS (Figure 5), here we discuss spindle pole bodies (SPBs), which exist in fungi as the equivalent of centrosomes. SPBs are layered structures embedded in the nuclear envelop of budding yeast (*Saccharomyces cerevisiae*). Two types of microtubules, nuclear and cytosolic, grow out from SPBs. As one of the best-studied SPBs, yeast SPB consists of at least 18 different proteins, which assemble into a cylindrical organelle with a diameter of 100 nm. The core components of SPBs assemble into three vertical layers, named outer, inner, and central plaques. The outer and the inner plaques face the cytoplasm and the nucleoplasm, respectively, to organize cytoplasmic MTs and the nuclear MTs. Containing a two-dimensional crystal of the protein Spc42, the central plaque embeds in the nuclear membrane to anchor and interconnect the outer and inner plaques.[137] The kinase Cdc28 directly phosphorylates Spc42 to control its assembly into the SPB.[138] Moreover, Cdc28 also phosphorylates the Mps1 kinase,[139–141] which is known to regulate the phosphorylation and assembly of Spc42. Such multiple enzymes or multilevel controls of supramolecular assemblies (Figure 17B) support that ENS is a unifying theme in cell biology.

Midbody.—The midbody is a transient assembly at the intercellular bridge that connects two daughter cells at the end of mitosis (Figure 18A, B).[142] Midbody, controlling the final separation site of the daughter cells (Figure 18C),[143] plays roles in cell fate, polarity, tissue organization, and cilium and lumen formation. The dynamic nature of midbody implicates that the assembly process is controlled by enzymes. Indeed, a recent study on the interactomes of midbody reveals that MYPT1/PP1β phosphatase regulates microtubule dynamics and dephosphorylates the kinesin component MKLP1/KIF23 of the centralspindlin complex at the end of mitosis.[143] Specifically, after the completion of furrow ingression, the phosphatase MYPT1/PP1β accumulates at the midbody to dephosphorylate MKLP1. This dephosphorylation antagonizes the actions of kinase aurora B, thus strengthening the association of centralspindlin with PRC1. This result indicates that, during mitosis, the distribution of kinases and counteracting phosphatases controls the assembly and dynamic of cytokinesis proteins. Such control mechanisms indicate that the cellular functions of PP1 family phosphatases would likely involve in other ENS processes, such as the formation of cleavage furrow in early telophase.[75,143]

Mitochondria.—Mitochondria are complex organelles that play a central role in key cellular processes, particularly in acting as the hub for bioenergetic, biosynthetic, and signaling events.[144–150] The advances in mitochondrial biology have revealed that mitochondria, carrying their own DNA (mtDNA)[151–152] and constantly undergoing turnover,[153] fission,[154] and fusion,[155] are essential for metabolism,[156] stress response,[157] and cell death.[149] Because of the dynamic nature of mitochondria, it is not surprising that ENS plays roles in many mitochondrial processes. One interesting example of mitochondrial ENS is the aggregation of mitochondrial antiviral-signaling protein (MAVS) to form prion-like filaments for activating innate immune response against viruses.[158–160] Without infection, RIG-I bears constitutively phosphorylated serine or threonine residues in their CARDs and C-terminal domains, which represent a signaling-repressed state (i.e., an intramolecular interaction between the helicase domain and the CARDs of RIG-I resulting in an auto-repressed conformation). During infection, RIG-I binds to RNA to undergo an ATPase-dependent conformational change, which releases the CARDs for binding to several regulatory molecules, including phosphatase PP1—PP1α or PP1γ isoforms. PP1 removes the inhibitory phosphorylation marks in their CARDs. Then, the E3 ubiquitin ligases (e.g., TRIM25 or Riplet) attach ubiquitin polymers onto the CARDs and C-terminal domain for the tetramerization of RIG-I. The RIG-I tetramer interacts with the adaptor protein MAVS at the outer membrane of mitochondria to active MAVS. The activated MAVS self-assembles into prion-like filament structures, which further initiate the cascade of immune response.[160] Several enzymatic reactions (e.g., ATPase activity of RIG-I, dephosphorylation by PP1, and ligation of ubiquitin by E3 ligases) participate in the formation of MAVS filaments. Thus, MAVS assembly is a fine example of sophisticated ENS processes.

Mitotic Spindle.—The mitotic spindle is the cytoskeletal structure formed during mitosis of eukaryotic cells for separating chromosomes between the daughter cells.[162] The major components of the spindle are microtubule polymers, therefore, the ENS process for microtubule dynamics plays a role. Besides tubulins acting as GTPases, many other enzymes, obviously, regulate the assembly of the mitotic spindle (Figure 20A).[163] For example, the attachment of chromosomes to spindle microtubules through kinetochores during mitosis is essential for genome integrity. The dynamic of kinetochore–microtubule (k–MT) attachment is regulated by multiple enzymes (Figure 20B),[164] such as polo-like kinase 1 (PLK1), aurora B kinase (AURKB), cyclin–cyclin-dependent kinases (CDKs), and phosphatases PP1 and PP2A. These enzymes regulate the phosphorylation status of their substrates (e.g., kinesin family member 2B (KIF2B), BUB1-related kinase 1 (BUBR1), bi-orientation of chromosomes in cell division 1 (BOD1), and survivins), thus collectively controlling the k–MT attachment stability.

The nucleus is the largest and probably the most important membrane-bound organelle in eukaryotic cells. Being discovered about three centuries ago, the nucleus stores the genes of cells in the form of chromosomes and acts as the control center of the cell. The nucleus consists of several major components, such as the nuclear envelope, the nuclear matrix, nuclear bodies (e.g., nucleoli), and nuclear speckles (Figure 2). The nucleus regulates numerous cell functions, including gene expression, processing of pre-mRNA, through many dynamic processes. These dynamic processes constantly undergo assembly and disassembly

of higher-order structures, which are under the control of enzymatic reactions, as shown in the cases of nuclear bodies, nuclear membranes, nuclear speckles, nucleoli, nucleoli fibrillar centers, and the nucleoplasm.

Nuclear Bodies.—Nuclear bodies are membraneless structures inside the cell nucleus (Figure 21). There are several types of nuclear bodies, including Cajal bodies (CBs),[165–166] nucleolus,[167] promyelocytic leukemia protein (PML) nuclear bodies,[168] and ND10s.[169] CBs, being discovered by Cajal in 1903, can vary in size from 200 nm to 2 μm. Containing protein and RNA, CBs dynamically associate with cell cycle or cell stress. Recent advances of in vivo detection and imaging methods have revealed many insights on CBs, and support that multiple enzymatic reactions regulate the dynamic of CBs.[166,170] For example, coilin is the protein marker of Cajal bodies. One interesting feature of the components in CBs is that they also exist at other cellular locations. This observation suggests that enzyme catalyzed PTMs likely regulate these components. Increased evidence supports this notion. Hebert et al. reported that the interactions between coilin and RNA decreased when coilin was hyperphosphorylated,[171] and Lazo et al. reported that VRK1 regulates Cajal body dynamics and protects coilin from proteasomal degradation during cell cycle.[170] Such studies have led to a hypothesized model about PTMs on the dynamics of colin and CB formation (Figure 21C), which involves kinases, ubiquitinases, methylases, and probably phosphatases. Future studies on the enzymatic regulation of CBs may shed more light on the detail of the dynamics of CBs. Similar to the formation of CBs, enzymatic reactions also control the formation of PML nuclear bodies.[172] As shown in Figure 21D, oligomerization of non-SUMOylated PML monomers occurs via noncovalent interactions through the RBCC motif and covalent di-sulfide bonds between cysteine residues. A SUMO ligase, UBC9, then promotes (poly-)SUMOylation of the PML moieties for multiple SUMO–SUMO interacting motifs (SIM) interaction to form larger aggregates. Other binding partners carrying SIMs and/or SUMO residues can interact with the preassembled aggregates. These assemblies further self-organize to form a normal PML body.

Nuclear Membranes.—Nuclear membrane, also referred to as the nuclear envelope (NE), is a double lipid bilayer that encloses the nucleus. Consisting of an outer nuclear membrane (ONM), an inner nuclear membrane (INM)), nuclear pore complexes (NPC), and the nuclear lamina, the NE disassembles and assembles to coordinate with the segregation of sister chromatids in each cell division cycle. Not surprisingly, multiple enzymatic reactions control such dynamic processes. For example, a key feature in the NE is the nuclear pore complexes (NPC),[175] which consist of around 1000 protein subunits (Figure 22A).[176] While it is reported that mitotic disassembly of NPC involves CDK1- and PLK1-mediated phosphorylation of key interconnecting nucleoporins,[177] increasing number of studies suggest that phosphatases play important roles in the NPC re-assembly.[178] Since phosphorylation and hyperphosphorylation of nucleoporins trigger NPC disassembly, dephosphorylation at the end of mitosis would likely promote NPC assembly (Figure 22B). Desai et al. reported the nucleoporin ELYS as a scaffold to recruit PP1.[179] Lamond identified another PP1 binding protein, Repo-Man.[180] The study of Repo-Man during mitotic exit suggests that Repo-man binds stably to PP1 for the accumulation of some NPC components, namely Nup153 and importin β.[181] Moreover, the local activation of the

phosphatase is able to trigger NPC reformation even in the presence of high CDK1 and PLK1 activity. Another phosphatase, PP2A may dephosphorylate Nup153 for the reformation of NPC. In addition, Nup153 is also a PP1 substrate.[178] More studies likely will reveal the important role of phosphatases for controlling large protein assemblies like NPC.

Nuclear Speckles.—Nuclear speckles (NSs) or splicing speckles, also called interchromatin granule clusters, are self-organizing membraneless structures for the storage and modification of splicing factors[183] and may play a general role in RNA metabolism. Recent advances suggest that many enzymes act within NSs to facilitate the regulation of gene expression.[184–185] The best known molecular mechanism of nuclear speckle localization is a phosphorylation/dephosphorylation cycle of the arginine/serine repeat (RS) domain of serine rich (SR) proteins. Although it is generally believed that RS domain phosphorylation drives SR proteins from NSs to the nucleoplasm,[186] a recent study reveals that synergistic interplay between PP1 and two splicing kinases (SRPK1 and CLK1) regulate the location of SR proteins, such as SRSF1.[187] Adams et al. reported that SRSF1 binds to PP1 through the RRM1 domain and represses the catalytic activity of PP1 through an allosteric mechanism. This interaction would allow phosphorylation of hypophosphorylated SRSF1 to act as the substrates of kinases (e.g., SRPK1 and CLK1). The intermediate phosphorylated SRSF1 would reside in the NSs. Further phosphorylation would generate hyperphosphorylated SRSF1 to leave the NSs and to enter the nucleoplasm. The PP1 can dephosphorylate the hyperphosphorylated SRSF1 and bring it back to NSs. Thus, the balanced actions of phosphatase and kinases would result in the NS localization of SR proteins (Figure 23B).[187] Obviously, SR proteins inside the NS would interact with other proteins to form protein assemblies for RNA storage and modification.

Nucleoli.—As the largest membraneless organelle inside the nucleus, the nucleolus[167] is the site of ribosome biogenesis and a cellular stress sensor. Nucleoli contain three substructures: the fibrillar centers (FCs), dense fibrillar component (DFC), and the granular component (GC). Ribosomes synthesize proteins from amino acids according to the need of cells for new proteins. Nature has evolved elaborated mechanisms to assemble ribosomes in the nucleolus, which, of course, involves enzymatic reactions to regulate assembling processes. For example, one of the proteins found at high levels in the nucleolus is nucleophosmin (NPM), which binds with the proteins containing arginine-motifs (R-motifs). One binding mode is the multimer of NPM interacting with multiple R-motifs of other proteins. Such a binding is dynamic or reversible, and is controlled by enzymatic switch: phosphorylation and dephosphorylation. Kriwacki et. al. reported that the unphosphorylated N-terminal domain of NPM (NPM-N) predominantly populates the pentameric state. Phosphorylation of pentameric NPM-N destabilizes the oligomeric structure, and leads to conformational changes to expose additional, otherwise buried sites for further phosphorylation. The phosphorylation at the buried sites results in monomeric folded or monomeric disordered structures.[188] Thus, enzymes control the degree and state of phosphorylation to regulate the functions of NPM (Figure 24A), which interacts with more than one hundred proteins inside cells. The same lab also proposed that such multivalent interactions with proteins containing R-motifs and ribosomal RNA (rRNA) is one mechanism of nucleolar localization, and involves phase separation of proteins within the

nucleolus.[189] This mode of action appears to operate in the context of the tumor suppressor p14arf (Figure 24B).[190]

Nucleoli Fibrillar Center.—In the nucleolus, fibrillar centers (FCs) and dense fibrillar components (DFCs) are sites for rDNA transcription and pre-rRNA processing. A recent study by Chen et al. reported the assembly of DFC for sorting nascent pre-rRNA. They found that fibrillarin (FBL) self-assembles to form clusters, which integrate into the DFC surrounding the FC. The nascent pre-rRNA binds FBL. Because FBL diffuses to the DFC, the clusters immobilize FBL-interacting pre-rRNA, thus facilitating pre-rRNA processing and DFC formation. The authors attributed this pre-RNA sorting to liquid-liquid phase separation. The logical question would be what factors control the phase separation? The presence of ubiquitylation sites and phosphorylation sites on FBL implicates that enzymatic control of the PTMs of FBLs likely involves the formation of the clusters of FBLs. This presumption is supported by the report of Komada et al., which reported that USP36 plays a crucial role in regulating the structure and function of nucleoli by deubiquitylating various nucleolar substrate proteins, including fibrillarin.[191] Other enzymes, such as Pol I, also play a role in the formation of this dynamic interface of FC and DFC.

Nucleoplasm.—The nucleus contains the nucleolus and nucleoplasm, which are mainly nucleoproteins and nucleic acids. The most important content of the nucleoplasm is chromatin, a complex of DNA and protein. Chromatin serves as the basic constituent of the chromosomes, which is the site of gene storage. There are two types of chromatin materials: heterochromatin and euchromatin. While the former is metabolically and genetically inert, the latter contains metabolically active DNA and is genetically important. Recently, to account for the dynamic features of heterochromatin, Narlikar et al. reported that human HP1α protein (also known as CBX5) displays liquid demixing in vitro, and the HP1α demixing requires N-terminal phosphorylation or DNA binding.[193] They proposed a model (Figure 26) in which N-terminal extensional phosphorylation of HP1α leads to conformation change, which results in the dimerization of HP1α, which can assemble on the chromatin. Further increase in the concentration of the phosphorylated HP1α promotes the oligomerization, which interacts with chromatin to result in phase separation. This liquid phase would incorporate the macromolecules that interact with HP1α and exclude non-interacting molecules. In a related study, Karpen et al. proposed that the formation of heterochromatin domains was mediated by phase separation by examining the behavior of heterochromatin protein 1 (HP1) in Drosophila cells.[194] But phosphorylation appears missing from the cases of HP1 in Drosophila, implicating that other enzymatic reaction or interaction with other partners may control the phase separation.

Peroxisome.—Peroxisomes, existing in virtually all eukaryotic cells, are single membrane-bound metabolic organelles mainly for degrading fatty acids via β-oxidation and detoxifying hydrogen peroxide. Peroxisomes are highly dynamic and may undergo drastic changes in size, shape, abundance, and protein composition according to the need of cells. To meet the demand of fast dynamics of peroxisomes, cells rely on protein phosphorylation to govern peroxisome biogenesis and functions.[195] For example, in the study of the autophagy in yeast that involves peroxisomes, which is called pexophagy, a Hrr25-mediated

phosphorylation of Atg36 is necessary to form the assembly on the surface of peroxisomes for priming the peroxisome for autophagy (Figure 27A).[195] Unlike the case of yeast, which relies more on phosphorylation, mammalian cells employs ubiquitination of the pexophagy. Under stress conditions, ubiquitination of PEX5 and ABCD3 occurs, which leads to the binding of NBR1. This binding allows the tether of peroxisomes to the phagophore.[196] Since the peroxisome is a sophisticated organelle, other peroxisomal membrane proteins involve phosphorylation and ubiquitination to initiate pexophagy. Further studies with more emphasis on enzymatic controls would likely reveal more insights on the biogenesis and functions of peroxisomes.

Plasma Membrane.—The plasma membrane (also known as the cell membrane), is a biological membrane to protect the cell from its environment. As a lipid bilayer made of mainly cholesterols and phospholipids, the plasma membrane contains many protein molecules as its integral components and is the site for important cellular functions, including signaling and endocytosis. The dynamic compositions and shapes of the plasma membrane, again, imply the enzymatic control of assemblies (or oligomerization).. For example, one of the most studied lipid families is phosphoinositides. Multiple inositol lipid kinases and phosphatases regulate the degree of phosphorylation of the inositol ring in membrane phosphoinositides to control protein assemblies on the plasma membrane for cell signaling.[197] That is, the binding of inactive proteins ($E_{inactive}$) and appropriate phosphoinositides at the plasma membrane can activate or recruit additional proteins, and the activated proteins (E_{active}) can return to the cytosol as effectors for further actions (Figure 28A). In a recent study, Yuan et al. reported that, during the necroptosis mediated by the RIPK1-RIPK3-MLKL signaling, RIPK3 and TAM kinases phosphorylate Ser358 and Tyr376 of MLKL, respectively. These enzymatic reactions lead to the oligomerization of MLKL on the plasma membrane and cause membrane rupture, thus resulting in cell death (Figure 28B).[198] Many receptor-mediated signaling events also take place near the plasma membrane, especially those involving kinases.[199–200]

Rods and Rings.—Originally discovered by the use of human autoantibodies, rods and rings (RRs) are filament-like cytoplasmic structures containing proteins involved in the biosynthesis of nucleotides.[201] The size, shape, and quantity of RRs vary and are context-dependent (e.g., depending on cell types), suggesting that RRs may be transient and are likely resulted from ENS. A recent study on the composition complexity of the RRs formed by inosine monophosphate dehydrogenase (IMPDH)[202] supports this notion. In the presence of its inhibitors (e.g., mycophenolic acid (MPA) or ribavirin), IMPDH self-assembles to form polymers that appear as RRs across a wide variety of cell types. Although it was suggested that RRs play a role in the regulation of *de novo* guanine nucleotide synthesis, the function and regulation of RRs is largely unclear. Kahn et al. show that a regulatory GTPase, ARL2, a subset of its binding partners, and several ER resident proteins localize to RRs (Figure 29A). They found that RRs matured with IMPDH first forming aggregates, followed by ARL2, and only later calnexin, a marker of the ER, suggesting that the formation of RRs was complicated and likely regulated by enzymatic reactions. In fact, inhibiting IMPDH to result in the aggregation of IMPDH confirms that the enzyme activity of IMPDH regulates the assembly of IMPDH. CTP synthase (CTPS) is another enzyme known to form RRs.

Recent study by Kollman et al.[203] reveals that human CTP synthase 1 (hCTPS1) polymerizes in the presence of UTP and ATP substrates, but not in the presence of CTP and ADP, which differs from the bacterial CTPS1 (Figure 29B). They also found that hCTPS1 assembled into filaments, which likely locked hCTPS1 in a more active conformation, thus resulting in enhanced activity. Interestingly, the formation of the tetramer from the CTPS requires phosphorylation,[204] which further supports the enzymatic regulation of RRs formation.

Vesicles.—Vesicles are membrane-bound organelles, consisting of liquid or cytoplasm enclosed by a lipid bilayer, such as endocytic vesicles, secretory granules, peroxisomes, and lipid droplets. About 10% of human proteins localize to vesicles, which define the biological functions of vesicles. One of the most studied types of vesicles are synaptic vesicles (SVs) (Figure 30A), which are the secretory organelles that store and secrete non-peptide neurotransmitters at the synapse. The association of synapsins, which are highly abundant phosphoproteins,[205] during the dynamics of SVs (e.g., generation and regeneration) indicates phosphorylation-dependent interactions are likely controlled by enzymatic reactions. For example, synapsins are substrates for several protein kinases. The phosphorylation of synapsins is a response to a wide range of chemical and electrical stimuli. That is, PKA phosphorylated synapsins would detach synapsins from SVs and diffuse in the synaptic bouton and into the axonal compartment. After the stimulation (or in the recovery phase), phosphatase (e.g., PP2A) removes the phosphate groups from synapsins to allow the reclustering of the SVs (Figure 30B).[206] This process, of course, is complicated and involves other proteins. Other proteins, such as amphiphysin I and II, dynamin I, and synaptojanin, exhibit a similar phosphorylation/dephosphorylation cycle. Such a dephosphorylation step is required for these proteins to initiate the process of SV endocytosis. Moreover, multiple enzymes (e.g., V-ATPase and trimeric GTPase) present on the surface of SVs, further support that enzymatic reactions regulate the dynamics of SVs.

2.2. Extracellular ENS

Cells must respond to its surroundings, such as interacting with neighboring cells in tissues or adapting their environment for survival. To carry out these essential functions, cells have evolved extracellular matrices (ECMs) and cell adhesion molecules to transduce signals into the cells and to coordinate with the cytoskeleton dynamics. Increasing evidence suggests that the assembly of these molecules functioning in extracellular space are controlled by enzymatic reactions,[208–209] as illustrated by the following representative cases.

Extracellular Matrices.—Extracellular matrices (ECMs), consisting of the assemblies of proteins and polysaccharides, render distinctive mechanical properties to the tissues and mediate intercellular interactions. To provide a wide range of physical strengths, ECMs are networks of oligomeric assemblies of ECM molecules. To adapt to the environment or to meet the need of intercellular communications, ECMs constantly undergo remodeling, which is regulated by enzymatic reactions. For example, the formation collagen fibers[210–211] is a classic example of ENS of protein assemblies. In animal tissues, collagens exist as very long fibers with a unique axial periodicity (Figure 31A). The fibers act as the major biomechanical scaffold for cell attachment and macromolecular anchorage, thus defining the

shape and form of tissues. The collagen molecules self-assemble to form a trimer called procollagen. The procollagen consists of a triple-helical domain that can be as long as 300 nm with non-helical domains at the N-terminal and the C-terminal. Procollagen N-proteinase and procollagen C-proteinase cleave the N-propeptide and C-propeptide regions, respectively, to allow the triple-helical domains to form fibers. The oxidation by lysyl oxidase further crosslinks the fibers to modulate the mechanical strength of the collagen fibers (Figure 31B).

Cell junctions.—Cell junctions are the regions where cells meet and their plasma membranes closely face each other (Figure 32A).[212] There are four main types of cell-cell junctions: tight junctions,[213] adherens junctions,[214] desmosomes,[215] and gap junctions.[216] There are two types of cell-ECM junctions: focal adhesions and hemidesmosomes. The molecules that constitute the junction typically have ectodomains (exocellular parts) and endodomains (intracellular parts). In epithelial cells, junctional molecular complexes interact with cytoskeletons (e.g., intermediate filaments) to modulate the intercellular communications and to coordinate the morphogenesis and homeostasis of tissues.[217] These processes require a dynamic continuum of higher-order structures, which usually involve enzymatic reactions and self-assembly. For example, a recent study of the formation of tight junctions, by Honigmann et al.,[218] reveals that multivalent interactions and enzymatic reactions (de-/phosphorylation) regulate the phase transition of zonula occludens (ZO) proteins to form the supramolecular assembly and tight junctions as continuous networks of adhesion strands between cells.[218] Because ZO1 and ZO2 are phosphoproteins and their phosphorylation state involves tight-junction formation,[219–221] the authors tested whether the phosphorylation state affected the phase-separation ability of ZO proteins. Using casein kinase-2 (CK2) and lambda phosphatase, respectively, to phosphorylate and to dephosphorylate ZO1, ZO2, and ZO3 in vitro, they found that dephosphorylated ZO1, ZO2, and ZO3 efficiently phase separated into liquid droplets. But all phosphorylated ZOs are unable to phase separate under the tested conditions. Using mass spectrometry, they reported that CK2 phosphorylated ZO1 at 47 residues (Figure 32B). These results indicate that dephosphorylation likely actively triggers phase separation of ZO1 and ZO2 in a locally controlled manner.

Focal Adhesion Sites.—Focal adhesion[108] is one type of cell junction between the cell and extracellular matrix (ECM) (Figure 32A). At the focal adhesion sites, the transmembrane proteins, such as integrins, interact with their extracellular ligands, and transduce both mechanical and biochemical signals into the cells via the intracellular multipleprotein assemblies that connect to the actin cytoskeleton. While the enzymatic control of the intracellular molecular assemblies at the focal adhesion sites[222] is well-established (Figure 11), the understanding of the extracellular domains of focal adhesion sites focuses more on the ligand-receptor binding. This includes the binding of integrins with the RGD-motif on the ECM proteins. The accumulation of the knowledge on the phosphorylation of ECM proteins[208] implies that enzymatic reactions in extracellular spaces also likely play a role in focal adhesion sites, which remain to be elucidated.

3. Enzymatic Noncovalent Synthesis in Cell Free Conditions

Despite significant advancement in noncovalent synthesis and the observations of enzyme-controlled assembly of proteins, little attention was paid to the development of ENS until the report of using enzymatic reaction to trigger self-assembly of small molecules in water to form supramolecular hydrogels.[37] Hydrogels formed by three-dimensional elastic networks whose interstitial spaces are filled with water present many useful properties. Although enzymes can catalyze the formation of covalent bonds to crosslink polymers to form hydrogels,[223] there was no report on using enzymes to control self-assembly of small molecules for forming supramolecular hydrogels (via noncovalent bonds). That is, until the use of alkaline phosphatase (ALP) to catalytically dephosphorylate Fmoc-phosphotyrosine for generating Fmoc-tyrosine, a hydrogelator, to form a hydrogel, was reported.[37] This work illustrates a simple and reliable way to explore the emergent properties of small molecules in water, such as self-assembly or phase transition. Because it is easy to observe sol-gel phase transition, the use of enzymes to trigger the formation of supramolecular hydrogels becomes a facile assay to identify the substrates for ENS. Some of those examples[37,102,224–285] have been summarized in a recent review on supramolecular hydrogels.[286] The following section mainly discusses the works published after that review, according to the types of the enzymes.

3.1. Phosphatases

3.1.1. The Early Example and A Protocell Model—Phosphatases remove phosphate group(s) from a substrate. According to the pH for its optimal activity, nonspecific phosphatases fall into two categories: alkaline and acid phosphatases.[287] According to its substrates, specific phosphatases are of three kinds: tyrosine,[288] serine and threonine,[289] and histidine[290]. Because the broad substrate scope and rapid kinetics of ALP provide a platform for demonstrating many concepts of ENS of man-made molecules, ENS catalyzed by alkaline phosphatases (ALP) has received the most extensive exploration. The first case of ENS of small molecules employs ALP to dephosphorylate a simple substrate N-(fluorenyl-methoxycarbonyl) tyrosine phosphate (Fmoc-$_p$Y, **1**) (Figure 33A).[37] In that work, 50 mM of **1** at basic pH (9.6) exists as a solution, which turns into a hydrogel (Figure 33B) 30 minutes after the addition of ALP (0.15 U/mL). TEM reveals the nanofibers of Fmoc-Y (**2**) in the hydrogel (Figure 33C). The formation of a hydrogel or hydrogelation itself turns out to be a facile assay for indicating ENS if the substrate concentration is adequate. Depending on its concentration and pH, it is feasible for **1** to self-assemble to form micelle-like structures, as elucidated from the mechanistic study reported by Ulijn et al.[291] This result also suggests successive dephosphorylation by ALP, an overlooked subtlety. Nevertheless, this rather simple demonstration[37] established the feasibility of ENS of synthetic molecules and led to the researches of ENS of man-made molecules, as summarized by some recent reviews.[102,292–297]

Recently, Mann et al. demonstrated the use of ENS catalyzed by ALP for spatiotemporal control of hydrogelation in a model system such as protocells.[298] Based on their previous work of protocells,[299] the authors prepared ALP-containing water-in-water silica colloidosomes. The addition of **1** to the aqueous continuous phase allows the diffusion of **1**

through the semipermeable membrane and results in ALP-catalyzed dephosphorylation of **1**. The subsequent production of **2** leads to spontaneous self-assembly to form nanofibers. This simple model system produces a time-dependent sequence of supramolecular assemblies over three stages: First forming an outer wall of **2** on the external surface of the colloidosome; then forming a cytoskeletal-like matrix within the interior of the microcapsules; and finally forming denser assemblies of **2** as an extended matrix of colloidosomes. Although this is a simple model system that could benefit from more quantitative analysis, the simple coupling of ENS and compartmentation is able to result relatively sophisticated colloidosomes comprising spatially delineated regions of hydrogels, further implying the importance of ENS in the context of the origin of life. The same lab also further extended the colloidosome-based protocells to mimic phagocytosis.[300] Although phagocytosis is a highly complicated process in living cells, the use of a model system to mimic the essence of biological phenomena is able to reveal useful insights and principles for the design of ENS processes for future applications.

3.1.2. The Broad Substrate Scope of ALP—A unique advantage of ENS catalyzed by ALP is the broad substrate scope of ALP. It even allows otherwise water insoluble molecules to self-assemble in water, as reported by Yang et al.[240] In that study, a highly hydrophobic small molecule, Fmoc-Tyr-OMe (**4**, Figure 34A), being insoluble in water, can't form a hydrogel by either changing pH or adjusting temperature. But Fmoc-$_p$Tyr-OMe (**3**), the phosphorylated **4**, exhibits relatively good solubility in water. The addition of ALP to the solution of **3** results in the hydrogel of **4** (Figure 34B). This simple demonstration underscores that ENS is a powerful approach for exploring the self-assembly of a wide range of molecules, including hydrophobic molecules that have extremely poor water solubility.[237] One class of such molecules that remain to be explored would be hydrophobic drug candidates known to form aggregates.[301] Moreover, the broad substrate scope of ALP permits the evaluation of ENS of known self-assembling building blocks by a simple phosphorylation to make a substrate of ALP. For example, it is known that the core segment (GNNQQNY) of yeast prion Sup35 is able to self-assemble to form cross-β spine structures. The attachment of naphthyl (Nap) group to the N-terminal of GNNQQNY produces a hydrogelator Nap-GNNQQNY (**6**, Figure 34C). The phosphorylation of tyrosine in **6** generates Nap-GNNQQN$_p$Y (**5**). The addition of ALP to the solution of **5** converts **5** to **6**, which results in the hydrogel consisting of the nanofibers of **6** formed by noncovalent interactions (Figure 34C). ALP also is able to dephosphorylate D-phosphopeptide, Nap-gnnqqn$_p$y (**7**, which is the enantiomer of **5**) to form a hydrogel (here, the lower-case letters represent D-amino acids, same for the rest of this review). The hydrogel of **8** is relatively compatible to cells.[302] It would be interesting to examine whether the ENS of other cross-β spine forming peptides leads to supramolecular hydrogels and their cell compatibility.

Following their work of the ENS of **4** and their pioneering study of using ENS formed hydrogels as vaccine adjuvants, Yang et al. further evaluated the L- and D-peptide hydrogels formed by ENS.[303] They synthesized two phosphotripeptides, Nap-GFF$_p$Y-OMe (**9**) and Nap-Gff$_p$y-OMe (**11**) (Figure 35A). After confirming the formation of hydrogels of Nap-GFFY-OMe (**10**) and Nap-Gffy-OMe (**12**), they used the hydrogels as vaccine adjuvants and found that both L- and D-peptide hydrogels are more potent than the clinically used alum

adjuvant in the increase of the IgG production of OVA. Notably, the OVA encapsulated D-peptide hydrogel exhibits a slightly more efficient accumulation of OVA in the lymph nodes for preventing tumor growth than the L-peptide hydrogel does. This study, indeed, has led to several impressive follow up reports[304–312] on adjuvant studies from the same lab. Markedly, Yang et al. combined tuftsin (TKPR) and Nap-Gffy to develop a novel self-assembling molecule Nap-GffyTKPR, and reported that the nanofibers of Nap-GffyTKPR enhanced the phagocytic activity of macrophages, promoted the maturation of DCs, stimulated the expression of cytokines, and elicited a strong $CD8^+$ T immune response. As suggested by the authors, this work[313] demonstrated a powerful immune stimulating nanomaterial for cancer immunotherapy. Based on the application of Gffy, Liu et al. also used Gffy to enable the self-assembly of fenofibrate and ketoprofen for treating nonalcoholic fatty liver disease.[314]

One often overlooked factor for enabling the self-assembly of molecules is the concentration of the self-assembling building blocks. Thus, it is rather easy to observe hydrogelation from ENS if the self-assembling blocks have adequate concentrations, even without the attachment of a naphthyl or Fmoc group, as evidenced by the ENS of an immunoreceptor tyrosine based inhibitory motif (ITIM).[315] As shown in Figure 35B, the hexapeptide, LYYYYL (**14**), is a ITIM.[316] ALP catalytically dephosphorylates **13** (at 0.5 wt% and pH 7.4) to form **14**, which self-assembles in water to form a hydrogel. ALP is able to catalyze the dephosphorylation of the enantiomer (**15**) or retro-inverso isomer (**17**) of **13** to form the same peptide (**16**), which also self-assembles in water to result in supramolecular hydrogels. Although dephosphorylating **15** or **17** should give the same hydrogel of **16**, the hydrogel formed by dephosphorylating **17** is more cell compatible than the gel formed by dephosphorylating **15**. For example, when three mammalian cell lines, Saos2, HeLa, and HS-5, which express high, medium, and low levels of ALP, respectively were incubated with **16**, all the cells are quite viable. **17** exhibits much lower cytotoxicity to Saos2 cells than **15** does, though the dephosphorylation products from **15** and **17** both are **16**. Similarly, the hydrogel formed by ENS from **17** is the most compatible with HeLa cells. This result implies that the process or the history of ENS likely determines the properties of the peptide assemblies, which has profound implications in biomedical applications of ENS. Since immunomodulatory peptides play important roles in biology, further exploration of ENS of other ITIMs or immunoreceptor tyrosine-based activation motifs (ITAMs) may lead to useful soft materials for immunology.

Although it is used extensively to remove the phosphate group from a tyrosine residue, ALP is able to dephosphorylate phosphoserine for self-assembly, as shown by the enzymatic hydrogelation of the peptides containing phosphoserine.[317] In that study, a series of precursors contain the Nap-FF motif and an L- or D-phosphoserine residue (**18** and **20**), or both L- or D-phosphoserine and L- or D-phosphotyrosine residues (**22–28**) (Figure 35C). At the concentration of 0.5 wt%, the addition of ALP into the solutions of these precursors results in the nanofibers formed by the corresponding dephosphorylated peptides (**19**-**29**). Hydrogelation, however, only occurs for the peptides that incorporate tyrosine residues (**23**-**29**). While it indicates that tyrosine increases the ability of self-assembly of the peptides, this work, again, confirms the broad substrate scope of ALP for exploring ENS.

ALP also catalyzes the dephosphorylation of nanoparticles for self-assembly, as reported in the case of magnetic nanoparticles.[278] Recently, Shu and Ding have shown that ALP triggers self-assembly of quantum dots (QDs) by catalytically dephosphorylating the phosphopeptides attached on the QDs.[318] The authors attached the phosphorylated peptide ($GGFF_pY$) on the QDs (Figure 36A). ALP hydrolyzes the phosphorylated peptide to form peptide self-assemblies on the QDs surfaces, which also enable the self-assembly of QDs (Figure 36B). According to the authors, this ENS process, coupling with fluorescence resonance energy transfer (FRET) between phosphopeptide modified QDs and dansyl chloride (DNS), has a significant advantage, such as detecting ALP at an exceedingly low detection limit, 0.001 U/L, which is remarkable.

The substrates for ALP-catalyzed ENS also can be other solids (microparticles), as shown by transforming biocomposites of phosphopeptides and calcium (or strontium) ions to supramolecular hydrogels.[319] Having strong affinity alkaline metal ions (e.g., Ca^{2+} or Sr^{2+}), a heterochiral phosphotripeptide (**30**, Figure 36C) forms precipitates with the addition of calcium chloride. The addition ALP to the suspension of the precipitates results in a hydrogel consisting of the nanofibers of (**31**) and the microcrystals of calcium phosphates (Figure 36D). As the first example of ENS to assist the dissolution of a solid to form supramolecular nanofibers/hydrogel composites, this approach may find applications in understanding and generating calcified soft tissues.

Based on their pioneering exploration of dipeptides for emulsion,[320] Ulijn et al. used ALP for ENS to form interfacial nanofiber networks for stabilizing emulsions.[321] By mixing the Fmoc-$_pYL$ (**32**, Figure 37A) in water with chloroform and shaking the mixture, they obtained the emulsion, which is relatively weak and phase separates after 1 hour. Shaking after the addition of ALP in the mixture results in the emulsions stabilized by interfacial nanofiber networks of **33**. One unique feature of this simple method is that, even after storing the biphasic mixture for weeks, enzyme addition and shaking create the emulsion. It also appears the concentration of **32** should be at a proper range (e.g., 5 mM) to prevent hydrogelation due to the self-assembly of **33**. It would be interesting to see how the emulsion behaves when the non-aqueous phase is another organic solvent.

Since ALP maintains its activity in heterogeneous conditions,[319] it also catalyzes the formation of hydrogels in emulsion, as shown by the subsequent study of Ulijn and Tuttle.[322] Without the need of the Fmoc motif, the authors used an unprotected tripeptide, KYF (**35**), as the self-assembling building block for generating hydrogels by enzymatic dephosphorylation catalyzed by ALP. Particularly, they synthesized the phosphotripeptide, K_pYF (**34**, Figure 37B), which is a non-gelator. In addition to that ALP converted **34** to **35** to form a hydrogel of KYF (**35**), the amount of ALP kinetically controls the fiber network formed by KYF (Figure 36C). When the ALP catalyzed self-assembly occurs in biphasic mixtures, nanofibers of **35** form at the oil water interface and throughout the surrounding buffer to stabilize the oil-in-water droplets (Figure 37C). This work illustrates a facile on-demand formation and stabilization of emulsion by ENS, and would probably be very useful for making food or cosmetic products.

3.1.3. Context-Dependent—Differing from self-assembly at thermodynamic equilibrium, ENS is inherently irreversible and context-dependent. Yang et al. reported an example that ENS and heating–cooling processes result in different supramolecular assemblies.[323] They synthesized Ada-Gff$_p$y (**36,** Figure 38A), which is a substrate of ALP. Without the heating-cooling process, enzymatic dephosphorylation of **36** to generated the nanoparticles of Ada-Gffy (**37**), which is a viscous solution. Subjecting the solution to a heating–cooling cycle results in a hydrogel consisting of nanofibers and nanoparticles. Using the nanoparticles and the nanofibers as a protein vaccine adjuvant, the authors found that the nanoparticles resulted in accelerated DC maturation and stronger T-cell cytokine production than the nanofibers. The authors also suggested that ENS gave higher molecular order and conserved the more ordered conformation of the peptides. Although the detailed mechanism remains to be elucidated, this result indicates an entropy driven self-assembly by a heat-cooling process. Moreover, their work demonstrated that ENS is a useful method for preparing supramolecular nanomaterials for enhanced bioactivity. In another related study, Yang et al., reported that ALP catalyzed ENS at different temperatures generated peptide assemblies that had different morphology and exhibited different emergent properties, such as gel or sol.[324] The authors developed a fluorescent phosphopeptide (**38**, Figure 38B) that, underwent ENS catalyzed by ALP. When **38** is incubated with 0.1 U/mL ALP at 37 °C (or 1 U/mL ALP at 4 °C), the relatively slow rate of dephosphorylation allows the resultant peptide (**39**) to distribute evenly and self-assemble to form a hydrogel, consisting of nanofibers of **39**. When **38** is incubated with 1 U/mL ALP at 37 °C, fast dephosphorylation of **38** creates high local concentration of **39** near the enzymes and results in a solution of nanoparticles (Figure 38C). This work highlights the spatiotemporal control offered by ENS in the context of different temperature and different enzyme concentrations. Interestingly, the authors reported that 3T3 cells uptake about ten times more of the nanofibers than the nanoparticles. It would be useful to elucidate the underlying mechanism, especially by using other types of cells for the cell uptake study.

Besides their works to show that ENS results in different morphologies of the assemblies (of the same peptide) at different temperature, Yang et al. demonstrated that different precursors of the same hydrogelator formed different assemblies after undergoing ENS.[325] They synthesized three phosphorylated peptides (Nap-$_p$YYY (**40**), Nap-Y$_p$YY (**41**), Nap-YY$_p$Y (**42**)), which were the precursors of the same peptide (Nap-YYY (**43**)) (Figure 38D). Upon the addition of ALP, **41** is dephosphorylated to form uniform nanofibers in a stable hydrogel. The dephosphorylation of the other two precursors (**40** and **42**) by ALP, however, produces metastable hydrogels containing mixed nanostructures. The authors used TEM to show that the preorganization of **41** likely contributes to the formation of the stable hydrogel of **43** (Figure 38E). Another notable feature is that the nanofibers of **43**, being made from **42**, exhibit quite extensive interfibrillar interactions to form ribbon-like and higher-order structures. This work indicates that the assemblies of the precursors, acting as context-dependent signals, provide a useful strategy to control the outcomes of ENS, such as cellular uptake.[326] It also highlights that the molecular space of the precursors is a key factor for controlling ENS.

Recently, Yang et al. reported that the self-assembly catalyzed by ALP can make a micelle solution that turns into a hydrogel up increasing temperature, as a thermogel.[327] They synthesized two relatively long phosphopeptides (Figure 39A) with the structures of Nap-FFGG$_p$YGSSSRRAPQT (**44**) and NBD-GFF$_p$YGAVPIAQK (**46**). Adding ALP to dephosphorylate **44** or **46** at 4°C results in **45** or **47**, respectively. **45** and **47** both self-assemble to form micelles or short fibers at 4°C, but remain as solutions (Figure 39B). At a physiological temperature of 37°C, the solution of **45** or **47** undergoes sol-to-gel transformations, likely being driven by the increase of entropy. According to the authors, this thermogel may find promising applications such as three-dimensional (3D) cell culture. This work also highlights the opportunity to control the properties of the assemblies of oligopeptides via ENS.

From the discussion in section 2, the most common context-dependent signals used by cells for ENS are ligand-receptor interactions, as evidenced by ENS and ligand–receptor interactions of proteins often occuring together, for example in signalosomes. To understand how ligand–receptor interaction modulates the ENS of small molecules, it would be useful to develop ENS for generating supramolecular assemblies in the presence of a specific and strong ligand-receptor interaction, as shown in a recent study that uses ligand-receptor interaction to modulate the kinetics of ENS (Figure 40).[328] In that study, the ligand-receptor pair is vancomycin (**48**) and D-Ala-D-Ala, which serves as the basis for vancomycin against Gram-positive bacteria.[329–330] The attachment of D-Ala-D-Ala to the C-terminal of Nap-FFYGG produces a peptide (**50**) that self-assembles to form nanoribbons. Replacing tyrosine in **50** by phosphotyrosine generates a substrate (Nap-FF$_p$YGGaa, **49**, Figure 40A) of ALP for ENS. Without interacting with **48**, enzymatic dephosphorylation of **49** makes **50**, which is a hydrogelator and self-assembles to form long nanofibers of **50** (Figure 40B). In the presence of **48** (i.e., the ligand–receptor interaction), enzymatic dephosphorylation of **49** leads to precipitous aggregates containing short nanofibers that are made of **48** and **50** (Figure 40B). An excess amount of **48** can disrupt the nanofibers of **50** and result in the precipitates (of **48** and **50**). Directly adding **50** in water results in the nanoribbons of **50**, which hardly interact with **48**. This result also confirms that the assemblies of **50** exhibit different properties from that of individual molecules of **50**. This work represents the first case of using ligand-receptor interactions to control ENS of small molecules. Further exploration of this direction may lead to useful applications of ENS, especially when this type of modulation integrates with cellular functions.[331–332]

Nature also uses the ENS process, as context-dependent signals, to control another ENS process, such as the control of the dynamics of actins. Dynamic self-assembly, indeed, is an emerging concept in supramolecular chemistry.[333–335] Ulijn et al. pioneered the combination of dynamic self-assembly and enzymatic reaction. Taking advantage of the dephosphorylation of **1** by ALP and the amide bond formation catalyzed by thermolysin, Ulijn et al. reported an intriguing self-assembly cascade that utilized those two enzymatic reactions for generating transient (or interconverting) nanostructures.[336] As shown in Figure 40C, ALP dephosphorylates **1** to generate nanofibers of **2**; thermolysin catalyzes the (reversible) amide hydrolysis and condensation of **2** and C-terminal capped phenylalanine (F-NH$_2$). The authors examined the morphology of the resulting assemblies by sequential

addition or co-addition of the enzymes. In pathway I, ALP converts the spheres of **1** to the fibers of **2**, the subsequent addition of thermolysin and F-NH_2 generates Fmoc-YF-NH_2 (**52**) which self-assembles to form nanosheets. In pathway II, thermolysin catalyzes the condensation between Fmoc-$_p$Y and F-NH_2 to produce Fmoc-$_p$YF-NH_2 (**51**), which self-assembles to form nanotubes/tapes. The subsequent addition of ALP removes phosphate group from tyrosine phosphate to result in the nanosheets of **52**. By varying the ratios of the enzymes and co-addition of the enzymes in the mixtures of **1** and F-NH_2 (Pathway III), it is possible to control the morphological transition of the mixtures to make the system evolve more like pathway I or II. This work is an excellent example of how to use multiple ENS processes to control self-assembly, and provides important insights for designing soft nanostructures that exhibit tunable dynamic properties. Recently, Zhang Y. reported an elegant example of a Dual-Enzyme-Instructed Hierarchical Assembly.[337] The next step, besides more rigorous kinetic analysis, is how to translate these concepts and insights into useful applications.

3.1.4. On A Surface—The fast kinetics of ALP catalyzed dephosphorylation allows rapid buildup of the concentration of the products. When the product is a building block for self-assembly, such a rapid ENS process enables localization of the assemblies at the position of the enzymes.[267] One way to help increase the local concentrations of the products is to provide a binding site for the products, as shown by the elegant work of Schaaf and Boulmedais.[338] They generated a seed layer composed of poly(acrylic acid) that carried Fmoc-FFC as the pendants. After confirming that PAA-CFF-Fmoc (**53**) interacted with Fmoc-FF$_p$Y (**54**) to promote ALP catalyzed enzymatic hydrogelation, they embedded ALP in a polyelectrolyte multilayer, which had **53** as the top layer (Figure 41A). With the top layer acting as the nucleation site for the self-assembly of the Fmoc-FFY peptide (**55**), a nanofiber network starts to form almost instantaneously when the multilayers come in contact with the solution of **54**. The network is able to extend up to several micrometers into the solution after several hours. The authors also demonstrated that changing the peptide density allowed the active seed layer to control the self-assembly kinetics and the geometric features of the fiber network. This model system may provide a useful insight for understanding ENS for spatiotemporal control of molecular assemblies in a more complicated microenvironment, such as cells.[267]

Instead of attaching phosphopeptides to nanoparticles, Schaaf and Jierry also covalently linked ALP to nanoparticles to catalyze self-assembly in a spatiotemporally controlled manner.[339] In that work, the substrate is **54**, and the enzyme is the ALP linked on silica nanoparticles (NPs). As shown in Figure 41B, after the dephosphorylation, the self-assembled peptide nanofibers grow from the NPs, which are able to form a hydrogel that consists of the silica nanoparticles and the nanofibers of **55**. The authors reported an unexpected macroscopic shape change of the hydrogel over time, resulted from a phase separation leading to a dense phase (in NPs and nanofibers) in the center of the vial and surrounded by a dilute one, which still contained NPs and peptide self-assemblies (Figure 41C). Although it is similar to a syneresis process, this change only occurs when the ALP is being attached to the NPs. Thus, the authors speculated that the strong interactions of self-assembled peptide nanofibers with the enzymes on the NPs resulted in the dense phase.

Since the interaction between the nanofibers and ALP is less explored,[233] this work may reveal a useful insight for further investigation of the allosteric interaction of the peptides with the ALP. In another related study, Schaaf, Jierry, and Boulmedais made a polymeric hydrogel that incorporated ALP for ENS inside the hydrogel.[340] Because of its small size, **54** easily diffuses into the polymeric hydrogel and allows the dephosphorylation of **54**. This approach is able to tune the elastic moduli of the hydrogels, but only moderately. Recently, the same group of authors also reported the use of glutathione reductase[341] for controlling the self-assembly of Fmoc-peptides for gelation that was initiated exclusively from the surface.

Schaaf and Jierry also reported an exciting use of ENS on a surface to generate self-assembled peptide nanofibers for catalysis in the context of flow chemistry.[342] To avoid the mechanical fragility of peptide nanofibers in the hydrogels, the authors immobilized ALP on a multilayer film based on a commercial open-cell melamine foam. After packing the foam into a column and passing the solution of Fmoc-GFF$_p$YGH$_p$Y (**56**, Figure 41D)[343] through the functionalized column, the hydrogel consisting of the nanofibers of Fmoc-GFFYGHY (**59**) forms in the pores of the foam. The authors demonstrated that this supramolecular hydrogel was able to catalyze the hydrolysis of an activated ester, 4-nitrophenyl acetate, and the kinetic resolution of racemates. Most impressively, being reusable and stable over months, the resulting hybrid material is robust enough to be a component in continuous flow reactors. This innovative work illustrates ENS as a facile approach to control the emergent functionalities of supramolecular assemblies.

It is difficult to detect enzyme-induced color change in colored medium, such as blood. Yang et al. reported an facile way to detect the activity of ALP in blood via ENS.[344] They designed and synthesized NBD-FF$_p$Y (**60**, Figure 41E) that was able to be converted to NBD-FFY (**61**) upon dephosphorylation catalyzed by ALP. Taking the advantage of a positively charged surface, they allowed the negatively charged **61**, being generated by ALP (in serum), to be attracted to the surface modified with positive charges. This process results in nanofibers/hydrogels on the surface. After removing the serum, the fluorescence turned on at the glass surface reveals activity of the enzyme (ALP). According to the authors, the color depth of hydrogels at the surface is visible even by naked eyes, thus providing a convenient assay for detecting enzymes.

3.1.5. Coupling with Other Controlling Mechanisms—The enzymatic control of the dynamics of self-assembly also is suitable to couple with other controlling mechanisms, such as photochemistry, as shown by Zhang et al.[345] Inspired by the dynamic and reciprocal interactions between ECM and cells, the authors developed two building blocks that contained coumarin and acted as self-assembling hydrogelators (Figure 42A). While the peptide derivative (**63**) self-assembles into nanofibers, the benzoate molecule (**64**) forms nanobelts. These two molecules exhibit different dynamic profiles and form self-sorted nanostructures. One interesting feature of this two-component mixture is that the growth of the nanofibers of **63** enables the nanobelts of **64** to turn into a layer-by-layer nanosheet (with nine-fold increase in height). This behavior resembles crowding effects to promote protein assemblies. The authors also demonstrated that light and ALP (Figure 42A) were able to

control the height and morphology of the self-sorted nanostructures. This kind of dual control appears to have interesting potential applications, but it remains to be explored.

In a different study, Yang and Wang et al. reported the first combination of amine-reactive aldehyde with ALP catalyzed self-assembly.[346] As shown in Figure 40B, the phosphopeptide (Nap-gff$_p$y-CHO, **68**), in addition to a phosphotyrosine residue, bears an aldehyde group at the C-terminal. **68**, despite bearing an aldehyde group, still can be dephosphorylated by ALP. The authors reported that **68**, forming a clear solution in PBS buffer, turned into a hydrogel of Nap-gffy-CHO (**69**) after ALP dephosphorylated 85% of **68** in the solution. Because the drug containing an amino group can form pH-responsive Schiff bases with **69**, the hydrogels are useful for encapsulating amine drugs, such as doxorubicin, for controlled release.

To reduce the autofluorescence in biological samples, Liang et al. came up with an original approach that combined ENS and chemiluminescence (CL) catalyzed by ALP.[347] The authors used **54** for the ALP catalyzed self-assembly of Fmoc-FFY (**55**). Using a commercial chemiluminescence agent AMPPD (**70**, Figure 42C) to incubate with **54** in the presence of ALP, the authors were able to employ CL for characterizing and imaging the simultaneous ENS process of **54**. They also found that **54** and **70** competed for ALP, thus **54** delayed the peak of CL and **70** slightly slowed down the gelation (Figure 42D). The further applications of this simple mixture, however, remains to be demonstrated.

3.1.6. Acid Phosphatases—Only a few studies[257,348] have used acid phosphatases (ACP) for ENS after the early example of screening the inhibitors of ACPs based on hydrogelation resulted from ENS.[224] Borner et al. used ACP to dephosphorylate polymer-peptide conjugates for self-assembly.[348] As shown in Figure 43, the polymer–peptide conjugates consist of five repeats of alternating threonine and valine diads ((TV)$_5$) at the N-terminal and a polyethylene glycol (PEO) block at the C-terminal. The (TV)$_5$ repeats favor the formation of β-sheets in water. Containing three phosphothreonine ($_p$T) residues, the phosphorylate conjugates (**73**) dissolve well in acidic water to form a solution, and the phosphorylated peptide segments adopt a coil conformation. The addition of ACP dephosphorylates the phosphothreonine residues on the conjugates and leads to rapid conformation change of the peptides from the coil conformation to β-sheet. However, only after a relatively long time (7 days) incubation with ACP, did the resulting dephosphorylated conjugates self-assemble to form uniform nanofibers. This work illustrates that the concept of ENS is applicable to large synthetic molecules. It remains to be seen if the peptide segment can be phosphorylated by a kinase. If this is true, a more dynamic control of the polymer-peptide conjugates may be achieved.

3.1.7. Protein Phosphatases—Enzymatic phosphorylation/dephosphorylation is a putative mechanism used by cells to control the conformation of proteins and to modulate the protein functions. Thus, it is reasonable and logical to use enzymatic reaction for modulating the conformation of peptides for self-assembly, as shown by Schneider et al.[349] Based on their seminal work on the self-assembly of peptide hairpins,[350–352] the authors designed and synthesized the peptides by having a phosphothreonine at different positions of the hairpins (Figure 44A). The phosphopeptides disfavor the folded and assembled state,

thus largely reside in unstructured states (Figure 44B). The addition of lambda protein phosphatase (LPP) almost quantitatively dephosphorylates the peptide (**75**) within hours. Such dephosphorylation leads to a distinct conformational change from random coil to β-sheet, which assembles into well-defined monomorphic fibrils (~4 nm). The position of the phosphothreonine hardly affects the dephosphorylation kinetics, but modulate the dynamics of self-assembly. The authors also investigated the cytocompatibility of a hydrogel resulting from dephosphorylation of the phosphopeptides (**75** & **77**) and found that human dermal fibroblasts (HDFs) remain viable on top of the resulting hydrogels. One notable result reported in this work is that **75** appears to be a more suitable substrate to the protein phosphatase than to ALP. Because of the abundance and specificity of protein phosphatases in cells, it is likely that carefully designed ENS substrates of protein phosphatases would lead to more useful applications.

3.1.8. Coupling with A Disassembly Process—It is well-established that cells use a pair of enzymes that have counteracting activities to switch the functions of proteins.[353] Such an enzyme-switch is a common feature that associates with ENS, which would result in phase-transition (as shown Figure 32B[218]). In fact, the study of ENS of small molecules has confirmed that it is feasible to use a kinase/phosphatase switch for regulating phase transition.[226] As shown in Figure 45A&B, a hydrogelator Nap-FFGEY (**82**) forms a gel. The addition of a kinase and ATP to the gel of **82** allows the phosphorylation of **82** to generate Nap-FFGE$_p$Y (**81**). Because **81** is more hydrophilic than **82**, the kinase turns the gel of **82** to the solution of **81**. Adding ALP to the resulting solution leads to sol-gel transition because ALP converts **81** back to **82** (Figure 45B). TEM reveals that ALP catalyzed ENS also generates nanofibers with monodispersed diameters (Figure 45C), which are more-ordered than the nanofibers in the gel of **82** formed by changing pH. In vivo study (i.e., subcutaneous injection of **81** in mice) confirms that ENS is able to generate the gel of **82** *in vivo*.[226] Stupp et al., using a peptide amphiphile (**84**, Figure 45D) as the substrate of protein kinase A and alkaline phosphatase, also demonstrated the enzymatic switch of the gel of **84**.[354]

Recently, to detect the presence of tyrosine kinase, Liang et al. combined ALP catalyzed self-assembly with disassembly catalyzed by kinase, as shown in Figure 45E.[355] The authors synthesized a ^{19}F-fluorinated hydrogelator (**86**), as well as its phosphorylated precursor (**85**). ALP catalyzed dephosphorylation generates the hydrogel of **86**, which is silent in F-19 NMR (Figure 45E) because **86** is unable to rotate freely in the nanofibers of **86** in the hydrogel. According to the authors, treating the hydrogel of **86** with tyrosine kinase generates **85** and results in the disassembly of the nanofibers. As the soluble molecule, **85** is F-19 NMR active (Figure 45E), thus the disassembly constitutes a “turn-on” process of the F-19 based MRI. The authors also used the cell lysates of H1975 cells (EGFR overexpression) and LoVo cells (ALP overexpression) to demonstrate the ON/OFF MRI signals. This work, being the first case of using ^{19}F NMR/MRI to sense the activity of tyrosine kinase and phosphatase, underscores the importance of incorporating ENS into a dynamic process. In related studies,[356–357] Liang et al. also reported the use of liquid-phase scanning tunneling microscopy (L-STM) to directly visualize enzymatic self-assembly/disassembly of nanofibers of an analog, in which F replaces the CF_3 group in **85**.

To develop an enzyme probe for reporting tyrosinase, Yang et al. combined ALP catalyzed assembly and tyrosinase catalyzed disassembly, as shown in Figure 45G.[274] The authors developed a phosphopeptide (**87**) containing a fluorinate phenylalanine residue and an adamantane at the N-terminal. After ALP removes the phosphates, the resulting peptide (**88**) self-assembles to form a nanoparticle suspension, which is silent on F-19 NMR due to the aggregation of **88**. The addition of tyrosinase catalyzes the oxidation of **88** to form **89**, causing the disassembly of the nanoparticles, thus turning on the F-19 NMR signals. Although the amount of tyrosinases, used in this demonstration, is relatively high, the principle illustrated in this work should be applicable for detecting other enzymes that have high activity and result in disassembly. The above results illustrate ENS for phase transition and promise a versatile way to design and to construct biomaterials for various applications (See Section 4).

3.2. Proteases

In addition to the use of enzymatic dephosphorylation for controlling self-assembly of molecules, enzymatic proteolysis is another type of enzymatic reaction being used to regulate the self-assembly of various substrates. Unlike ALP, protease catalyzed ENS of synthetic molecules has received less exploration, so the following discussion adheres to more of a chronological order than thematic arrangement. Because proteases are evolved for breaking bonds in large molecules, such as proteins,[358] it is rather common to cleave peptide segments from a polymer for enabling self-assembly of nanoparticles, as pioneered by Bhatia et al.[359] As shown in Figure 46A, the authors generated superparamagnetic Fe_3O_4 nanoparticles coated with biotin or neutravidin that attach to polyethylene glycol (PEG) polymers (10 kDa) via a GPLGVRGC peptide segment. Because GPLGVRGC is a substrate of matrix metalloproteinase-2 (MMP-2), MMP-2 can proteolytically remove the PEG to allow the binding of biotin and neutravidin, thus initiating the self-assembly of the Fe_3O_4 nanoparticles. The authors reported that ten to hundreds of nanoparticles assemble together 3 h after MMP-2 addition. Using MRI, the authors also showed that MMP-2 initiated assembly to amplify the transverse (T2) relaxation of the nanoparticles and suggested that these MMP-2 responsive magnetic nanoparticles may allow MRI detection of tumors. This approach has been applied to the design of polymer nanoparticles for drug delivery that targets cancer cells.[360]

One of the known drawbacks of nanoparticles for imaging is the accumulation of nanoparticles by mononuclear phagocytic and renal systems.[361] One approach to address this problem is to form the nanoparticles in situ on the tumors by ENS of small molecules. Indeed, it is feasible to use proteases to instruct the self-assembly of small molecules.[238] Because the tetraphenylalanine (FFFF) is an efficient supramolecular hydrogelator with the minimum gelation concentration (mgc) at about 0.4 wt% in water at pH7.4, it is feasible to create a soluble precursor (**90**) by adding the pentapeptide, CGLDD, at the C-terminal of the tetraphenylalanine. As a substrate of MMP-9, FFFFCGLDD (**90**), is able to undergo proteolysis catalyzed by MMP9 (Figure 46B). At pH > 6.6, **90** (0.6 wt%) exists as a clear solution. The addition of MMP-9 to the aqueous solution of **90** at room temperature results in the sol-gel transition after 45 minutes. Although only 47% of **90** is converted to **91**, TEM shows the nanofibers in the hydrogel (Figure 46C), confirming that MMP-9 catalyzes the

proteolysis to initiate the self-assembly of the peptide mixture, which consists of **90**, **91**, and **92**.

To achieving passive monitoring of biological environments by soft materials, Kofinas et al. developed color changing close-packed nanoparticles—hydrogel composites.[362] They suspended silica nanoparticles in the solution of 4-arm norbornene-PEG (PEG4NB (**93**), Figure 46D) and a dicysteine capped peptide **(94)** for photo crosslinking to make the nanoparticle—hydrogel composites. Proteases, either chymotrypsin or trypsin, catalytically cleave the peptides in hydrogel network, thus initiating self-assembly to form a secondary, physically cross-linked network. This change causes a 1200% increase in storage modulus. The increased packing of the silica particles also results in color change of the composites (Figure 46E). This result is rather counterintuitive because proteolytic cleavage usually results in dissociation of molecular aggregates.[363] The authors suggested that such protease responsive hydrogel nanocomposites may find biomedical applications as degradation-stiffening and collapsing materials.

Based on the work of Ulijn et al.,[225] Huang and Qi investigated the use of α-chymotrypsin for enzymatic hydrogelation.[364] In that study, the substrates are Fmoc-F, Fmoc-W, Fmoc-A, Fmoc-S, F-OMe, F-OEt, and Y-OMe. Rapid hydrogelation occurs when the substrates are Fmoc-F and F-OMe (or Y-OMe) and α-chymotrypsin is the enzyme. Without the addition of the enzyme, the substrate exhibits poor solubility and exists as a milky suspension. The authors also suggested the interactions between the substrates and the enzyme promote the self-assembly of the substrates and the product of the enzymatic reaction. This assumption appears to be reasonable since the amount of α-chymotrypsin or trypsin, used in that study, is relatively high (1 mg/mL).[364] Ulijn et. al., based on the reverse hydrolysis catalyzed by thermolysin, recently used reversible and irreversibly immobilized enzymes on a surface for ENS of peptide assemblies.[365] The authors used bioinspired polydopamine and polyphenol coatings to study the effects of surface anchoring and surface release of enzymes on the self-assembly process. Their studies reveal that the enzymes reversibly bound to the surface catalyze the coupling of the precursors Fmoc-T (**95**, Figure 47A) and F-NH_2 (**96**) to result in a bulk gel made of **97**. The enzymes, which are irreversibly bound to the surface, catalyze the conversion of the precursors only at the surface, thus restricting self-assembly of the gelator **97** to form nanofibers/hydrogel at the surface (Figure 47B). The work may lead to a useful model system to understand pericellular ENS catalyzed by membrane-anchored enzymes and secreted enzymes, especially when the enzymes are proteases.

While MMPs have received much attention in ENS, transmembrane serine proteases (TMPRSS)[366] only are being explored for enzymatic self-assembly recently.[367–368] Enterokinase (ENTK/TMPRSS15) is an enteropeptidase discovered by Pavlov.[369] ENTK specifically cleaves the peptide sequence DDDDK from proteins and has led to the development of FLAG-tag (DYKDDDK) for protein purification.[370] As shown in Figure 47C, attaching the FLAG-tag as a peptidic branch to a self-assembling motif[371] affords a negatively charged, soluble, branched peptide (**98**). **98** self-assembles to form micelles. ENTK catalyzes the cleavage of the hydrophilic FLAG branch to generate a peptide (**99**) that forms nanofibers, which results in supramolecular hydrogels. This ENTK-based ENS induces both sol-gel and morphological (micelles-to-nanofibers) transitions (Figure 47D).

This work is also the first case of using a protease to cut branched peptides for generating supramolecular hydrogels, and opens a new way explore ENS of branched peptides.

To develop oligopeptide hydrogels for localized protein delivery, He and Mo used substrate-selective proteases to catalyze ENS of **103** (Figure 48A) for encapsulating proteins by an innovative design,[372] as shown in Figure 48B. In that study, the authors first used polymeric networks to encapsulate a protease (WQ9–2) to prevent the proteolysis of protein cargos, then they mixed the proteins and peptide substrates (**101** and **102**) of the proteases. Because of the small size of the peptides, it enters the polymeric networks and acts as the substrates of the protease for reverse hydrolysis. This process leads to the buildup of the peptide hydrogelators and results in a supramolecular hydrogel for loading the proteins. The authors used the resulting oligopeptide hydrogels for delivering of an antiangiogenic protein, hirudin, and an apoptosis-inducing cytokine, TRAIL, in a mice model, and observed enhanced synergistic antitumor effects both in vitro and in vivo.[372] Although proteins would be the natural substrates for proteases, the combination of protein and protease is much less explored for self-assembly. Recently, Li et al. reported an interesting example of this approach.[373] Using bacillus licheniformis protease (BLP) to catalyze the partial hydrolysis of α-lactalbumin, the authors generated amphiphilic α-lactalbumin peptides that self-assembled to form peptosomes. The authors used the peptosomes to encapsulate a therapeutic peptide and curcumin for drug delivery. According to the authors, this system exhibits enhanced antitumor and antimetastatic activities in vitro and in vivo. This work bears similarity to earlier work on anticancer α-lactalbumin done by Svanborg.[374] Further study is needed for identifying the molecular species formed upon partial hydrolysis.

Based on their innovative approach of surface immobilized ALP for supramolecular hydrogelation, Schaaf and Boulmedais used proteases for localized enzyme-assisted self-assembly (LEASA).[375] As shown in Figure 48C, the enzyme is α-chymotrypsin and the substrate is KL-OEt (**104**, K: lysine; L: leucine; OEt ethyl ester). After the absorption of α-chymotrypsin and bovine serum albumin (BSA) on a surface made of poly(ethylene imine) and tannic acid, the authors allowed the surface to contact the solution of **104** so that α-chymotrypsin catalytically converted **104** to $(KL)_n$OEt oligopeptides (**105**). After reaching a critical concentration near the surface, the formed oligopeptides self-assembled into β-sheets resulting in a fibrillar network localized at the interface. The authors were able to control the lag time (i.e., the time before starting the self-assembly process) by finely tuning the surface density in α-chymotrypsin and the concentration of **104**. This model system would be extremely useful if it can mimic the ENS processes that occur on a cell surface. In a related study, Bai et al. devised an interesting application of ENS for making peptide cages.[376] Specifically, the authors absorbed thermolysin on porous $CaCO_3$ microparticles to catalyze the condensation reaction of Fmoc-Y (**2**) and L-NH_2 in a water/hexane emulsion. This biphasic system limits the self-assembly of Fmoc-YL-NH_2 on $CaCO_3$ surface. After the removal of the $CaCO_3$, the authors were able to obtain the peptide cages made by Fmoc-YL-NH_2.

One of advantages of using peptides as the pendant groups of block copolymers is to produce nanoparticles that exhibit narrow size distribution, as shown by the work of Gianneschi et al.[377] The authors used the fully water-soluble quaternary amine based

Hoveyda–Grubbs type catalyst to initiate the ROMP of the L-amino acid–based norbornene dicarboximide, generating a block copolymer that contains GPLGLAGGWGERDGS as the pendants in the peptide stabilizer block. This type of open-to-air aqueous-phase ring-opening metathesis polymerization induced self-assembly (ROMPISA) forms well-defined peptide polymer nanoparticles. Upon the addition of the protease thermolysin, these nanoparticles further rearrange into larger aggregates. These innovative block copolymers seem to be excellent synthetic substrates to generate a dynamic continuum of particles with different morphologies, as shown by the same lab previously.[378]

3.3. Esterases

Esterases, as an enzyme commonly used for activating prodrugs, also find applications for the ENS of man-made molecules.[227,249] Ragona and Galeotti reported an innovative approach that indirectly applies acetylcholinesterase (AchE) to trigger the self-assembly of a perylene diimide-theorine derivative (PDI-Thr, **106**).[379] As shown in Figure 49A, B, myristoylcholine chloride (**107**) acts as a cationic surfactant, which is able to disperse PDI-Thr. AchE catalyzes the hydrolysis of **107** to result in the self-assembly of **106**. One attractive feature accompanying this process is the change of the fluorescence of the assemblies with and without the presence of the AchE. Hydrolysis of esters is a facile way to trigger self-assembly. For example, Zhong et al. reported a simple hydrogelator (**111**, Figure 49C), which is formed by the hydrolysis of an ester (**110**).[380] The authors used sodium carbonate to trigger the hydrogelation for the encapsulation of 10-hydroxy camptothecin (HCPT) to make the HCPT hydrogel. The authors suggested that the HCPT hydrogel possessed satisfactory stability and recoverability for localized injectable drug delivery. **110** also can act as a substrate of esterase for ENS, as reported earlier.[249]

3.4. Kinases

Although kinases are an important type of enzyme for cell functions, including endogenous ENS, the use of kinase for controlling the self-assembly of man-made molecules is much less explored. A close related recent example, in fact, is the self-assembly of kinase, as reported by Xiang and Yan.[381] In their study, they selected an adenylate kinase (AKe) as the building block for self-assembly. Bearing dual substrate-recognition domains for binding adenosine triphosphate (ATP) and adenosine monophosphate (AMP), AKe switches its conformations between closed and open states. This switch in conformation traps these two substrates for enzymatic conversion of an ATP and an AMP to two ADP molecules. The authors also produced a protein amphiphile containing one AKe head and a hydrophobic polypeptide tail. While this protein amphiphile self-assembled to form 1D nanofibers, the addition of a specific ligand, diadenosine-5-pentaphosphate (Ap5A), compresses the AKe conformation to generate 2D nanosheets. This elegant example may provide useful insights for the design of other man-made substrates for ENS catalyzed by kinases.

3.5. Beta-lactamases

As a type of bacterial specific enzyme, β-Lactamases hydrolyze the four-membered β-lactam ring in antibiotics and cause the most widespread antimicrobial drug resistance.[382] During the development of a facile approach for detecting the presence of β-lactamases and

screening their inhibitors, β-lactamase based ENS was explored.[228] As shown in Figure 50, the substrate (**112**) of β-Lactamases consists of the cephem nucleus as the linker, a hydrophilic group, and a hydrogelator. The substrate, bearing the hydrophilic group, is too soluble to form a hydrogel. Upon the action of a β-lactamase, the β-lactam ring opens to release the hydrogelator (**113**). Self-assembling to form nanofibers, **113** results in a hydrogel after reaching adequate concentration. Indeed, the lysates of bacteria (e.g., *E. coli*) containing different types of β-lactamases are able to catalyze hydrogelation. Besides providing a simple, low-cost strategy to identify β-lactam antibiotic resistant pathogens, this work may provide a way to induce intracellular gel-sol transition in cells with controlled-expression of β-lactamases, an application that remains to be realized. In addition, this study also establishes the feasibility of using microorganism specific enzymes for the development of ENS.

3.6. DNAzymes

DNAzymes are able to recognize specific DNA sequences and cut at an RNA base site. Ganneschi et al. pioneered the use of DNAzymes to control the self-assembly of DNA-brush copolymers.[383] The authors synthesized the DNA-brush copolymer amphiphiles containing a RNA base (rA) as an enzymatic cleavage site. The DNA-brush copolymer amphiphiles self-assemble into spherical micelles. The addition of a DNA-based phosphodiesterase (DNAzyme), which recognizes a given DNA sequence and cuts at the RNA base, catalytically generates a truncated ssDNA sequence. This enzymatic reaction also leads to a subsequent sphere-to-cylinder phase transition. Adding a 19-base input DNA sequence can trigger a cylinder-to-sphere morphological transition. This work illustrates a combination of ENS and DNA hybridization for dynamically controlling a phase transition.

4. Biomedical Applications of ENS

The previous two sections have shown the ubiquity of ENS processes in biology and the easiness of using enzymatic reactions to generate/control the noncovalent assemblies (or aggregates) of synthetic molecules in supramolecular chemistry. The obvious logical question would be what are the properties and functions of these assemblies formed by ENS. Since nature uses ENS for functions, it is not surprising that it becomes possible to use ENS for designing/controlling functions of the assemblies of synthetic molecules, as shown in the exploration of potential applications of ENS in biomedicine.[384] The following subsections focus on the ENS of synthetic molecules in cellular environment. Because the field is rapidly evolving, we divide the subsections, roughly, according the cellular locations of ENS, such as intercellular, pericellular/intracellular, and subcellular. We choose not to differentiate pericellular and intracellular ENS processes because they often are related. We present the results in each subsection in chronological order (more or less) so that it is easier for the readers to follow the advances of the research.

4.1. Intercellular ENS

Though it is much less explored, intercellular ENS likely promises important applications, such as controlling cell morphogenesis. It is well-established that intercellular interactions in a three-dimensional (3D) environment differ profoundly from a monolayer of cells (2D).[385]

In addition, increasing numbers of reports suggest that 3D cell organization provides better in vitro models that represent the actual in vivo microenvironment[386–391] more accurately than 2D monolayers do. Such insights have led to the development of 3D in vitro models of human cells in the hopes of bridging the discontinuity between in vitro systems and in vivo animal models for drug discovery, stem cell research, cancer cell biology, and tissue engineering and implantation.[392–394] There is renewed interest in generating cell spheroids as the 3D in vitro models of human cells. Although many efforts have focused on generating cell spheroids, the current procedures are still time-consuming (e.g., > 72 h). Intercellular ENS turns out to be a simple and physiologically-relevant way to generate cell spheroids, as shown in Figure 51.[331] The ligand-receptor interaction between **48** and **49** results in a complex (**48**:**49**), which is also a supramolecular phosphoglycopeptide (sPGP) because **48** is a glycopeptide and **49** a phosphopeptide (Figure 51A). The sPGP further self-assembles in water to form nanoparticles with diameters of 8±2 nm. ALP dephosphorylates the sPGP to turn the nanoparticles of **48**:**49** into nanofibers of **48**:**50** with diameters of 8±2 nm (Figure 51B). Being incubated with fibroblast cells and partially dephosphorylated, the sPGP forms dynamic assemblies in situ on the cell surface (Figure 51C). The dynamic assemblies interact with extracellular matrix molecules and effectively abolish contact inhibition of locomotion (CIL) of the fibroblast cells to result in 3D cell spheroids. This work demonstrates that ENS can generate a dynamic continuum of man-made molecules for regulating cell behavior.

Context-dependent signaling is a ubiquitous phenomenon in nature. Because one of the unique features of ENS is contextual-dependendency, that is, the resulting assemblies from ENS are highly dependent on the path (or the history of molecular transformation) or local microenvironment, ENS of man-made molecules can mimic the context-dependent signaling in cells. This is shown by a recent study[332] on incubating **48**:**49** with cancer cells (Saos2) or the co-culture of the cancer cells (Saos2) and stromal cells (HS-5). Depending on the amount of the inhibitor for inhibiting the ALPL overexpressed by Saos2 cells, the assemblies of the **48:49** can either result in cell death or induces 3D cell spheroids (Figure 51D). Similarly, adjusting the ratio of the stromal and cancer cells in a co-culture is able to modulate the expression of ectophosphatase so that ENS of **48:50** enables cell spheroids. The spheroids formed in the co-culture also can mimic the tumor microenvironment for drug screening. As the first example of the self-assembly of small molecules for context-dependent signaling, this work underscores the promises of intercellular ENS as multifunctional processes for controlling cell behaviors.

To assist the formation of functional vascular networks in regenerative tissues, Sun and Li employed ENS to develop an injectable hydrogel of a glycopeptide, which served as a scaffold to release deferoxamine (DFO).[395] As shown in Figure 52A, the authors synthesized the glycopeptide precursor (**115**) that consisted of a naphthyl group, a tetrapeptide segment (Phe-Phe-Asp-Tyr(H_2PO_3)), and a sugar moiety (D-glucosamine) on the side chain of Asp. Using ALP to remove the phosphate from the precursor, the authors produced the glycopeptide hydrogel that incorporates DFO. After subcutaneous injection of the DFO-containing hydrogel in mice, the authors reported the hydrogel acting as an effective matrix to trigger the generation of new blood capillaries in vivo (Figure 52B). This

work illustrates a novel approach to generate supramolecular assemblies of a glycopeptide to mimic the glycosylated microenvironment of extracellular matrix.

The intercellular ENS process seems particularly useful for mimicking the protein dynamics in ECM for inducing cell spheroids. A single component molecule precursor (**117**), which differs from the sPGP (**48:49**), is able to act as a substrate of ENS to enable 2D to 3D cell morphogenesis.[396] As shown in Figure 53A, the biotinylated D-phosphotetrapeptide (**117**) is a substrate of phosphatases. Biotin serves as a cell compatible ligand of cell surface receptors.[397] Before dephosphorylation, **117** self-assembles to form nanoparticles, which turn into nanofibers upon dephosphorylation catalyzed by phosphatases to generate **118**. After incubating with HS-5 cells, some of the molecules of **117** become dephosphorylated and result in nanofibers consisting of the mixture of **117** and **118** at the intercellular space (Figure 53B). The formation of the intercellular nanofibers transforms a 2D cell sheet to 3D cell spheroids (Figure 53C). The formation of the 3D cell spheroids depends on dephosphorylation, cell surface binding motif, and proteolytic resistance of the precursor. Similar to the recent report of ENS of proteins for cellular junctions,[218] this work illustrates ENS as a versatile approach to mimic protein dynamics for modulating intercellular interactions. One of the potential applications that remain to be explored is to apply ENS for modulating supracellular networks[398–400] during morphogenesis for tissue engineering.

4.2. Peri/intracellular ENS

Pericellular and intracellular ENS processes are common features of cells. Although intracellular ENS of man-made molecules was explored in 2007,[227,229] a bona fide pericellular ENS of synthetic molecules was a rather recent event.[267] In that study, a proteolytically stable, D-phosphotripeptide (**119**) turns out to be the substrate of ALP. After being dephosphorylated, **119** becomes **120** (Figure 54A), which self-assembles to form hydrogel/nanofibers in water. This transformation is likely benefited from the promiscuity of ALP to their substrates. That is, ALP is able to catalyze the dephosphorylation of both L- and D-peptide substrates.[263] The addition of **119** to the culture of HeLa cells results in hydrogelation of culture medium. Further investigation reveals that the nanofibers form on the surface of the HeLa cells. The most significant insight is that overexpression of ALP on cancer cells leads to the formation of the pericellular nanofibers (Figure 54B, C), which block cellular mass exchange to induce apoptosis of cancer cells, including multidrug-resistance (MDR) cancer cells, MES-SA/Dx5. Moreover, the substrate is innocuous to normal cells. This discovery is largely due to the use of D-phosphopeptides, which are proteolytically resistant and ALP susceptible. In addition, the pericellular hydrogel/nanonets can entrap secretory proteins, which serves as a medium for enriched secretomes of cancer cells.[401]

To further understand the mechanism on how the pericellular nanofibers formed by ENS selectively kill cancer cells, a more detailed study was carried out.[402] The elucidation of the cell death mechanism of HeLa cells reveals that the nanofibers of **120**, form locally on the surface of the HeLa cells and act as a pericellular nanonet around cancer cells specifically. The fibers are able to present the secreted, different proapoptotic ligands (e.g., TNFα and TRAIL) from cancer cells to bind with different extrinsic cell death receptors (e.g.,

TNFR1/2 and DR4/5), or directly interact with the death receptors (e.g., CD95) (Figure 55A). These actions lead to the death of cancer cells only. Further investigation on other co-cultures implies that **119** inhibits cancer cells likely via different ENS processes and different mechanisms. Incubated **119** with the co-culture of HeLa and HS-5 confirms that ALP-catalyzed ENS of the nanofibers of **120** selectively kills the cancer cells in the co-culture (Figure 55B). Moreover, the ENS of **120** nanofibers kills cancer cells selectively in different co-cultures.[402] In addition, inhibiting ALP reduces the dephosphorylation of **119**, thus rescuing the cells in the co-culture (Figure 55C); adding extra ALP converts **119** to **120** before **119** reaches the cell surface, also rescues the HeLa cells in the co-culture (Figure 55D). These results confirm that the nanofibers of **120** have to be generated in situ for inhibiting cancer cells, which explains the exceptional selectivity of ENS against the cancer cells. Although the inhibitory concentration of **119** against cancer cells is relatively high in this case, this work indicates that ENS, as a molecular process, increases inhibitory efficacy to cancer cells without increasing toxicity to normal cells. Moreover, the pericellular localization of the nanofibers of **120** appear to be determined by the D-Phe-D-Phe backbone because replacing D-Phe-D-Phe in **119** by D-Trp-D-Trp results in the ENS product localizing in the lysosome and the corresponding ENS process hardly inhibits the HeLa cells.[403]

Because cells lack specific receptors or transporters for D-peptides, the result above implies that the cytotoxicity likely originates from the nanofibers rather than individual molecules. Thus, ENS for inhibiting cancer cells should be independent to the building blocks of the nanofibers, which is also revealed by the work of Pires and Ulijn.[275] In their work, they used a simple carbohydrate amphiphile (**121**) bearing a phosphate group. After enzymatic dephosphorylation by ALP, **121** turns into **122**, which self-assembles to form nanofibers. The authors used an osteosarcoma cell line, Saos2, which overexpresses ALP to incubate with **121**, and found that hydrogelation and nanofibers formed mainly on the cell surface. By monitoring the metabolic activity of the Saos2 cells, they found that gelation of the pericellular environment reduced metabolic activity at an initial stage (≤7 h), and eventually caused cell death at longer exposure periods (≥24 h). Using prechondrocytes ATDC5 (that exhibits ~15–20 times lower ALP activity compared to Saos2) as a control cell line, they found that ATDC5 was hardly affected by **121** at concentrations ≤1 mM. Since **121** is a simple carbohydrate phosphate derivative unlikely to bind to a receptor with high affinity, this work, along with the example above, confirms that ENS generates the assemblies of small molecules in pericellular space (Figure 56A) for controlling cell fate. In a follow up study, the authors suggested that **121**/**122** also antagonized the glucose transporter (GLU1) for inhibiting the metabolism of the cancer cells.[404]

The use of proteases for ENS[225,238] suggests that it is feasible to use proteases to generate nanofibers in cellular environment, as first demonstrated by Maruyama et. al.[405] As shown in Figure 56B, the authors designed a peptide amphiphile (**123**) that was a substrate of matrix metalloproteinase-7 (MMP-7). Being proteolytically cleaved by MMP, **123** becomes a supramolecular hydrogelator (**124**). Being incubated with cancer cells overexpressing MMP-7, molecules of **123** are hydrolyzed by MMP-7. The cancer cells likely uptake the resulting **124**, which is able to self-assemble inside the cancer cells to form nanofibers. The

nanofibers disrupt cellular function and thus result in the death of cancer cells. This work also demonstrates that the intracellular self-assembly of the supramolecular gelator selectively kills cancer cells. Although the concentration required for killing cancer cells is still high, the excellent selectivity towards the cancer cells (Figure 56B) promises a fundamentally new approach for developing anticancer drugs. Using a fluorophore (NBD) linked to the peptide to generate the fluorescent analogue of **124**, the authors, using fluorescence recovery after photobleaching (FRAP) (Figure 56C), also confirmed the increase of intracellular viscosity by the ENS of those peptide amphiphiles.

Although it is feasible to develop D-peptides that bind to certain cellular targets,[406–410] D-peptides lack interactions with endogenous transporters, thus are usually unable to enter cells efficiently. Taurine, a natural amino acid, is able to boost the cellular uptake of small D-peptides, as reported by recent studies.[411–412] Specifically, the conjugation of taurine at the C-terminal of a D-peptide through an ester bond generates the precursor, **127** (Figure 57A). After entering the cells, intracellular carboxylesterases (CES) catalytically cleaves the taurine group and results in a hydrophobic D-peptide (**128**), which self-assembles intracellularly to form nanofibers (Figure 57B). Since the nanofibers of **128** hardly diffuse out the cells, **128** accumulates inside the cells (Figure 57C). It is shown that, when the incubation concentrations of the D-peptides are about 200 μM, taurine conjugation, in combination with intracellular ENS, is able to increase the cellular uptake of small D-peptides in mammalian cells by >10-fold, from 118 μM (without conjugating taurine) to >1.6 mM (after conjugating taurine).[411] A more carefully mechanistic study[412] reveals that, for dynamin 1, 2, and 3 triple knockout (TKO) mouse fibroblasts, the cells uptake **127** via macropinocytosis and dynamin-dependent endocytosis. Further study using Drosophila larval blood cells derived from endocytic mutants confirms multiple endocytosis pathways contribute to the uptake of **127**. Since the uptake is most efficient at 200 μM of **127**, it is likely that **12**7 forms nanoparticles before entering cells, which was confirmed by TEM. These studies indicate that the cellular uptake of negatively charged substrates, including D-peptides, likely results from the aggregation of these relatively hydrophobic molecules.

For developing a radioactive probe for PET imaging, Liang et al. used the condensation reactions firstly developed by Rao et al.[280] for intracellular ENS in tumor cells.[413] As shown Figure 57D, the authors synthesized a peptide substrate (**130**), which carried cyanobenzothiazole (CBT) at the C-terminal, a substrate of furin at the N-terminal, and a F-18 radioactive isotope label at the side chain. Intracellular furin catalytically cleaves the N-terminal to generate **131**, which exposes the N-terminal of cysteine which condenses with CBT to form a dimer (**132**). The self-assembly of **132** results in nanoparticles with the F-18 labels. After using the F-19 analog to confirm the condensation reactions, the authors tested the F-18 probes in a tumor grafted murine model. MicroPET imaging of MDA-MB-468 tumor-bearing mice indicates that mice co-injected with **130** and the F-19 analog show higher uptake and longer attenuation of radioactivity in tumors than those mice only injected with same dosage of **130**. These results indicate that self-assembly is critical for the retention of the probe and provides a useful approach for developing PET imaging agents based on ENS. In another study of intracellular ENS, Liang et al. also introduced iodine into the substrate of ALP for ENS.[414] They designed an iodinated hydrogelator precursor Nap-F-

F(I)-$_p$Y (**133,** Figure 57E). After being generated by ALP catalyzed dephosphorylation, Nap-F-F(I)-Y (**134**) self-assembles to form nanofibers, which result in a hydrogel. Notably, the authors applied **133** for direct nano-computed tomography (nano-CT) imaging, and demonstrated the detection of ALP activity in bacteria.[414] This pioneering work promises better nano-CT imaging of ALP activity if high contrast agents can be developed.

To address the problem of drug resistance in cancer therapy, Liang and Zhang used intracellular ENS for generating the nanoparticles of taxol inside cancer cells.[415] They developed a taxol derivative Ac-RVRR-C(StBu)-K(taxol)-CBT (**135**, Figure 58A) as a substrate for the furin. Furin cleaves **135** to generate CBT-taxol (**136**), which self-condensates to form dimers that self-assemble.[280] According to the authors, **135** exhibits 1.5-fold increase of efficacy for inhibiting the taxol-resistant HCT116 cancer cells in vivo in a murine model, suggesting that **135** selectively targets cancer cells. This work suggests that protease catalyzed intracellular ENS (Figure 58B) may lead to a new strategy for overcoming MDR. This furin triggered condensation reaction is highly versatile for intracellular ENS, especially in developing imaging probes, as reported by Liang et al. to form F-19 MRI probes[416] and by Lin et al. to form PET probes.[417] In a related study using taxol,[418] Liang, taking the advantage of the biphasic effect of taxol on axonal branching, recently reported a taxol derivative Fmoc-FF-K(taxol)-$_p$Y (**137**, Figure 58C), which was an ENS substrate, for promoting axonal branching. The authors found that ALP catalyzed the dephosphorylation of **137** to form the nanofibers of **138**. While **137**, at 10 μM, inhibits cell proliferation, at 10 nM, not only does it promote neurite elongation, as taxol does, but it also induces axonal branching. Although the mechanisms of this extremely interesting observation remain to be elucidated, this study shows the application of ENS outside of cancer therapy.

Rao et al. recently reported the first case of using ENS catalyzed by caspases for generating a tracer for positron emission tomography (PET).[419–420] The authors synthesized a substrate (**139**, Figure 59A) bearing a F-18 radioisotope. **139** carries the caspase cleavable N-terminal and a protected cysteine. After **139** enters tumor cells, intracellular caspases (i.e., caspases 3/7) catalytically cleave **139**, then glutathione reduces the protected cysteine. These two reactions generate **140**, which undergoes intramolecular cyclization to form **141**. The self-assembly of **141** leads to the accumulation of **141** in tumor cells as nanoaggregates, which can act as a tracer for imaging tumors in vivo in a murine model. It appears, however, that most of the nanoaggregates are still trapped in the liver, which is a likely result from the considerable amount of glutathione in the liver.[421]

Combining intracellular ENS with anticancer drugs provides a new way to boost the activity of drugs against drug-resistant cancers without increasing systemic toxicity.[422] As shown in Figure 59B, the small peptide precursors (Nap-ff-es-taurine, **142**, and Nap-FF-es-taurine, **143**), being a substrate of CES, undergo CES-catalyzed hydrolysis to lose the hydrophilic taurine group and to form hydrophobic products (Nap-ff-es, **144**, and Nap-FF, **145**). **144** and **145** self-assembles in water to form nanofibers. After entering the cancer cells that overexpress CES, **142** and **143** turn into the nanofibers of **144** and **145**, respectively, inside the cells. The formation of the intracellular peptide assemblies disrupts actin dynamics and results in the death of cancer cells (Figure 59C). At optimal concentration, **142** (or **143**),

being innocuous to cells, doubles or triples the activity of cisplatin against the drug resistant ovarian cancer cells, such as SKOV3 and A2780cis (Figure 59D). This work illustrates that ENS of small peptides is a useful strategy for combination therapy of cisplatin without increasing systemic burden or other side effects.

In fact, even without cisplatin, intracellular ENS to form peptide nanofibers is effective for selectively killing cancer cells.[423] In the subsequent study of the CES substrates, both the D- and L-peptide precursors, **144** and **145**, were tested on a panel of cancer cells. As shown in Figure 59C, intracellular CES catalyzes the cleavage of the ester bond to remove hydrophilic taurine groups, thus generating nanofibers of short peptides for selectively inhibiting cancer cells. The intracellular nanofibers disrupt actin dynamics, thus leading to cell death. This intracellular ENS approach allows selective inhibition of a range of cancer cells that exhibit relatively high CES activities, including drug resistant cancer cells (e.g., triple negative breast cancer (TNBC) cells (HCC1937) and platinum-resistant ovarian cells (SKOV3, A2780cis)). Generally, the D-dipeptide precursors exhibit lower IC_{50} values (25–44 μg/mL) than those of L-dipeptide precursors (28–80 μg/mL) against the cancer cells. Most importantly, this intracellular ENS of dipeptides is innocuous to normal cells. Such selectivity is also valid in the co-cultures of cancer and normal cells. In addition, these precursors are non-toxic to normal tissues in mice, though the in vivo activity against cancer cells remains to be tested.

To address two shortcomings, that is, high uptake by the reticuloendothelial system and low uptake in tumors, of nanoparticle-based delivery systems, Chen et al. innovatively applied ENS, using Nap-FFK_pY (**146**, Figure 59E) as the precursor, to co-assemble **147** with indocyanine green (ICG) for in vivo cancer theranostics.[424] ICG is a near-infrared (NIR) tricarbocyanine dye, which has been approved by the FDA for clinical imaging. Because ICG has a very short half-life (2–4 min) in vivo before biliary excretion, the uptake of ICG in tumor cells is low. To explore the potential of ICG for anticancer photothermal therapy (PTT), the authors mixed ICG with **146** and found that the mixture formed micelles, likely due to the interaction between the sulfonate group of ICG with the lysine groups of **146**. After treating the micelles with ALP, the micelles turn into nanofibers of **147** and ICG adopts a J-aggregate arrangement. J-aggregates of ICG exhibit red-shift of absorbance, which is advantageous for PTT. The authors demonstrated that intravenous injection of the micelles in xenograft tumor mice models, greatly increased the tumor uptake of ICG (25-fold higher than that of the free ICG) and achieved high T/N ratios (>15) that clearly distinguished tumors from the surrounding normal tissue. In addition to being the first case of in vivo formation of tumor-specific ICG-doped nanofibers for PTT theranostics, this work illustrates the versatility and compatibility of ENS with other therapeutic approaches.

Reversible phosphorylation/dephosphorylation is a canonical mechanism for cell signaling. While most of the studies are focus on intracellular phosphorylation and kinases, ectophosphatases, such as ALP, in extracellular domains have received less attention. It has been recently recognized that cancer cells, overexpressing ALP for immunosuppression, resist cancer immunotherapy.[425] Thus, profiling the activity of ALP on cancer cells becomes a necessary effort for immunotherapy, but most phosphatase probes are unable to serve as activity probes for imaging tumor specific phosphatases on cancer cells. ENS turns out to be

a versatile approach for imaging the activity of ALP on live cancer cells.[426] As shown in Figure 60A, a phosphorylated and nitrobenzoxadiazole (NBD) conjugated D-peptide (**148**) acts as a substrate of ALPs. Being dephosphorylated, **148** forms **149** which self-assembles to generate fluorescent nanofibers. Being non-diffusive, the nanofibers of **149** localize with ALP, thus revealing the activities of ALPs on live cells. This work, indeed, confirmed the significantly higher activities of ALP on cancer cells than on stromal cells in their co-culture (Figure 60B). Further developing this type of ENS-based molecular tool may ultimately lead to a probe for precision medicine that selectively targets cancer cells. Moreover, since ALP is a key enzyme in bacteria, the method shown in Figure 60B is also useful for profiling the activity of ALP in bacteria, as recently reported by Yang et al.[427]

Increasing the therapeutics index for selectively killing cancer cells without harming normal cells remains a holy grail in cancer therapy. ENS, as a multiple step molecular process, is able to enhance the efficiency for killing cancer cells without increasing toxicity to normal cells, as shown in the report of the molecular and cellular validation of ENS for selectively killing cancer cells.[428] As shown in Figure 61, nine tetrapeptide derivatives (**150–158**) share a similar backbone, which consists of D-Phe and D-Tyr. In addition to the slight difference in the sequence of the backbone, they also differ in terms of the state of phosphorylation. The D-tetrapeptide precursors contain one or two phosphotyrosine residues. After enzyme-catalyzed dephosphorylation, the D-phosphotetrapeptides or the D-diphosphotetrapeptides turn into self-assembling tetrapeptides to form nanofibers in water. While the un-phosphorylated D-tetrapeptides are innocuous to several cancer cell lines and one normal cell line, the mono- and diphosphorylated D-tetrapeptides selectively inhibit the cancer cells, but remain nontoxic to the normal cell. Generally, the D-phosphotetrapeptides exhibit higher inhibitory activity against the cancer cells than the D-diphosphotetrapeptides do, confirming the importance of peptide assemblies for cancer inhibition. The cancer cell lines that express higher levels of ALPs are more susceptible to inhibition by the phosphorylated D-tetrapeptides. The cell death modality, either apoptosis or necroptosis, likely also associates with the interactions between nanofibers and the death receptors on different cancer cells. This work is the first comprehensive validation of ENS as a multiple step process for selectively killing multiple cancer cell lines, thus establishing the spatiotemporal defined supramolecular processes/assemblies for developing anticancer therapeutics.

ENS is able to regulate the rate of the formation of molecular assemblies, which is one of the fundamental features of cells. This feature is useful for selectively targeting cancer cells. The molecular design is rather simple—tailoring the number of phosphates on peptidic substrates of alkaline phosphatases to make **153** and **154**, as shown in Figure 61A.[429] The pair of cell lines are HepG2 (liver hepatocellular carcinoma) and Saos2 (osteosarcoma), both known to express ALPL, but Saos2 expresses a much higher level of ALPL than HepG2 does. Utilizing different substrates, ENS is able to amplify this difference.. As shown in Figure 61E, the rate for generating the peptide assemblies of **155** should be slower with the diphosphorylated substrates (**153**) than with the monophosphorylated substrates (**154**) because the former requires dephosphorylation twice. Therefore, **153** should be more toxic to Saos2 than to HepG2, which is confirmed by cell viability assays: **153** and **154** exhibit similar inhibitory activities against Saos2 cells, but **153** is less cytotoxic than **154** towards

HepG2 cells. This result establishes rate regulation of a multiple-step process to inhibit cells selectively, which may provide a way to target cancer cells in a specific organ.

It is facile to combine pericellular ENS with other cellular processes, such as intracellular condensation, as shown by the work of Liang et al.[430] The authors developed a phosphopeptide ((SEt)CE_pYFFG-CBT, **159**), which carried an ethylthiolester at the N-terminal and CBT at the C-terminal. **159** acts as the precursor of the hydrogelator (SEt)CE_pYFFG-CBT (**160**), which forms a cyclic dimer (**161**) via condensation reaction in the presence of intracellular glutathione (GSH). After confirming that both **160** and **161** were able to form hydrogels, the authors used **159** to incubate with HeLa cells. The ALP on the HeLa cells dephosphorylates **159** to form **160**, which self-assembles to produce nanofibers of **160**. After uptake by the cells via endocytosis, **160** forms the cyclic dimer **161** after the condensation initiated by intracellular GSH. **161** self-assembles into nanofibers that exhibit enhanced mechanical strength. This work illustrates an innovative way to modify peptide assemblies for a hierarchical morphological transition process in cellular environment.

Drug resistance remains the biggest challenge in cancer treatment. Among various types of drug resistance, platinum-resistant ovarian cancer is one of the hardest to treat. Resistance arises from multiple mechanisms, including cholesterol as an inducer.[431] Intriguingly, ENS of a cholesterol derivative (**162**, Figure 63A) is able to minimize acquired drug resistance for inhibiting ovarian cancer cells. This unusual feature originates from the multifaceted assemblies of **162**/**163** which are able to modulate multiple cellular processes.[432] Specifically, conjugating cholesterol with a D-phosphotyrosine generates a precursor (**162**) for ENS catalyzed by ALP. It turns out that **162** inhibits A2780cis cells and is more potent than cisplatin. The IC_{50} of **162** is 13±1.3 μM (8.7 ±0.8 μg/mL, 48 h), which is about five times lower than the IC_{50} of cisplatin against A2780cis—71±1.2 μM (21.2±0.4 μg/mL, 48 h). The inhibition of ALP only partially reduces the activity of **162**, indicating multiple mechanisms contribute to killing the cancer cells. After the report that ENS, in-situ on or inside the cancer cells, generates the assemblies of the conjugate of cholesterol and D-tyrosine (**163**) to activate extrinsic and intrinsic cell death signaling simultaneously, a more extensive mechanistic study on the action of **162** further confirms multiple action mechanisms from the assemblies of **163**.[433] As shown Figure 63B, the assemblies, acting as polypharmaceuticals, augment lipid rafts, aggregate extrinsic cell death receptors (e.g., DR5, CD95, or TRAILR), modulate the expression of oncoproteins (e.g., Src and Akt), disrupt the dynamics of cytoskeletons (e.g., actin filaments or microtubules), induce endoplasmic reticulum stress, and increase the production of reactive oxygen species, thus resulting in cell death and preventing acquired drug resistance. These results validate that ENS of small molecules is a multifaceted strategy for amplifying the genetic difference between cancer and normal cells and for overcoming drug resistance in cancer therapy. A recent study shows that **162** promotes pro-inflammatory macrophages and induces apoptosis of cancer cells.[434] Moreover, ENS enables an exceedingly simple lipid (e.g., the conjugate of phosphotyrosine and dodecyl amine) to target cancer cells selectively.[435] These studies imply that ENS, as a molecular process, may lead to a new kind of multitargeting drugs.[436]

To improve photoacoustic signal for imaging, one approach is to use ENS to generate the assemblies of the fluorophores, as shown by Wang et al.[437] The authors developed a peptide (**164**, Figure 64A), consisting of a chlorophyll, a substrate of caspase-1, and a cell penetrating peptide (YGRKKRRQRRR). Upon enzymatic cleavage of the YVHDC at the D/C sites, **164** becomes a more hydrophobic molecule (**165**), which self-assembles to form the nanofibers that produce enhanced photoacoustic signals. According to the authors, this dynamic process allows monitoring of the activity of caspase-1 via ratiometric photoacoustic signals (Figure 64B). The authors suggested that this ENS process could offer a noninvasive method for real-time monitoring of bacterial infection, which associated with the upregulation of caspase-1 in the early stage. This type of protease catalyzed ENS also finds applications in delivering anticancer drugs, as reported by Ulijn et al.[438] For example, they utilized MMP-9 overexpressed by cancer cells to enable ENS for enhancing drug specificity against cancer cells. Specifically, the authors synthesized a substrate of MMP-9, Ph-FFAGLDD (**166**, Figure 64C), which underwent proteolysis in the presence of MMP-9 to form hydrophobic segments, Ph-FFAGL (**167**) and Ph-FFAG (**168**). The authors reported that **166** formed micelles, which turned into fibrillar nanostructures upon the addition of MMP-9. The authors demonstrated that this ENS process allowed slow release doxorubicin to cancer cells (Figure 64D) for inhibiting tumor growth in a murine model.

Both gain-of-functions (i.e., upregulation) and loss-of-functions (i.e., down-regulation) can lead to cancer. Molecular therapy, based on inhibitory binding, is able to suppress gain-of-function in cancer cells, but it is unable to act on down-regulated targets in cancer cells. ENS of peptides is able to target down-regulation in cancer cells by a proper design, as shown in Figure 65.[439] The key feature is to combine enzymatic assembly and disassembly. For example, in order to target down-regulation of carboxylesterases (CES) in OVSAHO, an ovarian cancer cell line, peptidic precursors (**169** and **173**) act as the substrates of both CES and ALP. The precursors, being dephosphorylated by ALP, turn into self-assembling molecules (**170** and **174**) to form nanofibers. In the presence of CES, **170** and **174** undergo hydrolysis to cleave the ester bonds and become **172** and **176**, respectively. **172** (or **176**), being hydrophilic, results in the disassembly of nanofibers of **170** (or **174**). Thus, the precursors selectively inhibit OVSAHO, which down-regulates CES. But the same precursors are innocuous to HepG2, a hepatocyte that overexpresses CES. In addition to illustrating ENS as a potential approach for targeting down-regulation (or loss-of-functions) in cancer cells, this work also shows that **173** is more potent than cisplatin for inhibiting OVSAHO cells. The work also illustrates a multiple responsive approach for targeting tumors, which hold great promises, as evidenced by a recent work of Zhong et al. that uses multiple response to design a smart drug release depot for treating prostate cancer.[440]

The study of the precursors of ALP and CES also allows evaluating a series of C-terminal capped phosphopeptides (Figure 66), which reveal that self-assembling ability is the key factor for ENS to inhibit cancer cells.[441] Based on the precursor (**173**) for ENS, five precursors (**177**, **178**, **179**, **180**, and **181**) were made. These precursors, differing from **173** in terms of N-terminal capping, C-terminal modification, stereochemistry, or regiochemistry, aim to elucidate the effect of structural differences (i.e., N-terminal capping, C-terminal modification, stereochemistry, and regiochemistry) to the morphologies of assemblies and

the contribution of the self-assembling abilities of either the phosphorylated precursors or the dephosphorylated products. That is, what features determine the efficacy of ENS for inhibiting cancer cells. Examining these ENS precursors reveals that, regardless of the stereochemistry and the regiochemistry of their tetrapeptidic backbones, the anticancer activities of these precursors largely match their self-assembling abilities. As the first case to correlate thermodynamic properties (e.g., self-assembling ability) of small molecules with the efficacy of ENS processes against cancer cells, this work provides an important designing principle for developing ENS for potential cancer therapy.

Induced pluripotent stem cells (iPSCs) are another type of cells, besides certain cancer cells, that overexpress ALP. Taking advantage of the difference in ALP expression between iPSCs and normal cells, Saito et al. used ENS for the selective removal of human iPSC cells after using the iPSCs for generating muscle cells.[442] The authors tested four D-phosphopeptides, which are the substrates of ENS catalyzed by ALP, for inhibiting iPSCs, and found that a D-phospho-tetrapeptide (Nap-fff$_p$y, **182**, Figure 67A) is most effective. After dephosphorylation of **182** (at 0.35 mg/mL) by the ALP expressed on the iPSCs, the resulting D-peptide, Nap-fffy (**183**) self-assembles to kill the iPSCs within 1 hr. But **182** is largely innocuous to non-iPSCs, including primary hepatocytes and iPSC-derived cardiomyocytes. According to the authors, alkaline phosphatase, being highly expressed on iPSCs, induces dephosphorylation of the peptides. The spatial-temporal accumulation of dephosphorylated peptides around iPSCs generates peptide aggregates in situ that trigger cell stress and iPSC death. The absence or low expression of ecto-alkaline phosphatase in other cell types makes them tolerant to **182**. The authors reported that two hours of incubation with **182** could efficiently eliminate iPSCs, even in the co-cultures spiked with increasing ratios of iPSCs. Using a mouse tumorigenicity assay, the authors confirmed that **182**, being an ENS substrate of ALP, prevented the growth of residual iPSC to form induced teratomas in vivo. These results, again, highlight the excellent cell selectivity of ENS. This innovative work underscores the application of ENS in regenerative medicine based on iPSCs.

It is a challenge to make short peptides (with <5 amino acids) adopt an α-helical conformation, but Yang et al. reported that ENS may provide a way to assist the self-assembly of peptides into such a conformation.[443] The authors synthesized a peptide, chlorambucil-Gffy (CRB-Gffy, **184**, Figure 68A), and its corresponding phosphopeptide, CRB-Gff$_p$y (**185**). After a heating–cooling process, **184** adopts a conformation more similar to a β-sheet and self-assembles into nanoparticles, which result in a suspension. Adding ALP to the solution of **185**, at 4 °C, generates **184**, which adopts an α-helical conformation and self-assembles into stable nanofibers and hydrogels (Figure 68B). Interestingly, the nanofiber solution exhibits better stability against proteinase K digestion and results in an enhanced cellular uptake. Using a panel of cancer cells and a murine tumor model, the authors reported that the nanofibers of **184** were more effective than the nanoparticles of **184** for inhibiting cancer cells in vitro and in vivo (Figure 68C). Moreover, the authors also reported that **184** was more compatible to white blood cells than CRB. This result is particularly attractive because it may lower the major side effects of CRB. This study shows the unique advantages of ENS to control peptide folding and self-assembly. It would be

interesting to know the molecular arrangements in these two types of nanostructures, in addition to the conformational differences of the building blocks.

ALP, being a promiscuous ectoenzyme on the cell membrane, can enable the ENS of a wide range of substrates for many innovative applications, such as the patching of lipid rafts, as reported by Zhang et al.[444] As shown in Figure 69, the authors used the metal complex Ru(II)$(bpy)_3$ as a three-dimensional (3D) core to conjugate with the D-phosphotetrapeptide (Nap-ffk$_p$y[263]) to generate a metal complex (**186**) as the substrate of ALP. The authors, after confirming that ALP converted the solution of **186** to a hydrogel, incubated **186** with HeLa, HS-5, Ect1/E6E7, and A375 cells. Ru(II)$(bpy)_3$, being fluorescent and having a long fluorescent life time, allows the authors to monitor the ENS of **186** on the surface of HeLa cells and to examine how the pericellular assemblies affect the dynamics of cytoskeleton. Based on the imaging results, the authors reported that ALP in the lipid rafts catalyzed the dephosphorylation of **186**, thus creating the self-assembled nanofibrils patch on lipid rafts. This patch, inducing lipid raft dysfunction and reinforcing focal adhesion, glues the lipid rafts together to raft-associated receptors to provoke opposing cell migration against focal adhesion. Such contradictory motions eventually cause cell rupture and cell death. This rather comprehensive study underscores the versatility of ENS as a multiple step process for modulating multiple cellular functions.

To develop an MRI contrasting agent to report ALP expression, Liang et al. reported an ALP substrate, Nap-FFF$_p$Y-EDA-DOTA(Gd) (**187**, Figure 70A), which self-assembled into gadolinium nanofibers upon the action of ALP. After confirming the self-assembly of the peptide Nap-FFFY-EDA-DOTA(Gd) (**188**) by hydrogelation, the authors injected **187** in mice to image a tumor. According to the in vivo T2-weighted MRI at 9.4 T, **187** is able to reveal the HeLa tumor on mice in vivo (Figure 70B). The MRI signal intensity of the HeLa tumor in the mice injected with **187** is higher than the mice injected with Gd-DTPA, suggesting the accumulation of the nanofibers of **188** in the tumor. It remains to be seen if the contrast enhancement will be preserved in a magnetic field with lower strength.

To establish a new approach for enhancing the efficacy of dexamethasone (Dex), a steroid for treating inflammation, Liang et al. developed a simple approach that used ENS to co-assemble Dex with a hydrogelator for making hydrogels.[445] To avoid the formation of Dex precipitates after using ALP to dephosphorylate dexamethasone sodium phosphate (**191**, Figure 70C), they mixed the hydrogelator precursor Nap-FF$_p$Y (**189**) with **191**. Adding ALP to the solution of a 1:1 (molar ratio) mixture of **189** and **191**, they obtained a hydrogel due to co-assembly by ENS of Nap-FFY (**190**) and Dex (**192**). According to the authors, intracellular ALP triggered the co-assembly of **190** and Dex and boosted the anti-inflammation efficacy of Dex on two types inflammatory cell models (Figure 70D). This simple approach illustrates a useful application of ENS for intracellular co-assembly, which appears to be a rather general approach[446] for further development. In fact, Jiang et al. recently reported the use of ENS of **189** to control intermolecular forces for generating β-sheets based on a multi-modal analytical system that satisfied both point-of-care testing (POCT) and laboratory-based testing.[447]

Besides proteases or phosphatases for bond breaking, ligases, such as transglutaminases (TGase),[223] provide a useful approach for intracellular polymerization and self-assembly, as reported by Wang et al.[449] They used elastin-based peptide sequences bearing a functional motif (e.g., fluorophore) and one or two pairs of the substrates of the TGases. The TGase-instructed polymerization occurs via formation of an isopeptide bond between the side chains of glutamine and lysine. According to the authors, the substrates enter the cells to undergo intracellular enzyme-catalyzed polymerization, which results in nanoparticles or 3D gel-like structures, depending on the elastin sequences. While the nanoparticles are cell compatible, the 3D gels are cytotoxic. Although more detailed characterization of the 3D gel is warranted, these findings illustrate the versatility of intracellular ENS for biomedical applications.

Autophagy, being an endogenous mechanism of the cell, removes unnecessary or dysfunctional components in cells. Wang et al. recently reported the use of intracellular ENS for monitoring of autophagy.[450] As shown in Figure 71A, a bis(pyrene) derivative (BP) is connected to a dendrimer core by a peptide linker that is a substrate of an autophagy-specific enzyme, ATG4B, to generate nanoparticles (**193**). On the nanoparticles, the fluorescence of BP is quenched. Inside cells, ATG4B cleaves the peptide GTFGFSGKG at the G/F site, releases the BP-peptide conjugates (**194**), which self-assemble to form nanofibers and “turn-on” the fluorescence (Figure 71B). According to the authors, this in situ intracellular self-assembly strategy provides a rapid, effective, real-time, and quantitative method for monitoring autophagy in living cells. Verification of whether the relatively high concentration of nanoparticles also induce autophagy is still needed. Using the same ATG4B substrate, but replacing BP with purpurin-18, the same lab generated another type of nanoparticle (**195**) as a photoacoustic (PA) nanoprobe for real-time and quantitative detection of autophagy in mice for the first time.[451] That is, ATG4B cleaves the peptide at G/F site to generate **196** for self-assembly. This innovative design, developed earlier by Gianneschi et al.,[452] which uses enzymes to cleave peptides off polymers or dendrimers to enable the self-assembly of peptides, likely would lead to many other advances in the applications of intracellular ENS. This includes inducing or evading macrophage cell uptake.[453]

In fact, it is possible to enable the self-assembly of peptides when the peptides are still attached to the nanoparticles, as shown by the work of Wang and Li et al. that combine ENS with gold nanoparticles.[454] Peptide modified spherical gold nanoparticles (AuNPs@**197**/**199** in Figure 71C), with a 16:1 ratio of **197** and **199**, are able to be monodispersed over a wide range of ionic strengths, pH, and fetal bovine serum (FBS). After **197** is cleaved by matrix metalloproteinase-2 (MMP-2), **199** becomes exposed and interacts with **199** from other gold nanoparticles, which results in the aggregation of the gold nanoparticles. The aggregation leads to a red shift in localized surface plasmon resonance (LSPR) and selective accumulation of the nanoparticles on tumor sites. Taking advantage of the red-shift to the NIR window and enhanced retention in tumor sites, the authors achieved improved photothermal treatment (PTT) against the tumors. One of the remaining issues is the aggregation of the gold nanoparticles in vivo.

To develop a molecular probe to reveal the localization and activity of phosphatases, Liang et al. reported a simple peptide substrate of phosphatase, as shown in Figure 71D.[455] The peptide (**200**), bearing a tetraphenylethylene (TPE) at the N-terminal of a phosphotripeptide Y_pYY, undergoes dephosphorylation, catalyzed by ALP, to form TPE-YYY (**201**). Notably, it appears that ALP converts the fibrillar aggregates of **200** to the nanoparticles of **201**. Although it was reported that **200** diffused into cells rapidly, the fluorescence of **201** inside the cells was diffusive and relatively weak. More studies are needed to determine whether TPE binds to other targets inside cells or how stable **201** is inside the cells.

The versatility of ENS allows it to be combined with other stimuli for controlling self-assembly of peptides, as shown by the work of Zhang et al., which integrates ENS with photo-response.[456] As shown in Figure 72A, the authors developed a phosphopeptide (Tet-Gf_py, **202**), bearing a biaryl-substituted tetrazole with an o-allyloxy group on the N-phenyl ring (Tet). **202** turns into Tet-Gfy (**203**) after the dephosphorylation of **202** catalyzed by ALP, and **203**, being a hydrogelator, forms a supramolecular hydrogel. Photo-irradiation transforms the Tet motif to pyrazoline (Pyr), accompanied by fluorescence. Since the self-assembling ability of Pyr-Gfy (**204**) is lower than that of **203**, photo-irradiation also induces gel-sol transition. The authors also demonstrated the combination of ENS and photo-response on the surface of cells, showing that photo-irradiation disassembled the assemblies of **203** formed by pericellular ENS (Figure 72B). This innovative work may lead to a new way to modulate pericellular dynamics for selectively controlling cell death and survival, which may find applications in controlling the fate of iPSCs.[442]

Because ENS is able to selectively target cancer cells, it boosts the efficacy of other cancer therapeutics without increasing side effects, as shown by a recent study in Figure 72C, D.[457] In that study, ENS exhibits strong synergism with the inhibitors, bortezomib (BTZ)[458] and BAY 11–7085 (BAY),[459] both of which target the transcription factor nuclear factor-κB (NF-κB). The substrate, C-terminal methylated phosphotetrapeptide (**205**), of ALP results in extra- and intracellular assemblies of the C-terminal methylated tetrapeptide (**206**). The assemblies of **206**, though unable to kill cells, causes cell stress, results in inductive expression of tumor necrosis factor receptor 2 (TNFR2),[460] and decreases the expression of three key proteins (PI3K,[461–462] Akt,[463] and MEKK3[464]) at the up-stream of NF-κB signaling in cancer cells. In the presence of the inhibitors targeting NF-κB signaling, **205** drastically decreases cancer cell viability (about an order of magnitude). Further mechanistic study indicates that the combination of the ENS of **206** and NF-κB inhibitors decreases the expressions of those up-stream proteins, which eventually results in cell death via necroptosis. This work implies that ENS, combined with clinical cancer therapeutics, may facilitate the translation of key regulatory circuits into promising targets of cancer therapy.

In cellular environment, it is common for the same enzymes to present at different locations (e.g., extra- and intracellular) in different amounts. When the substrates of the enzymes are used for ENS, it is necessary to analyze the kinetics of ENS to understand the efficacy of the substrates for functions, such as cancer cell inhibition, as shown in Figure 73.[465] That study has examined three substrates of CES (**142**, **207**, and **209**, Figure 77A) for intracellular ENS. In studying hydrolysis catalyzed by CES, these substrates result in hydrogelators, which self-assemble in water to form nanofibers. Because CES exists both extra- and

intracellularly, these substrates, being incubated with ovarian cancer cells, undergo intracellular hydrolysis to form intracellular nanofibers in addition to some extracellular hydrolysis. While the three substrates selectively kill cancer cells, **142** and **209** exhibit the highest and the lowest activities, respectively, a trend that inversely correlates with the rates of converting the substrates to the hydrogelators in PBS buffer. Detailed kinetic modeling provides quantification of the key rate constants (Figure 77B) of ENS inside cells and calculates the activity of each substrates for killing the cancer cells (Figure 77C). The kinetic analysis also reveals that (i) substrate stereochemistry determines the rate of enzymatic conversion and the morphology of the assemblies; (ii) less extracellular hydrolysis of the substrates leads to more intracellular ENS; (iii) the self-assembling ability of the ENS molecules also dictate the cytotoxicity of intracellular ENS. This work illustrates that stereochemistry is a useful modulator for developing anticancer ENS in the complex extra- and/or intracellular environment.

To address the problems of low drug loading and loss of function due to the covalent modification of the antibody in antibody-based medicine, Yang et al. reported an innovative application of ENS.[466] As shown in Figure 74A, a phosphopeptide (NBD-Gff$_p$y, **38**) is mixed with anti-HER2 antibody to form a solution. The addition of ALP to the solution, at 4 °C, produces a clear hydrogel (Figure 74B). This simple process loads >30 wt% of the antibody and significantly improves the stability of the antibody at 37 °C (>15 d in vitro). According to the authors, the nanofibers exhibit high affinity for HER2+ cancer cells and efficiently enters the cells. Using a murine tumor model, the authors demonstrated the shrinkage of the tumors when CRB-HA-Gff$_p$y (**185**) was mixed with the antibody for making the hydrogel/nanofibers. This study illustrates using ENS to combine antibody and alkylating agents for cancer therapy.

Yang et al. recently developed an innovative tandem molecular self-assembly that is controlled by ENS and an intracellular redox reaction.[467] As shown in Figure 74C, the peptide (**211**) consists of two segments, NBD-GFF$_p$Y and ERGD, that are linked by a disulfide motif. **211**, upon dephosphorylation catalyzed by ALP, becomes **212**, which self-assembles to form a micelle solution. The addition of GSH, reductively cleaving the disulfide bond, generates **213**, whose assemblies become nanofibers to form a hydrogel. The authors demonstrated this tandem self-assembly using liver cancer cells that exhibited higher concentrations of both phosphatase and GSH than normal cells. It is also interesting that the morphologies of nanofibers in the two liver cancer cell lines, HepG2 and QGY7703, differ, which may be worth further investigation. This unique utilization of both extracellular and intracellular reactions to trigger tandem molecular self-assembly is exciting and promising for the development of cancer diagnostics and therapy.

Taking the advantage of the long lifetime of ($Ru(bpy)_3^{2+}$) complex,[468] Liang et al. developed a substrate for intracellular imaging.[469] The molecule (Cys(StBu)-Lys-($Ru(bpy)_3^{2+}$)-CBT**, 214**, Figure 75A) consists of a latent cystine at the N-terminal, $Ru(bpy)_3^{2+}$ at the side chain of lysine of the peptide, and CBT at the C-terminal. As shown in Figure 75B, **214**, after entering the cells and being reduced to expose the thiol group in cysteine, undergoes a condensation reaction to form a trimer of **215**, which self-assembles to form nanoparticles of **215** with non-quenchable, persistent phosphorescence. The authors

also demonstrated the fluorescence from **214** for imaging HepG2 cancer cells in a tumor murine model. It appears, however, that the efficiency of imaging remains to be improved.

To develop a strategy for treating hepatic fibrosis, Liang et al. further developed ENS for delivering Dex[470] after their earlier report that intracellular co-assembly boosted the antiinflammation capacity of dexamethasone.[445] As shown in Figure 75C, they made a hydrogelator precursor Nap-FFK(Dex)$_p$Y (**216**) for the slow release of Dex by ENS and enzymatic release. That is, the action of ALP produces Nap-FFK(Dex)Y (**217**), which self-assembles into nanofibers. Because Dex is linked to lysine via an ester bond, the action of esterase cleaves Dex from the nanofibers for slow release of Dex. This work illustrates the importance of designing ENS not only for assembly, but also for disassembly. More useful applications applying this concept[439] will likely emerge.

To develop probes for photoacoustic (PA) imaging, Liang et al. conjugated a NIR dye with a substrate of ALP for tumor imaging.[471] As shown in Figure 75D, they designed and synthesized a NIR probe IR775-FF$_p$Y (**218**), which, being catalytically dephosphorylated by ALP, became IR775- FFY (**219**). After ENS forms the nanoparticles of **219**, the PA signal is enhanced 6.4-fold. The authors reported that in vivo tumor PA imaging exhibited 2.3 folds increase due to the ENS of **219** catalyzed by ALP. This work represents the first example of an ALP-activatable probe for enhanced PA imaging of tumors.

It is relatively easy to combine ENS with photo activatable molecules for selectively targeting certain cancer cells, as reported by Ding et al.[472] They designed and synthesized a substrate, **220** (Figure 76A), that consisted of a fluorophore (TPE-Py) and a short peptide with three tyrosine phosphates ($_p$Y). **220**, being the first reported triphosphoheptapeptide, exhibits good aqueous solubility, weak fluorescence, and negligible ROS generation ability. After ALP of Saos2 cells, enzymatic action dephosphorylates **220**, then, the ALP-catalyzed product (**221**) self-assembles to form nanoscale aggregates, which are highly fluorescent and are able to produce ROS efficiently during irradiation (Figure 76B). Cellular studies reveal that **220** is specific towards Saos2 cells. It is, however, less clear on how to use photoactivated ROS for treating solid tumors formed by Saos2.

To target prostate cancer, Wang et al. combined gold nanoparticles (AuNPs) with a phosphopeptide for ENS, which facilitated photothermal therapy.[473] As shown in Figure 79, the authors synthesized a phosphopeptide, CREKA$_p$YPFFK(Nph) (**222**, Figure 76C). The sequence CREKA is a pentapeptide structure binding to fibronectin and forming Au–S bonds with AuNPs via the cysteine residue. The conjugation of AuNPs with **222** affords AuNPs@**222**, which have diameters of 13 nm. Using ALP to treat the AuNPs@**222**, the authors confirmed the aggregation of the nanoparticles after dephosphorylation converted **222** to CREKAYPFFK(Nph) (**223**). They incubated PC-3 and MCF-7 cells with AuNPs@**222** and found more accumulation of the AuNP@**223** in the PC-3 cells than in MCF-7 cells. After AuNPs@**222** were injected into mice, the accumulation of AuNPs@**223** in tumor sites allowed effective photothermal therapy in vivo (Figure 76D). This work demonstrates, again, that inorganic nanoparticles, with a proper surface modification, can act as the substrates for intracellular ENS.

Using the enzyme attached on the nanoparticles of silica, Wang et al. reported an innovative approach to core–shell nanogels for drug delivery.[474] As shown in Figure 80, CES, being immobilized on the surface of silicon nanoparticles (SNPs), catalyzes the hydrolysis of a substrate (Nap-FF-*es*, **224**, Figure 76E) to form a hydrogelator (Nap-FF-*e*, **225**). The self-assembly of **225** forms a layer of hydrogel around the silica nanoparticles to generate the core–shell SNP nanogels (Figure 76F). Changing the concentrations of **224** controls the growth of the gel layer. The nanogels can encapsulate drugs, such as doxorubicin (Dox), and release the Dox when proteases cleave the peptides (**225**) on the surface of the nanoparticles. The Dox-loaded nanogels, being incubated with HeLa cells, undergo endocytosis and release Dox to the cell nuclei within 24 h.

To combine MRI and PDT, Han et al. reported a peptide conjugate that consisted of protoporphyrin IX (PpiX), a proteolytic site, and DOTA(Gd), as shown in Figure 77A, B.[475] This chimeric peptide PpiX-PEG8-SSSPLGLAK(DOTA)-PEG6F4 (denoted as Ppdf-Gd, **226**), being a substrate of MMP-2, aims to amplify MRI for guided photodynamic therapy (PDT) of tumors. **226**, being amphiphilic, self-assembles to form spherical nanoparticles, which turn into nanofibers upon the action of MMP-2 that hydrolyzes the Pro-Leu-Gly-Leu-Ala (PLGLA) peptide sequence at the site of G/L. One notable feature is that the sphere-to-fiber switch results in a higher relaxation rate of DOTA(Gd). The incorporation of protoporphyrin IX also allows **226** to be an agent for PDT. The in vivo examination of the nanoparticles of the chimeric peptide indicates high accumulation of the particles in the liver, which is a common drawback of nanoparticles.

The study of immunosuppression reveals that immunosuppressive adenosine[425] in the tumor microenvironment is a major cause for patients' unresponsiveness to the treatment[476] of cancer immunotherapy based on checkpoint blockade.[477] ALP can rapidly convert ATP to adenosine which causes immunosuppression in the tumor microenvironment. While it is still a challenge to develop suitable inhibitors[478] for ALP, ENS catalyzed by ALP can target tumors overexpressing ALP, as shown in Figure 77C.[479] A recent study shows that **173**, the substrate of ALP and CES, uses ENS to inhibit osteosarcoma in orthotopic murine models. The key feature of **173** is that, being a substrate of CES, it selectively inhibits osteosarcoma without affecting liver cells. Compared to the control (saline solution), **173** significantly inhibits the progression of Saos2-luc and its metastatic subline Saos2-lung (Figure 77C). Validating the in vivo anticancer efficacy of ENS of peptides for the first time, this work ultimately may lead to a fundamentally new way to target immunosuppressive cancer cells and establish immune normalization for cancer treatment.

To develop approaches for promoting antibodies to recognize phosphorylated proteins, Yang et al. reported an innovative method for the efficient production of antibodies of phosphorylated proteins.[304] They used Ca^{2+} to induce the self-assembly of a phosphopeptide, Nap-Gff$_p$y (**227**, Figure 77D), to form a hydrogel (i.e., Y-Gel). Because the hydrogel, as a medium to encapsulate phosphorylated antigens, reduces the dephosphorylation of the antigen, the ratio of the antibodies for phosphorylated proteins increases (Figure 77E). Although the mechanism remains to be elucidated, this study opens a new way for producing antibodies that recognize specific posttranslational modifications in proteins.

To increase inhibitory capacity and decrease systemic toxicity, Yang et al. combined ligand-receptor binding and pericellular ENS.[480] As show in Figure 78A, they designed a substrate (**229**) of ALP containing the CCK-6 peptide (Nle-Gly-Trp-Nle-Asp-Phe), a specific ligand of the human cholecystokinin-2 receptor (CCK2R), at the C-terminal of **60**. Using two cancer cell lines (HeLa and HepG2) that overexpressed CCK2R, the authors showed that HeLa cells treated by **229** were covered by large amounts of nanofibers made of **230** (Figure 78B). Using RGD connected to the C-terminal of **60** and **60** as the controls, the authors confirmed the selectivity of **229** to the CCK2R expressed cancer cell lines. This work illustrates a facile approach to enhance the selectivity of pericellular ENS for detecting or inhibiting cancer cells.

To selectively inhibit lung cancer, Yang et al. further developed their tandem self-assembly approach.[481] As shown in Figure 78C, they designed a peptide derivative, NBD-GFF$_p$YG-N=N-ERGD (**233**), which was the substrate of both ALP and reductase. According to the authors, ectoenzyme, ALP, converts **233** to NBD-GFFYG-N=N-ERGD (**234**). **234** self-assembles to form nanoparticles or short nanofibers for efficient endocytosis. After the mitochondrial accumulation of **234**, the reductase in the mitochondrial membrane likely converts **234** to NBD-GFFYG-aniline (**235**), which further self-assembles into nanofibers in the mitochondria to disrupt the mitochondrial membrane. These events could result in cytochrome c (Cyt c) release and reactive oxygen species (ROS) production, which can increase ER stress, activate unfolded protein response (UPR), and lead to selective inhibition of lung cancer cells. Using the A549 lung cancer cell line, the authors demonstrated their concept in cell assays and in a mice model. This innovative study may provide a feasible strategy for developing ENS for treating lung cancer.

Yang et al. reported a rather less explored application of ENS, the removal of senescent cells.[482] They designed a substrate of β-galactosidase (GLB1), NBD-FFY(gal)G (**236**, Figure 79A), because GLB1 was overexpressed in senescent cells.[483–484] The authors incubated senescent HeLa cells with **236** and its control (NBD-FFYG, **237**) and showed that the nanofibers of **237** formed in the cells treated by **236**, not by **237** (Figure 79B). The formation of nanofibers reduces the expression of p53, p21, and p16INK4a in the cells, which is evidence of reducing endothelial cell senescence. According to the authors, the ENS of **236**/**237** is able to selectively remove senescent endothelial cells by inducing apoptosis. Since GLB1 overexpresses in certain cancer cells, this work illustrates a new way to remove senescent endothelial cells for cancer therapy.

Using ENS to control the conformation of peptides in supramolecular assemblies, Yang et al. demonstrated a simple way to modulate the activities of peptides in the assemblies.[485] They designed and synthesized a peptide, Nap-FFGGYGSSSRRAPQT (**45**), consisting of the self-assembling motif (Nap-FF) and a peptide from insulin-like growth factor-I (GYGSSSRRAPQT, IGF-1). Folding into β-sheet conformation, **45**, forming a hydrogel (Gel-A), almost preserves its ability to bind with the IGF-1 receptor (IGF-1R) It also has a K_d of 11.5 nM, which is comparable to that of IGF-1 (K_d = 4.3 nM). Without the self-assembling motif, the peptide (Nap-GGYGSSSRRAPQT, **238**, Figure 79C) exhibits weak affinities to IGF-1R (K_d = 381 nM). With β-sheet conformation, **45**, at 10 nM, efficiently activates IGF-1 downstream signaling and prevents cell apoptosis. In the hydrogel formed by

heating-cooling cycle, **45** adopts a β-sheet conformation and is more effective than IGF-1 to improve ischemic hind-limb salvage in vivo. Enzymatic dephosphorylation of the phosphorylated peptide (Nap-FFGG$_p$YGSSSRRAPQT, **44**) results in a gel (Gel-B), in which **45** adopts an α-helix conformation but is less effective than IGF-1 in vivo (Figure 79D). While this study provides a useful strategy to modulate peptide conformations in assemblies for mimicking protein functions, it, again, reveals that ENS differs fundamentally from self-assembly at thermodynamic equilibrium.

PET is commonly used in tumor imaging with high sensitivity. However, tumor-targeted PET probes that can distinguish and image specific tumors are underdeveloped. In a work reported by Liang et al.,[486] a tumor targeting PET imaging probe CBT-^{68}Ga (**239**, Figure 80A) was designed. It utilizes a furin substrate peptide (RVRR) to target specific tumor cells overexpressing furin. After furin activation, the probe undergoes CBT-Cys condensation and intracellular self-assembly to form nanoparticles with average diameters of 258.3 nm. In vivo microPET imaging suggested the co-injection of CBT-^{68}Ga (**239**) with its cold analogue CBT-Ga (**240**) would lead to the formation of CBT-^{68}Ga/CBT-Ga nanoparticles inside the MDA-MB-468 tumors and have a 9.1-fold increase of the tumor/liver ratio comparing to that of the mice only injected with CBT-^{68}Ga (Figure 80B). This work is the first report of a furin-targeted ^{68}Ga radiotracer for enhanced tumor microPET imaging. Replacing the furin substrate with other enzyme-specific peptides may give us a hint in developing other sensitive microPET probes.

Cathepsin B (CTSB) is a lysosomal protease that functions in catabolic pathways after protein internalization. Aberrant expression of CTSB is a hallmark of certain cancer, such as esophageal cancer.[487] In a study reported by Liang et al., a bioluminescence probe Val-Cit-AL (**241**, Figure 80C) is designed to detect CTSB both *in vitro* and *in vivo*.[488] Upon activation, it has a 67-fold “turn-on” intensity with good linear relationship from 0–40 U/L. It has an excellent lower detection limit of 27 mU/L. Notably, the author reported that the ratio of turnover number (kcat)/Michaelis constant (Km) of CTSB for **241** was about 500-fold higher than that of a Gly-Phe-Leu-Gly (GFLG)-based nanoparticle probe.[489] Likely benefited from its rapid enzymatic kinetics, this CTSB-specific bioluminescence probe is capable of cancer cell imaging, hardly being interfered by common intracellular substances such as cations, some tumor markers, and proteases. After injecting into MDA-MB-231 tumor-bearing nude mice, the probe can rapidly target tumors within 30 min (Figure 80D). This article is the first example of using bioluminescence to target CTSB, reaching good selectivity both *in vitro* and *in vivo*. One of the reasonable questions is the selectivity of **241** for other cathepsins. If **241** is exceptionally specific toward CTSB, it may lead to a useful assay for CTSB.

Liang et al. also applied the concept of “turn-on” nanoparticles for developing NIR nanoprobes based on ENS catalyzed by carboxylesterase (CES).[490] Specifically, the authors designed H_2N-Cys(StBu)-Lys(Biotin)-Ser(Cy5.5)-CBT (NIR-CBT) (**242**, Figure 81A), which was a substrate of CES and a ligand of biotin receptors. The NIR-CBT probe is subjected to reduction-controlled condensation and self-assembles to form “OFF” NIR-CBT nanoparticles. After being recognized by biotin receptors overexpressed on tumor cells, intracellular CES catalyzes the cleavage and turns the Cy5.5 fluorescence signal “ON”

(Figure 81B). After demonstrating that the nanoparticles of **242** exhibit a 69 fold increase of fluorescence once incubated with CES for 6 h, the authors incubated the nanoparticles of **242** with HepG2 cells. They reported that biotin receptor-assisted endocytosis and intracellular CES hydrolysis turned on the fluorescence. Moreover, these nanoparticles of **243** are able to image the HepG2 tumors, which express biotin receptors and CES, in a murine model.

To develop MRI contrasting agents, Liang et al. designed a “smart” Gd-based probe Glu-Cys(StBu)Lys(DOTA-Gd)-CBT (**244**, Figure 81C), which underwent ENS catalyzed by γ-glutamyltranspeptidase (GGT).[491] According to the authors, GGT cleaves glutamine to allow the intracellular CBT-Cys condensation reaction to form Gd nanoparticles of **246** for enhancing the T2-weighted MR contrast of a tumor in vivo at 9.4 T. One of the future challenges of this study is to prove that the MRI enhancement is significant when the magnetic field strength is at the clinical range.

To develop an approach for reducing tumor recurrence, Qiao and Wang recently reported the use of intracellular ENS from constructing a long-term drug depot.[492] The molecule, CPT-LVFFGFLG-PEG-RGD (**247**, Figure 82A), consists of a hydrophobic anticancer drug (camptothecin, CPT) at the N-terminal and a PEG-RGD at the C-terminal. CTSB recognizes GFLG sequence and catalyzes the cleavage of GF/LG to form CPT-LVFFGF and LG-PEG-RGD. The authors reported that **247** self-assembled to form nanoparticles, which transformed to nanofibers after being treated by CTSB. Based on *in vitro* and *in vivo* results, the authors proposed the mechanism of action of **247** (Figure 82B): The nanoparticles of **247** enter cancer cells, CTSB cleaves **247** to form nanofibers of CPT-LVFFGF, the nanofibers slowly dissociate and release CPT intracellularly. The authors reported that, after the resection surgery on mice model, the sustained release of CPT from the nanofiber depot in the remnant cancer cells prevented postsurgical local tumor recurrences. Probably due to the relatively high expression of CTSB in liver cells,[493] the liver still accumulates more **247** than tumor sites. Therefore, more optimization of this substrate is required. In a related work, the authors used PEG to synthesize polymer–peptide conjugates (PPCs) that underwent an acid-induced intracellular self-assembly in the tumor microenvironment for enabling drug delivery deep inside the tumor.[494]

A recent study by Wang et al.[495] has reported a new NIR probe (**248**, Figure 82C) that is activatable by a prolyl endopeptidase, fibroblast activation protein-α (FAP-α). The peptide (**248**) consists of four major parts: hydrophilic motifs, FAP substrate, self-assembly motif, and a cyanine dye. Molecule **248** shows no significant cytotoxicity when its concentration reaches 300 μM. Upon FAP cleaving GPA at the P/A site, the resulting peptide increases hydrophobicity and self-assembles to form nanofibers (Figure 82D). In vivo, when the FAP on the surface of cancer associated fibroblasts (CAFs) cleaves **248**, the probe selectively accumulates around the tumor (with 4- and 5-fold higher intensity over liver and kidney, respectively). The enzymatic formation of nanofibers not only enables extended retention time (over 48h detectable windows) but also enhances the signal of the probe (5.5-fold signal enhancement). Similar to the earlier work by Chen et al.,[424] this study is a successful example that combines ENS with clinically used cyanine dyes for functions.

Fan and Ren reported enhanced anticancer selectivity and efficiency when they combined ENS with a novel inhibitor of histone deacetylase.[496] They designed a novel peptide, Nap-Gff$_p$YSV (**249**, Figure 83A), which is a substrate of ALP for ENS. The authors tested the cytotoxicity of **249** and the dephosphorylated product, Nap-GffYSV (**250**), on several cancer cell lines and a normal cell line (L929) and measured the secreted ALP by the cells (Figure 83B). One notable difference of this work in contrast to other reports is that **249** is pretreated by ALP prior to being incubated with the cells. Moreover, **249** is more potent than Nap-ff$_p$y (**119**) for inhibiting HeLa cells, supporting that YSV acts as an inhibitor of histone deacetylase. Although YSV is claimed to act as an anticancer peptide, it hardly inhibits HeLa cells. It is possible that the self-assembly of **250** promotes endocytosis for inhibiting the HeLa cells. Thus, more analogs of **249** or more cell lines need to be tested for elucidating the mechanism of the cytotoxicity of **249** or **250**.

To mimic the multivalence exhibited by sugar moieties on glycoproteins, Tian and Li developed a glycopeptide for ENS.[497] Attaching mannose at the serine, as shown in Figure 83C, the glycopeptide (**252**), can be phosphorylated at the tyrosine residue to give the phosphoglycopeptide, **251**. Using ALP to dephosphorylate **251** generates the hydrogel of **252**. According to the authors, the hydrogel of **252**, bearing multiple mannose ligands on its self-assembled structure and engaging multivalent carbohydrate–lectin interactions, is able to bind *E. coli* with high specificity, which results in bacterial adhesion, membrane disruption, and subsequent bacterial death (Figure 83C). The authors also reported that an in vivo wound healing assay (in a full-thickness skin defect mouse model) showed this glycopeptide hydrogel promoting wound healing and preventing *E. coli* infection. This work illustrates that ENS, combined with specific saccharide–lectin interactions, is suitable for generating multivalent interactions to mimic glycoproteins.

To achieve simultaneously multimodality imaging, Ye et al. developed an impressive bimodal probe that was an ENS substrate for in vivo imaging.[498] As shown in Figure 83D, the small molecule probe (P-Cy-FF-Gd, **253**) consists of an ALP-activatable near-infrared (NIR) fluorophore, a self-assembling dipeptide, and a magnetic resonance (MR) contrasting agent. The authors reported that endogenous ALP, overexpressed on cancer cell membranes, removed the phosphate group on the fluorophore (Cy), resulting the dephosphorylated probe (Cy-FF-Gd, **254**) to self-assemble into nanoparticles, as visualized by cryo-SEM. This ENS process, simultaneously enhanced NIR fluorescence over 70-fold and r1 relaxivity about 2-fold, and enabled real-time, high-sensitivity, high-spatial-resolution imaging of the ALP activity of tumor cells in a mice model. One notable result is that, compared to the control molecule (P-Cy-Gd) without the self-assembling motif, **253** significantly enhances the fluorescent and MRI signals from the HeLa tumors in mice. It is also impressive that **253** results in higher MRI signal in the tumor than in the liver of the mice model (Figure 83E). This work illustrates the merit of ENS for designing other activatable multimodal probes to image the activity and locations of enzymes in vivo and in real time.

To develop a self-delivery system consisting of lonidamine (LND) for selective inhibition of cancer cells, Zhong et al. synthesized a substrate (**255**, Figure 84A) of phosphatase.[499] **255**, consisting of lonidamine and GFF$_p$Y, turns into **256** (or LND-GFFY) after dephosphorylation. After confirming that **255** is a substrate of ENS catalyzed by ALP, the

authors showed that cancer cells uptake more **255** than normal cells do. Moreover, **255** inhibits tumor growth in a HeLa xenograft murine model. The authors suggested this approach should be generally applicable to the delivery of other hydrophobic cancer drugs.

To detect the high expression of furin in live cells, Zhou and Yi developed a relatively simple peptide substrate (RVRRFFF-NBD (**257**), Figure 84B) of furin.[500] **257** self-assembles to form a β-sheet nanostructure that is capable of a rapid and specific response to furin in only 5 min in aqueous solution because of the existence of the RVRR motif in **257**. The nanostructures of **257** thus can selectively distinguish high furin-expressing cancer cells, like MDA-MB-231 cells, a kind of human breast cancer cell, from normal cells. According to the authors, the nanoparticles of **257** self-assembles and enters cells. The furin in the MDA-MB-231 cells catalytically cleaves the **257** to generate FFF-NBD (**258**), which is fluorescent. The authors reported that the assemblies **257** was able to stay in live cells for a long time and were capable of durable detection of intracellular furin. Since the intensity of the fluorescence in the cells treated by **257** correlates well with the concentrations of **257**, it is likely that **258** also self-assembles inside cells after being cleaved by furin.

The use of furin for intracellular ENS[280,501] has received more attention for developing theranostics, as recently reported by Bulte et al. on chemical exchange saturation transfer magnetic resonance (CEST) imaging.[502] To enhance the tumor retention of imaging agents for CEST, the authors developed a peptide conjugate (**259**) that connected olsalazine on the side chain of lysine,[503] RVRR at the N-terminal, and 2-cyanobenzothiazole[280,282,284] at the C-terminal. Based on the condensation reaction reported by Rao et al.,[280] furin cleaves **259** to generate **260**, which forms a dimer of olsalazine (**261**) in the presence of GSH. **261** self-assembles to form nanoparticles. According to the authors, both **259** and the nanoparticles of **261** are readily detected with CEST due to the exchangeable hydroxyl protons on olsalazine. Using murine xenografts, the authors showed that the CEST signal from olsalazine and anti-tumor therapeutic effect increased 6.5- and 5.2-folds, respectively. Although the concentration of the probe is too high to be clinically useful, this work illustrated that intracellular ENS is an attractive approach for developing MRI based theranostic agents.

The substrates for ENS can be almost any type molecules that self-assemble. Recently, Zhang et al. reported a polyaromatic molecule to selectively alter cell permeability for inducing cell death.[504] As shown in Figure 85A, the authors, inspired by pore forming toxin, designed and synthesized a substrate (**262**) of ALP. **262**, as nontoxic water-soluble molecular precursors, distributes in extracellular fluid. In the case of cancer cells, ALPs, being overexpressed on the cancer cells, catalytically dephosphorylate **262** to **263**. The aromatic motifs in **263**, as hydrophobic building blocks, promote the self-assembly of **263**, which results in rigid aggregates to insert into the hydrocarbon core of membrane. The insertion of the aggregates of **263** leads to membrane permeability alteration by blocking the transportation of molecules, eventually causing the death of the cancer cells (Figure 85B). This work is the first example that uses the expanded π-conjugation system with an extremely high rigidity and long linear length for ENS-guided membrane insertion. Since there are many rigid molecular motifs known to be able to insert into cell membranes to form pores or channels,[505] this strategy may eventually lead to cancer cell death without causing drug resistance.

While most of studies use one of the enantiomers of the peptide-based ENS substrates to interact with cells, Zhang et al. reported that the co-administration of the two stereoisomers of ALP substrates in cancer cells led to molecular assembly targeting of both the plasma membrane and the lysosomes.[506] As shown in Figure 85C, they synthesized homochiral-peptide-based boron diketonate complexes (**264** and **266**) by coupling a boron diketone fluorophore with a pair of homochiral peptides that bear a taurine group at the C-terminals. **264** and **266**, being the substrates of ALP, turn into **265** and **267**, respectively, upon dephosphorylation. After confirming that **265** or **267** self-assembles to form nanofibers, the authors used it to incubate HeLa cells and found that the assemblies of **265** mainly localized at the plasma membrane and the assemblies **267** mainly in the lysosome. Then the authors showed that co-administration of the two stereoisomers in cancer cells also led to molecular assembly at both organelles, but inhibition of the ALP prevented the assemblies on or in the cells (Figure 85D). The dual-targeted-assembly may generate a synergistic anticancer effect, as suggested by the authors.

Wang et al. recently developed an ingenious application of the ENS of **1** to deliver enzymes into cells for anticancer therapy. Neutrophil-dependent cell inactivation relies neutrophil lysosomes to produce cytotoxic reactive oxygen species (ROS) by a cascade of enzymatic reactions. Based on this fact, he authors chose to load superoxide dismutase (SOD) and chloroperoxidase (CPO) in the hydrogels formed on magnetic nanoparticles (MNPs) as a multifunctional SOD/CPO-loaded nanogel system (SCNG).[507] As shown in Figure 86A, SOD catalyzes the dismutation of $^{\cdot}O_2^{-}$ to form H_2O_2, which serves as a substrate of CPO to produce HOCl. The reaction of HOCl and H_2O_2 generates singlet oxygen ($^1O_2$) for cell destruction. To build a suitable carrier to entrap CPO and SOD, the authors attached ALP on MNPs and added **1**, which produced hydrogel nanoparticles with about several hundred nanometers in diameter. The nanogels, acting as a matrix to protect enzymes from proteolytic deactivation, are suitable for loading SOD and CPO to form the SCNG. The relatively higher level of ROS in tumor microenvironment thus enables the SCNG to generate $^1O_2$ to inhibit tumors (Figure 86B). The authors used intratumoral injection of the SCNG to demonstrate the functions of the SCNG. Although the dosage of the SCNG remains high, the use of a simple ENS molecule (**1**) to enable a sophisticated enzyme cascade is stimulating. The authors also proposed a highly promising concept, enzyme dynamic therapy (EDT), for taking full advantage of redox enzymatic reactions in the tumor microenvironment to treat cancer by $^1O_2$. The success of this approach likely depends on the kinetics of $^1O_2$ formation by SCNG. In fact, Wang et al. already made progress on enhancing the production of H_2O_2 and $^1O_2$ in cancer cells.[508] Specifically, they combined magnetic hyperthermia with enzyme catalysis by using an alternating magnetic field (AMF) to heat up the MNP@Nanogels for generating H_2O_2 and the MNP-CPO@Nanogels for producing $^1O_2$. They named such a construction magnetocaloric–enzymatic tandem therapy (METT). As suggested by the authors, the programmed alternating magnetic field (AMF), similar to the neutrophil activator, elevates H_2O_2 levels in cancer cells, and the CPO within the protective peptide nanolayer converts the H_2O_2 into $^1O_2$ in a sustained manner. As a proof of concept, the authors confirmed that both the H_2O_2 and $^1O_2$ in cancer cells increase stepwise under a programmed alternating magnetic field (Figure 86C). The authors also reported the effective inhibition of cancer cells in vitro and suppression of tumor growth in

animal models. Although the in vivo studies were done via local administrations, this work represents an innovative combination of physical and biochemical approaches for anticancer therapy, which will likely stimulate more research activities along this direction.

Although nuclear accumulation would greatly enhance the efficacy of anticancer drugs, it remains a challenge to enhance nucleus targeting. Yang et al. recently used conformation control by ENS to enhance cellular uptake and nuclear accumulation.[509] They designed and synthesized four peptides (Figure 87A), NBD-βA-$FF_pYGTSFAEYWNLLSP$ (**268**) NBDβA-FFYGTSFAEYWNLLSP (**269**), HCPT-$FF_pYGTSFAEYWNLLSP$ (**270**), and HCPT-FFYGTSFAEYWNLLSP (**271**). The sequence, TSFAEYWNLLSP (PMI), is capable of binding with the MDM2 and MDMX in the cell nucleus for activating the p53 gene. The authors tuned the peptide conformations by heating-cooling or ENS. They found that the assemblies formed by ENS at 4 °C showed enhanced cellular uptake and nuclear accumulation (Figure 87B). Impressively, against HepG2, A549 and U87MG cells, the IC_{50} values of **271** formed by ENS at 37 °C are 0.66, 1.43 and 1.94 μM, respectively, and the IC_{50} values of **271** formed by ENS at 4 °C are 0.22, 0.26 and 0.87 μM, respectively. Moreover, **271** formed by ENS at 4 °C exhibits the highest in vivo activity. This study, taking advantage of HCPT, a highly potent drug candidate, illustrates a powerful way for modulating the emergent properties of peptide-based supramolecular nanomedicine to enhance efficacy in cancer therapy.

To develop probes for image-guided surgery, Wang et al. recently reported a peptide-based probe for imaging renal cell carcinoma (RCC).[510] As shown in Figure 86C, the peptide, RGDRDDRDDPLGYLGFFC(Cy) (**272**), consists of a targeting motif, an enzyme cleavable site, and a NIR fluorophore. Specifically, the modular molecular design includes (i) RGD, as a recognition motif, for recognizing the highly expressed αvβ3 integrins in RCC, (ii) PLGYLG, as an enzyme-responsive peptide linker and a substrate to be cleaved by MMP-2/9, (iii) a self-assembly motif (YLGFFC), and (iv) a fluorophore (Cy). According to the design by the authors, the peptide binds to the integrins overexpressed on the cancer cells, and MMP2/9 enzymes overexpressed by the cancer cells cleave the peptide to release the self-assembling peptide attached with the cyanine dye to form fluorescent nanoparticles on the surface of cancer cells. After confirming the in situ enzyme triggered self-assembly of the NIR peptide probes on cancer cells, the authors tested the probes on tumor lesions in a mice model. The authors have shown that the nanofibers formed by the self-assembly of the probes, exhibiting an excretion-retarded effect in the kidney, enabled identifying tiny lesions for complete tumor removal, and significantly reduced the postoperative recurrence of tumors compared with traditional surgery. Moreover, using an ex vivo kidney perfusion model, they also demonstrated the tumor-specific excretion-retarded (TER) effect. Although the detailed enzyme kinetics remain to be elucidated, this work illustrates the promises of the concept of ENS in developing imaging probes.

To target castration-resistant prostate cancer (CRPC) cells, a small D-phosphopeptide (**274**) has been developed to undergo prostatic acid phosphatase (PAP) catalyzed ENS to inhibit prostate cancer cells.[511] As shown in Figure 88A, while dephosphorylating **274** by PAP forms uniform nanofibers that inhibit VCaP, a CRPC cell, a non-hydrolysable phosphate analogue, **276**, is ineffective for inhibiting VCap. Although the efficacy of **274** remains to be

improved, this work confirms that PAP-catalyzed ENS is critical for selective inhibition of CRPC cells.

Although protein kinases are the most attractive targets in drug discovery, it is rather difficult to use protein kinase to enable ENS for targeting cancer cells. Recently, Gao et al. reported innovative progress on utilizing protein kinase A (PKA) to design PKA-triggered supramolecular assemblies with anticancer activities.[512] They grafted a suitable peptide to PNIPAM to increase the lower critical solution temperature (LCST) of the polymer (**277**, Figure 88B) to above body temperature. Upon phosphorylation by PKA, the resulting polymer (**278**) exhibited a critical temperature below body temperature to result in the PKA-triggered supramolecular assembly. They demonstrated that the PKA-triggered assembly occurred selectively in PKA-upregulated MCF-7 cells, which could be used to sensitize tumors for Dox in vivo. This PKA-catalyzed supramolecular assembly would likely lead to a new strategy for combating kinase-upregulated cancer, especially in the case of drug resistance to kinase inhibitors.

Because ENS builds up non-diffusive molecular assemblies, it would increase the local concentration of the desired molecules for further reactions, as shown by the innovative combination of ENS and biorthogonal reactions[513] demonstrated by Rao et al.[514] To image the activity of enzyme in tissues, the authors further developed target-enabled in situ ligand aggregation, a powerful platform technology that they developed for molecular imaging.[515] As shown in Figure 89A, the key molecule is **279**, consists of a caspase cleave site, a protected aminothiol group, an aromatic nitriles, and a trans-cyclooctene (TCO). Such a design allows **279** to undergo two bioorthogonal reactions—the condensation reaction of aromatic nitriles and aminothiols and the inverse-electron demand Diels–Alder reaction between tetrazine and trans-cyclooctene (TCO). Specifically, caspase 3/7 cleaves the DEVD sequence off **279** to expose the N-terminal amine, and GSH deprotects the thiol group. These two reactions lead to intramolecular cyclization to form **280**. Being more hydrophobic than **279**, **280** self-assembles to form nanoaggregates. Bearing the TCO group, **280** is able to couple tetrazine on a fluorescent substrate (**281**) via the intermolecular click reaction. After validating this design in vitro, the authors demonstrated the application of this approach in vivo using a mice xenograft with tumors. According to the procedure illustrated in Figure 89B, 24 h after the intratumoral injection of cisplatin to induce cell death, **279** was injected intravenously into the mice, followed by intravenous injection of **281** after 30 min. The authors found significant retention of fluorescent signal in the cisplatin-treated mouse group compared to the untreated group. These results support the versatility of the ENS process for coupling with multiple bioorthogonal reactions in vivo. The concentration of **279** used in the study is still high, probably because the TCO is buried inside the nanoaggregates. Structural elucidation of the nanoaggregates may help address this limitation in the future.

Gao et al. recently devised an innovative indirect ENS process for reducing methicillin-resistant staphylococcus epidermidis (MRSE) infection.[516] Taking the cues from neutrophil extracellular traps (NETs), which stick to bacteria and activate the sudden increase of reactive oxygen species (ROS), the authors developed a molecular mimic of NETs. The authors synthesized a quinazolinone derivative (BQA-GGFF, **283**, Figure 90A) with a typical aryl boronate immolative linker,[517–518] which underwent oxidation to yield BQH-

GGFF (**284**). **284** self-assembles to form nanofibers and results in a hydrogel. Upon the oxidation of the hydrogen peroxide produced by glucose oxidase (Gox) and glucose, **283** turns to **284**, thus resulting in hydrogelation. After confirming that the nanofibers of **284** within the hydrogel tightly stuck to the bacteria and inhibited bacterial growth in vitro, the authors tested **283** at the bacterial infection site on mice. The authors reported that inflammatory condition (i.e., high level of ROS including hydrogen peroxide) at the infection site induced the formation of fluorescent assemblies of **284**. The nanofibers of **284** were able to trap the bacteria, thus lessening bacterial translocation and increasing the overall mice survival ratio (Figure 90B). The use of inflammation to enable ENS for forming in situ supramolecular assemblies would likely have broad applications beyond infection control, especially if this approach is able to reduce inflammation induced tissue injury.

One of the remaining challenges for intracellular ENS is to visualize the formation of supramolecular nanofibers in live cells. Gao and coworkers recently made considerable progress by combining direct stochastic optical reconstruction microscopy (dSTORM) imaging with ALP catalyzed ENS in cancer cells.[519] The authors, aiming to elucidate the dynamic assemblies formed by ALP catalyzed ENS, designed and synthesized two molecules **285** and **287** (Figure 91A). As an assembly precursor, **285** is able to undergo ENS upon ALP catalyzed dephosphorylation to generate **286**. Bearing a tetrazine group, **285** reacts with a TCO-modified Cy5 dye to form **287**, which is a fluorescent assembly precursor and a substrate of ALP. Using super-resolution fluorescence microscopy, the authors confirmed that ALP catalyzed ENS resulted in the nanofibers of the co-assembly of **286**/**288** (Figure 91B). After treating HeLa and Saos2 cells with **285** and **287**, the authors fixed the cells and used dSTROM to image the nanofibers with the resolution below 50 nm (Figure 91C). Moreover, the authors reported that supramolecular assemblies behaved differently in HeLa and in Saos2 cells. In HeLa cells, the supramolecular nanofibers appear to be transcytosis: they form inside cells, but are excreted from the HeLa cells. In Saos2 cells, the supramolecular assemblies form first on the cell surface with granular morphology, then transform into nanofibers and accumulate in cells, which eventually induces Saos2 cell death via ROS upregulation. Considering that HeLa and Saos2 express different isozymes of ALP and at different levels and locations, these results are reasonable. The dynamics of the D-enantiomers of **285** and **287** also remains to be determined. Nevertheless, this excellent work illustrates the need to develop a method to capture the dynamic morphology of the intracellular molecular assemblies formed by ENS. Furthermore, itshows fluorescent imaging as a methodology to identify the morphology of other classes of ENS assemblies for correlating dynamics of assembly and bioactivities of ENS. Moreover, the observation of exocytosis in HeLa cells, in this work, is very intriguing. Similar phenomena appears in the case of using ENS for imaging lipid rafts.[520] These results suggest that ENS may promote exosome secretion, which remains to be confirmed.

While using the self-assembly[521] of synthetic molecules to form peptide filaments has been successful *in vitro*[522–525] or extracellularly,[267,275,426] the generation of artificial intracellular filaments has not been possible. The challenge largely arises from dynamics and crowding of the intracellular environment,[526] which makes it difficult to carry out self-assembly, a thermodynamic equilibrium process, of synthetic molecules inside cells. Thus, it is

reasonable to use ENS to generate intracellular filaments. Although increased number of reports indicate that it is feasible to use enzymatic reaction to control self-assembly of small molecules inside cells,[227,253,519,527] the formation of bona fide artificial intracellular filaments is only a recent result (Figure 92).[528] The self-assembly of a phosphorylated and trimethylated heterochiral tetrapeptide (**289**, Figure 92A) forms nanoparticles. Enzymatic dephosphorylation reduces repulsive intermolecular electrostatic interactions and converts the nanoparticles of **289** into two types of filaments (types 1 and 2) of **290**. Cryo-EM reveals that type 1 filaments exhibit distinct types of cross-β structures with either C7 or C2 symmetries (Figure 92B), with the hydrophilic C-terminal residues at the periphery of the helix (Figure 92C). After the Saos2 cells uptake the nanoparticles, intracellular ALP converts the nanoparticles of **289** to the filaments of **290**. Due to the intracellular crowdedness, the peptide filaments form bundles that extend from the plasma membrane to nuclear membrane (Figure 92D). Electron tomography confirms the intracellular filaments of **290** forming bundles, which hardly interact with endogenous components, including cytoskeletons (Figure 92E). Structural analogs of **289** indicate that stereochemistry and multiple post-translational modification (PTM) of peptides, that is, phosphorylation and trimethylation, are critical for generating the intracellular bundles. This work, as the first case of artificial intracellular filament, illustrates the power of ENS and provides molecular insights for understanding normal and aberrant intracellular filaments. This work also raises other interesting questions, such as the mechanisms of the endocytic pathway and endosomal escape of the nanoparticles, which remain to be elucidated. In addition, intracellular filaments only form from the heterochiral tetrapeptide, which demands more exploration of the molecular space of the precursors so that a general design principle can be formulated.

4.3. Subcellular ENS

The presence of enzymes in subcellular organelles should allow the use of ENS for targeting specific organelles, which is much less explored despite the promising implications for biomedicine. An early report on using ENS for targeting mitochondria[529] actually combines ENS and a well-established mitochondria targeting motif (triphenyl phosphonium (TPP)[530]). As shown in Figure 93A, attaching TPP to a phosphotetrapeptide produces the precursors (**291** or **293**) that self-assemble form noncovalent oligomers. **291** (or **293**), being incubated with Saos2 cells, undergoes dephosphorylation catalyzed by ALP overexpressed on the cells to form **292** (or **294**), which further self-assembles to result in large aggregates on the surface of Saos2 cells to facilitate the endocytosis of **292** (or **294**). The assemblies of **292** (or **294**), escape from the lysosome, and target mitochondria because of TPP. The accumulation of **292** (or **294**) on mitochondria induces dysfunction of mitochondria to release cytochrome c, and results in cell death (Figure 93B). One notable result from this work is that Saos2 is unable to evolve acquired drug resistance to **291** (or **293**) (Figure 93C), likely due to the assemblies of **292** (or **294**) targeting mitochondria. This study, though still relies on pericellular ENS, highlights the feasibility and underscores the importance of using ENS to target subcellular organelles.

In fact, it is possible to target mitochondria by perimitochondrial ENS, as shown in a recent serendipitous observation.[367] As shown in Figure 94, a branched peptide (**295**), consisting of

a well-established protein tag (i.e., FLAG-tag: DYKDDDDK)[370] as the branch, Nap-ff as the self-assembling motif,[531–533] and NBD as the fluorophore,[253] is a substrate of enterokinase (ENTK).[369] **295** self-assembles in water to form micelles, which turn into nanofibers after ENTK cuts off the FLAG motif (DDDDK). After fluorescent microscopy of HeLa cells reveals that the product (**296**) of ENTK cleavage localizes mainly at mitochondria, TEM of the isolated mitochondria confirms the conversion of the micelles to nanofibers at the mitochondria. This result is the first case of ENS on mitochondria by a synthetic molecule. In addition, the mitochondrial ENS is able to deliver molecular cargos (proteins or small molecules) to mitochondria of cancer cells selectively. This work, indicating ENTK as a perimitochondrial enzyme in cancer cells, illustrates a fundamentally new way for targeting mitochondria by enzymatic reactions. In fact, a recent study reveals that this kind of Flag-branched peptide also enables the trafficking of histone protein (H2B), a nuclear protein, to the mitochondria in cancer cells, likely resulted from the ENTK catalyzed proteolysis of **98**.[534]

The perimitochondrial proteolysis catalyzed by enterokinase (ENTK/TMPRSS15) of cancer cells allows the use of ENS for selectively targeting mitochondria of cancer cells, as demonstrated by delivering chloramphenicol (CLRP) into the mitochondria of cancer cells, especially liver cancer cells.[535] Liver cells detoxify CLRP *via* glucuronidation[536] catalyzed by a cytosolic enzyme, but mitochondria lack the enzyme for glucuronidation. Because CLRP inhibits protein synthesis, delivering the CLRP into the mitochondria of liver cancer cells should inhibit mitochondrial protein synthesis, thus leading to selective death of cancer cells. Such perimitochondrial ENS has delivered CLRP into the mitochondria of HepG2 and HeLa cells, and reduced protein synthesis and ATP production of the cancer cells.[535] As shown in Figure 95, the conjugation of the Flag-tag[370] to 2-amino-dibutylhexadecanediamide makes a peptide-lipid conjugate Flag-$(C16)_2$ (**297**), which forms micelles to encapsulate CLRP. The micelles selectively enter cancer cells and accumulate at the mitochondria to release CLRP into the mitochondria of cancer cells. As expected, CLRP inside mitochondria inhibits mitochondrial protein synthesis and decreases cancer cell proliferation. Moreover, after the enzymatic cleavage of **297**, the resulting lipids (**298**) also promote mitochondrial outer membrane permeabilization (MOMP) for apoptosis.[537] Thus, MOMP and the inhibition of mitochondrial protein synthesis synergistically reduces the viability of cancer cells (Figure 95). Most importantly, this selective targeting of mitochondria increases the efficacy of inhibiting liver cancer cells without increasing the toxicity to normal liver cells.[535] This work, as the first example of ENS to repurpose clinically approved ribosome inhibitors, may provide a new way to interrupt the metabolism of cancer cells for cancer treatment.

Endoplasmic reticulum (ER), being the largest subcellular organelle, performs a wide range of functions in eukaryotic cells.[538–539] Although disrupting ER functions is emerging as a new strategy for anticancer therapies,[540–542] selectively targeting the ER of cancer cells is less explored. ENS offers a new strategy for targeting the ER, as reported recently.[543] In that study, a substrate of phosphatase, **299**, bearing L-homoarginine at the C-terminal, is able to undergo relatively slow dephosphorylation on cancer cells to generate **300** (Figure 96A). The mixture of **299** and **300** self-assembles to form crescent-shaped supramolecular

assemblies, which interact with the cell membrane to cause curvatures and disrupt cell membranes. The crescent-shaped assemblies enter cells and accumulate at the ER, a location enriched with protein tyrosine phosphatases ($PTP1B^{253}$). The further dephosphorylation at the ER promotes the self-assembly of **300**, causes ER stress and subsequently activates the caspase signaling cascade for cell death (Figure 96B). Because the ALP overexpressed by cancer cells results in the formation of the crescent-shaped assemblies, **299** selectively targets the ER of cancer cells to exhibit potent activities for inhibiting cancer cells (e.g., HeLa, A2780cis, and OVSAHO), but not normal cells (e.g., HS-5) (Figure 96C). This work illustrates an approach for *in situ* generation of membrane binding scaffolds to disrupt the cell membrane and target ER of cancer cells.

The enrichment of PTP1B at the ER also provides a way to use ENS to generate liquid-like condensates for sequestrating enzymes to the ER, as shown in Figure 97.[527] In order to sequestrate enzymes to this target organelle, naproxen (a nonsteroidal anti-inflammatory drug (NSAID) and a ligand of cyclooxygenase-2 (COX-2)) replaces the naphthyl group in **299** to generate a phosphopeptide (**301**) as a substrate of phosphatases. **301**, acting as the precursor of a hydrogelator (**302**), slowly undergoes dephosphorylation catalyzed by phosphatases to form supramolecular assemblies on the ER. The assemblies, containing **301** and **302** molecules, are able to bind both COX-2 and PTP1B, thus sequestrating them on the ER. The examination of the structural analogs of **301** suggests that the NSAID motif, the phosphotyrosine, and the enzymatic dephosphorylation of **301** are necessary for the enzyme sequestration. This work, for the first time, illustrates the use of subcellular ENS for associating enzymes in cells and provides biochemical insights for understanding intracellular liquid condensates.

Recently, Zhang reported an innovative way to target the ER of cancer cells by esterase catalyzed ENS.[544] Based on massive accumulation of alcohol derivatives around the ER to cause ER stress and cell death, the authors designed and synthesized a N-hydroxylethyl peptide (**303**, Figure 98A) for cytosolic self-assembly. They conjugated Nap-FF with ethanolamine to generate the alcohol derivative (**145**). Attaching the fluorescent coumarin derivative (**304**) to the hydroxyl group of **145** produces the esterase substrate **303**. They also made two control molecules, **305** and **306**. In the presence of CES, **303** was hydrolyzed to form **145** and **304**. While **305** hydrolyzes faster than **303**, **306** is resistant to hydrolysis catalyzed by esterase. The authors found that HeLa cells cultured with **303** or **305** exhibited strong fluorescence from coumarin in the cytosol, but not in the HeLa cells incubated with **306** (Figure 98B). Notably, cell viability assays on ovarian cancer (SKOV3 and drug resistant OVCAR-3), liver cancer (HepG2), and metastatic pancreatic cancer (PANC-1) reveals potent anticancer activity of **303**, especially with the inhibition shown within 24 h (Figure 98C). If the liver cytotoxicity of **303** could be reduced, this approach might lead to an effective prodrug for ER targeting of cancer cells.

Another type of enzyme for targeting the ER is proteases, as shown by an unexpected observation that trypsin-1 (PRSS1) catalyzes ENS of a branched peptide on the ER of cancer cells.[545] As shown in Figure 99A, the branched peptide (**307**), consisting of a D-tetrapeptide backbone and a branch with the sequence of KYDKKKKDG, turns to be a substrate of PRSS1. That is, PRSS1 catalyzes the cleavage of **307** to produce **308** and **309**, which self-

assemble to form nanofibers (Figure 99B). Based on the cancer cell line encyclopedia (CCLE), the authors incubated OVSAHO, a high-grade serous ovarian cancer cell line, with **307** because OVSAHO overexpresses PRSS1. After using cell assays to confirm that **307** inhibited the proliferation of OVSAHO cells, but not the control cells expressing normal or low level PRSS1, the authors used immunostaining and fluorescent imaging of a fluorescent analog of **307** to reveal the overexpression PRSS1 on the ER of OVSAHO (Figure 99C). This work, illustrating the inhibition of cancer cells by ENS on ER for the first time, offers a new way to target the ER of cancer cells because many enzymes are synthesized at the ER. However, it remains to be determined whether the enzyme activity of PRSS1 at the ER is an aberrant feature of cancer cells.

One unique advantage of ENS is that it can serve as a context-dependent signal for targeting the ER of cancer cells, as shown in the case of ENS generating the assemblies from the antagonist (AVPI) of inhibitors of apoptotic proteins (IAPs).[546] Since ALP presents on the surface of certain cancer cells, but not normal cells,[426] ALP on the cell surface acts as a context-dependent signal for increasing the efficacy of BTZ[458] against cancer cells and reducing the known side effect of BTZ (toxicity to bone marrow stromal cells (e.g., HS-5)). As shown in Figure 100A, conjugating AVPI, a binding motif against IAPs,[547] to the Ɛ-NH_2 of lysine in a phosphotyrosine-bearing peptide generates a branched proapoptotic peptide (**311**), which self-assembles to form micelles. After ALP catalyzed dephosphorylation converts **311** to **312**, the micelles turn into nanofibers. When the micelles of **311** (co-incubated with BTZ) enter cancer cells via the caveolin-dependent endocytosis, **311** undergoes dephosphorylation to form the nanofibers of **312** at the ER. Thus, the assemblies of **312**, in the cancer cells, sequestrate the IAPs so that the cancer cells become more sensitive to BTZ and commit apoptosis (Figure 100B&C). In the case of HS-5 cells, the micelles of **311** and BTZ enter HS-5 cells via macropinocytosis, but localize in the lysosome of HS-5. Thus, BTZ is unable to reach its target (proteasomes) so the toxicity of BTZ decreases (Figure 100B). Therefore, the phosphopeptide not only forms assemblies to deactivate the IAPs in cancer cells, but also rescues normal cells (e.g. HS-5) from the side effects of BTZ. Incubating **313**, the fluorescent analog of **311**, with Saos2, HeLa, and HS-5 cells shows that the assemblies of **314**, after ENS, indeed localizes at the ER of the cancer cells (i.e., Saos2 and HeLa), but in the lysosomes of the normal cells (i.e., HS-5) (Figure 100D). This work illustrates that ENS, as a context-dependent process, controls endocytosis for selectively targeting the ER of cancer cells. Although it is conceivable that ALP catalyzes the formation of nanofibers to facilitate the endosomal escape of the peptide assemblies, the quantitative role of ENS for endosomal escape remains to be elucidated.

5. Conclusion and Outlook

Bioinspiration.

The discussions on the ENS of nature have illustrated that ENS is, at least, one of the universal controlling mechanisms of intermolecular interactions in molecular ensembles for cellular functions. That is, ENS, integrating these two non-genetic features, enzymatic reaction and self-assembly, of cells, represents an overlooked organizing principle of proteins (and other molecules) in cells. Self-assembly, clearly, is a non-genetic feature of

cells. Though enzymes are genetically controlled, enzymatic reactions are beyond genetic control. Considering that the cell is a complicated heterogeneous mixture, enzymatic reactions increase the number of molecular components and confer context-dependent specificities. Also, self-assembly provides a facile way for modulating the quantitative aspects of signaling transduction, such as location, duration, thresholds, and amplitudes. Most importantly, self-assembly creates higher-order assemblies, in specific locations, to exhibit emergent properties and functions that are absent in individual molecules. Apparently, the most efficient way to control or organize the higher-order assemblies, being selected by evolution, is enzymatic reaction. From this viewpoint, ENS, arguably, is one of the rules of life. One the other hand, as shown by many examples in nature, enzymes trigger hierarchical self-assembly to create large biological entities like microtubules, biomolecular machines and so on. This feature can likely serve as a general guide for the uniqueness of ENS or supramolecular synthesis. Thus, from the perspective of biomimetics, it is highly attractive to use man-made molecules to explore the principles and applications of ENS. The exploration of ENS of man-made molecules in the last decade has validated the notion that it is feasible to design functions from molecular processes such as ENS. Although the use of enzymes to control the emergent properties of man-made molecules is in its infancy, the promises and opportunities are abundant. The advancement of cell biology is an unlimited source of inspiration for the development of ENS.

Kinetic Analysis.

Compared to molecular self-assembly at thermodynamic equilibrium, which sometimes lead to heterogeneous assemblies (even with one kind of building block), ENS usually produces homogeneous, self-limiting, monodispersed, or more-ordered structures, even when the building blocks or reaction environments are heterogeneous.[57,226] This apparently counterintuitive observation, resembling the formation of Turning patterns by the Belousov–Zhabotinsky reaction,[548] underscores the pivotal role of kinetics regulated by enzymatic reaction. It would be instructive if such a phenomena could be examined in terms of reaction-diffusion[39] by rigorous kinetic and thermodynamic analysis.[465,549–550] To do that, more detailed enzyme kinetics should be examined in the context of self-assembly, which is still a rather less explored area.[551] One important characteristic of ENS is ultrafast (comparing to crystallization) in which reaction and assembly can complete in minutes or seconds. This feature is particularly useful for functions of molecular assemblies, especially in cellular environment. It is likely that close collaboration between molecular scientists and applied mathematicians would provide more insights for the development of ENS.

Structures, imaging, and modeling.

To understand the emergent properties of the assemblies formed by ENS, it is necessary to elucidate the structures of the assemblies. The rapid advancement of cryo-EM will likely be able to address the needs of structure elucidation.[552–556] However, molecular assemblies in cells are neither static nor crystalline. The understanding of the biological functions of ENS requires further development of new biophysical tools that provide the information of enzyme reaction in real time and in live cells. To extract such dynamic information over a large area and relatively long time, correlated light and electron microscopy and whole cell NMR or a combination of these can probably shine more light for molecular understanding.

Obviously, any tools that can provide dynamic information of ENS[519] would be useful. But such kinds of tools remain to be developed. The major challenge is that one has to examine enzymatic and spatiotemporal control of the supramolecular assemblies of proteins or synthetic molecules over multiple length scales (e.g., subcellular, intracellular, or intercellular space) and extended time scales (e.g., milliseconds, seconds, and hours) for elucidating biological functions of ENS. Intriguingly, properly designed ENS-based fluorescent probes, at certain conditions, are able to achieve high resolution imaging over large area and extended time.[520] In addition, to fill the experimental gaps, molecular dynamic simulation[528,557–561] would be highly valuable for providing insights that help understand these dynamic processes,[562] especially with the increase of computational power and the advancement of computational methods.

Integration with other processes.

While most of the reports on ENS of man-made molecules have focused on the formation of assemblies, the reverse process, disassembly, is equally important for biological functions, as revealed by enzymatically regulated assembly and disassembly of proteins in cellular environment. Combining assembly and disassembly for designing ENS approaches remains challenging, but the success in this direction may lead to new therapeutics that achieve spatial control and precise regulation for treating diseases. For example, the combination of ENS with disassembly has greatly increased the therapeutic windows for targeting tumors.[439,479] With more understanding of biological processes, it is likely that more elaborated, enzyme-controlled assembly and disassembly[563–565] will emerge for a wide range of applications. In fact, regulation of disassembly has already attracted considerable research attention in the field of controlled drug release.[566–567] Moreover, coupling ENS and disassembly would be an effective approach to mimic the cellular signal transduction cascades with feedback loops.[568] In addition, it would be fruitful to introduce other local changes (e.g., ligand–receptor interactions,[328,569] coordination,[570–571] pH-response,[494] ionic interaction,[572] redox reactions,[518,573–576] bioorthogonal reactions[513,575,577–578], and dynamic covalent bonds[579–583]) into the substrates of ENS for designing sophisticated molecular systems that can control emergent properties of molecular assemblies and modulate cellular functions.

Molecules and molecular processes.

While its essence is to use reactions to control assemblies, ENS has been explored under other names, such as enzyme-responsive assembly, biocatalytic self-assembly, enzyme-instructed self-assembly, enzyme-assisted self-assembly, or directed assembly, which are familiar to chemists. In fact, some of the studies may unknowingly involve enzyme reactions to generate assemblies, such as the synthetic polymers that use peptides as pendants,[584] or may be helped by ENS, such as the attempt to carry out enzymatic polymerization[585] in vivo.[586] The molecular building blocks used for exploring ENS are largely peptides because the bioactivities of peptides and considerable advances in the self-assembly of peptides.[384,587–590] Other building blocks, such as small organic molecules,[591–594] lipids,[595] polymers,[596] proteins,[27,597–598] nanoparticles,[599] or drug candidates,[600–601] for self-assembly should be useful as the substrates for ENS as well. The most important advantage of ENS is to confer functions to molecular processes. This feature, functions by kinetics or

by rate control,[429] is a feature of life. Thus, further advancing ENS research will impact both basic and translational biomedical research, including understanding cell biology and addressing the challenges in oncology, neuroscience, and infectious diseases. Having the ability to make (almost) any sophisticated molecule and the understanding of noncovalent interactions, chemists are well-equipped to develop molecular assemblies with emergent properties and to explore the functions of molecular processes by ENS. Since nature uses ENS for functions, ENS is a universal theme for understanding the functions and locations of molecular ensembles in cellular environments. For example, from the perspective of ENS, it would be easy to understand liquid-liquid phase separation[29] in cells and to design approaches for controlling those biochemical phenomena, though they appear to be biophysical. On the other hand, the exploration of enzyme-controlled noncovalent synthesis in the context of cells will open a new paradigm of supramolecular assemblies in cell biology. Thus, providing a necessary path for functions,[602] such as controlling cell fate, understanding diseases, and developing therapeutics. Certainly, many challenges remain. The ENS of man-made molecules, compared to that of natural molecules, is still relatively primitive. But the path for functions clearly centers on chemistry.[603–604] The interdisciplinary collaboration of chemists, biochemists, molecular biologists, physicists, physiologists, structural biologists, clinicians as well as engineers will likely meet those challenges and make exciting discoveries in the future research of controlling molecular assemblies by reactions.

Acknowledgements:

This work was partially supported by NIH (R01CA142746 and R21CA252364) and NSF (MRSEC-2011846).

Biography of the authors:

Hongjian He obtained his bachelor's degree from Tongji University, Shanghai, China, in 2015. He joined Brandeis University as a graduate student in 2015. He is currently in his fifth year as a graduate student in the Department of Chemistry with Prof. Bing Xu at Brandeis University. His current works focus on the design of molecular self-assembly for mitochondria targeting.

Weiyi Tan obtained his B.S. degree in the College of Chemistry, Chemical Engineering and Material Science at Soochow University in 2018. He is currently in his second year as a graduate student in chemistry supervised under Prof. Bing Xu at Brandeis University. His current research interest lies in designing self-assembling materials for biological applications.

Jiaqi Guo received her B.S. degree in chemical biology from Xiamen University in 2018. In the same year, she joined the laboratory of Prof. Bing Xu at Brandeis University where she is now a third-year graduate student focusing on peptide assemblies and their emergent properties in cells.

Meihui Yi obtained her B.S. degree in the School of Chemistry and Materials Science at Nanjing Normal University in 2018. During her undergraduate study, she investigated

mesoporous silica nanomotor. Now she is a third-year graduate student in Prof. Bing Xu's lab at Brandeis University. Her research interest focuses on designing peptide assemblies for cancer therapy.

Adrianna N. Shy obtained her B.S. degree in chemistry from Hampton University in 2017. She was admitted to Brandeis University that same year where she joined the laboratory of Prof. Bing Xu. Currently, she is a fourth year PhD candidate where she focuses on the self-assembly of small peptides for various applications.

Bing Xu, after receiving his BS and MS from Nanjing University in 1987 and 1990, respectively, obtained his PhD under the supervision of Prof. Timothy Swager in 1996 from the University of Pennsylvania. Before starting his independent research at the Hong Kong University of Science and Technology (HKUST) on the Aug. 2000, he was an NIH postdoctoral fellow in the Whitesides lab at Harvard University. He was tenured as an associated professor in Jan 2006 and became a full professor in July 2008 at HKUST before moving to Brandeis. Based on his works at HKUST and Brandeis, Bing Xu is identified on the "Highly-Cited Researchers 2014 in Chemistry" list. He has made contributions to metallogels, biofunctional magnetic nanoparticles, self-delivery drugs, enzyme-responsive materials, and supramolecular hydrogels. His current research focuses on enzymatic noncovalent synthesis in materials, biology, and medicine.

Abbreviations

3D	three-dimensional
AAK1	AP2-associated protein kinase 1
ABCD3	ATP-binding cassette sub-family D member 3
ABPs	actin binding proteins
AchE	acetylcholinesterase
ACP	acid phosphatase
ADAM	disintegrin and metalloproteinase domain-containing protein
ADP	adenosine diphosphate
Ake	adenylate kinase
Akt	protein kinase B
ALP	alkaline phosphatase
ALPL	tissue non-specific alkaline phosphatase
AMP	adenosine monophosphate
AP2	adaptor protein 2

AP2M1	AP2 complex subunit mu
Ap5A	diadenosine-5-pentaphosphate
ARL2	ADP-ribosylation factor-like protein 2
ASC	the adaptor molecule apoptosis-associated speck-like protein containing a CARD
ATG4B	autophagy-related protein 4 homolog B
Atg11	Autophagy-related protein 11
Atg30	autophagy-related protein 30
Atg36	autophagy-related protein 36
ATL	atlastin
ATP	adenosine triphosphate
AURKB	aurora B kinase
BAY	BAY 11–7085
Bla	β-lactamase
BLP	bacillus licheniformis protease
BMP-1	bone morphogenetic protein 1
BOD1	bi-orientation of chromosomes in cell division 1
BRCC3	Lys-63-specific deubiquitinase BRCC36
BTZ	bortezomib
BUBR1	BUB1-related kinase 1
CAFs	cancer associated fibroblasts
CARD	caspase activation and recruitment domain
CBs	Cajal bodies
CBT	cyanobenzothiazole
CBX5	chromobox protein homolog 5
CCK2R	cholecystokinin-2 receptor
CCP	clathrin-coated pit
Cdc28	Cdk1 protein kinase
CD	chromodomain

CD95	tumor necrosis factor receptor superfamily member 6
CDDP	cisplatin
CDK1	cyclin–cyclin-dependent kinase1
CES	carboxylesterases
CEST	chemical exchange saturation transfer magnetic resonance
CFTR	cystic fibrosis transmembrane conductance regulator
CIL	contact inhibition of locomotion
CITK	citron Rho-interacting kinase
CK	casein kinase-2
CLSM	confocal laser scanning microscopy
CME	clathrin-mediated endocytosis
Cnn	centrosomin
COX-2	cyclooxygenase-2
CPEB1	cytoplasmic polyadenylation element-binding protein 1
CPK	space-filling calotte
CPT	camptothecin
CRB	chlorambucil
CRPC	castration-resistant prostate cancer
CSD	chromoshadowdomain
nano-CT	nano-computed tomography
CTD	carboxy-terminal domain
CTE	C-terminal extension
CTSB	cathepsin B
CTP	cytidine triphosphate
CTPS	cytidine triphosphate synthase
ecCTPS	*E. coli* cytidine triphosphate synthase
hCTPS1	human cytidine triphosphate synthase 1
Cyt c	cytochrome c
DAPI	4′,6-diamidino-2-phenylindole

DC	dendritic cell
DCP1a	mRNA-decapping enzyme 1A
Dex	dexamethasone
DFC	dense fibrillar component
DFO	deferoxamine
DMEM	
DNA	deoxyribonucleic acid
mtDNA	mitochondria DNA
DNS	dansyl chloride
DOTA	1,4,7,10-tetraazacyclododecane-1,4,7,10-tetraacetic acid
Dox	doxorubicin
DR4/5	death receptor 4/5
dSTORM	direct stochastic optical reconstruction microscopy
E1	ubiquitin-activating enzyme
E2	ubiquitin-conjugating enzyme
E3	ubiquitin ligase
ECM	extracellular matrix
ECS	enzymatic covalent synthesis
EDC4	mRNA-decapping protein 4
EGFR	epidermal growth factor receptor
EIF4ENIF1	eukaryotic translation initiation factor 4E transporter
EISA	enzyme-instructed self-assembly
cryo-EM	cryo-electron microscopy
ENS	enzymatic noncovalent synthesis
ENTK	
ER	endoplasmic reticulum
ERK	mitogen-activated protein kinase
ESCRT-I	endosomal sorting complex I required for transport
ESCRT-II	endosomal sorting complex II required for transport

ESCRT-III	endosomal sorting complex III required for transport
ELYS	embryonic large molecule derived from yolk sac
F-actin	filamented actin
FA	Focal adhesion
FAK	focal adhesion kinase
FAP-α	fibroblast activation protein-α
FBL	fibrillarin
FBS	fetal bovine serum
FC	fibrillar center
FITM	fat storage-inducing transmembrane protein
Fmoc	N-(fluorenyl-methoxycarbonyl)
FLAG	Asp-Tyr-Lys-Asp-Asp-Asp-Asp-Lys
FRAP	fluorescence recovery after photobleaching
FRET	fluorescence resonance energy transfer
G-actin	globular actin
GC	granular component
GDP	guanosine diphosphate
GFP	green fluorescent protein
GGT	γ-glutamyltranspeptidase
GLB1	β-galactosidase
GRASP65	Golgi peripheral membrane protein p65
GLU1	glucose transporter
GSH	glutathione
GTP	guanosine triphosphate
H2B	histone protein 2B
HADC6	histone deacetylase
HCPT	10-hydroxy camptothecin
HER2	Receptor tyrosine-protein kinase erbB-2
HP1α	heterochromatin protein 1 homolog alpha

HP1	heterochromatin protein 1
Hrr25	casein kinase I homolog HRR25
ICG	indocyanine green
IF	Intermediate filament
cIF	cytoplasmic intermediate filament
IFB-1	intermediate filament protein B1
IGF-1	insulin-like growth factor-I
IGF-1R	IGF-1 receptor
IKKε	IκB kinase-ε
IL 1	intermediate layer 1
IL 2	intermediate layer 2
IMPDH	inosine-5’-monophosphate dehydrogenase
INM	inner nuclear membrane
ITAM	immunoreceptor tyrosine-based activation motif
ITIM	immunoreceptor tyrosine based inhibitory motif
JNK	c-Jun N-terminal kinase
KIF2B	kinesin family member 2B
LCST	lower critical solution temperature
LD	lipid droplet
LEASA	localized enzyme-assisted self-assembly
LPP	lambda protein phosphatase
LRP6	low-density lipoprotein receptor-related protein 6
LSPR	localized surface plasmon resonance
L-STM	liquid-phase scanning tunneling microscopy
MAP	microtubule-associate protein
MAPK	mitogen-activated protein kinase
MKLP1/KIF23	mitotic kinesin-like protein 1
MAVS	mitochondrial antiviral-signaling protein
MDR	multidrug-resistance

MEKK3	Mitogen-activated protein kinase kinase kinase 3
MEL28	maternal effect lethal protein 28
MM	midbody matrix
MMP-2	matrix metalloproteinase-2
MMP-7	matrix metalloproteinase-7
MMP-9	
MPA	mycophenolic acid
MRI	magnetic resonance imaging
MRLC	myosins regulatory light-chain
Mps1	monopolar spindle protein 1
MT	microtubule
cMT	cytoplasmic microtubules
k–MT	kinetochore–microtubule
nMT	nuclear microtubule
MLKL	mixed lineage kinase domain-like protein
MTOC	microtubule-organizing center
MTT	3-(4,5-dimethylthiazol-2-yl)-2,5-diphenyltetrazolium bromide
MYPT1	protein phosphatase 1 regulatory subunit 12A
NBD	nitrobenzoxadiazole
NBR1	next to BRCA1 gene 1 protein
ND10	nuclear domain 10
NE	nuclear envelope
NECAP	adaptin ear-binding coat-associated protein 1
NF-κB	nuclear factor kappa-light-chain-enhancer of activated B cells
NIR	near-infrared
NLRP3	NACHT, LRR and PYD domains-containing protein 3
NMR	nuclear magnetic resonance
NPs	nanoparticles

NPC	nuclear pore complexes
NPM	nucleophosmin
NPM-N	N-terminal domain of NPM
NS	nuclear speckles
NSAID	nonsteroidal anti-inflammatory drug
NTE	N-terminal extension
Nup153	nuclear pore complex protein Nup153
OGT	O-GlcNAc transferase
Olsa	olsalazine
ONM	outer nuclear membrane
OVA	ovalbumin
p14arf	p14ARF/p16INK4a fusion protein
p16INK4a	cyclin-dependent kinase 4 inhibitor A
p21	cyclin-dependent kinase inhibitor 1
p42ERK	p42 extracellular signal-regulated kinase
p53	tumor protein p53
PA	photoacoustic
PAP	prostatic acid phosphatase
P-bodies	processing bodies
PBS	phosphate-buffered saline
PCM	pericentriolar material
PDI	perylene diimide
PDT	photodynamic therapy
PE	primary human pancreatic epithelial cells
PEG	polyethylene glycol
PEO	polyethylene glycol
PET	positron emission tomography
PEX5	peroxin-5
Pex14	peroxin-14

sPGP	supramolecular phosphoglycopeptide
PHF	paired helical filament
PI3K	phosphatidylinositol 4,5-bisphosphate 3-kinase
PIDA	photo-induced disassembly
PKA	protein kinase A
PKD	protein kinase D
Pkh1/2	3-phosphoinositide-dependent protein kinase 1/2
PLK1	polo-like kinase 1
PML	promyelocytic leukemia protein
Pol I	POL polyprotein I
Polo	serine/threonine-protein kinase polo
PP1	protein phosphatase 1
PP1α	serine/threonine-protein phosphatase PP1-alpha
PP1γ	serine/threonine-protein phosphatase PP1-gamma
PP2A	serine/threonine-protein phosphatase 2A
PPI	protein-protein interaction
PpiX	protoporphyrin IX
PRC1	protein regulator of cytokinesis 1
iPSCs	induced pluripotent stem cells
PtdIns(x,y)Pn	phosphatidylinositol x,y-n-phosphate
PTM	posttranslational modification
PTP1B	protein tyrosine phosphatase
PTT	photothermal therapy
PYD	pyrin domain
QD	quantum dot
RBCC	N-terminal RING finger/B-box/coiled coil
RER	rough endoplasmic reticulum
RGD	Arg-Gly-Asp
Rheb	Ras homolog enriched in brain

RhoA	Ras homolog family member A
RhoA-GTP	Rho family of GTPases
RhoA-GAP	RhoA GTPase-accelerating proteins
Rho-GEF	Rho guanin exchange factor
RIG-I	retinoic acid-inducible gene 1 protein
RIPK1	receptor-interacting serine/threonine-protein kinase 1
RIPK3	receptor-interacting serine/threonine-protein kinase 1
mRNA	messenger RNA
sRNP	small nuclear ribonucleoprotein
ROK	Rho-associated protein kinase
ROMP	ring-opening metathesis polymerization
ROMPISA	ROMP induced self-assembly
ROS	reactive oxygen species
RR	rods and ring
RS	arginine/serine repeat
SEM	scanning electron microscopy
SER	smooth endoplasmic reticulum
Sey1P	
SF	straight filaments
SH2	Src homology 2
SIM	SUMO–SUMO interacting motif
SMN	survival motor neuron protein
SMOC	supramolecular organization centers
SNP	silica nanoparticle
SNX9	sorting nexin-9
Spc42	spindle pole body component SPC42
Spd-2	spindle-defective protein 2
SPB	spindle pole bodies
SQSTM1	sequestosome-1

SR	serine rich
Src	proto-oncogene tyrosine-protein kinase Src
SRPK1	SRSF protein kinase 1
SRSF1	serine/arginine-rich splicing factor 1
SVs	synaptic vesicles
TAG	triacylglycerol
TAM	TAM (Tyro3, Axl, and Mer) kinase
TBK1	TANK-binding kinase 1
TCO	trans-cyclooctene
TEM	transmission electron microscopy
TER	tumor-specific excretion-retarded
TGase	transglutaminase
TKO	triple knockout
TMPRSS	transmembrane serine proteases
TNBC	triple negative breast cancer
TNFα	tumor necrosis factor alpha
TNFR1/2	tumor necrosis factor receptor 1/2
mTORC1	serine/threonine-protein kinase mTOR
TPP	triphenyl phosphinium
TRAIL	tumor necrosis factor related apoptosis inducing ligand
TRAILR	tumor necrosis factor related apoptosis inducing ligand receptor
TRIM25	E3 ubiquitin/ISG15 ligase TRIM25
Ub	ubiquitin
UBC9	SUMO-conjugating enzyme UBC9
ULF	unit length filament
UPR	unfolded protein response
USP36	ubiquitin carboxyl-terminal hydrolase 36
Vps27	vacuolar protein sorting-associated protein 27

VRK1	Serine/threonine-protein kinase VRK1
WRAP53	telomerase Cajal body protein 1
Yop1p	yeast homolog of the polyposis locus protein 1
ZO	zonula occludens

References.

(1). McCord JM; Fridovich I Superoxide Dismutase. An Enzymic Function for Erythrocuprein (Hemocuprein). J. Biol. Chem 1969, 244, 6049–6055. [PubMed: 5389100]

(2). Habig WH; Pabst MJ; Jakoby WB Glutathione S Transferases. The First Enzymatic Step in Mercapturic Acid Formation. J. Biol. Chem 1974, 249, 7130–7139. [PubMed: 4436300]

(3). Knowles JR Enzyme-Catalyzed Phosphoryl Transfer Reactions. Annu. Rev. Biochem 1980, 49, 877–919. [PubMed: 6250450]

(4). Conway EJ; Macdonnell E Carboxylase and Carbonic Acid [13]. Nature 1945, 156, 752–753. [PubMed: 21007636]

(5). Garner RL; Grannis GF Phosphogalactoisomerase. Science 1951, 114, 501–502. [PubMed: 14892777]

(6). Mazia D; Hinegardner RT Enzymes of DNA Synthesis in Nuclei of Sea Urchin Embryos. Proc. Natl. Acad. Sci. U.S.A 1963, 50, 148–156. [PubMed: 13934206]

(7). Atkinson DE Regulation of Enzyme Function. Annu. Rev. Microbiol 1969, 23, 47–68. [PubMed: 4900062]

(8). Lehn J-M Supramolecular Chemistry: Concepts and Perspectives; Wiley-VCH, 1995.

(9). Fruton JS Proteolytic Enzymes. Annu. Rev. Biochem 1947, 16, 35–54. [PubMed: 20259055]

(10). Wynne AM Non-Oxidative Enzymes. Annu. Rev. Biochem 1946, 15, 35–74. [PubMed: 20995963]

(11). Jencks WP Mechanism of Enzyme Action. Annu. Rev. Biochem 1963, 32, 639–676. [PubMed: 14140708]

(12). Boyer PD Mechanism of Enzyme Action. Annu. Rev. Biochem 1960, 29, 15–44. [PubMed: 13803583]

(13). Cleland WW Enzyme Kinetics. Annu. Rev. Biochem 1967, 36, 77–112. [PubMed: 18257716]

(14). Hammes GG; Wu CW Kinetics of Allosteric Enzymes. Annu. Rev. Biophys. Bioeng 1974, 3, 1–33. [PubMed: 4371650]

(15). Kirsch JF Mechanism of Enzyme Action. Annu. Rev. Biochem 1973, 42, 205–234. [PubMed: 4354313]

(16). Haschemeyer RH; De Harven E Electron Microscopy of Enzymes. Annu. Rev. Biochem 1974, 43, 279–301. [PubMed: 4136708]

(17). Sigman DS; Mooser G Chemical Studies of Enzyme Active Sites. Annu. Rev. Biochem 1975, 44, 899–931. [PubMed: 237464]

(18). Schlichting I; Berendzen J; Chu K; Stock AM; Maves SA; Benson DE; Sweet RM; Ringe D; Petsko GA; Sligar SG The Catalytic Pathway of Cytochrome P450cam at Atomic Resolution. Science 2000, 287, 1615–1622. [PubMed: 10698731]

(19). Niphakis MJ; Cravatt BF Enzyme Inhibitor Discovery by Activity-Based Protein Profiling. Annu. Rev. Biochem 2014, 83, 341–377. [PubMed: 24905785]

(20). Industrial Biotransformations; Liese A; Seelbach K; Wandrey C, Eds.; Wiley-VCH: Weiheim, 2006.

(21). Vaissier Welborn V; Head-Gordon T Computational Design of Synthetic Enzymes. Chem. Rev 2019, 119, 6613–6630. [PubMed: 30277066]

(22). Lewis JC; Coelho PS; Arnold FH Enzymatic Functionalization of Carbon-Hydrogen Bonds. Chem. Soc. Rev 2011, 40, 2003–2021. [PubMed: 21079862]

(23). Giver L; Gershenson A; Freskgard PO; Arnold FH Directed Evolution of a Thermostable Esterase. Proc. Natl. Acad. Sci. U.S.A 1998, 95, 12809–12813. [PubMed: 9788996]

(24). Arnold FH Design by Directed Evolution. Acc. Chem. Res 1998, 31, 125–131.

(25). Mildvan AS Mechanism of Enzyme Action. Annu. Rev. Biochem 1974, 43, 357–399. [PubMed: 4212156]

(26). Alberts B The Cell as a Collection of Protein Machines: Preparing the Next Generation of Molecular Biologists. Cell 1998, 92, 291–294. [PubMed: 9476889]

(27). Wu H; Fuxreiter M The Structure and Dynamics of Higher-Order Assemblies: Amyloids, Signalosomes, and Granules. Cell 2016, 165, 1055–1066. [PubMed: 27203110]

(28). Du M; Chen ZJ DNA-Induced Liquid Phase Condensation of Cgas Activates Innate Immune Signaling. Science 2018, 361, 704–709. [PubMed: 29976794]

(29). Kato M; McKnight SL A Solid-State Conceptualization of Information Transfer from Gene to Message to Protein. Annu. Rev. Biochem 2018, 87, 351–390. [PubMed: 29195049]

(30). Rai AK; Chen JX; Selbach M; Pelkmans L Kinase-Controlled Phase Transition of Membraneless Organelles in Mitosis. Nature 2018, 559, 211–216. [PubMed: 29973724]

(31). Reinkemeier CD; Girona GE; Lemke EA Designer Membraneless Organelles Enable Codon Reassignment of Selected Mrnas in Eukaryotes. Science 2019, 363, eaaw2644. [PubMed: 30923194]

(32). Nakamura H; Lee AA; Afshar AS; Watanabe S; Rho E; Razavi S; Suarez A; Lin YC; Tanigawa M; Huang B et al. Intracellular Production of Hydrogels and Synthetic Rna Granules by Multivalent Molecular Interactions. Nat. Mater 2018, 17, 79–89. [PubMed: 29115293]

(33). Woodruff JB; Hyman AA; Boke E Organization and Function of Non-Dynamic Biomolecular Condensates. Trends Biochem. Sci 2018, 43, 81–94. [PubMed: 29258725]

(34). Maharana S; Wang J; Papadopoulos DK; Richter D; Pozniakovsky A; Poser I; Bickle M; Rizk S; Guillen-Boixet J; Franzmann TM et al. Rna Buffers the Phase Separation Behavior of Prion-Like Rna Binding Proteins. Science 2018, 360, 918–921. [PubMed: 29650702]

(35). Boeynaems S; Alberti S; Fawzi NL; Mittag T; Polymenidou M; Rousseau F; Schymkowitz J; Shorter J; Wolozin B; Van Den Bosch L et al. Protein Phase Separation: A New Phase in Cell Biology. Trends Cell Biol. 2018, 28, 420–435. [PubMed: 29602697]

(36). Dolgin E Cell Biology's New Phase. Nature 2018, 555, 300–301.

(37). Yang Z; Gu H; Fu D; Gao P; Lam JK; Xu B Enzymatic Formation of Supramolecular Hydrogels. Adv. Mater 2004, 16, 1440–1444.

(38). Sanchez T; Chen DT; DeCamp SJ; Heymann M; Dogic Z Spontaneous Motion in Hierarchically Assembled Active Matter. Nature 2012, 491, 431–434. [PubMed: 23135402]

(39). Epstein IR; Xu B Reaction-Diffusion Processes at the Nano- and Microscales. Nat. Nanotechnol 2016, 11, 312–319. [PubMed: 27045215]

(40). Desai A; Mitchison TJ Microtubule Polymerization Dynamics. Annu. Rev. Cell Dev. Biol 1997, 13, 83–117. [PubMed: 9442869]

(41). Song N; Li T Regulation of Nlrp3 Inflammasome by Phosphorylation. Front Immunol 2018, 9, 2305. [PubMed: 30349539]

(42). Yang Y; Wang H; Kouadir M; Song H; Shi F Recent Advances in the Mechanisms of Nlrp3 Inflammasome Activation and Its Inhibitors. Cell Death Dis. 2019, 10, 128. [PubMed: 30755589]

(43). Orgel JP; Irving TC; Miller A; Wess TJ Microfibrillar Structure of Type I Collagen in Situ. Proc. Natl. Acad. Sci. U.S.A 2006, 103, 9001–9005. [PubMed: 16751282]

(44). Vardy ER; Catto AJ; Hooper NM Proteolytic Mechanisms in Amyloid-Beta Metabolism: Therapeutic Implications for Alzheimer's Disease. Trends Mol. Med 2005, 11, 464–472. [PubMed: 16153892]

(45). Johnson GV; Stoothoff WH Tau Phosphorylation in Neuronal Cell Function and Dysfunction. J. Cell Sci 2004, 117, 5721–5729. [PubMed: 15537830]

(46). Shin Y; Brangwynne CP Liquid Phase Condensation in Cell Physiology and Disease. Science 2017, 357, eaaf4382. [PubMed: 28935776]

(47). Ellis RJ Macromolecular Crowding: Obvious but Underappreciated. Trends Biochem. Sci 2001, 26, 597–604. [PubMed: 11590012]

(48). Zhou HX; Rivas G; Minton AP Macromolecular Crowding and Confinement: Biochemical, Biophysical, and Potential Physiological Consequences. Annu. Rev. Biophys 2008, 37, 375–397. [PubMed: 18573087]

(49). Rivas G; Minton AP Toward an Understanding of Biochemical Equilibria within Living Cells. Biophys. Rev 2018, 10, 241–253. [PubMed: 29235084]

(50). Munishkina LA; Cooper EM; Uversky VN; Fink AL The Effect of Macromolecular Crowding on Protein Aggregation and Amyloid Fibril Formation. J. Mol. Recognit 2004, 17, 456–464. [PubMed: 15362105]

(51). Derham BK; Harding JJ The Effect of the Presence of Globular Proteins and Elongated Polymers on Enzyme Activity. BBA - Proteins Proteom. 2006, 1764, 1000–1006.

(52). Jiang M; Guo Z Effects of Macromolecular Crowding on the Intrinsic Catalytic Efficiency and Structure of Enterobactin-Specific Isochorismate Synthase. J. Am. Chem. Soc 2007, 129, 730–731. [PubMed: 17243787]

(53). Thul PJ; Akesson L; Wiking M; Mahdessian D; Geladaki A; Ait Blal H; Alm T; Asplund A; Bjork L; Breckels LM et al. A Subcellular Map of the Human Proteome. Science 2017, 356, aal3321.

(54). Bugyi B; Kellermayer M The Discovery of Actin: "To See What Everyone Else Has Seen, and to Think What Nobody Has Thought". J Muscle Res Cell Motil 2020, 41, 3–9. [PubMed: 31093826]

(55). Straub FB; Feuer G Adenosinetriphosphate the Functional Group of Actin. Biochim. Biophys. Acta 1950, 4, 455–470.

(56). Bugyi B; Carlier MF Control of Actin Filament Treadmilling in Cell Motility. Annu. Rev. Biophys 2010, 39, 449–470. [PubMed: 20192778]

(57). Pollard TD; Borisy GG Cellular Motility Driven by Assembly and Disassembly of Actin Filaments. Cell 2003, 112, 453–465. [PubMed: 12600310]

(58). Doherty GJ; McMahon HT Mechanisms of Endocytosis. Annu. Rev. Biochem 2009, 78, 857–902. [PubMed: 19317650]

(59). Boldogh IR; Pon LA Interactions of Mitochondria with the Actin Cytoskeleton. BBA - Mole. Cell Res 2006, 1763, 450–462.

(60). Hatch AL; Gurel PS; Higgs HN Novel Roles for Actin in Mitochondrial Fission. J. Cell Sci 2014, 127, 4549–4560. [PubMed: 25217628]

(61). Betzig E; Patterson GH; Sougrat R; Lindwasser OW; Olenych S; Bonifacino JS; Davidson MW; Lippincott-Schwartz J; Hess HF Imaging Intracellular Fluorescent Proteins at Nanometer Resolution. Science 2006, 313, 1642–1645. [PubMed: 16902090]

(62). Burridge K; Chrzanowska-Wodnicka M Focal Adhesions, Contractility, and Signaling. Annu. Rev. Cell Dev. Bi 1996, 12, 463–519.

(63). Rao JN; Madasu Y; Dominguez R Mechanism of Actin Filament Pointed-End Capping by Tropomodulin. Science 2014, 345, 463–467. [PubMed: 25061212]

(64). Chou SZ; Pollard TD Mechanism of Actin Polymerization Revealed by Cryo-Em Structures of Actin Filaments with Three Different Bound Nucleotides. Proc. Natl. Acad. Sci. U.S.A 2019, 116, 4265–4274. [PubMed: 30760599]

(65). Johnston JA; Ward CL; Kopito RR Aggresomes: A Cellular Response to Misfolded Proteins. J. Cell Biol 1998, 143, 1883–1898. [PubMed: 9864362]

(66). Kopito RR Aggresomes, Inclusion Bodies and Protein Aggregation. Trends Cell Biol. 2000, 10, 524–530. [PubMed: 11121744]

(67). Junn E; Lee SS; Suhr UT; Mouradian MM Parkin Accumulation in Aggresomes Due to Proteasome Impairment. J. Biol. Chem 2002, 277, 47870–47877. [PubMed: 12364339]

(68). Olzmann JA; Li A; Chudaev MV; Chen J; Perez FA; Palmiter RD; Chin LS Parkin-Mediated K63-Linked Polyubiquitination Targets Misfolded Dj-1 to Aggresomes Via Binding to Hdac6. J. Cell Biol 2007, 178, 1025–1038. [PubMed: 17846173]

(69). Burnett BG; Pittman RN The Polyglutamine Neurodegenerative Protein Ataxin 3 Regulates Aggresome Formation. Proc. Natl. Acad. Sci. U.S.A 2005, 102, 4330–4335. [PubMed: 15767577]

(70). García-Mata R; Bebök Z; Sorscher EJ; Sztul ES Characterization and Dynamics of Aggresome Formation by a Cytosolic Gfp- Chimera. J. Cell Biol 1999, 146, 1239–1254. [PubMed: 10491388]

(71). Doxsey S Re-Evaluating Centrosome Function. Nat. Rev. Mo.l Cell. Biol 2001, 2, 688–698.

(72). Humphrey JE Nucleoli and Centrosomes. Ann. Bot-london 1894, os-8, 373–376.

(73). Raff JW Phase Separation and the Centrosome: A Fait Accompli? Trends Cell Biol. 2019, 29, 612–622. [PubMed: 31076235]

(74). Sillibourne JE; Bornens M Polo-Like Kinase 4: The Odd One out of the Family. Cell Division 2010, 5, 25. [PubMed: 20920249]

(75). D'Avino PP How to Scaffold the Contractile Ring for a Safe Cytokinesis - Lessons from Anillin-Related Proteins. J. Cell Sci 2009, 122, 1071–1079. [PubMed: 19339546]

(76). D'Avino PP; Giansanti MG; Petronczki M Cytokinesis in Animal Cells. Cold Spring Harb. Perspect. Biol 2015, 7, a015834. [PubMed: 25680833]

(77). Bashkirov VI; Scherthan H; Solinger JA; Buerstedde JM; Heyer WD A Mouse Cytoplasmic Exoribonuclease (Mxrn1p) with Preference for G4 Tetraplex Substrates. J. Cell Biol 1997, 136, 761–773. [PubMed: 9049243]

(78). Parker R; Sheth U P Bodies and the Control of Mrna Translation and Degradation. Mol. Cell 2007, 25, 635–646. [PubMed: 17349952]

(79). Hubstenberger A; Courel M; Benard M; Souquere S; Ernoult-Lange M; Chouaib R; Yi Z; Morlot JB; Munier A; Fradet M et al. P-Body Purification Reveals the Condensation of Repressed Mrna Regulons. Mol. Cell 2017, 68, 144–157 e145. [PubMed: 28965817]

(80). Youn JY; Dunham WH; Hong SJ; Knight JDR; Bashkurov M; Chen GI; Bagci H; Rathod B; MacLeod G; Eng SWM et al. High-Density Proximity Mapping Reveals the Subcellular Organization of Mrna-Associated Granules and Bodies. Mol. Cell 2018, 69, 517–532 e511. [PubMed: 29395067]

(81). Eulalio A; Behm-Ansmant I; Schweizer D; Izaurralde E P-Body Formation Is a Consequence, Not the Cause, of Rna-Mediated Gene Silencing. Mol. Cell Biol 2007, 27, 3970–3981. [PubMed: 17403906]

(82). Serman A; Le Roy F; Aigueperse C; Kress M; Dautry F; Weil D Gw Body Disassembly Triggered by Sirnas Independently of Their Silencing Activity. Nucleic. Acids. Res 2007, 35, 4715–4727. [PubMed: 17604308]

(83). Andrei MA; Ingelfinger D; Heintzmann R; Achsel T; Rivera-Pomar R; Luhrmann R A Role for Eif4e and Eif4e-Transporter in Targeting Mrnps to Mammalian Processing Bodies. RNA 2005, 11, 717–727. [PubMed: 15840819]

(84). Kim Y; Myong S Rna Remodeling Activity of Dead Box Proteins Tuned by Protein Concentration, Rna Length, and Atp. Mol. Cell 2016, 63, 865–876. [PubMed: 27546789]

(85). Mugler CF; Hondele M; Heinrich S; Sachdev R; Vallotton P; Koek AY; Chan LY; Weis K Atpase Activity of the Dead-Box Protein Dhh1 Controls Processing Body Formation. Elife 2016, 5, e18746. [PubMed: 27692063]

(86). Rzeczkowski K; Beuerlein K; Muller H; Dittrich-Breiholz O; Schneider H; Kettner-Buhrow D; Holtmann H; Kracht M C-Jun N-Terminal Kinase Phosphorylates Dcp1a to Control Formation of P Bodies. J. Cell Biol 2011, 194, 581–596. [PubMed: 21859862]

(87). Tenekeci U; Poppe M; Beuerlein K; Buro C; Muller H; Weiser H; Kettner-Buhrow D; Porada K; Newel D; Xu M et al. K63-Ubiquitylation and Traf6 Pathways Regulate Mammalian P-Body Formation and Mrna Decapping. Mol. Cell 2016, 62, 943–957. [PubMed: 27315556]

(88). Kagan JC; Magupalli VG; Wu H Smocs: Supramolecular Organizing Centres That Control Innate Immunity. Nat. Rev. Immunol 2014, 14, 821–826. [PubMed: 25359439]

(89). Lu A; Magupalli VG; Ruan J; Yin Q; Atianand MK; Vos MR; Schroeder GF; Fitzgerald KA; Wu H; Egelman EH Unified Polymerization Mechanism for the Assembly of Asc-Dependent Inflammasomes. Cell 2014, 156, 1193–1206. [PubMed: 24630722]

(90). Goedert M Tau Filaments in Neurodegenerative Diseases. FEBS. Lett 2018, 592, 2383–2391. [PubMed: 29790176]

(91). Fitzpatrick AWP; Falcon B; He S; Murzin AG; Murshudov G; Garringer HJ; Crowther RA; Ghetti B; Goedert M; Scheres SHW Cryo-Em Structures of Tau Filaments from Alzheimer's Disease. Nature 2017, 547, 185–190. [PubMed: 28678775]

(92). Drewes G Marking Tau for Tangles and Toxicity. Trends Biochem. Sci 2004, 29, 548–555. [PubMed: 15450610]

(93). Wang JZ; Grundke-Iqbal I; Iqbal K Kinases and Phosphatases and Tau Sites Involved in Alzheimer Neurofibrillary Degeneration. Eur. J. Neurosci 2007, 25, 59–68. [PubMed: 17241267]

(94). Wainaina MN; Chen Z; Zhong C Environmental Factors in the Development and Progression of Late-Onset Alzheimer's Disease. Neurosci. Bull 2014, 30, 253–270. [PubMed: 24664867]

(95). Hengartner MO The Biochemistry of Apoptosis. Nature 2000, 407, 770–776. [PubMed: 11048727]

(96). Shi Y Mechanical Aspects of Apoptosome Assembly. Curr. Opin. Cell Biol 2006, 18, 677–684. [PubMed: 17046227]

(97). Baud V; Karin M Signal Transduction by Tumor Necrosis Factor and Its Relatives. Trends Cell Biol. 2001, 11, 372–377. [PubMed: 11514191]

(98). Wajant H; Pfizenmaier K; Scheurich P Tumor Necrosis Factor Signaling. Cell Death Differ. 2003, 10, 45–65. [PubMed: 12655295]

(99). Schulte M; Reiss K; Lettau M; Maretzky T; Ludwig A; Hartmann D; de Strooper B; Janssen O; Saftig P Adam10 Regulates Fasl Cell Surface Expression and Modulates Fasl-Induced Cytotoxicity and Activation-Induced Cell Death. Cell Death Differ. 2007, 14, 1040–1049. [PubMed: 17290285]

(100). Hanada K.-i.; Wang QJ; Inozume T; Yang JC Molecular Identification of an Mhc-Independent Ligand Recognized by a Human A/B T-Cell Receptor. Blood 2011, 117, 4816–4825. [PubMed: 21300979]

(101). Black RA; Rauch CT; Kozlosky CJ; Peschon JJ; Slack JL; Wolfson MF; Castner BJ; Stocking KL; Reddy P; Srinivasan S et al. A Metalloproteinase Disintegrin That Releases Tumor-Necrosis Factor-A from Cells. Nature 1997, 385, 729–733. [PubMed: 9034190]

(102). Zhou J; Xu B Enzyme-Instructed Self-Assembly: A Multistep Process for Potential Cancer Therapy. Bioconjugate. Chem 2015, 26, 987–999.

(103). Powers RE; Wang S; Liu TY; Rapoport TA Reconstitution of the Tubular Endoplasmic Reticulum Network with Purified Components. Nature 2017, 543, 257. [PubMed: 28225760]

(104). Hu J; Prinz WA; Rapoport TA Weaving the Web of Er Tubules. Cell 2011, 147, 1226–1231. [PubMed: 22153070]

(105). Wrobel AG; Kadlecova Z; Kamenicky J; Yang JC; Herrmann T; Kelly BT; McCoy AJ; Evans PR; Martin S; Muller S et al. Temporal Ordering in Endocytic Clathrin-Coated Vesicle Formation Via Ap2 Phosphorylation. Dev. Cell 2019, 50, 494–508 e411. [PubMed: 31430451]

(106). Agajanian MJ; Walker MP; Axtman AD; Ruela-de-Sousa RR; Serafin DS; Rabinowitz AD; Graham DM; Ryan MB; Tamir T; Nakamichi Y et al. Wnt Activates the Aak1 Kinase to Promote Clathrin-Mediated Endocytosis of Lrp6 and Establish a Negative Feedback Loop. Cell Rep. 2019, 26, 79–93 e78. [PubMed: 30605688]

(107). Geiger B; Spatz JP; Bershadsky AD Environmental Sensing through Focal Adhesions. Nat. Rev. Mol. Cell Bio 2009, 10, 21–33. [PubMed: 19197329]

(108). Burridge K; Fath K; Kelly T; Nuckolls G; Turner C Focal Adhesions: Transmembrane Junctions between the Extracellular Matrix and the Cytoskeleton. Annu. Rev. Cell Biol 1988, 4, 487–525. [PubMed: 3058164]

(109). Geiger B; Bershadsky A; Pankov R; Yamada KM Transmembrane Crosstalk between the Extracellular Matrix and the Cytoskeleton. Nat. Rev. Mol. Cell Bio 2001, 2, 793–805. [PubMed: 11715046]

(110). Westhoff MA; Serrels B; Fincham VJ; Frame MC; Carragher NO Src-Mediated Phosphorylation of Focal Adhesion Kinase Couples Actin and Adhesion Dynamics to Survival Signaling. Mol. Cell Biol 2004, 24, 8113–8133. [PubMed: 15340073]

(111). Kulkarni-Gosavi P; Makhoul C; Gleeson PA Form and Function of the Golgi Apparatus: Scaffolds, Cytoskeleton and Signalling. FEBS. Lett 2019, 593, 2289–2305. [PubMed: 31378930]

(112). Barr FA; Puype M; Vandekerckhove J; Warren G Grasp65, a Protein Involved in the Stacking of Golgi Cisternae. Cell 1997, 91, 253–262. [PubMed: 9346242]

(113). Huang S; Wang Y Golgi Structure Formation, Function, and Post-Translational Modifications in Mammalian Cells. F1000Res 2017, 6, 2050. [PubMed: 29225785]

(114). Lazarides E Intermediate Filaments as Mechanical Integrators of Cellular Space. Nature 1980, 283, 249–255. [PubMed: 7188712]

(115). Etienne-Manneville S Cytoplasmic Intermediate Filaments in Cell Biology. Annu. Rev. Cell Dev. Biol 2018, 34, 1–28. [PubMed: 30059630]

(116). Snider NT; Omary MB Post-Translational Modifications of Intermediate Filament Proteins: Mechanisms and Functions. Nat. Rev. Mo.l Cell. Biol 2014, 15, 163–177.

(117). Thompson LJ; Bollen M; Fields AP Identification of Protein Phosphatase 1 as a Mitotic Lamin Phosphatase. J. Biol. Chem 1997, 272, 29693–29697. [PubMed: 9368037]

(118). Kaminsky R; Denison C; Bening-Abu-Shach U; Chisholm AD; Gygi SP; Broday L Sumo Regulates the Assembly and Function of a Cytoplasmic Intermediate Filament Protein in C. Elegans. Dev. Cell 2009, 17, 724–735. [PubMed: 19922876]

(119). Tarbet HJ; Dolat L; Smith TJ; Condon BM; O'Brien ET 3rd; Valdivia RH; Boyce M Site-Specific Glycosylation Regulates the Form and Function of the Intermediate Filament Cytoskeleton. Elife 2018, 7, e31807. [PubMed: 29513221]

(120). Lopez CG; Saldanha O; Huber K; Koster S Lateral Association and Elongation of Vimentin Intermediate Filament Proteins: A Time-Resolved Light-Scattering Study. Proc. Natl. Acad. Sci. U.S.A 2016, 113, 11152–11157. [PubMed: 27655889]

(121). Boren J; Taskinen MR; Olofsson SO; Levin M Ectopic Lipid Storage and Insulin Resistance: A Harmful Relationship. J. Intern. Med 2013, 274, 25–40. [PubMed: 23551521]

(122). Jackson CL Lipid Droplet Biogenesis. Curr. Opin. Cell Biol 2019, 59, 88–96. [PubMed: 31075519]

(123). Wang H; Becuwe M; Housden BE; Chitraju C; Porras AJ; Graham MM; Liu XN; Thiam AR; Savage DB; Agarwal AK et al. Seipin Is Required for Converting Nascent to Mature Lipid Droplets. Elife 2016, 5, e16582. [PubMed: 27564575]

(124). Hayes M; Choudhary V; Ojha N; Shin JJ; Han GS; Carman GM; Loewen CJ; Prinz WA; Levine T Fat Storage-Inducing Transmembrane (Fit or Fitm) Proteins Are Related to Lipid Phosphatase/Phosphotransferase Enzymes. Microb. Cell 2017, 5, 88–103. [PubMed: 29417057]

(125). Sui X; Arlt H; Brock KP; Lai ZW; DiMaio F; Marks DS; Liao M; Farese RV Jr.; Walther TC Cryo-Electron Microscopy Structure of the Lipid Droplet-Formation Protein Seipin. J. Cell Biol 2018, 217, 4080–4091. [PubMed: 30327422]

(126). Pyc M; Cai Y; Greer MS; Yurchenko O; Chapman KD; Dyer JM; Mullen RT Turning over a New Leaf in Lipid Droplet Biology. Trends Plant Sci. 2017, 22, 596–609. [PubMed: 28454678]

(127). Saftig P; Klumperman J Lysosome Biogenesis and Lysosomal Membrane Proteins: Trafficking Meets Function. Nat. Rev. Mol. Cell Bio 2009, 10, 623–635. [PubMed: 19672277]

(128). Radulovic M; Schink KO; Wenzel EM; Nahse V; Bongiovanni A; Lafont F; Stenmark H Escrt-Mediated Lysosome Repair Precedes Lysophagy and Promotes Cell Survival. Embo. J 2018, 37, e99753. [PubMed: 30314966]

(129). Guizetti J; Gerlich DW Escrt-Iii Polymers in Membrane Neck Constriction. Trends Cell Biol. 2012, 22, 133–140. [PubMed: 22240455]

(130). Morvan J; Rinaldi B; Friant S Pkh1/2-Dependent Phosphorylation of Vps27 Regulates Escrt-I Recruitment to Endosomes. Mol. Biol. Cell 2012, 23, 4054–4064. [PubMed: 22918958]

(131). Lawrence RE; Cho KF; Rappold R; Thrun A; Tofaute M; Kim DJ; Moldavski O; Hurley JH; Zoncu R A Nutrient-Induced Affinity Switch Controls Mtorc1 Activation by Its Rag Gtpase–Ragulator Lysosomal Scaffold. Nat. Cell Biol 2018, 20, 1052–1063. [PubMed: 30061680]

(132). Li P; Gu M; Xu H Lysosomal Ion Channels as Decoders of Cellular Signals. Trends Biochem. Sci 2019, 44, 110–124. [PubMed: 30424907]

(133). Al-Bassam J; Chang F Regulation of Microtubule Dynamics by Tog-Domain Proteins Xmap215/Dis1 and Clasp. Trends Cell Biol. 2011, 21, 604–614. [PubMed: 21782439]

(134). Manka SW; Moores CA Microtubule Structure by Cryo-Em: Snapshots of Dynamic Instability. Essays. Biochem 2018, 62, 737–751. [PubMed: 30315096]

(135). McIntosh JR; O'Toole E; Morgan G; Austin J; Ulyanov E; Ataullakhanov F; Gudimchuk N Microtubules Grow by the Addition of Bent Guanosine Triphosphate Tubulin to the Tips of Curved Protofilaments. J. Cell Biol 2018, 217, 2691–2708. [PubMed: 29794031]

(136). Gadadhar S; Bodakuntla S; Natarajan K; Janke C The Tubulin Code at a Glance. J. Cell Sci 2017, 130, 1347–1353. [PubMed: 28325758]

(137). Seybold C; Schiebel E Spindle Pole Bodies. Curr. Biol 2013, 23, R858–860. [PubMed: 24112974]

(138). Jaspersen SL; Huneycutt BJ; Giddings TH Jr.; Resing KA; Ahn NG; Winey M Cdc28/Cdk1 Regulates Spindle Pole Body Duplication through Phosphorylation of Spc42 and Mps1. Dev. Cell 2004, 7, 263–274. [PubMed: 15296722]

(139). Liu X; Winey M The Mps1 Family of Protein Kinases. Annu. Rev. Biochem 2012, 81, 561–585. [PubMed: 22482908]

(140). Weiss E; Winey M The Saccharomyces Cerevisiae Spindle Pole Body Duplication Gene Mps1 Is Part of a Mitotic Checkpoint. J. Cell Biol 1996, 132, 111–123. [PubMed: 8567717]

(141). Castillo AR; Meehl JB; Morgan G; Schutz-Geschwender A; Winey M The Yeast Protein Kinase Mps1p Is Required for Assembly of the Integral Spindle Pole Body Component Spc42p. J. Cell Biol 2002, 156, 453–465. [PubMed: 11827982]

(142). D'Avino PP; Capalbo L Regulation of Midbody Formation and Function by Mitotic Kinases. Semin. Cell Dev. Biol 2016, 53, 57–63. [PubMed: 26802517]

(143). Capalbo L; Bassi ZI; Geymonat M; Todesca S; Copoiu L; Enright AJ; Callaini G; Riparbelli MG; Yu L; Choudhary JS et al. The Midbody Interactome Reveals Unexpected Roles for Pp1 Phosphatases in Cytokinesis. Nat. Commun 2019, 10, 4513. [PubMed: 31586073]

(144). Green DR; Kroemer G The Pathophysiology of Mitochondrial Cell Death. Science 2004, 305, 626–629. [PubMed: 15286356]

(145). McBride HM; Neuspiel M; Wasiak S Mitochondria: More Than Just a Powerhouse. Curr. Biol 2006, 16, R551–R560. [PubMed: 16860735]

(146). Kujoth GC; Hiona A; Pugh TD; Someya S; Panzer K; Wohlgemuth SE; Hofer T; Seo AY; Sullivan R; Jobling WA et al. Mitochondrial DNA Mutations, Oxidative Stress, and Apoptosis in Mammalian Aging. Science 2005, 309, 481–484. [PubMed: 16020738]

(147). Balaban RS; Nemoto S; Finkel T Mitochondria, Oxidants, and Aging. Cell 2005, 120, 483–495. [PubMed: 15734681]

(148). Pattingre S; Tassa A; Qu XP; Garuti R; Liang XH; Mizushima N; Packer M; Schneider MD; Levine B Bcl-2 Antiapoptotic Proteins Inhibit Beclin 1-Dependent Autophagy. Cell 2005, 122, 927–939. [PubMed: 16179260]

(149). Green DR; Reed J, C. Mitochondria and Apoptosis. Science 1998, 281, 1309–1312. [PubMed: 9721092]

(150). Nunnari J; Suomalainen A Mitochondria: In Sickness and in Health. Cell 2012, 148, 1145–1159. [PubMed: 22424226]

(151). Wallace DC; Zheng XX; Lott MT; Shoffner JM; Hodge JA; Kelley RI; Epstein CM; Hopkins LC Familial Mitochondrial Encephalomyopathy (Merrf) - Genetic, Pathophysiological, and Biochemical-Characterization of a Mitochondrial-DNA Disease. Cell 1988, 55, 601–610. [PubMed: 3180221]

(152). Giles RE; Blanc H; Cann HM; Wallace DC Maternal Inheritance of Human Mitochondrial-DNA. Proc.Natl. Acad.Sci.U. S. A 1980, 77, 6715–6719. [PubMed: 6256757]

(153). Cuervo AM; Bergamini E; Brunk UT; Dröge W; Ffrench M; Terman A Autophagy and Aging: The Importance of Maintaining "Clean" Cells. Autophagy 2014, 1, 131–140.

(154). Wang W; Wang Y; Long J; Wang J; Haudek SB; Overbeek P; Chang BH; Schumacker PT; Danesh FR Mitochondrial Fission Triggered by Hyperglycemia Is Mediated by Rock1 Activation in Podocytes and Endothelial Cells. Cell Metab. 2012, 15, 186–200. [PubMed: 22326220]

(155). Chan DC Fusion and Fission: Interlinked Processes Critical for Mitochondrial Health. Annu. Rev. Genet 2012, 46, 265–287. [PubMed: 22934639]

(156). Matoba S; Kang J-G; Patino WD; Wragg A; Boehm M; Gavrilova O; Hurley PJ; Bunz F; Hwang PM P53 Regulates Mitochondrial Respiration. Science 2006, 312, 1650–1653. [PubMed: 16728594]

(157). Zhao Q A Mitochondrial Specific Stress Response in Mammalian Cells. EMBO J. 2002, 21, 4411–4419. [PubMed: 12198143]

(158). Hou F; Sun L; Zheng H; Skaug B; Jiang QX; Chen ZJ Mavs Forms Functional Prion-Like Aggregates to Activate and Propagate Antiviral Innate Immune Response. Cell 2011, 146, 448–461. [PubMed: 21782231]

(159). Rawling DC; Fitzgerald ME; Pyle AM Establishing the Role of Atp for the Function of the Rig-I Innate Immune Sensor. Elife 2015, 4, e09391. [PubMed: 26371557]

(160). Chan YK; Gack MU Viral Evasion of Intracellular DNA and Rna Sensing. Nat. Rev. Microbiol 2016, 14, 360. [PubMed: 27174148]

(161). Xu H; He X; Zheng H; Huang LJ; Hou F; Yu Z; de la Cruz MJ; Borkowski B; Zhang X; Chen ZJ et al. Structural Basis for the Prion-Like Mavs Filaments in Antiviral Innate Immunity. Elife 2014, 3, e01489. [PubMed: 24569476]

(162). McIntosh JR; Landis SC The Distribution of Spindle Microtubules During Mitosis in Cultured Human Cells. J. Cell Biol 1971, 49, 468–497. [PubMed: 19866774]

(163). Walczak CE; Heald R Mechanisms of Mitotic Spindle Assembly and Function. Int. Rev. Cytol 2008, 265, 111–158. [PubMed: 18275887]

(164). Godek KM; Kabeche L; Compton DA Regulation of Kinetochore–Microtubule Attachments through Homeostatic Control During Mitosis. Nat. Rev. Mol. Cell Bio 2014, 16, 57. [PubMed: 25466864]

(165). Cioce M; Lamond AI Cajal Bodies: A Long History of Discovery. Annu. Rev. Cell Dev. Bi 2005, 21, 105–131.

(166). Hebert MD; Poole AR Towards an Understanding of Regulating Cajal Body Activity by Protein Modification. RNA Biol 2017, 14, 761–778. [PubMed: 27819531]

(167). Boisvert FM; Van Koningsbruggen S; Navascués J; Lamond AI The Multifunctional Nucleolus. Nat. Rev. Mol. Cell Bio 2007, 8, 574–585. [PubMed: 17519961]

(168). Zhong S; Salomoni P; Pandolfi PP The Transcription Role of Pml and the Nuclear Body. Nat. Cell Biol 2000, 2, E85–E90. [PubMed: 10806494]

(169). Maul GG Nuclear Domain 10, the Site of DNA Virus Transcription and Replication. Bioessays 1998, 20, 660–667. [PubMed: 9780840]

(170). Cantarero L; Sanz-García M; Vinograd-Byk H; Renbaum P; Levy-Lahad E; Lazo PA Vrk1 Regulates Cajal Body Dynamics and Protects Coilin from Proteasomal Degradation in Cell Cycle. Sci. Rep 2015, 5, 10543. [PubMed: 26068304]

(171). Enwerem II; Velma V; Broome HJ; Kuna M; Begum RA; Hebert MD Coilin Association with Box C/D Scarna Suggests a Direct Role for the Cajal Body Marker Protein in Scarnp Biogenesis. Biol. Open 2014, 3, 240–249. [PubMed: 24659245]

(172). Hoischen C; Monajembashi S; Weisshart K; Hemmerich P Multimodal Light Microscopy Approaches to Reveal Structural and Functional Properties of Promyelocytic Leukemia Nuclear Bodies. Front Oncol 2018, 8, 125. [PubMed: 29888200]

(173). Sun J; Xu H; Subramony SH; Hebert MD Interactions between Coilin and Piasy Partially Link Cajal Bodies to Pml Bodies. J. Cell Sci 2005, 118, 4995–5003. [PubMed: 16219678]

(174). Pena E; Berciano MT; Fernandez R; Ojeda JL; Lafarga M Neuronal Body Size Correlates with the Number of Nucleoli and Cajal Bodies, and with the Organization of the Splicing Machinery in Rat Trigeminal Ganglion Neurons. J. Comp. Neurol 2001, 430, 250–263. [PubMed: 11135260]

(175). von Appen A; Kosinski J; Sparks L; Ori A; DiGuilio AL; Vollmer B; Mackmull M-T; Banterle N; Parca L; Kastritis P et al. In Situ Structural Analysis of the Human Nuclear Pore Complex. Nature 2015, 526, 140. [PubMed: 26416747]

(176). Kosinski J; Mosalaganti S; von Appen A; Teimer R; DiGuilio AL; Wan W; Bui KH; Hagen WJ; Briggs JA; Glavy JS et al. Molecular Architecture of the Inner Ring Scaffold of the Human Nuclear Pore Complex. Science 2016, 352, 363–365. [PubMed: 27081072]

(177). Linder MI; Kohler M; Boersema P; Weberruss M; Wandke C; Marino J; Ashiono C; Picotti P; Antonin W; Kutay U Mitotic Disassembly of Nuclear Pore Complexes Involves Cdk1- and Plk1-Mediated Phosphorylation of Key Interconnecting Nucleoporins. Dev. Cell 2017, 43, 141–156 e147. [PubMed: 29065306]

(178). Huguet F; Flynn S; Vagnarelli P The Role of Phosphatases in Nuclear Envelope Disassembly and Reassembly and Their Relevance to Pathologies. Cells 2019, 8, 687.

(179). Hattersley N; Cheerambathur D; Moyle M; Stefanutti M; Richardson A; Lee KY; Dumont J; Oegema K; Desai A A Nucleoporin Docks Protein Phosphatase 1 to Direct Meiotic Chromosome Segregation and Nuclear Assembly. Dev. Cell 2016, 38, 463–477. [PubMed: 27623381]

(180). Trinkle-Mulcahy L; Andersen J; Lam YW; Moorhead G; Mann M; Lamond AI Repo-Man Recruits Pp1 Gamma to Chromatin and Is Essential for Cell Viability. J. Cell Biol 2006, 172, 679–692. [PubMed: 16492807]

(181). Vagnarelli P; Ribeiro S; Sennels L; Sanchez-Pulido L; de Lima Alves F; Verheyen T; Kelly DA; Ponting CP; Rappsilber J; Earnshaw WC Repo-Man Coordinates Chromosomal Reorganization with Nuclear Envelope Reassembly During Mitotic Exit. Dev. Cell 2011, 21, 328–342. [PubMed: 21820363]

(182). Weberruss M; Antonin W Perforating the Nuclear Boundary - How Nuclear Pore Complexes Assemble. J. Cell Sci 2016, 129, 4439–4447. [PubMed: 27856507]

(183). Lamond AI; Spector DL Nuclear Speckles: A Model for Nuclear Organelles. Nat. Rev. Mol. Cell Bio 2003, 4, 605–612. [PubMed: 12923522]

(184). Galganski L; Urbanek MO; Krzyzosiak WJ Nuclear Speckles: Molecular Organization, Biological Function and Role in Disease. Nucleic. Acids. Res 2017, 45, 10350–10368. [PubMed: 28977640]

(185). Chen Y; Belmont AS Genome Organization around Nuclear Speckles. Curr. Opin. Genet. Dev 2019, 55, 91–99. [PubMed: 31394307]

(186). Sanchez-Hernandez N; Prieto-Sanchez S; Moreno-Castro C; Munoz-Cobo JP; El Yousfi Y; Boyero-Corral S; Sune-Pou M; Hernandez-Munain C; Sune C Targeting Proteins to Rna Transcription and Processing Sites within the Nucleus. Int. J. Biochem. Cell Biol 2017, 91, 194–202. [PubMed: 28600144]

(187). Aubol BE; Hailey KL; Fattet L; Jennings PA; Adams JA Redirecting Sr Protein Nuclear Trafficking through an Allosteric Platform. J. Mol. Biol 2017, 429, 2178–2191. [PubMed: 28576472]

(188). Mitrea DM; Grace CR; Buljan M; Yun MK; Pytel NJ; Satumba J; Nourse A; Park CG; Madan Babu M; White SW et al. Structural Polymorphism in the N-Terminal Oligomerization Domain of Npm1. Proc. Natl. Acad. Sci. U.S.A 2014, 111, 4466–4471. [PubMed: 24616519]

(189). Mitrea DM; Cika JA; Guy CS; Ban D; Banerjee PR; Stanley CB; Nourse A; Deniz AA; Kriwacki RW Nucleophosmin Integrates within the Nucleolus Via Multi-Modal Interactions with Proteins Displaying R-Rich Linear Motifs and Rrna. Elife 2016, 5, e13571. [PubMed: 26836305]

(190). Luchinat E; Chiarella S; Franceschini M; Di Matteo A; Brunori M; Banci L; Federici L Identification of a Novel Nucleophosmin-Interaction Motif in the Tumor Suppressor P14arf. FEBS J. 2018, 285, 832–847. [PubMed: 29283500]

(191). Endo A; Matsumoto M; Inada T; Yamamoto A; Nakayama KI; Kitamura N; Komada M Nucleolar Structure and Function Are Regulated by the Deubiquitylating Enzyme Usp36. J. Cell Sci 2009, 122, 678–686. [PubMed: 19208757]

(192). Yao RW; Xu G; Wang Y; Shan L; Luan PF; Wang Y; Wu M; Yang LZ; Xing YH; Yang L et al. Nascent Pre-Rrna Sorting Via Phase Separation Drives the Assembly of Dense Fibrillar Components in the Human Nucleolus. Mol. Cell 2019, 76, 767–783. [PubMed: 31540874]

(193). Larson AG; Elnatan D; Keenen MM; Trnka MJ; Johnston JB; Burlingame AL; Agard DA; Redding S; Narlikar GJ Liquid Droplet Formation by Hp1α Suggests a Role for Phase Separation in Heterochromatin. Nature 2017, 547, 236. [PubMed: 28636604]

(194). Strom AR; Emelyanov AV; Mir M; Fyodorov DV; Darzacq X; Karpen GH Phase Separation Drives Heterochromatin Domain Formation. Nature 2017, 547, 241. [PubMed: 28636597]

(195). Oeljeklaus S; Schummer A; Mastalski T; Platta HW; Warscheid B Regulation of Peroxisome Dynamics by Phosphorylation. Biochim. Biophys. Acta 2016, 1863, 1027–1037. [PubMed: 26775584]

(196). Eberhart T; Kovacs WJ Pexophagy in Yeast and Mammals: An Update on Mysteries. Histochem. Cell Biol 2018, 150, 473–488. [PubMed: 30238155]

(197). Balla T Inositol-Lipid Binding Motifs: Signal Integrators through Protein-Lipid and Protein-Protein Interactions. J. Cell Sci 2005, 118, 2093–2104. [PubMed: 15890985]

(198). Najafov A; Mookhtiar AK; Luu HS; Ordureau A; Pan H; Amin PP; Li Y; Lu Q; Yuan J Tam Kinases Promote Necroptosis by Regulating Oligomerization of Mlkl. Mol. Cell 2019, 75, 457–468 e454. [PubMed: 31230815]

(199). Simons K; Toomre D Lipid Rafts and Signal Transduction. Nat. Rev. Mol. Cell Bio 2000, 1, 31–39. [PubMed: 11413487]

(200). Manning G; Whyte DB; Martinez R; Hunter T; Sudarsanam S The Protein Kinase Complement of the Human Genome. Science 2002, 298, 1912–1934. [PubMed: 12471243]

(201). Carcamo WC; Calise SJ; von Muhlen CA; Satoh M; Chan EK Molecular Cell Biology and Immunobiology of Mammalian Rod/Ring Structures. Int. Rev. Cell. Mol. Biol 2014, 308, 35–74. [PubMed: 24411169]

(202). Schiavon CR; Griffin ME; Pirozzi M; Parashuraman R; Zhou W; Jinnah HA; Reines D; Kahn RA Compositional Complexity of Rods and Rings. Mol. Biol. Cell 2018, 29, 2303–2316. [PubMed: 30024290]

(203). Lynch EM; Hicks DR; Shepherd M; Endrizzi JA; Maker A; Hansen JM; Barry RM; Gitai Z; Baldwin EP; Kollman JM Human Ctp Synthase Filament Structure Reveals the Active Enzyme Conformation. Nat. Struct. Mol. Biol 2017, 24, 507–514. [PubMed: 28459447]

(204). Pappas A; Yang WL; Park TS; Carman GM Nucleotide-Dependent Tetramerization of Ctp Synthetase from Saccharomyces Cerevisiae. J. Biol. Chem 1998, 273, 15954–15960. [PubMed: 9632643]

(205). Chanaday NL; Cousin MA; Milosevic I; Watanabe S; Morgan JR The Synaptic Vesicle Cycle Revisited: New Insights into the Modes and Mechanisms. J. Neurosci 2019, 39, 8209–8216. [PubMed: 31619489]

(206). Cesca F; Baldelli P; Valtorta F; Benfenati F The Synapsins: Key Actors of Synapse Function and Plasticity. Prog. Neurobiol 2010, 91, 313–348. [PubMed: 20438797]

(207). Takamori S; Holt M; Stenius K; Lemke EA; Gronborg M; Riedel D; Urlaub H; Schenck S; Brugger B; Ringler P et al. Molecular Anatomy of a Trafficking Organelle. Cell 2006, 127, 831–846. [PubMed: 17110340]

(208). Klement E; Medzihradszky KF Extracellular Protein Phosphorylation, the Neglected Side of the Modification. Mol. Cell Proteom 2017, 16, 1–7.

(209). Yalak G; Vogel V Extracellular Phosphorylation and Phosphorylated Proteins: Not Just Curiosities but Physiologically Important. Sci Signal 2012, 5, re7. [PubMed: 23250399]

(210). Kadler KE; Holmes DF; Trotter JA; Chapman JA Collagen Fibril Formation. Biochem. J 1996, 316 (Pt 1), 1–11. [PubMed: 8645190]

(211). Kadler KE Fell Muir Lecture: Collagen Fibril Formation in Vitro and in Vivo. Int. J. Exp. Pathol 2017, 98, 4–16. [PubMed: 28508516]

(212). Shilova ON; Shilov ES; Lieber A; Deyev SM Disassembling a Cancer Puzzle: Cell Junctions and Plasma Membrane as Targets for Anticancer Therapy. J. Control Release 2018, 286, 125–136. [PubMed: 30030181]

(213). Furuse M; Hirase T; Itoh M; Nagafuchi A; Yonemura S; Tsukita S; Tsukita S Occludin: A Novel Integral Membrane Protein Localizing at Tight Junctions. J. Cell Biol 1993, 123, 1777–1788. [PubMed: 8276896]

(214). Nishimura T; Takeichi M Chapter 2 Remodeling of the Adherens Junctions During Morphogenesis. Curr. Top. Dev. Biol 2009, 89, 33–54. [PubMed: 19737641]

(215). Proksch E; Brandner JM; Jensen JM The Skin: An Indispensable Barrier. Exp. Dermatol 2008, 17, 1063–1072. [PubMed: 19043850]

(216). Kumar NM; Gilula NB The Gap Junction Communication Channel. Cell 1996, 84, 381–388. [PubMed: 8608591]

(217). Herrmann H; Bar H; Kreplak L; Strelkov SV; Aebi U Intermediate Filaments: From Cell Architecture to Nanomechanics. Nat. Rev. Mo.l Cell. Biol 2007, 8, 562–573.

(218). Beutel O; Maraspini R; Pombo-Garcia K; Martin-Lemaitre C; Honigmann A Phase Separation of Zonula Occludens Proteins Drives Formation of Tight Junctions. Cell 2019, 179, 923–936 e911. [PubMed: 31675499]

(219). Dorfel MJ; Huber O Modulation of Tight Junction Structure and Function by Kinases and Phosphatases Targeting Occludin. J. Biomed. Biotechnol 2012, 2012, 807356. [PubMed: 22315516]

(220). Rao RK; Basuroy S; Rao VU; Karnaky KJ Jr.; Gupta A Tyrosine Phosphorylation and Dissociation of Occludin-Zo-1 and E-Cadherin-Beta-Catenin Complexes from the Cytoskeleton by Oxidative Stress. Biochem. J 2002, 368, 471–481. [PubMed: 12169098]

(221). Sallee JL; Burridge K Density-Enhanced Phosphatase 1 Regulates Phosphorylation of Tight Junction Proteins and Enhances Barrier Function of Epithelial Cells. J. Biol. Chem 2009, 284, 14997–15006. [PubMed: 19332538]

(222). Mitra SK; Hanson DA; Schlaepfer DD Focal Adhesion Kinase: In Command and Control of Cell Motility. Nat. Rev. Mol. Cell Bio 2005, 6, 56–68. [PubMed: 15688067]

(223). Hu BH; Messersmith PB Rational Design of Transglutaminase Substrate Peptides for Rapid Enzymatic Formation of Hydrogels. J. Am. Chem. Soc 2003, 125, 14298–14299. [PubMed: 14624577]

(224). Yang ZM; Xu B A Simple Visual Assay Based on Small Molecule Hydrogels for Detecting Inhibitors of Enzymes. Chem. Commun 2004, 2424–2425.

(225). Toledano S; Williams RJ; Jayawarna V; Ulijn RV Enzyme-Triggered Self-Assembly of Peptide Hydrogels Via Reversed Hydrolysis. J. Am. Chem. Soc 2006, 128, 1070–1071. [PubMed: 16433511]

(226). Yang ZM; Liang GL; Wang L; Xu B Using a Kinase/Phosphatase Switch to Regulate a Supramolecular Hydrogel and Forming the Supramolecular Hydrogel in Vivo. J. Am. Chem. Soc 2006, 128, 3038–3043. [PubMed: 16506785]

(227). Yang ZM; Xu KM; Guo ZF; Guo ZH; Xu B Intracellular Enzymatic Formation of Nanofibers Results in Hydrogelation and Regulated Cell Death. Adv. Mater 2007, 17, 3152–3156.

(228). Yang ZM; Ho PL; Liang GL; Chow KH; Wang QG; Cao Y; Guo ZH; Xu B Using Beta-Lactamase to Trigger Supramolecular Hydrogelation. J. Am. Chem. Soc 2007, 129, 266–267. [PubMed: 17212393]

(229). Yang ZM; Liang GL; Guo ZF; Guo ZH; Xu B Intracellular Hydrogelation of Small Molecules Inhibits Bacterial Growth. Angew. Chem. Intl. Ed 2007, 46, 8216–8219.

(230). Yang ZM; Liang GL; Ma ML; Gao Y; Xu B In Vitro and in Vivo Enzymatic Formation of Supramolecular Hydrogels Based on Self-Assembled Nanofibers of a Beta-Amino Acid Derivative. Small 2007, 3, 558–562. [PubMed: 17323399]

(231). Yang Z; Liang G; Xu B Enzymatic Control of the Self-Assembly of Small Molecules: A New Way to Generate Supramolecular Hydrogels. Soft Matter 2007, 3, 515–520. [PubMed: 32900012]

(232). Das AK; Collins R; Ulijn RV Exploiting Enzymatic (Reversed) Hydrolysis in Directed Self-Assembly of Peptide Nanostructures. Small 2008, 4, 279–287. [PubMed: 18214877]

(233). Wang QG; Yang ZM; Gao Y; Ge WW; Wang L; Xu B Enzymatic Hydrogelation to Immobilize an Enzyme for High Activity and Stability. Soft Matter 2008, 4, 550–553. [PubMed: 32907219]

(234). Yang Z; Liang G; Xu B Enzymatic Hydrogelation of Small Molecules. Acc. Chem. Res 2008, 41, 315–326. [PubMed: 18205323]

(235). Williams RJ; Smith AM; Collins R; Hodson N; Das AK; Ulijn RV Enzyme-Assisted Self-Assembly under Thermodynamic Control. Nat. Nanotechnol 2009, 4, 19–24. [PubMed: 19119277]

(236). Thornton K; Smith AM; Merry CLR; Ulijn RV Controlling Stiffness in Nanostructured Hydrogels Produced by Enzymatic Dephosphorylation. Biochem. Soc. T 2009, 37, 660–664.

(237). Das AK; Hirst AR; Ulijn RV Evolving Nanomaterials Using Enzyme-Driven Dynamic Peptide Libraries (Edpl). Faraday. Discuss 2009, 143, 293–303. [PubMed: 20334108]

(238). Yang Z; Ma M; Xu B Using Matrix Metalloprotease-9 (Mmp-9) to Trigger Supramolecular Hydrogelation. Soft Matter 2009, 5, 2546–2548.

(239). Gao Y; Kuang Y; Guo ZF; Guo ZH; Krauss IJ; Xu B Enzyme-Instructed Molecular Self-Assembly Confers Nanofibers and a Supramolecular Hydrogel of Taxol Derivative. J. Am. Chem. Soc 2009, 131, 13576–13577. [PubMed: 19731909]

(240). Gao J; Wang HM; Wang L; Wang JY; Kong DL; Yang ZM Enzyme Promotes the Hydrogelation from a Hydrophobic Small Molecule. J. Am. Chem. Soc 2009, 131, 11286–11287. [PubMed: 19630424]

(241). Miller AF; Guilbaud JB; Vey E; Boothroyd S; Smith AM; Ulijn RV; Saiani A Enzymatic Catalyzed Synthesis and Triggered Gelation of Ionic Peptides. Langmuir 2010, 26, 11297–11303. [PubMed: 20408518]

(242). Hirst AR; Roy S; Arora M; Das AK; Hodson N; Murray P; Marshall S; Javid N; Sefcik J; Boekhoven J et al. Biocatalytic Induction of Supramolecular Order. Nat. Chem 2010, 2, 1089–1094. [PubMed: 21107375]

(243). Li XM; Gao YA; Kuang Y; Xu B Enzymatic Formation of a Photoresponsive Supramolecular Hydrogel. Chem. Commun 2010, 46, 5364–5366.

(244). Wang HM; Ren CH; Song ZJ; Wang L; Chen XM; Yang ZM Enzyme-Triggered Self-Assembly of a Small Molecule: A Supramolecular Hydrogel with Leaf-Like Structures and an Ultra-Low Minimum Gelation Concentration. Nanotechnology 2010, 21, 1–5.

(245). Sadownik JW; Leckie J; Ulijn RV Micelle to Fibre Biocatalytic Supramolecular Transformation of an Aromatic Peptide Amphiphile. Chem. Commun 2011, 47, 728–730.

(246). Hughes M; Xu HX; Frederix PWJM; Smith AM; Hunt NT; Tuttle T; Kinloch IA; Ulijn RV Biocatalytic Self-Assembly of 2d Peptide-Based Nanostructures. Soft Matter 2011, 7, 10032–10038.

(247). Zhao F; Weitzel CS; Gao Y; Browdy HM; Shi JF; Lin HC; Lovett ST; Xu B Beta-Galactosidase-Instructed Formation of Molecular Nanofibers and a Hydrogel. Nanoscale 2011, 3, 2859–2861. [PubMed: 21637882]

(248). Li XM; Kuang Y; Shi JF; Gao Y; Lin HC; Xu B Multifunctional, Biocompatible Supramolecular Hydrogelators Consist Only of Nucleobase, Amino Acid, and Glycoside. J. Am. Chem. Soc 2011, 133, 17513–17518. [PubMed: 21928792]

(249). Zhao F; Gao Y; Shi J; Browdy HM; Xu B Novel Anisotropic Supramolecular Hydrogel with High Stability over a Wide Ph Range. Langmuir 2011, 27, 1510–1512. [PubMed: 21138331]

(250). Li XM; Kuang Y; Lin HC; Gao Y; Shi JF; Xu B Supramolecular Nanofibers and Hydrogels of Nucleopeptides. Angew. Chem. Int. Ed 2011, 50, 9365–9369.

(251). Gao J; Zheng W; Kong D; Yang Z Dual Enzymes Regulate the Molecular Self-Assembly of Tetra-Peptide Derivatives. Soft Matter 2011, 7, 10443–10448.

(252). Cao CY; Chen Y; Wu FZ; Deng Y; Liang GL Caspase-3 Controlled Assembly of Nanoparticles for Fluorescence Turn On. Chem. Commun 2011, 47, 10320–10322.

(253). Gao Y; Shi J; Yuan D; Xu B Imaging Enzyme-Triggered Self-Assembly of Small Molecules inside Live Cells. Nat. Commun 2012, 3, 1033. [PubMed: 22929790]

(254). Hughes M; Frederix PWJM; Raeburn J; Birchall LS; Sadownik J; Coomer FC; Lin IH; Cussen EJ; Hunt NT; Tuttle T et al. Sequence/Structure Relationships in Aromatic Dipeptide Hydrogels Formed under Thermodynamic Control by Enzyme-Assisted Self-Assembly. Soft Matter 2012, 8, 5595–5602.

(255). Du XW; Li JF; Gao Y; Kuang Y; Xu B Catalytic Dephosphorylation of Adenosine Monophosphate (Amp) to Form Supramolecular Nanofibers/Hydrogels. Chem. Commun 2012, 48, 2098–2100.

(256). Yang CH; Li DX; Liu Z; Hong G; Zhang J; Kong DL; Yang ZM Responsive Small Molecular Hydrogels Based on Adamantane-Peptides for Cell Culture. J. Phys. Chem. B 2012, 116, 633–638. [PubMed: 22111956]

(257). Li JY; Li XM; Kuang Y; Gao Y; Du XW; Shi JF; Xu B Self-Delivery Multifunctional Anti-Hiv Hydrogels for Sustained Release. Adv. Healthc. Mater 2013, 2, 1586–1590. [PubMed: 23616384]

(258). Li JY; Kuang Y; Gao Y; Du XW; Shi JF; Xu B D-Amino Acids Boost the Selectivity and Confer Supramolecular Hydrogels of a Nonsteroidal Anti-Inflammatory Drug (Nsaid). J. Am. Chem. Soc 2013, 135, 542–545. [PubMed: 23136972]

(259). Hughes M; Debnath S; Knapp CW; Ulijn RV Antimicrobial Properties of Enzymatically Triggered Self-Assembling Aromatic Peptide Amphiphiles. Biomater. Sci 2013, 1, 1138–1142. [PubMed: 32481936]

(260). Debnath S; Roy S; Ulijn RV Peptide Nanofibers with Dynamic Instability through Nonequilibrium Biocatalytic Assembly. J. Am. Chem. Soc 2013, 135, 16789–16792. [PubMed: 24147566]

(261). Gao Y; Kuang Y; Du XW; Zhou J; Chandran P; Horkay F; Xu B Imaging Self-Assembly Dependent Spatial Distribution of Small Molecules in a Cellular Environment. Langmuir 2013, 29, 15191–15200. [PubMed: 24266765]

(262). Scott G; Roy S; Abul-Haija YM; Fleming S; Bai S; Ulijn RV Pickering Stabilized Peptide Gel Particles as Tunable Microenvironments for Biocatalysis. Langmuir 2013, 29, 14321–14327. [PubMed: 24144273]

(263). Li J; Gao Y; Kuang Y; Shi J; Du X; Zhou J; Wang H; Yang Z; Xu B Dephosphorylation of D-Peptide Derivatives to Form Biofunctional, Supramolecular Nanofibers/Hydrogels and Their Potential Applications for Intracellular Imaging and Intratumoral Chemotherapy. J. Am. Chem. Soc 2013, 135, 9907–9914. [PubMed: 23742714]

(264). Gao Y; Berciu C; Kuang Y; Shi J; Nicastro D; Xu B Probing Nanoscale Self-Assembly of Nonfluorescent Small Molecules inside Live Mammalian Cells. Acs Nano 2013, 7, 9055–9063. [PubMed: 24067160]

(265). Gao J; Zheng WT; Zhang JM; Guan D; Yang ZM; Kong DL; Zhao Q Enzyme-Controllable Delivery of Nitric Oxide from a Molecular Hydrogel. Chem. Commun 2013, 49, 9173–9175.

(266). Tang AM; Wang WJ; Mei B; Hu WL; Wu M; Liang GL Devd-Based Hydrogelator Minimizes Cellular Apoptosis Induction. Sci. Rep 2013, 3, 1–7.

(267). Kuang Y; Shi J; Li J; Yuan D; Alberti KA; Xu Q; Xu B Pericellular Hydrogel/Nanonets Inhibit Cancer Cells. Angew. Chem. Intl. Ed 2014, 53, 8104–8107.

(268). Bai S; Debnath S; Gibson K; Schlicht B; Bayne L; Zagnoni M; Ulijn RV Biocatalytic Self-Assembly of Nanostructured Peptide Microparticles Using Droplet Microfluidics. Small 2014, 10, 285–293. [PubMed: 23913836]

(269). Zhou J; Du X; Gao Y; Shi J; Xu B Aromatic-Aromatic Interactions Enhance Interfiber Contacts for Enzymatic Formation of a Spontaneously Aligned Supramolecular Hydrogel. J. Am. Chem. Soc 2014, 136, 2970–2973. [PubMed: 24512553]

(270). Abul-Haija YM; Roy S; Frederix P; Javid N; Jayawarna V; Ulijn RV Biocatalytically Triggered Co-Assembly of Two-Component Core/Shell Nanofibers. Small 2014, 10, 973–979. [PubMed: 24027125]

(271). Yuan D; Zhou R; Shi J; Du X; Li X; Xu B Enzyme-Instructed Self-Assembly of Hydrogelators Consisting of Nucleobases, Amino Acids, and Saccharide. RSC Adv. 2014, 4, 26487–26490. [PubMed: 25071934]

(272). Shi J; Du X; Yuan D; Zhou J; Zhou N; Huang Y; Xu B D-Amino Acids Modulate the Cellular Response of Enzymatic-Instructed Supramolecular Nanofibers of Small Peptides. Biomacromolecules 2014, 15, 3559–3568. [PubMed: 25230147]

(273). Wang W; Qian J; Tang A; An L; Zhong K; Liang G Using Magnetic Resonance Imaging to Study Enzymatic Hydrogelation. Anal. Chem 2014, 86, 5955–5961. [PubMed: 24856317]

(274). Gao J; Shi Y; Wang YZ; Cai YB; Shen J; Kong DL; Yang ZM Enzyme-Controllable F-Nmr Turn on through Disassembly of Peptide-Based Nanospheres for Enzyme Detection. Org. Biomol. Chem 2014, 12, 1383–1386. [PubMed: 24457904]

(275). Pires RA; Abul-Haija YM; Costa DS; Novoa-Carballal R; Reis RL; Ulijn RV; Pashkuleva I Controlling Cancer Cell Fate Using Localized Biocatalytic Self-Assembly of an Aromatic Carbohydrate Amphiphile. J. Am. Chem. Soc 2015, 137, 576–579. [PubMed: 25539667]

(276). Wu D; Du X; Shi J; Zhou J; Zhou N; Xu B The First Cd73-Instructed Supramolecular Hydrogel. J. Colloid Interf. Sci 2015, 447, 269–272.

(277). Yuan D; Du X; Shi J; Zhou N; Zhou J; Xu B Mixing Biomimetic Heterodimers of Nucleopeptides to Generate Biocompatible and Biostable Supramolecular Hydrogels. Angew. Chem. Int. Ed 2015, 54, 5705–5708.

(278). Du X; Zhou J; Xu B Ectoenzyme Switches the Surface of Magnetic Nanoparticles for Selective Binding of Cancer Cells. J. Colloid Interf. Sci 2015, 447, 273–277.

(279). Xu C; Xing B; Rao J A Self-Assembled Quantum Dot Probe for Detecting Beta-Lactamase Activity. Biochem. Biophys. Res. Commun 2006, 344, 931–935. [PubMed: 16631595]

(280). Liang G; Ren H; Rao J A Biocompatible Condensation Reaction for Controlled Assembly of Nanostructures in Living Cells. Nat. Chem 2010, 2, 54–60. [PubMed: 21124381]

(281). Liang G; Ronald J; Chen Y; Ye D; Pandit P; Ma ML; Rutt B; Rao J Controlled Self-Assembling of Gadolinium Nanoparticles as Smart Molecular Magnetic Resonance Imaging Contrast Agents. Angew. Chem. Int. Ed 2011, 50, 6283–6286.

(282). Ye D; Liang G; Ma ML; Rao J Controlling Intracellular Macrocyclization for the Imaging of Protease Activity. Angew. Chem. Int. Ed 2011, 50, 2275–2279.

(283). Ye D; Pandit P; Kempen P; Lin J; Xiong L; Sinclair R; Rutt B; Rao J Redox-Triggered Self-Assembly of Gadolinium-Based Mri Probes for Sensing Reducing Environment. Bioconjugate. Chem 2014, 25, 1526–1536.

(284). Ye D; Shuhendler AJ; Cui L; Tong L; Tee SS; Tikhomirov G; Felsher DW; Rao J Bioorthogonal Cyclization-Mediated in Situ Self-Assembly of Small-Molecule Probes for Imaging Caspase Activity in Vivo. Nat. Chem 2014, 6, 519–526. [PubMed: 24848238]

(285). Ye D; Shuhendler AJ; Pandit P; Brewer KD; Tee SS; Cui L; Tikhomirov G; Rutt B; Rao J Caspase-Responsive Smart Gadolinium-Based Contrast Agent for Magnetic Resonance Imaging of Drug-Induced Apoptosis. Chem. Sci 2014, 5, 3845–3852.

(286). Du X; Zhou J; Shi J; Xu B Supramolecular Hydrogelators and Hydrogels: From Soft Matter to Molecular Biomaterials. Chem. Rev 2015, 115, 13165–13307. [PubMed: 26646318]

(287). Greenstein JP Distribution of Acid and Alkaline Phosphatase in Tumors, Normal Tissues, and the Tissues of Tumor-Bearing Rats and Mice. J. Natl. Cancer I 1942, 2, 511–524.

(288). Hof P; Pluskey S; Dhe-Paganon S; Eck MJ; Shoelson SE Crystal Structure of the Tyrosine Phosphatase Shp-2. Cell 1998, 92, 441–450. [PubMed: 9491886]

(289). Brautigan DL; Shenolikar S Protein Serine/Threonine Phosphatases: Keys to Unlocking Regulators and Substrates. Annu. Rev. Biochem 2018, 87, 921–964. [PubMed: 29925267]

(290). Rigden DJ The Histidine Phosphatase Superfamily: Structure and Function. Biochem. J 2008, 409, 333–348. [PubMed: 18092946]

(291). Thornton K; Abul-Haija Y; Hodson N; Ulijn R Mechanistic Insights into Phosphatase Triggered Self-Assembly Including Enhancement of Biocatalytic Conversion Rate. Soft Matter 2013, 9, 9430–9439.

(292). Ren C; Wang Z; Wang Q; Yang C; Liu J Self-Assembled Peptide-Based Nanoprobes for Disease Theranostics and Diseas-Related Molecular Imaging. Small Methods 2020, 4, 1900403.

(293). Mehwish N; Dou X; Zhao Y; Feng CL Supramolecular Fluorescent Hydrogelators as Bio-Imaging Probes. Mater. Horiz 2019, 6, 14–44.

(294). Kim BJ; Yang D; Xu B Emerging Applications of Supramolecular Peptide Assemblies. Trends Chem. 2019, 2, 71–83.

(295). Wang H; Feng Z; Xu B D-Amino Acid-Containing Supramolecular Nanofibers for Potential Cancer Therapeutics. Adv. Drug Deliver. Rev 2017, 110–111, 102–111.

(296). Gao J; Zhan J; Yang Z Enzyme-Instructed Self-Assembly (Eisa) and Hydrogelation of Peptides. Adv. Mater 2020, 32, 1805798.

(297). Yao Q; Huang Z; Liu D; Chen J; Gao Y Enzyme-Instructed Supramolecular Self-Assembly with Anticancer Activity. Adv. Mater 2019, 31, 1804814.

(298). Akkarachaneeyakorn K; Li M; Davis SA; Mann S Secretion and Reversible Assembly of Extracellular-Like Matrix by Enzyme-Active Colloidosome-Based Protocells. Langmuir 2016, 32, 2912–2919. [PubMed: 26981922]

(299). Kumar RK; Yu X; Patil AJ; Li M; Mann S Cytoskeletal-Like Supramolecular Assembly and Nanoparticle-Based Motors in a Model Protocell. Angew. Chem. Int. Ed 2011, 50, 9343–9347.

(300). Rodríguez-Arco L; Li M; Mann S Phagocytosis-Inspired Behaviour in Synthetic Protocell Communities of Compartmentalized Colloidal Objects. Nat. Mater 2017, 16, 857–863. [PubMed: 28604713]

(301). McGovern SL; Caselli E; Grigorieff N; Shoichet BK A Common Mechanism Underlying Promiscuous Inhibitors from Virtual and High-Throughput Screening. J. Med. Chem 2002, 45, 1712–1722. [PubMed: 11931626]

(302). Yuan D; Shi J; Du X; Huang Y; Gao Y; Baoum AA; Xu B The Enzyme-Instructed Assembly of the Core of Yeast Prion Sup35 to Form Supramolecular Hydrogels. J. Mater. Chem. B 2016, 4, 1318–1323. [PubMed: 27134750]

(303). Wang H; Luo Z; Wang Y; He T; Yang C; Ren C; Ma L; Gong C; Li X; Yang Z Enzyme-Catalyzed Formation of Supramolecular Hydrogels as Promising Vaccine Adjuvants. Adv. Funct. Mater 2016, 26, 1822–1829.

(304). Wang Y; Li X; Zhang Y; Wang L; Yang Z A Supramolecular Hydrogel to Boost the Production of Antibodies for Phosphorylated Proteins. Chem. Commun 2019, 55, 12388–12391.

(305). Wang YZ; Gao J; Yang ZM Short Peptide-Based Hydrogels: Mild Preparation Methods and Their Application as Vaccine Adjuvant. Acta Polym. Sin 2018, 9–20.

(306). Liu Y; Wang Y; Yu F; Zhang Z; Yang Z; Zhang W; Wang PG; Zhao W Potentiating the Immune Response of Muc1-Based Antitumor Vaccines Using a Peptide-Based Nanovector as a Promising Vaccine Adjuvant. Chem. Commun 2017, 53, 9486–9489.

(307). Luo Z; Wu Q; Yang C; Wang H; He T; Wang Y; Wang Z; Chen H; Li X; Gong C et al. A Powerful Cd8(+) T-Cell Stimulating D-Tetra-Peptide Hydrogel as a Very Promising Vaccine Adjuvant. Adv. Mater 2017, 29, 1601776.

(308). Wang Z; Cai Y; Yi L; Gao J; Yang Z Supramolecular Hydrogels of Indole-Capped Short Peptides as Vaccine Adjuvants. Chinese. J. Chem 2017, 35, 1057–1062.

(309). Wang Z; Liang C; Shi F; He T; Gong C; Wang L; Yang Z Cancer Vaccines Using Supramolecular Hydrogels of Nsaid-Modified Peptides as Adjuvants Abolish Tumorigenesis. Nanoscale 2017, 9, 14058–14064. [PubMed: 28895610]

(310). Wang Z; Shang Y; Tan Z; Li X; Li G; Ren C; Wang F; Yang Z; Liu J A Supramolecular Protein Chaperone for Vaccine Delivery. Theranostics 2020, 10, 657–670.

(311). Xu Y; Wang Y; Yang Q; Liu Z; Xiao Z; Le Z; Yang Z; Yang C A Versatile Supramolecular Nanoadjuvant That Activates Nf-Kb for Cancer Immunotherapy. Theranostics 2019, 9, 3388–3397. [PubMed: 31244959]

(312). Yang C; Shi F; Li C; Wang Y; Wang L; Yang Z Single Dose of Protein Vaccine with Peptide Nanofibers as Adjuvants Elicits Long-Lasting Antibody Titer. ACS Biomater-Sci. Eng 2018, 4, 2000–2006.

(313). Li X; Wang Y; Wang S; Liang C; Pu G; Chen Y; Wang L; Xu H; Shi Y; Yang Z A Strong Cd8(+) T Cell-Stimulating Supramolecular Hydrogel. Nanoscale 2020, 12, 2111–2117.

(314). Wang Z; Ma C; Shang Y; Yang L; Zhang J; Yang C; Ren C; Liu J; Fan G; Liu J Simultaneous Co-Assembly of Fenofibrate and Ketoprofen Peptide for the Dual-Targeted Treatment of Nonalcoholic Fatty Liver Disease (Nafld). Chem. Commun 2020, 56, 4922–4925.

(315). Yamagata N; Chen X; Zhou J; Li J; Du X; Xu B Enzymatic Self-Assembly of an Immunoreceptor Tyrosine-Based Inhibitory Motif (Itim). Org. Biomol. Chem 2017, 15, 5689–5692. [PubMed: 28675212]

(316). Janeway CJ; Travers P; Walport M; Shlomchik MJ Immunobiology: The Immune System in Health and Disease; 5 ed.; Garland Science: New York, 2001.

(317). Zhou J; Du X; Wang J; Yamagata N; Xu B Enzyme-Instructed Self-Assembly of Peptides Containing Phosphoserine to Form Supramolecular Hydrogels as Potential Soft Biomaterials. Front. Chem. Sci. Eng 2017, 11, 509–515. [PubMed: 29403673]

(318). Shu C; Li D; Li T; Ji S; Ding L Sensitive and Accurate Detection of Alp Activity Using a Fluorescence on-Off-on Switch and Mass Barcode Signal Amplification. RSC Adv. 2018, 8, 36527–36533.

(319). Shi J; Yuan D; Haburcak R; Zhang Q; Zhao C; Zhang X; Xu B Enzymatic Dissolution of Biocomposite Solids Consisting of Phosphopeptides to Form Supramolecular Hydrogels. Chem. Eur. J 2015, 21, 18047–18051. [PubMed: 26462722]

(320). Bai S; Pappas C; Debnath S; Frederix PW; Leckie J; Fleming S; Ulijn RV Stable Emulsions Formed by Self-Assembly of Interfacial Networks of Dipeptide Derivatives. ACS Nano 2014, 8, 7005–7013. [PubMed: 24896538]

(321). Moreira IP; Sasselli IR; Cannon DA; Hughes M; Lamprou DA; Tuttle T; Ulijn RV Enzymatically Activated Emulsions Stabilised by Interfacial Nanofibre Networks. Soft Matter 2016, 12, 2623–2631. [PubMed: 26905042]

(322). Moreira IP; Piskorz TK; Van Esch JH; Tuttle T; Ulijn RV Biocatalytic Self-Assembly of Tripeptide Gels and Emulsions. Langmuir 2017, 33, 4986–4995. [PubMed: 28463516]

(323). Yang C; Ren X; Ding D; Wang L; Yang Z Enzymatic Induction of Supramolecular Order and Bioactivity. Nanoscale 2016, 8, 10768–10773. [PubMed: 27161242]

(324). Zhan J; Cai Y; Ji S; He S; Cao Y; Ding D; Wang L; Yang Z Spatiotemporal Control of Supramolecular Self-Assembly and Function. ACS Appl. Mater. Interfaces 2017, 9, 10012–10018. [PubMed: 28252276]

(325). Wang Z; Liang C; Shang Y; He S; Wang L; Yang Z Narrowing the Diversification of Supramolecular Assemblies by Preorganization. Chem. Commun 2018, 54, 2751–2754.

(326). Liang C; Wang Z; Xu T; Chen Y; Zheng D; Zhang L; Zhang W; Yang Z; Shi Y; Gao J Preorganization Increases the Self-Assembling Ability and Antitumor Efficacy of Peptide Nanomedicine. ACS Appl. Mater. Interfaces 2020, 12, 22492–22498. [PubMed: 32352747]

(327). Shang Y; Wang Z; Zhang R; Li X; Zhang S; Gao J; Li X; Yang Z A Novel Thermogel System of Self-Assembling Peptides Manipulated by Enzymatic Dephosphorylation. Chem. Commun 2019, 55, 5123–5126.

(328). Haburcak R; Shi J; Du X; Yuan D; Xu B Ligand-Receptor Interaction Modulates the Energy Landscape of Enzyme-Instructed Self-Assembly of Small Molecules. J. Am. Chem. Soc 2016, 138, 15397–15404. [PubMed: 27797504]

(329). Reynolds PE Structure, Biochemistry and Mechanism of Action of Glycopeptide Antibiotics. Eur. J. Clin. Microbiol 1989, 8, 943–950.

(330). Bugg TDH; Wright GD; Walsh CT; Dutka-Malen S; Arthur M; Courvalin P Molecular Basis for Vancomycin Resistance in Enterococcus Faecium Bm4147: Biosynthesis of a Depsipeptide Peptidoglycan Precursor by Vancomycin Resistance Proteins Vanh and Vana. Biochemistry 1991, 30, 10408–10415. [PubMed: 1931965]

(331). Wang H; Shi J; Feng Z; Zhou R; Wang S; Rodal AA; Xu B An in Situ Dynamic Continuum of Supramolecular Phosphoglycopeptides Enables Formation of 3d Cell Spheroids. Angew. Chem. Int. Ed 2017, 56, 16297–16301.

(332). Wang H; Feng Z; Xu B Instructed Assembly as Context-Dependent Signaling for the Death and Morphogenesis of Cells. Angew. Chem. Int. Ed 2019, 58, 5567–5571.

(333). Huc I; Lehn JM Virtual Combinatorial Libraries: Dynamic Generation of Molecular and Supramolecular Diversity by Self-Assembly. Proc. Natl. Acad. Sci. U.S.A 1997, 94, 2106–2110. [PubMed: 9122156]

(334). Sreenivasachary N; Lehn JM Gelation-Driven Component Selection in the Generation of Constitutional Dynamic Hydrogels Based on Guanine-Quartet Formation. Proc. Natl. Acad. Sci. U.S.A 2005, 102, 5938–5943. [PubMed: 15840720]

(335). Boekhoven J; Hendriksen WE; Koper GJ; Eelkema R; van Esch JH Transient Assembly of Active Materials Fueled by a Chemical Reaction. Science 2015, 349, 1075–1079. [PubMed: 26339025]

(336). Sahoo JK; Pappas CG; Sasselli IR; Abul-Haija YM; Ulijn RV Biocatalytic Self-Assembly Cascades. Angew. Chem. Int. Ed 2017, 56, 6828–6832.

(337). Zhang S; Cortes W; Zhang Y Constructing Cross-Linked Nanofibrous Scaffold Via Dual-Enzyme-Instructed Hierarchical Assembly. Langmuir : the ACS journal of surfaces and colloids 2020, 36, 6261–6267. [PubMed: 32418429]

(338). Vigier-Carrière C; Garnier T; Wagner D; Lavalle P; Rabineau M; Hemmerlé J; Senger B; Schaaf P; Boulmedais F; Jierry L Bioactive Seed Layer for Surface-Confined Self-Assembly of Peptides. Angew. Chem. Int. Ed 2015, 54, 10198–10201.

(339). Criado-Gonzalez M; Fores JR; Carvalho A; Blanck C; Schmutz M; Kocgozlu L; Schaaf P; Jierry L; Boulmedais F Phase Separation in Supramolecular Hydrogels Based on Peptide Self-Assembly from Enzyme-Coated Nanoparticles. Langmuir 2019, 35, 10838–10845. [PubMed: 31334660]

(340). Criado-Gonzalez M; Rodon Fores J; Wagner D; Schröder AP; Carvalho A; Schmutz M; Harth E; Schaaf P; Jierry L; Boulmedais F Enzyme-Assisted Self-Assembly within a Hydrogel Induced by Peptide Diffusion. Chem. Commun 2019, 55, 1156–1159.

(341). Rodon Fores J; Criado-Gonzalez M; Schmutz M; Blanck C; Schaaf P; Boulmedais F; Jierry L Protein-Induced Low Molecular Weight Hydrogelator Self-Assembly through a Self-Sustaining Process. Chem. Sci 2019, 10, 4761–4766. [PubMed: 31160952]

(342). Rodon Fores J; Criado-Gonzalez M; Chaumont A; Carvalho A; Blanck C; Schmutz M; Serra CA; Boulmedais F; Schaaf P; Jierry L Supported Catalytically Active Supramolecular Hydrogels for Continuous Flow Chemistry. Angew. Chem. Int. Ed 2019, 58, 18817–18822.

(343). Yang C; Wang H; Li D; Wang L Molecular Hydrogels with Esterase-Like Activity. Chinese. J. Chem 2013, 31, 494–500.

(344). Xu T; Liang C; Ji S; Ding D; Kong D; Wang L; Yang Z Surface-Induced Hydrogelation for Fluorescence and Naked-Eye Detections of Enzyme Activity in Blood. Anal. Chem 2016, 88, 7318–7323. [PubMed: 27345959]

(345). Ji W; Zhang S; Yukawa S; Onomura S; Sasaki T; Miyazawa K; Zhang Y Regulating Higher-Order Organization through the Synergy of Two Self-Sorted Assemblies. Angew. Chem. Int. Ed 2018, 57, 3636–3640.

(346). Wang Y; Zhang Y; Li X; Li C; Yang Z; Wang L A Peptide-Based Supramolecular Hydrogel for Controlled Delivery of Amine Drugs. Chem. Asian J 2018, 13, 3460–3463. [PubMed: 29882291]

(347). Hai Z; Li J; Wu J; Xu J; Liang G Alkaline Phosphatase-Triggered Simultaneous Hydrogelation and Chemiluminescence. J. Am. Chem. Soc 2017, 139, 1041–1044. [PubMed: 28064496]

(348). Kuhnle H; Borner HG Biotransformation on Polymer-Peptide Conjugates: A Versatile Tool to Trigger Microstructure Formation. Angew. Chem. Int. Ed 2009, 48, 6431–6434.

(349). Shi J; Fichman G; Schneider JP Enzymatic Control of the Conformational Landscape of Self-Assembling Peptides. Angew. Chem. Int. Ed 2018, 57, 11188–11192.

(350). Hule RA; Nagarkar RP; Altunbas A; Ramay HR; Branco MC; Schneider JP; Pochan DJ Correlations between Structure, Material Properties and Bioproperties in Self-Assembled B;-Hairpin Peptide Hydrogels. Faraday. Discuss 2008, 139, 251–264. [PubMed: 19048999]

(351). Schneider JP; Pochan DJ; Ozbas B; Rajagopal K; Pakstis L; Kretsinger J Responsive Hydrogels from the Intramolecular Folding and Self-Assembly of a Designed Peptide. J. Am. Chem. Soc 2002, 124, 15030–15037. [PubMed: 12475347]

(352). Majumder P; Baxa U; Walsh STR; Schneider JP Design of a Multicompartment Hydrogel That Facilitates Time-Resolved Delivery of Combination Therapy and Synergized Killing of Glioblastoma. Angew. Chem. Int. Ed 2018, 57, 15040–15044.

(353). Lodish H Molecular Cell Biology; 5th ed.; W. H. Freeman Co.: New York, 2003.

(354). Webber MJ; Newcomb CJ; Bitton R; Stupp SI Switching of Self-Assembly in a Peptide Nanostructure with a Specific Enzyme. Soft Matter 2011, 7, 9665–9672. [PubMed: 22408645]

(355). Zheng Z; Sun H; Hu C; Li G; Liu X; Chen P; Cui Y; Liu J; Wang J; Liang G Using “on/Off” 19 F Nmr/Magnetic Resonance Imaging Signals to Sense Tyrosine Kinase/Phosphatase Activity in Vitro and in Cell Lysates. Anal. Chem 2016, 88, 3363–3368. [PubMed: 26901415]

(356). Zheng Z; Wang J; Chen P; Xie M; Zhang L; Hou Y; Zhang X; Jiang J; Wang J; Lu Q et al. Using L-Stm to Directly Visualize Enzymatic Self-Assembly/Disassembly of Nanofibers. Nanoscale 2016, 8, 15142–15146. [PubMed: 27492656]

(357). Wu C; Zheng Z; Guo Y; Tian C; Xue Q; Liang G Fluorine Substitution Enhances the Self-Assembling Ability of Hydrogelators. Nanoscale 2017, 9, 11429–11433. [PubMed: 28770916]

(358). Piejko M; Dec R; Babenko V; Hoang A; Szewczyk M; Mak P; Dzwolak W Highly Amyloidogenic Two-Chain Peptide Fragments Are Released Upon Partial Digestion of Insulin with Pepsin. J. Biol. Chem 2015, 290, 5947–5958. [PubMed: 25586185]

(359). Harris TJ; von Maltzahn G; Derfus AM; Ruoslahti E; Bhatia SN Proteolytic Actuation of Nanoparticle Self-Assembly. Angew. Chem. Int. Ed 2006, 45, 3161–3165.

(360). Guo F; Fu Q; Zhou K; Jin C; Wu W; Ji X; Yan Q; Yang Q; Wu D; Li A et al. Matrix Metalloprotein-Triggered, Cell Penetrating Peptide-Modified Star-Shaped Nanoparticles for Tumor Targeting and Cancer Therapy. J. Nanobiotech 2020, 18, 48.

(361). Wilhelm S; Tavares AJ; Dai Q; Ohta S; Audet J; Dvorak HF; Chan WCW Analysis of Nanoparticle Delivery to Tumours. Nat. Rev. Mater 2016, 1, 16014.

(362). Ayyub OB; Kofinas P Enzyme Induced Stiffening of Nanoparticle-Hydrogel Composites with Structural Color. ACS Nano 2015, 9, 8004–8011. [PubMed: 26196060]

(363). Ren C; Wang H; Mao D; Zhang X; Fengzhao Q; Shi Y; Ding D; Kong D; Wang L; Yang Z When Molecular Probes Meet Self-Assembly: An Enhanced Quenching Effect. Angew. Chem. Int. Ed 2015, 54, 4823–4827.

(364). Xie Y; Huang R; Qi W; Wang Y; Su R; He Z Enzyme-Substrate Interactions Promote the Self-Assembly of Amino Acid Derivatives into Supramolecular Hydrogels. J. Mater. Chem. B 2016, 4, 844–851. [PubMed: 32263156]

(365). Conte MP; Lau KHA; Ulijn RV Biocatalytic Self-Assembly Using Reversible and Irreversible Enzyme Immobilization. ACS Appl. Mater. Interfaces 2017, 9, 3266–3271. [PubMed: 28080020]

(366). Antalis TM; Buzza MS; Hodge KM; Hooper JD; Netzel-Arnett S The Cutting Edge: Membrane-Anchored Serine Protease Activities in the Pericellular Microenvironment. Biochem. J 2010, 428, 325–346. [PubMed: 20507279]

(367). He H; Wang J; Wang H; Zhou N; Yang D; Green DR; Xu B Enzymatic Cleavage of Branched Peptides for Targeting Mitochondria. J. Am. Chem. Soc 2018, 140, 1215–1218. [PubMed: 29328651]

(368). He H; Wang H; Zhou N; Yang D; Xu B Branched Peptides for Enzymatic Supramolecular Hydrogelation. Chem. Commun 2017, 54, 86–89.

(369). Pavlov IP; Thompson WH The Work of the Digestive Glands; Charles Griffin, 1902.

(370). Hopp TP; Prickett KS; Price VL; Libby RT; March CJ; Cerretti DP; Urdal DL; Conlon PJ A Short Polypeptide Marker Sequence Useful for Recombinant Protein Identification and Purification. Nat. Biotechnol 1988, 6, 1204–1210.

(371). Zhou J; Du X; Gao Y; Shi J; Xu B Aromatic–Aromatic Interactions Enhance Interfiber Contacts for Enzymatic Formation of a Spontaneously Aligned Supramolecular Hydrogel. J. Am. Chem. Soc 2014, 136, 2970–2973. [PubMed: 24512553]

(372). Jiang T; Shen S; Wang T; Li M; He B; Mo R A Substrate-Selective Enzyme-Catalysis Assembly Strategy for Oligopeptide Hydrogel-Assisted Combinatorial Protein Delivery. Nano Lett. 2017, 17, 7447–7454. [PubMed: 29172544]

(373). Li Y; Li W; Bao W; Liu B; Li D; Jiang Y; Wei W; Ren F Bioinspired Peptosomes with Programmed Stimuli-Responses for Sequential Drug Release and High-Performance Anticancer Therapy. Nanoscale 2017, 9, 9317–9324. [PubMed: 28426067]

(374). Ho CSJ; Rydstrom A; Trulsson M; Balfors J; Storm P; Puthia M; Nadeem A; Svanborg C Hamlet: Functional Properties and Therapeutic Potential. Future Oncol. 2012, 8, 1301–1313. [PubMed: 23130929]

(375). Vigier-Carrière C; Wagner D; Chaumont A; Durr B; Lupattelli P; Lambour C; Schmutz M; Hemmerlé J; Senger B; Schaaf P et al. Control of Surface-Localized, Enzyme-Assisted Self-Assembly of Peptides through Catalyzed Oligomerization. Langmuir 2017, 33, 8267–8276. [PubMed: 28749683]

(376). Feng L; Ren P; Hao L; Dong Q; Li J; Jian H; Wang M; Li X; Wang A; Bai S Fabrication of Short Peptide Cages by Interfacial Self-Assembly on Caco3 Templates. Coll.Surf. A: Physcochem. Eng. Asp 2019, 573, 22–29.

(377). Wright DB; Thompson MP; Touve MA; Carlini AS; Gianneschi NC Enzyme-Responsive Polymer Nanoparticles Via Ring-Opening Metathesis Polymerization-Induced Self-Assembly. Macromol. Rapid. Comm 2019, 40, 1800467.

(378). Wright DB; Ramírez-Hernández A; Touve MA; Carlini AS; Thompson MP; Patterson JP; De Pablo JJ; Gianneschi NC Enzyme-Induced Kinetic Control of Peptide-Polymer Micelle Morphology. ACS Macro Lett. 2019, 8, 676–681.

(379). Grisci G; Kozma E; Mróz W; Pagano K; Ragona L; Galeotti F Self-Assembly of a Water Soluble Perylene and Surfactant into Fluorescent Supramolecular Ensembles Sensitive to Acetylcholinesterase Activity. RSC Adv. 2016, 6, 64374–64382.

(380). Li RX; Shu C; Wang W; Wang XL; Li H; Xu DK; Zhong WY Encapsulation of 10-Hydroxy Camptothecin in Supramolecular Hydrogel as an Injectable Drug Delivery System. J. Pharm. Sci 2015, 104, 2266–2275. [PubMed: 25980666]

(381). Xu M; Zeng R; Xiang J; Yan Q Shaping Protein Amphiphilic Assemblies Via Allosteric Effect: From 1d Nanofilament to 2d Rectangular Nanosheet. J. Am. Chem. Soc 2019, 141, 13724–13728. [PubMed: 31434475]

(382). Walsh C Antibiotics: Actions, Origins, and Resistance; 1st ed.; ASM Press: Washington, D. C., 2003.

(383). Chien MP; Rush AM; Thompson MP; Gianneschi NC Programmable Shape-Shifting Micelles. Angew. Chem. Int. Ed 2010, 49, 5076–5080.

(384). Shy AN; Kim BJ; Xu B Enzymatic Noncovalent Synthesis of Supramolecular Soft Matter for Biomedical Applications. Matter 2019, 1, 1127–1147. [PubMed: 32104791]

(385). Cukierman E; Pankov R; Stevens DR; Yamada KM Taking Cell-Matrix Adhesions to the Third Dimension. Science 2001, 294, 1708–1712. [PubMed: 11721053]

(386). Imamura Y; Mukohara T; Shimono Y; Funakoshi Y; Chayahara N; Toyoda M; Kiyota N; Takao S; Kono S; Nakatsura T et al. Comparison of 2d- and 3d-Culture Models as Drug-Testing Platforms in Breast Cancer. Oncol. Rep 2015, 33, 1837–1843. [PubMed: 25634491]

(387). Falconnet D; Csucs G; Grandin HM; Textor M Surface Engineering Approaches to Micropattern Surfaces for Cell-Based Assays. Biomaterials. 2006, 27, 3044–3063. [PubMed: 16458351]

(388). Birgersdotter A; Sandberg R; Ernberg I Gene Expression Perturbation in Vitro--a Growing Case for Three-Dimensional (3d) Culture Systems. Semin. Cancer Biol 2005, 15, 405–412. [PubMed: 16055341]

(389). Weaver VM; Petersen OW; Wang F; Larabell CA; Briand P; Damsky C; Bissell MJ Reversion of the Malignant Phenotype of Human Breast Cells in Three-Dimensional Culture and in Vivo by Integrin Blocking Antibodies. J. Cell Biol 1997, 137, 231–245. [PubMed: 9105051]

(390). Bhadriraju K; Chen CS Engineering Cellular Microenvironments to Improve Cell-Based Drug Testing. Drug Discov. Today 2002, 7, 612–620. [PubMed: 12047872]

(391). Yamada KM; Cukierman E Modeling Tissue Morphogenesis and Cancer in 3d. Cell 2007, 130, 601–610. [PubMed: 17719539]

(392). Baharvand H; Hashemi SM; Kazemi Ashtiani S; Farrokhi A Differentiation of Human Embryonic Stem Cells into Hepatocytes in 2d and 3d Culture Systems in Vitro. Int. J. Dev. Biol 2006, 50, 645–652. [PubMed: 16892178]

(393). Benya PD; Shaffer JD Dedifferentiated Chondrocytes Reexpress the Differentiated Collagen Phenotype When Cultured in Agarose Gels. Cell 1982, 30, 215–224. [PubMed: 7127471]

(394). Nelson CM; Bissell MJ Modeling Dynamic Reciprocity: Engineering Three-Dimensional Culture Models of Breast Architecture, Function, and Neoplastic Transformation. Semin. Cancer Biol 2005, 15, 342–352. [PubMed: 15963732]

(395). Qi J; Yan Y; Cheng B; Deng L; Shao Z; Sun Z; Li X Enzymatic Formation of an Injectable Hydrogel from a Glycopeptide as a Biomimetic Scaffold for Vascularization. ACS Appl. Mater. Interfaces 2018, 10, 6180–6189. [PubMed: 29380599]

(396). Wang H; Feng Z; Xu B Intercellular Instructed-Assembly Mimics Protein Dynamics to Induce Cell Spheroids. J. Am. Chem. Soc 2019, 141, 7271–7274. [PubMed: 31033285]

(397). Russell-Jones G; McTavish K; McEwan J; Rice J; Nowotnik D Vitamin-Mediated Targeting as a Potential Mechanism to Increase Drug Uptake by Tumours. J. Inorg. Biochem 2004, 98, 1625–1633. [PubMed: 15458825]

(398). Röper K Integration of Cell-Cell Adhesion and Contractile Actomyosin Activity During Morphogenesis. Curr. Top. Dev. Biol 2015, 112, 103–127. [PubMed: 25733139]

(399). Saadaoui M; Rocancourt D; Roussel J; Corson F; Gros J A Tensile Ring Drives Tissue Flows to Shape the Gastrulating Amniote Embryo. Science 2020, 367, 453–458.

(400). Alert R; Trepat X Physical Models of Collective Cell Migration. Annu. Rev. Condens. Matter Phys 2020, 11, 77–101.

(401). Zhou R; Kuang Y; Zhou J; Du X; Li J; Shi J; Haburcak R; Xu B Nanonets Collect Cancer Secretome from Pericellular Space. PLoS One 2016, 11, e0154126. [PubMed: 27100780]

(402). Du X; Zhou J; Wang H; Shi J; Kuang Y; Zeng W; Yang Z; Xu B In Situ Generated D-Peptidic Nanofibrils as Multifaceted Apoptotic Inducers to Target Cancer Cells. Cell Death Dis. 2017, 8, e2614. [PubMed: 28206986]

(403). Yang D; Kim BJ; He H; Xu B Enzymatically Forming Cell Compatible Supramolecular Assemblies of Tryptophan-Rich Short Peptides Pept. Sci 2020, in press.

(404). Brito A; Pereira PMR; Soares da Costa D; Reis RL; Ulijn RV; Lewis JS; Pires RA; Pashkuleva I Inhibiting Cancer Metabolism by Aromatic Carbohydrate Amphiphiles That Act as Antagonists of the Glucose Transporter Glut1. Chem. Sci 2020, 11, 3737–3744.

(405). Tanaka A; Fukuoka Y; Morimoto Y; Honjo T; Koda D; Goto M; Maruyama T Cancer Cell Death Induced by the Intracellular Self-Assembly of an Enzyme-Responsive Supramolecular Gelator. J. Am. Chem. Soc 2015, 137, 770–775. [PubMed: 25521540]

(406). Schumacher TNM; Mayr LM; Minor DL Jr; Milhollen MA; Burgess MW; Kim PS Identification of D-Peptide Ligands through Mirror-Image Phage Display. Science 1996, 271, 1854–1857. [PubMed: 8596952]

(407). Eckert DM; Malashkevich VN; Hong LH; Carr PA; Kim PS Inhibiting Hiv-1 Entry: Discovery of D-Peptide Inhibitors That Target the Gp41 Coiled-Coil Pocket. Cell 1999, 99, 103–115. [PubMed: 10520998]

(408). Wei X; Zhan C; Shen Q; Fu W; Xie C; Gao J; Peng C; Zheng P; Lu W A D-Peptide Ligand of Nicotine Acetylcholine Receptors for Brain-Targeted Drug Delivery. Angew. Chem. Int. Ed 2015, 54, 3023–3027.

(409). Liu M; Li C; Pazgier M; Li C; Mao Y; Lv Y; Gu B; Wei G; Yuan W; Zhan C et al. D-Peptide Inhibitors of the P53-Mdm2 Interaction for Targeted Molecular Therapy of Malignant Neoplasms. Proc. Natl. Acad. Sci. U.S.A 2010, 107, 14321–14326. [PubMed: 20660730]

(410). He W; Yan J; Jiang W; Li S; Qu Y; Niu F; Yan Y; Sui F; Wang S; Zhou Y et al. Peptide-Induced Self-Assembly of Therapeutics into a Well-Defined Nanoshell with Tumor-Triggered Shape and Charge Switch. Chem. Mater 2018, 30, 7034–7046. [PubMed: 32982042]

(411). Zhou J; Du X; Li J; Yamagata N; Xu B Taurine Boosts Cellular Uptake of Small D -Peptides for Enzyme-Instructed Intracellular Molecular Self-Assembly. J. Am. Chem. Soc 2015, 137, 10040–10043. [PubMed: 26235707]

(412). Zhou J; Du X; Berciu C; Del Signore SJ; Chen X; Yamagata N; Rodal AA; Nicastro D; Xu B Cellular Uptake of a Taurine-Modified, Ester Bond-Decorated D-Peptide Derivative Via Dynamin-Based Endocytosis and Macropinocytosis. Mol. Ther 2018, 26, 648–658. [PubMed: 29396265]

(413). Liu Y; Miao Q; Zou P; Liu L; Wang X; An L; Zhang X; Qian X; Luo S; Liang G Enzyme-Controlled Intracellular Self-Assembly of 18f Nanoparticles for Enhanced Micropet Imaging of Tumor. Theranostics 2015, 5, 1058–1067. [PubMed: 26199645]

(414). Zheng Z; Tang A; Guan Y; Chen L; Wang F; Chen P; Wang W; Luo Y; Tian Y; Liang G Nanocomputed Tomography Imaging of Bacterial Alkaline Phosphatase Activity with an Iodinated Hydrogelator. Anal. Chem 2016, 88, 11982–11985. [PubMed: 27933762]

(415). Yuan Y; Wang L; Du W; Ding Z; Zhang J; Han T; An L; Zhang H; Liang G Intracellular Self-Assembly of Taxol Nanoparticles for Overcoming Multidrug Resistance. Angew. Chem. Int. Ed 2015, 54, 9700–9704.

(416). Wang D; Liang G 19f Mr Imaging Probe for Furin Detection in Vitro and in Living Cells. J. Univ. Sci. Tech. China 2015, 45, 112–116.

(417). Zhao X; Lv G; Li K; Peng Y; Liu Q; Qiu L; Lin J One-Step (18)F-Fluorination of Smart Positron Emission Tomography Tracer for Sensing Furin Activity in Tumors. Nucl. Med. Biol 2020, 82–83, 72–79.

(418). Mei B; Miao Q; Tang A; Liang G Enzyme-Instructed Self-Assembly of Taxol Promotes Axonal Branching. Nanoscale 2015, 7, 15605–15608. [PubMed: 26359218]

(419). Palner M; Shen B; Jeon J; Lin J; Chin FT; Rao J Preclinical Kinetic Analysis of the Caspase-3/7 Pet Tracer 18f-C-Snat: Quantifying the Changes in Blood Flow and Tumor Retention after Chemotherapy. J. Nucl. Med 2015, 56, 1415–1421. [PubMed: 26045308]

(420). Chen Z; Rao J Positron Emission Tomography Imaging of Tumor Apoptosis with a Caspase-Sensitive Nano-Aggregation Tracer [18f]C-Snat. Method Mol. Biol 2018, 1790, 181–195.

(421). Forman HJ; Zhang H; Rinna A Glutathione: Overview of Its Protective Roles, Measurement, and Biosynthesis. Mol. Asp. Med 2009, 30, 1–12.

(422). Li J; Kuang Y; Shi J; Zhou J; Medina JE; Zhou R; Yuan D; Yang C; Wang H; Yang Z et al. Enzyme-Instructed Intracellular Molecular Self-Assembly to Boost Activity of Cisplatin against Drug-Resistant Ovarian Cancer Cells. Angew. Chem. Int. Ed 2015, 54, 13307–13311.

(423). Li J; Shi J; Medina JE; Zhou J; Du X; Wang H; Yang C; Liu J; Yang Z; Dinulescu DM et al. Selectively Inducing Cancer Cell Death by Intracellular Enzyme-Instructed Self-Assembly (Eisa) of Dipeptide Derivatives. Adv. Healthc. Mater 2017, 6, 1601400.

(424). Huang P; Gao Y; Lin J; Hu H; Liao HS; Yan X; Tang Y; Jin A; Song J; Niu G et al. Tumor-Specific Formation of Enzyme-Instructed Supramolecular Self-Assemblies as Cancer Theranostics. ACS Nano 2015, 9, 9517–9527. [PubMed: 26301492]

(425). Di Virgilio F; Sarti AC; Falzoni S; De Marchi E; Adinolfi E Extracellular Atp and P2 Purinergic Signalling in the Tumour Microenvironment. Nat. Rev. Cancer 2018, 18, 601–618. [PubMed: 30006588]

(426). Zhou J; Du X; Berciu C; He H; Shi J; Nicastro D; Xu B Enzyme-Instructed Self-Assembly for Spatiotemporal Profiling of the Activities of Alkaline Phosphatases on Live Cells. Chem 2016, 1, 246–263. [PubMed: 28393126]

(427). Zhang X; Ren C; Hu F; Gao Y; Wang Z; Li H; Liu J; Liu B; Yang C Detection of Bacterial Alkaline Phosphatase Activity by Enzymatic in Situ Self-Assembly of the Aiegen-Peptide Conjugate. Anal. Chem 2020, 92, 5185–5190. [PubMed: 32207924]

(428). Zhou J; Du X; Yamagata N; Xu B Enzyme-Instructed Self-Assembly of Small D -Peptides as a Multiple-Step Process for Selectively Killing Cancer Cells. J. Am. Chem. Soc 2016, 138, 3813–3823. [PubMed: 26966844]

(429). Zhou J; Du X; Xu B Regulating the Rate of Molecular Self-Assembly for Targeting Cancer Cells. Angew. Chem. Int. Ed 2016, 55, 5770–5775.

(430). Zheng Z; Chen P; Xie M; Wu C; Luo Y; Wang W; Jiang J; Liang G Cell Environment-Differentiated Self-Assembly of Nanofibers. J. Am. Chem. Soc 2016, 138, 11128–11131. [PubMed: 27532322]

(431). Kopecka J; Trouillas P; Gašparović AČ; Gazzano E; Assaraf YG; Riganti C Phospholipids and Cholesterol: Inducers of Cancer Multidrug Resistance and Therapeutic Targets. Drug Resist. Update 2020, 49, 100670.

(432). Wang H; Feng Z; Wu D; Fritzsching KJ; Rigney M; Zhou J; Jiang Y; Schmidt-Rohr K; Xu B Enzyme-Regulated Supramolecular Assemblies of Cholesterol Conjugates against Drug-Resistant Ovarian Cancer Cells. J. Am. Chem. Soc 2016, 138, 10758–10761. [PubMed: 27529637]

(433). Wang H; Feng Z; Yang C; Liu J; Medina JE; Aghvami SA; Dinulescu DM; Liu J; Fraden S; Xu B Unraveling the Cellular Mechanism of Assembling Cholesterols for Selective Cancer Cell Death. Mol. Cancer Res 2019, 17, 907–917. [PubMed: 30552234]

(434). Hu Y; Wang H; Li C; Liu J; Xu B; Di W Enzyme-Instructed Assembly of a Cholesterol Conjugate Promotes Pro-Inflammatory Macrophages and Induces Apoptosis of Cancer Cells. Biomater. Sci 2020, 8, 2007–2017. [PubMed: 32073106]

(435). Wang J; Tan W; Li G; Wu D; He H; Xu J; Yi M; Zhang Y; Aghvami SA; Fraden S et al. Enzymatic Insertion of Lipids Increases Membrane Tension for Inhibiting Cancer Cells. Chemistry 2020.

(436). Deshaies RJ Multispecific Drugs Herald a New Era of Biopharmaceutical Innovation. Nature 2020, 580, 329–338. [PubMed: 32296187]

(437). Li LL; Zeng Q; Liu WJ; Hu XF; Li Y; Pan J; Wan D; Wang H Quantitative Analysis of Caspase-1 Activity in Living Cells through Dynamic Equilibrium of Chlorophyll-Based Nano-Assembly Modulated Photoacoustic Signals. ACS Appl. Mater. Interfaces 2016, 8, 17936–17943. [PubMed: 27341352]

(438). Kalafatovic D; Nobis M; Son J; Anderson KI; Ulijn RV Mmp-9 Triggered Self-Assembly of Doxorubicin Nanofiber Depots Halts Tumor Growth. Biomaterials. 2016, 98, 192–202. [PubMed: 27192421]

(439). Feng Z; Wang H; Zhou R; Li J; Xu B Enzyme-Instructed Assembly and Disassembly Processes for Targeting Downregulation in Cancer Cells. J. Am. Chem. Soc 2017, 139, 3950–3953. [PubMed: 28257192]

(440). He S; Mei L; Wu C; Tao M; Zhai Z; Xu K; Zhong W In Situ Hydrogelation of Bicalutamide-Peptide Conjugates at Prostate Tissue for Smart Drug Release Based on Ph and Enzymatic Activity. Nanoscale 2019, 11, 5030–5037. [PubMed: 30839985]

(441). Feng Z; Wang H; Chen X; Xu B Self-Assembling Ability Determines the Activity of Enzyme-Instructed Self-Assembly for Inhibiting Cancer Cells. J. Am. Chem. Soc 2017, 139, 15377–15384. [PubMed: 28990765]

(442). Kuang Y; Miki K; Parr CJC; Hayashi K; Takei I; Li J; Iwasaki M; Nakagawa M; Yoshida Y; Saito H Efficient, Selective Removal of Human Pluripotent Stem Cells Via Ecto-Alkaline Phosphatase-Mediated Aggregation of Synthetic Peptides. Cell Chem. Biol 2017, 24, 685–694.e684. [PubMed: 28529132]

(443). Liang C; Zheng D; Shi F; Xu T; Yang C; Liu J; Wang L; Yang Z Enzyme-Assisted Peptide Folding, Assembly and Anti-Cancer Properties. Nanoscale 2017, 9, 11987–11993. [PubMed: 28792044]

(444). Li G; Sasaki T; Asahina S; Roy MC; Mochizuki T; Koizumi K; Zhang Y Patching of Lipid Rafts by Molecular Self-Assembled Nanofibrils Suppresses Cancer Cell Migration. Chem 2017, 2, 283–298.

(445). Tang W; Yang J; Zhao Z; Lian Z; Liang G Intracellular Coassembly Boosts the Anti-Inflammation Capacity of Dexamethasone. Nanoscale 2017, 9, 17717–17721. [PubMed: 29130461]

(446). Kiran S; Hai Z; Ding Z; Wang L; Liu Y; Zhang H; Liang G Alkaline Phosphatase-Triggered Assembly of Etoposide Enhances Its Anticancer Effect. Chem. Commun 2018, 54, 1853–1856.

(447). Cao H; Wang Y; Gao Y; Deng X; Cong Y; Liu Y; Jiang X Molecular Design of -Sheet Peptide for the Multi-Modal Analysis of Disease. Angew. Chem. Int. Ed 2019, 58, 1626–1631.

(448). Dong L; Qian J; Hai Z; Xu J; Du W; Zhong K; Liang G Alkaline Phosphatase-Instructed Self-Assembly of Gadolinium Nanofibers for Enhanced T2-Weighted Magnetic Resonance Imaging of Tumor. Anal. Chem 2017, 89, 6922–6925. [PubMed: 28627868]

(449). Li LL; Qiao SL; Liu WJ; Ma Y; Wan D; Pan J; Wang H Intracellular Construction of Topology-Controlled Polypeptide Nanostructures with Diverse Biological Functions. Nat. Commun 2017, 8, 1276. [PubMed: 29097677]

(450). Lin YX; Qiao SL; Wang Y; Zhang RX; An HW; Ma Y; Rajapaksha RPYJ; Qiao ZY; Wang L; Wang H An in Situ Intracellular Self-Assembly Strategy for Quantitatively and Temporally Monitoring Autophagy. ACS Nano 2017, 11, 1826–1839. [PubMed: 28112893]

(451). Lin YX; Wang Y; Qiao SL; An HW; Wang J; Ma Y; Wang L; Wang H “In vivo Self-Assembled” Nanoprobes for Optimizing Autophagy-Mediated Chemotherapy. Biomaterials. 2017, 141, 199–209. [PubMed: 28689116]

(452). Callmann CE; Barback CV; Thompson MP; Hall DJ; Mattrey RF; Gianneschi NC Therapeutic Enzyme-Responsive Nanoparticles for Targeted Delivery and Accumulation in Tumors. Adv. Mater 2015, 27, 4611–4615. [PubMed: 26178920]

(453). Adamiak L; Touve MA; Leguyader CLM; Gianneschi NC Peptide Brush Polymers and Nanoparticles with Enzyme-Regulated Structure and Charge for Inducing or Evading Macrophage Cell Uptake. ACS Nano 2017, 11, 9877–9888. [PubMed: 28972735]

(454). Hu X; Yang P; He J; Liang R; Niu D; Wang H; Li Y In Vivo Self-Assembly Induced Retention of Gold Nanoparticles for Enhanced Photothermal Tumor Treatment. J. Mater. Chem. B 2017, 5, 5931–5936. [PubMed: 32264349]

(455). Zhao Y; Zhang X; Li Z; Huo S; Zhang K; Gao J; Wang H; Liang XJ Spatiotemporally Controllable Peptide-Based Nanoassembly in Single Living Cells for a Biological Self-Portrait. Adv. Mater 2017, 29, 1601128.

(456). Zhou Z; Xie X; Yi Q; Yin W; Kadi AA; Li J; Zhang Y Enzyme-Instructed Self-Assembly with Photo-Responses for the Photo-Regulation of Cancer Cells. Org. Biomol. Chem 2017, 15, 6892–6895. [PubMed: 28766648]

(457). Zhou J; Du X; Chen X; Wang J; Zhou N; Wu D; Xu B Enzymatic Self-Assembly Confers Exceptionally Strong Synergism with Nf-Kb Targeting for Selective Necroptosis of Cancer Cells. J. Am. Chem. Soc 2018, 140, 2301–2308. [PubMed: 29377688]

(458). Hideshima T; Chauhan D; Richardson P; Mitsiades C; Mitsiades N; Hayashi T; Munshi N; Dang L; Castro A; Palombella V et al. Nf-Kappa B as a Therapeutic Target in Multiple Myeloma. J. Biol. Chem 2002, 277, 16639–16647. [PubMed: 11872748]

(459). Baeuerle P; Baltimore D I Kappa B: A Specific Inhibitor of the Nf-Kappa B Transcription Factor. Science 1988, 242, 540–546. [PubMed: 3140380]

(460). Locksley RM; Killeen N; Lenardo MJ The Tnf and Tnf Receptor Superfamilies: Integrating Mammalian Biology. Cell 2001, 104, 487–501. [PubMed: 11239407]

(461). Carnero A; Blanco-Aparicio C; Renner O; Link W; Leal JFM The Pten/Pi3k/Akt Signalling Pathway in Cancer, Therapeutic Implications. Curr. Cancer Drug Targets 2008, 8, 187–198. [PubMed: 18473732]

(462). Kaileh M; Vazquez E; MacFarlane AWIV; Campbell K; Kurosaki T; Siebenlist U; Sen R Mtor-Dependent and Independent Survival Signaling by Pi3k in B Lymphocytes. PLoS One 2016, 11, e0146955. [PubMed: 26785352]

(463). Hers I; Vincent EE; Tavare JM Akt Signalling in Health and Disease. Cell Signal. 2011, 23, 1515–1527. [PubMed: 21620960]

(464). Blank JL; Gerwins P; Elliott EM; Sather S; Johnson GL Molecular Cloning of Mitogen-Activated Protein/Erk Kinase Kinases (Mekk) 2 and 3. Regulation of Sequential Phosphorylation Pathways Involving Mitogen-Activated Protein Kinase and C-Jun Kinase. J. Biol. Chem 1996, 271, 5361–5368. [PubMed: 8621389]

(465). Li J; Bullara D; Du X; He H; Sofou S; Kevrekidis IG; Epstein IR; Xu B Kinetic Analysis of Nanostructures Formed by Enzyme-Instructed Intracellular Assemblies against Cancer Cells. ACS Nano 2018, 12, 3804–3815. [PubMed: 29537820]

(466). Liang C; Zhang L; Zhao W; Xu L; Chen Y; Long J; Wang F; Wang L; Yang Z Supramolecular Nanofibers of Drug-Peptide Amphiphile and Affibody Suppress Her2+ Tumor Growth. Adv. Healthc. Mater 2018, 7, 1800899.

(467). Zhan J; Cai Y; He S; Wang L; Yang Z Tandem Molecular Self-Assembly in Liver Cancer Cells. Angew. Chem. Int. Ed 2018, 57, 1813–1816.

(468). Caspar JV; Meyer TJ Photochemistry of Tris(2,2'-Bipyridine)Ruthenium(2+) Ion (Ru(Bpy)32+). Solvent Effects. J. Am. Chem. Soc 1983, 105, 5583–5590.

(469). Li J; Hai Z; Xiao H; Yi X; Liang G Intracellular Self-Assembly of Ru(Bpy)32+ Nanoparticles Enables Persistent Phosphorescence Imaging of Tumors. Chem. Commun 2018, 54, 3460–3463.

(470). Tang W; Zhao Z; Chong Y; Wu C; Liu Q; Yang J; Zhou R; Lian ZX; Liang G Tandem Enzymatic Self-Assembly and Slow Release of Dexamethasone Enhances Its Antihepatic Fibrosis Effect. ACS Nano 2018, 12, 9966–9973. [PubMed: 30285414]

(471). Wu C; Zhang R; Du W; Cheng L; Liang G Alkaline Phosphatase-Triggered Self-Assembly of near-Infrared Nanoparticles for the Enhanced Photoacoustic Imaging of Tumors. Nano Lett. 2018, 18, 7749–7754. [PubMed: 30481463]

(472). Ji S; Gao H; Mu W; Ni X; Yi X; Shen J; Liu Q; Bao P; Ding D Enzyme-Instructed Self-Assembly Leads to the Activation of Optical Properties for Selective Fluorescence Detection and Photodynamic Ablation of Cancer Cells. J. Mater. Chem. B 2018, 6, 2566–2573. [PubMed: 32254475]

(473). Yang S; Yao D; Wang Y; Yang W; Zhang B; Wang D Enzyme-Triggered Self-Assembly of Gold Nanoparticles for Enhanced Retention Effects and Photothermal Therapy of Prostate Cancer. Chem. Commun 2018, 54, 9841–9844.

(474). Wu C; Hu W; Wei Q; Qiao L; Gao Y; Lv Y; Liu M; Li C; Wang X; Wang Q Controllable Growth of Core-Shell Nanogels Via Esterase-Induced Self-Assembly of Peptides for Drug Delivery. J. Biomed. Nanotech 2018, 14, 354–361.

(475). Zhang J; Mu YL; Ma ZY; Han K; Han HY Tumor-Triggered Transformation of Chimeric Peptide for Dual-Stage-Amplified Magnetic Resonance Imaging and Precise Photodynamic Therapy. Biomaterials. 2018, 182, 269–278. [PubMed: 30142526]

(476). Vijayan D; Young A; Teng MWL; Smyth MJ Targeting Immunosuppressive Adenosine in Cancer. Nat. Rev. Cancer 2017, 17, 709–724. [PubMed: 29059149]

(477). Sanmamed MF; Chen L A Paradigm Shift in Cancer Immunotherapy: From Enhancement to Normalization. Cell 2018, 175, 313–326. [PubMed: 30290139]

(478). Millán JL Mammalian Alkaline Phosphatases: From Biology to Applications in Mdicine and Biotechnology; John Wiley & Sons, 2006.

(479). Feng Z; Han X; Wang H; Tang T; Xu B Enzyme-Instructed Peptide Assemblies Selectively Inhibit Bone Tumors. Chem 2019, 5, 2442–2449. [PubMed: 31552305]

(480). Wang Y; Zhan J; Chen Y; Ai S; Li L; Wang L; Shi Y; Zheng J; Yang Z Selective Pericellular Hydrogelation by the Overexpression of an Enzyme and a Membrane Receptor. Nanoscale 2019, 11, 13714–13719. [PubMed: 31314031]

(481). Zheng D; Chen Y; Ai S; Zhang R; Gao Z; Liang C; Cao L; Chen Y; Hong Z; Shi Y et al. Tandem Molecular Self-Assembly Selectively Inhibits Lung Cancer Cells by Inducing Endoplasmic Reticulum Stress. Research 2019, 2019, 4803624. [PubMed: 31912037]

(482). Xu T; Cai Y; Zhong X; Zhang L; Zheng D; Gao Z; Pan X; Wang F; Chen M; Yang Z B;-Galactosidase Instructed Supramolecular Hydrogelation for Selective Identification and Removal of Senescent Cells. Chem. Commun 2019, 55, 7175–7178.

(483). Lee BY; Han JA; Im JS; Morrone A; Johung K; Goodwin EC; Kleijer WJ; DiMaio D; Hwang ES Senescence-Associated Beta-Galactosidase Is Lysosomal Beta-Galactosidase. Aging Cell 2006, 5, 187–195. [PubMed: 16626397]

(484). Gao Z; Gao H; Zheng D; Xu T; Chen Y; Liang C; Wang L; Ding D; Yang Z B;-Galactosidase Responsive Aie Fluorogene for Identification and Removal of Senescent Cancer Cells. Sci. China Chem 2020, 63, 398–403.

(485). Shang Y; Zhi D; Feng G; Wang Z; Mao D; Guo S; Liu R; Liu L; Zhang S; Sun S et al. Supramolecular Nanofibers with Superior Bioactivity to Insulin-Like Growth Factor-I. Nano Lett 2019, 19, 1560–1569. [PubMed: 30789273]

(486). Wang H; Chen P; Wu H; Zou P; Wu J; Liu Y; Liang G Furin-Guided Intracellular 68ga Nanoparticle Formation Enhancing Tumor Micropet Imaging. Anal. Chem 2019, 91, 14842–14845. [PubMed: 31718142]

(487). Yan Y; Zhou K; Wang L; Wang F; Chen X; Fan Q Clinical Significance of Serum Cathepsin B and Cystatin C Levels and Their Ratio in the Prognosis of Patients with Esophageal Cancer. Onco. Targets Ther 2017, 10, 1947–1954. [PubMed: 28435284]

(488). Ni Y; Hai Z; Zhang T; Wang Y; Yang Y; Zhang S; Liang G Cathepsin B Turning Bioluminescence “on” for Tumor Imaging. Anal. Chem 2019, 91, 14834–14837. [PubMed: 31726822]

(489). Lock LL; Cheetham AG; Zhang P; Cui H Design and Construction of Supramolecular Nanobeacons for Enzyme Detection. ACS Nano 2013, 7, 4924–4932. [PubMed: 23682734]

(490). Chen P; Kuang W; Zheng Z; Yang S; Liu Y; Su L; Zhao K; Liang G Carboxylesterase-Cleavable Biotinylated Nanoparticle for Tumor-Dual Targeted Imaging. Theranostics 2019, 9, 7359–7369. [PubMed: 31695773]

(491). Hai Z; Ni Y; Saimi D; Yang H; Tong H; Zhong K; Liang G Gamma-Glutamyltranspeptidase-Triggered Intracellular Gadolinium Nanoparticle Formation Enhances the T2-Weighted Mr Contrast of Tumor. Nano Lett 2019, 19, 2428–2433. [PubMed: 30856326]

(492). Cheng DB; Zhang XH; Gao YJ; Wang D; Wang L; Chen H; Qiao ZY; Wang H Site-Specific Construction of Long-Term Drug Depot for Suppression of Tumor Recurrence. Small 2019, 15, 1901813.

(493). Uhlen M; Fagerberg L; Hallstrom BM; Lindskog C; Oksvold P; Mardinoglu A; Sivertsson A; Kampf C; Sjostedt E; Asplund A et al. Proteomics. Tissue-Based Map of the Human Proteome. Science 2015, 347, 1260419. [PubMed: 25613900]

(494). Cong Y; Ji L; Gao YJ; Liu FH; Cheng DB; Hu Z; Qiao ZY; Wang H Microenvironment-Induced in Situ Self-Assembly of Polymer-Peptide Conjugates That Attack Solid Tumors Deeply. Angew. Chem. Int. Ed 2019, 58, 4632–4637.

(495). Zhao XX; Li LL; Zhao Y; An HW; Cai Q; Lang JY; Han XX; Peng B; Fei Y; Liu H et al. In Situ Self-Assembled Nanofibers Precisely Target Cancer-Associated Fibroblasts for Improved Tumor Imaging. Angew. Chem. Int. Ed 2019, 58, 15287–15294.

(496). Gao Y; Zhang C; Chang J; Yang C; Liu J; Fan S; Ren C Enzyme-Instructed Self-Assembly of a Novel Histone Deacetylase Inhibitor with Enhanced Selectivity and Anticancer Efficiency. Biomater. Sci 2019, 7, 1477–1485. [PubMed: 30672520]

(497). Li J; Liang S; Yan Y; Tian X; Li X O-Mannosylation Affords a Glycopeptide Hydrogel with Inherent Antibacterial Activities against E. Coli Via Multivalent Interactions between Lectins and Supramolecular Assemblies. Macromol. Biosci 2019, 19, 1900124.

(498). Yan R; Hu Y; Liu F; Wei S; Fang D; Shuhendler AJ; Liu H; Chen HY; Ye D Activatable Nir Fluorescence/Mri Bimodal Probes for in Vivo Imaging by Enzyme-Mediated Fluorogenic Reaction and Self-Assembly. J. Am. Chem. Soc 2019, 141, 10331–10341. [PubMed: 31244188]

(499). Wu C; Liu J; Tang X; Zhai ZR; Xu KM; Zhong WY An Enzyme-Assisted Self-Delivery System of Lonidamine-Peptide Conjugates for Selectively Killing Cancer Cells. Chem. Commun 2019, 55, 14852–14855.

(500). Li X; Cao C; Wei P; Xu M; Liu Z; Liu L; Zhong Y; Li R; Zhou Y; Yi T Self-Assembly of Amphiphilic Peptides for Recognizing High Furin-Expressing Cancer Cells. ACS Appl. Mater. Interfaces 2019, 11, 12327–12334. [PubMed: 30864434]

(501). Fu C; Zhan J; Huai J; Ma S; Li M; Chen G; Chen M; Cai Y; Ou C Furin-Instructed Molecular Self-Assembly Actuates Endoplasmic Reticulum Stress-Mediated Apoptosis for Cancer Therapy. Nanoscale 2020, 12, 12126–12132.

(502). Yuan Y; Zhang J; Qi X; Li S; Liu G; Siddhanta S; Barman I; Song X; McMahon MT; Bulte JW M. Furin-Mediated Intracellular Self-Assembly of Olsalazine Nanoparticles for Enhanced Magnetic Resonance Imaging and Tumour Therapy. Nat. Mater 2019, 18, 1376–1383. [PubMed: 31636420]

(503). Li X; Li J; Gao Y; Kuang Y; Shi J; Xu B Molecular Nanofibers of Olsalazine Form Supramolecular Hydrogels for Reductive Release of an Anti-Inflammatory Agent. J. Am. Chem. Soc 2010, 132, 17707–17709. [PubMed: 21121607]

(504). Du E; Hu X; Li G; Zhang S; Mang D; Roy S; Sasaki T; Zhang Y Self-Assembly-Directed Cancer Cell Membrane Insertion of Synthetic Analogues for Permeability Alteration. Langmuir 2019, 35, 7376–7382. [PubMed: 30091933]

(505). Sakai N; Matile S Synthetic Ion Channels. Langmuir 2013, 29, 9031–9040. [PubMed: 23631769]

(506). Mang D; Zhang S; Wu X; Hu X; Mochizuki T; Li G; Zhang Y Enzyme-Mediated Dual-Targeted-Assembly Realizes a Synergistic Anticancer Effect. Chem. Commun 2019, 55, 6126–6129.

(507). Wu Q; He Z; Wang X; Zhang Q; Wei Q; Ma S; Ma C; Li J; Wang Q Cascade Enzymes within Self-Assembled Hybrid Nanogel Mimicked Neutrophil Lysosomes for Singlet Oxygen Elevated Cancer Therapy. Nat. Commun 2019, 10, 240. [PubMed: 30651559]

(508). Zhang Q; Wu J; Wang J; Wang X; Wu C; Chen M; Wu Q; Lesniak MS; Mi Y; Cheng Y et al. A Neutrophil-Inspired Supramolecular Nanogel for Magnetocaloric-Enzymatic Tandem Therapy. Angew. Chem. Int. Ed 2020, 59, 3732–3738.

(509). Liang C; Yan X; Zhang R; Xu T; Zheng D; Tan Z; Chen Y; Gao Z; Wang L; Li X et al. Enhanced Cellular Uptake and Nuclear Accumulation of Drug-Peptide Nanomedicines Prepared by Enzyme-Instructed Self-Assembly. J. Control Release 2020, 317, 109–117. [PubMed: 31778740]

(510). An HW; Hou D; Zheng R; Wang MD; Zeng XZ; Xiao WY; Yan TD; Wang JQ; Zhao CH; Cheng LM et al. A near-Infrared Peptide Probe with Tumor-Specific Excretion-Retarded Effect for Image-Guided Surgery of Renal Cell Carcinoma. ACS Nano 2020, 14, 927–936. [PubMed: 31927974]

(511). Feng Z; Wang H; Yi M; Lo CY; Sallee A; Hsieh JT; Xu B Instructed-Assembly of Small Peptides Inhibits Drug-Resistant Prostate Cancer Cells. Pept. Sci 2019, 112, e24123.

(512). Liu D, Miao Z, Wu C, He F, Ren P, Bai S, Jiang X, Gao Y Isothermal Kinase-Triggered Supramolecular Assemblies as Drug Sensitizers. Chem. Sci 2020, 11, 1132–1139.

(513). Sletten EM; Bertozzi CR Bioorthogonal Chemistry: Fishing for Selectivity in a Sea of Functionality. Angew. Chem. Int. Ed 2009, 48, 6974–6998.

(514). Chen Z; Chen M; Zhou K; Rao J Pre-Targeted Imaging of Protease Activity through in Situ Assembly of Nanoparticles. Angew. Chem. Int. Ed 2020, 59, 7864–7870.

(515). Razgulin A; Ma N; Rao J Strategies for in Vivo Imaging of Enzyme Activity: An Overview and Recent Advances. Chem. Soc. Rev 2011, 40, 4186–4216. [PubMed: 21552609]

(516). Huang Z; Liu Y; Wang L; Ali A; Yao Q; Jiang X; Gao Y Supramolecular Assemblies Mimicking Neutrophil Extracellular Traps for Mrse Infection Control. Biomaterials. 2020, 253, 120124. [PubMed: 32447104]

(517). Dickinson BC; Chang CJ A Targetable Fluorescent Probe for Imaging Hydrogen Peroxide in the Mitochondria of Living Cells. J. Am. Chem. Soc 2008, 130, 9638–9639. [PubMed: 18605728]

(518). Huang Z; Yao Q; Chen J; Gao Y Redox Supramolecular Self-Assemblies Nonlinearly Enhance Fluorescence to Identify Cancer Cells. Chem. Commun 2018, 54, 5385–5388.

(519). Yao Q; Wang C; Fu M; Dai L; Li J; Gao Y Dynamic Detection of Active Enzyme Instructed Supramolecular Assemblies in Situ Via Super-Resolution Microscopy. ACS Nano 2020, 14, 4882–4889. [PubMed: 32233450]

(520). Wang H; Feng Z; Del Signore SJ; Rodal AA; Xu B Active Probes for Imaging Membrane Dynamics of Live Cells with High Spatial and Temporal Resolution over Extended Time Scales and Areas. J. Am. Chem. Soc 2018, 140, 3505–3509. [PubMed: 29481071]

(521). Whitesides GM; Grzybowski B Self-Assembly at All Scales. Science 2002, 295, 2418–2421. [PubMed: 11923529]

(522). Smith DJ; Brat GA; Medina SH; Tong D; Huang Y; Grahammer J; Furtmuller GJ; Oh BC; Nagy-Smith KJ; Walczak P et al. A Multiphase Transitioning Peptide Hydrogel for Suturing Ultrasmall Vessels. Nat. Nanotechnol 2016, 11, 95–102. [PubMed: 26524396]

(523). Bera S; Mondal S; Xue B; Shimon LJW; Cao Y; Gazit E Rigid Helical-Like Assemblies from a Self-Aggregating Tripeptide. Nat. Mater 2019, 18, 503–509. [PubMed: 30988450]

(524). Cui H; Pashuck ET; Velichko YS; Weigand SJ; Cheetham AG; Newcomb CJ; Stupp SI Spontaneous and X-Ray-Triggered Crystallization at Long Range in Self-Assembling Filament Networks. Science 2010, 327, 555–559. [PubMed: 20019248]

(525). Frederix PWJM; Scott GG; Abul-Haija YM; Kalafatovic D; Pappas CG; Javid N; Hunt NT; Ulijn RV; Tuttle T Exploring the Sequence Space for (Tri-)Peptide Self-Assembly to Design and Discover New Hydrogels. Nat. Chem 2015, 7, 30–37. [PubMed: 25515887]

(526). Dobson CM Chemical Space and Biology. Nature 2004, 432, 824–828. [PubMed: 15602547]

(527). Feng Z; Wang H; Xu B Instructed Assembly of Peptides for Intracellular Enzyme Sequestration. J. Am. Chem. Soc 2018, 140, 16433–16437. [PubMed: 30452246]

(528). Feng Z; Wang H; Wang F; Oh Y; Berciu C; Cui Q; Egelman EH; Xu B Artificial Intracellular Filaments. Cell Rep. Phys. Sci 2020, in press.

(529). Wang H; Feng Z; Wang Y; Zhou R; Yang Z; Xu B Integrating Enzymatic Self-Assembly and Mitochondria Targeting for Selectively Killing Cancer Cells without Acquired Drug Resistance. J. Am. Chem. Soc 2016, 138, 16046–16055. [PubMed: 27960313]

(530). Burns RJ; Smith RAJ; Murphy MP Synthesis and Characterization of Thiobutyltriphenylphosphonium Bromide, a Novel Thiol Reagent Targeted to the Mitochondrial Matrix. Arch. Biochem. Biophys 1995, 322, 60–68. [PubMed: 7574695]

(531). Reches M; Gazit E Casting Metal Nanowires within Discrete Self-Assembled Peptide Nanotubes. Science 2003, 300, 625–627. [PubMed: 12714741]

(532). Burattini S; Greenland BW; Merino DH; Weng W; Seppala J; Colquhoun HM; Hayes W; Mackay ME; Hamley IW; Rowan SJ A Healable Supramolecular Polymer Blend Based on Aromatic Π− Π Stacking and Hydrogen-Bonding Interactions. J. Am. Chem. Soc 2010, 132, 12051–12058. [PubMed: 20698543]

(533). Zhang Y; Kuang Y; Gao Y; Xu B Versatile Small-Molecule Motifs for Self-Assembly in Water and the Formation of Biofunctional Supramolecular Hydrogels. Langmuir 2010, 27, 529–537. [PubMed: 20608718]

(534). He H; Guo J; Lin X; Xu B Enzyme-Instructed Assemblies Enable Mitochondria Localization of Histone H2b in Cancer Cells. Angew. Chem. Int. Ed 2020, 59, 9330–9334.

(535). He H; Lin X; Guo J; Wang J; Xu B Perimitochondrial Enzymatic Self-Assembly for Selective Targeting the Mitochondria of Cancer Cells. ACS Nano 2020, in press.

(536). Chen M; LeDuc B; Kerr S; Howe D; Williams DA Identification of Human Ugt2b7 as the Major Isoform Involved in the O-Glucuronidation of Chloramphenicol. Drug Metab. Dispos 2010, 38, 368–375. [PubMed: 20008037]

(537). Chipuk J; Bouchier-Hayes L; Green D Mitochondrial Outer Membrane Permeabilization During Apoptosis: The Innocent Bystander Scenario. Cell Death Differ. 2006, 13, 1396. [PubMed: 16710362]

(538). Verfaillie T; Garg AD; Agostinis P Targeting Er Stress Induced Apoptosis and Inflammation in Cancer. Cancer Lett. 2013, 332, 249–264. [PubMed: 20732741]

(539). Schwarz DS; Blower MD The Endoplasmic Reticulum: Structure, Function and Response to Cellular Signaling. Cell Mol. Life Sci 2016, 73, 79–94. [PubMed: 26433683]

(540). Boelens J; Lust S; Offner F; Bracke ME; Vanhoecke BW The Endoplasmic Reticulum: A Target for New Anticancer Drugs. In Vivo 2007, 21, 215–226. [PubMed: 17436569]

(541). Healy SJM; Gorman AM; Mousavi-Shafaei P; Gupta S; Samali A Targeting the Endoplasmic Reticulum-Stress Response as an Anticancer Strategy. Eur. J. Pharmacol 2009, 625, 234–246. [PubMed: 19835867]

(542). Nam JS; Kang MG; Kang J; Park SY; Lee SJC; Kim HT; Seo JK; Kwon OH; Lim MH; Rhee HW et al. Endoplasmic Reticulum-Localized Iridium(Iii) Complexes as Efficient Photodynamic Therapy Agents Via Protein Modifications. J. Am. Chem. Soc 2016, 138, 10968–10977. [PubMed: 27494510]

(543). Feng Z; Wang H; Wang S; Zhang Q; Zhang X; Rodal AA; Xu B Enzymatic Assemblies Disrupt the Membrane and Target Endoplasmic Reticulum for Selective Cancer Cell Death. J. Am. Chem. Soc 2018, 140, 9566–9573. [PubMed: 29995402]

(544). Zhang S; Hu X; Mang D; Sasaki T; Zhang Y Self-Delivery of N-Hydroxylethyl Peptide Assemblies to the Cytosol Inducing Endoplasmic Reticulum Dilation in Cancer Cells. Chem. Commun 2019, 55, 7474–7477.

(545). Kim BJ; Fang Y; He H; Xu B Trypsin-Instructed Self-Assembly on Endoplasmic Reticulum for Selectively Inhibiting Cancer Cells. Adv. Healthc. Mater 2020, 9, 2000416.

(546). He H; Liu S; Wu D; Xu B Enzymatically-Formed Peptide Assemblies Sequestrate Proteins and Relocate Inhibitors for Selectively Killing Cancer Cells. Angewandte Chemie International Edition 2020.

(547). Wu G; Chai J; Suber TL; Wu J-W; Du C; Wang X; Shi Y Structural Basis of Iap Recognition by Smac/Diablo. Nature 2000, 408, 1008–1012. [PubMed: 11140638]

(548). Epstein IR; Vanag VK; Balazs AC; Kuksenok O; Dayal P; Bhattacharya A Chemical Oscillators in Structured Media. Acc. Chem. Res 2012, 45, 2160–2168. [PubMed: 22204671]

(549). Dadon Z; Wagner N; Ashkenasy G The Road to Non-Enzymatic Molecular Networks. Angew. Chem. Int. Ed 2008, 47, 6128–6136.

(550). Epstein IR; Pojman JA An Introduction to Nonlinear Chemical Dynamics: Oscillations, Waves, Patterns, and Chaos; Oxford University Press, 1998.

(551). Wong ASY; Pogodaev AA; Vialshin IN; Helwig B; Huck WTS Molecular Engineering of Robustness and Resilience in Enzymatic Reaction Networks. J. Am. Chem. Soc 2017, 139, 8146–8151. [PubMed: 28582616]

(552). Schwartz CL; Sarbash VI; Ataullakhanov FI; McIntosh JR; Nicastro D Cryo-Fluorescence Microscopy Facilitates Correlations between Light and Cryo-Electron Microscopy and Reduces the Rate of Photobleaching. J. Microsc 2007, 227, 98–109. [PubMed: 17845705]

(553). Zhang X; Settembre E; Xu C; Dormitzer PR; Bellamy R; Harrison SC; Grigorieff N Near-Atomic Resolution Using Electron Cryomicroscopy and Single-Particle Reconstruction. Proc. Natl. Acad. Sci. U.S.A 2008, 105, 1867–1872. [PubMed: 18238898]

(554). Egelman EH A Robust Algorithm for the Reconstruction of Helical Filaments Using Single-Particle Methods. Ultramicroscopy 2000, 85, 225–234. [PubMed: 11125866]

(555). Henderson R; Sali A; Baker ML; Carragher B; Devkota B; Downing KH; Egelman EH; Feng Z; Frank J; Grigorieff N et al. Outcome of the First Electron Microscopy Validation Task Force Meeting. Structure 2012, 20, 205–214. [PubMed: 22325770]

(556). Egelman EH Cryo-Em: Ice Is Nice, but Good Ice Can Be Hard to Find. Biophys. J 2020, 118, 1238–1239. [PubMed: 32061273]

(557). Monticelli L; Kandasamy SK; Periole X; Larson RG; Tieleman DP; Marrink SJ The Martini Coarse-Grained Force Field: Extension to Proteins. J. Chem. Theory Comput 2008, 4, 819–834. [PubMed: 26621095]

(558). Lu K; Jacob J; Thiyagarajan P; Conticello VP; Lynn DG Exploiting Amyloid Fibril Lamination for Nanotube Self-Assembly. J. Am. Chem. Soc 2003, 125, 6391–6393. [PubMed: 12785778]

(559). Johnson ER; Keinan S; Mori-Sanchez P; Contreras-Garcia J; Cohen AJ; Yang W Revealing Noncovalent Interactions. J. Am. Chem. Soc 2010, 132, 6498–6506. [PubMed: 20394428]

(560). Brooks BR; Brooks CL 3rd; Mackerell AD Jr.; Nilsson L; Petrella RJ; Roux B; Won Y; Archontis G; Bartels C; Boresch S et al. Charmm: The Biomolecular Simulation Program. J. Comput. Chem 2009, 30, 1545–1614. [PubMed: 19444816]

(561). Riccardi D; Schaefer P; Yang Y; Yu H; Ghosh N; Prat-Resina X; Konig P; Li G; Xu D; Guo H et al. Development of Effective Quantum Mechanical/Molecular Mechanical (Qm/Mm) Methods for Complex Biological Processes. J. Phys. Chem. B 2006, 110, 6458–6469. [PubMed: 16570942]

(562). Yao Q; Bao Q; Li X; Wang H; Yang Z; Shi X; Gao Y; Xu B Determination of the Packing Model of a Supramolecular Nanofiber Via Mass-Per-Length Measurement and De Novo Simulation. Nanoscale 2018, 10, 3990–3996. [PubMed: 29424852]

(563). Zhang C; Shafi R; Lampel A; MacPherson D; Pappas CG; Narang V; Wang T; Maldarelli C; Ulijn RV Switchable Hydrolase Based on Reversible Formation of Supramolecular Catalytic Site Using a Self-Assembling Peptide. Angew. Chem. Int. Ed 2017, 56, 14511–14515.

(564). Maki T; Yoshisaki R; Akama S; Yamanaka M Enzyme Responsive Properties of Amphiphilic Urea Supramolecular Hydrogels. Polym. J 2020, In press.

(565). Gao J; Wu P; Fernandez A; Zhuang J; Thayumanavan S Cellular and Gates: Synergistic Recognition to Boost Selective Uptake of Polymeric Nanoassemblies. Angew. Chem. Int. Ed 2020, In press.

(566). Mura S; Nicolas J; Couvreur P Stimuli-Responsive Nanocarriers for Drug Delivery. Nat. Mater 2013, 12, 991–1003. [PubMed: 24150417]

(567). Yu X; Zhang Z; Yu J; Chen H; Li X Self-Assembly of a Ibuprofen-Peptide Conjugate to Suppress Ocular Inflammation. Nanomedicine: Nanotech. Biol. Med 2018, 14, 185–193.

(568). Kholodenko BN Cell-Signalling Dynamics in Time and Space. Nat. Rev. Mol. Cell Bio 2006, 7, 165–176. [PubMed: 16482094]

(569). Yu G; Jie K; Huang F Supramolecular Amphiphiles Based on Host-Guest Molecular Recognition Motifs. Chem. Rev 2015, 115, 7240–7303. [PubMed: 25716119]

(570). Komatsu H; Matsumoto S; Tamaru S; Kaneko K; Ikeda M; Hamachi I Supramolecular Hydrogel Exhibiting Four Basic Logic Gate Functions to Fine-Tune Substance Release. J. Am. Chem. Soc 2009, 131, 5580–5585. [PubMed: 19331364]

(571). Chen Y; Huang F; Li Z-T; Liu Y Controllable Macrocyclic Supramolecular Assemblies in Aqueous Solution. Sci. China Chem 2018, 61, 979–992.

(572). Zhou Y; Lei L; Zhang Z; Zhang R; Song Q; Li X Cation Instructed Steroidal Prodrug Supramolecular Hydrogel. J. Colloid Interf. Sci 2018, 528, 10–17.

(573). Wei SM; Zhou XR; Huang ZT; Yao QX; Gao Y Hydrogen Sulfide Induced Supramolecular Self-Assembly in Living Cells. Chem. Commun 2018, 54, 9051–9054.

(574). Guo WW; Zhang ZT; Wei Q; Zhou Y; Lin MT; Chen JJ; Wang TT; Guo NN; Zhong XC; Lu YY et al. Intracellular Restructured Reduced Glutathione-Responsive Peptide Nanofibers for Synergetic Tumor Chemotherapy. Biomacromolecules 2020, 21, 444–453. [PubMed: 31851512]

(575). Chen Z; Chen M; Cheng Y; Kowada T; Xie J; Zheng X; Rao J Exploring the Condensation Reaction between Aromatic Nitriles and Amino Thiols to Optimize in Situ Nanoparticle Formation for the Imaging of Proteases and Glycosidases in Cells. Angew. Chem. Int. Ed 2020, 59, 3272–3279.

(576). Schleyer KA; Datko BD; Burnside B; Cui C; Ma X; Grey JK; Cui L Responsive Fluorophore Aggregation Provides Spectral Contrast for Fluorescence Lifetime Imaging. Chembiochem 2020, In press.

(577). Yao Q; Lin F; Fan X; Wang Y; Liu Y; Liu Z; Jiang X; Chen PR; Gao Y Synergistic Enzymatic and Bioorthogonal Reactions for Selective Prodrug Activation in Living Systems. Nat. Commun 2018, 9, 5032. [PubMed: 30487642]

(578). Fujita H; Zhang Y; Wu Z; Lindsey JS Chromogenic Agents Built around a Multifunctional Double-Triazine Framework for Enzymatically Triggered Cross-Linking under Physiological Conditions. New J. Chem 2020, 44, 3856–3867.

(579). Herrmann A Dynamic Combinatorial/Covalent Chemistry: A Tool to Read, Generate and Modulate the Bioactivity of Compounds and Compound Mixtures. Chem. Soc. Rev 2014, 43, 1899–1933. [PubMed: 24296754]

(580). Góngora-Benítez M; Tulla-Puche J; Albericio F Multifaceted Roles of Disulfide Bonds. Peptides as Therapeutics. Chem. Rev 2014, 114, 901–926. [PubMed: 24446748]

(581). Rowan SJ; Cantrill SJ; Cousins GRL; Sanders JKM; Stoddart JF Dynamic Covalent Chemistry. Angew. Chem. Int. Ed 2002, 41, 898–952.

(582). Mattia E; Pal A; Leonetti G; Otto S Mechanism of Building Block Exchange in Stacks of Self-Replicating Macrocycles. Synlett 2017, 28, 103–107.

(583). Pattillo CC; Moore JS A Tetrahedral Molecular Cage with a Responsive Vertex. Chem Sci 2019, 10, 7043–7048. [PubMed: 31588271]

(584). Liu Y; Zhang D; Qiao ZY; Qi GB; Liang XJ; Chen XG; Wang H A Peptide-Network Weaved Nanoplatform with Tumor Microenvironment Responsiveness and Deep Tissue Penetration Capability for Cancer Therapy. Adv. Mater 2015, 27, 5034–5042. [PubMed: 26198072]

(585). Kobayashi S; Uyama H; Kimura S Enzymatic Polymerization. Chem. Rev 2001, 101, 3793–3818. [PubMed: 11740921]

(586). Liu J; Kim YS; Richardson CE; Tom A; Ramakrishnan C; Birey F; Katsumata T; Chen S; Wang C; Wang X et al. Genetically Targeted Chemical Assembly of Functional Materials in Living Cells, Tissues, and Animals. Science 2020, 367, 1372–1376. [PubMed: 32193327]

(587). Hamley IW The Amyloid Beta Peptide: A Chemist's Perspective. Role in Alzheimer's and Fibrillization. Chem. Rev 2012, 112, 5147–5192. [PubMed: 22813427]

(588). Hendricks MP; Sato K; Palmer LC; Stupp SI Supramolecular Assembly of Peptide Amphiphiles. Acc. Chem. Res 2017, 50, 2440–2448. [PubMed: 28876055]

(589). Gazit E Reductionist Approach in Peptide-Based Nanotechnology. Annu. Rev. Biochem 2018, 87, 533–553. [PubMed: 29925257]

(590). Cui H; Webber MJ; Stupp SI Self-Assembly of Peptide Amphiphiles: From Molecules to Nanostructures to Biomaterials. Biopolymers. 2010, 94, 1–18. [PubMed: 20091874]

(591). Raeburn J; Zamith Cardoso A; Adams DJ The Importance of the Self-Assembly Process to Control Mechanical Properties of Low Molecular Weight Hydrogels. Chem. Soc. Rev 2013, 42, 5143–5156. [PubMed: 23571407]

(592). Kiyonaka S; Sugiyasu K; Shinkai S; Hamachi I First Thermally Responsive Supramolecular Polymer Based on Glycosylated Amino Acid. J. Am. Chem. Soc 2002, 124, 10954–10955. [PubMed: 12224923]

(593). Estroff LA; Hamilton AD Water Gelation by Small Organic Molecules. Chem. Rev 2004, 104, 1201–1218. [PubMed: 15008620]

(594). Liu M; Zhang L; Wang T Supramolecular Chirality in Self-Assembled Systems. Chem. Rev 2015, 115, 7304–7397. [PubMed: 26189453]

(595). Kunitake T Synthetic Bilayer Membranes: Molecular Design, Self-Organization, and Application. Angew. Chem. Int. Ed 1992, 31, 709–726.

(596). Brunsveld L; Folmer BJ; Meijer EW; Sijbesma RP Supramolecular Polymers. Chem. Rev 2001, 101, 4071–4098. [PubMed: 11740927]

(597). Woolfson N, The D Design of Coiled-Coil Structures and Assemblies. Adv. Protein Chem 2005, 70, 79–112. [PubMed: 15837514]

(598). Golub E; Subramanian RH; Esselborn J; Alberstein RG; Bailey JB; Chiong JA; Yan X; Booth T; Baker TS; Tezcan FA Constructing Protein Polyhedra Via Orthogonal Chemical Interactions. Nature 2020, 578, 172–176.

(599). Murray CB; Kagan CR; Bawendi MG Synthesis and Characterization of Monodisperse Nanocrystals and Close-Packed Nanocrystal Assemblies. Annu. Rev. Mater. Sci 2000, 30, 545–610.

(600). Irwin JJ; Duan D; Torosyan H; Doak AK; Ziebart KT; Sterling T; Tumanian G; Shoichet BK An Aggregation Advisor for Ligand Discovery. J. Med. Chem 2015, 58, 7076–7087. [PubMed: 26295373]

(601). Cheetham AG; Chakroun RW; Ma W; Cui H Self-Assembling Prodrugs. Chem. Soc. Rev 2017, 46, 6638–6663. [PubMed: 29019492]

(602). Whitesides GM Complex Organic Synthesis: Structure, Properties, and/or Function? Israel J. Chem 2018, 58, 142–150.

(603). Kornberg A The Two Cultures: Chemistry and Biology. Biochemistry 1987, 26, 6888–6891. [PubMed: 3427050]

(604). Walsh CT Chemical Biology: Here to Stay? Israel J. Chem 2018, 59, 7–17.

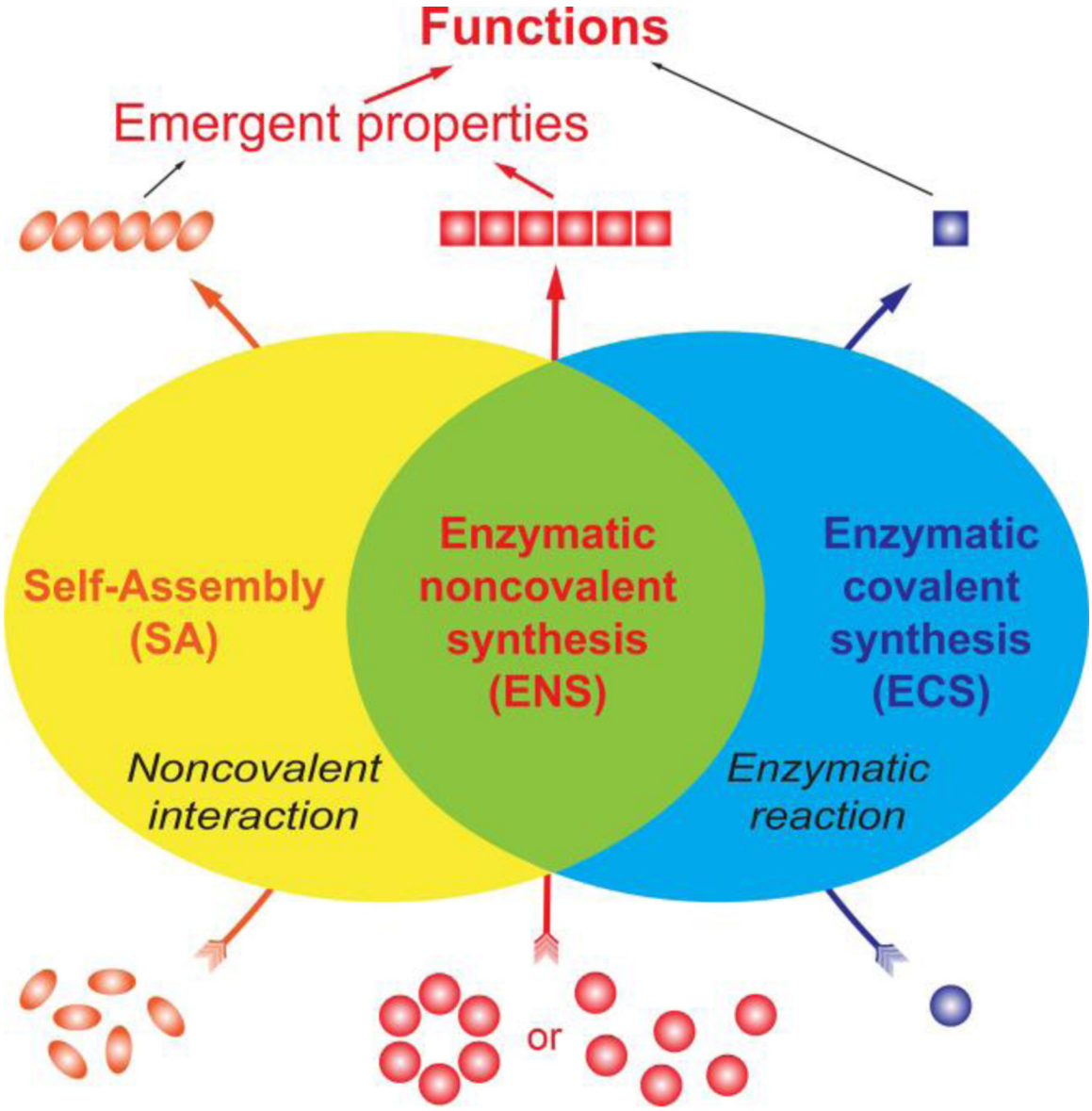

Figure 1.
The relationship among self-assembly, ECS, and ENS and the corresponding targets and products.

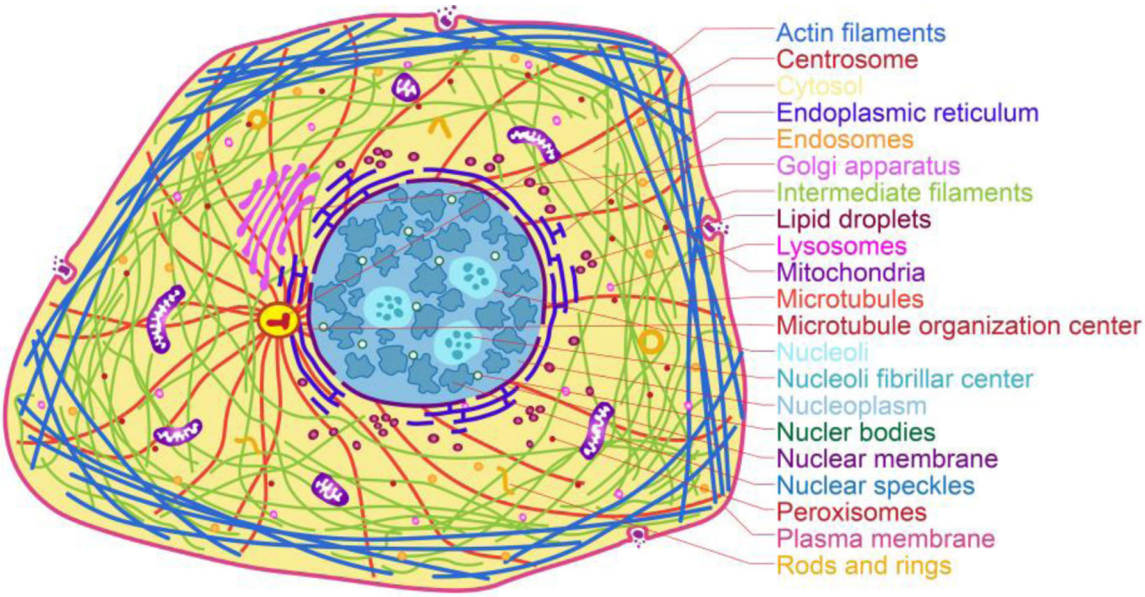

Figure 2.

Major intracellular functional structures. Adapted from Ref. 53. Copyright © 2017 by AAAS.

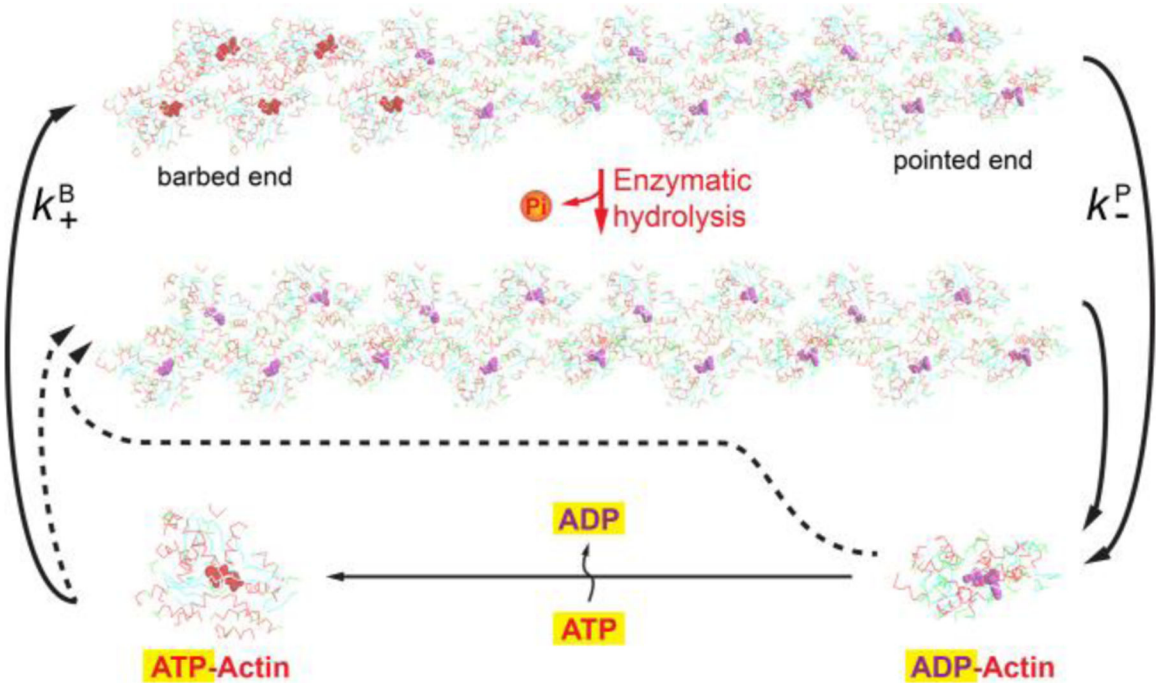

Figure 3.

Scheme of formation of an actin filament by ENS. Bold arrows show the net fluxes of pointed-end disassembly and barbed-end growth. The barbed ends, having two configurations, with bound ADP-Pi or ADP with different dissociation rates lead to that ATP hydrolysis affects length fluctuations at the barbed ends.[56] k^{B}_{+}: the association rate constant of ATP-G-actin to barbed ends; k^{P}_{-}: the dissociation rate constant of ADP-G-actin from pointed ends. The structures of ATP-actin (PDP ID: 4PKG[63]) and ADP-actin filament (PDB ID: 6DJO[64]) are adapted from PDB database.

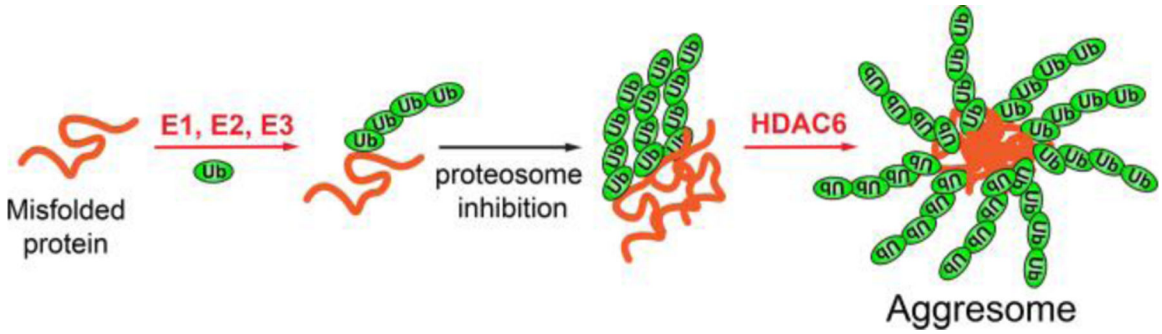

Figure 4.

Formation of aggresomes by ENS involving multiple enzymes and proteins.[66] Ub, E1, E2, E3 and HDAC6 are ubiquitin, ubiquitin-activating enzyme, ubiquitin-conjugating enzyme, ubiquitin ligase, and histone deacetylase, respectively.

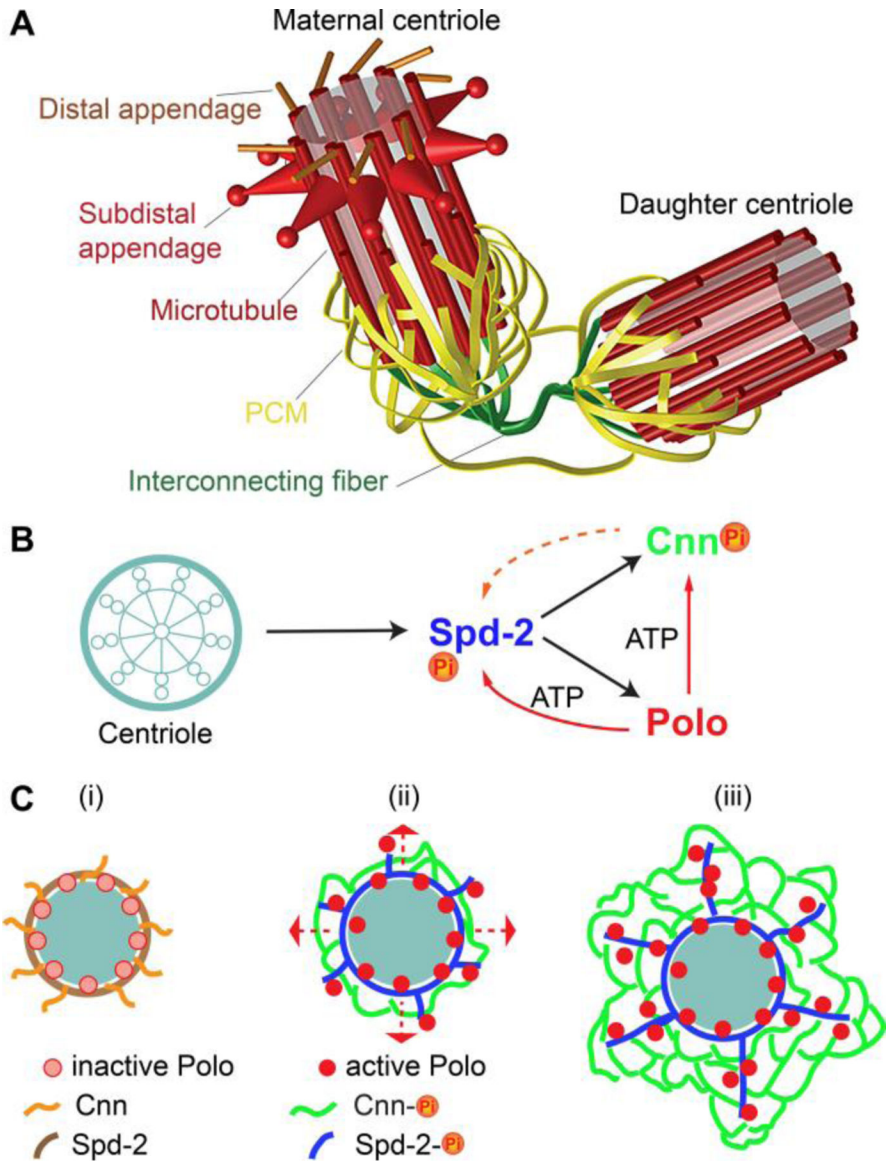

Figure 5.

(A) Centrosome structure. A pair of centrioles is shown, each with ninefold symmetry owing to the nine triplet microtubules. Each centriole has pericentriolar material (PCM) that nucleates microtubules around the ends closest to one another. Only the maternal centriole has two sets of extra appendages, distal and subdistal; the latter seems to anchor microtubules. A series of interconnecting fibers, different from the PCM, links the closest ends of the two centrioles. Adapted from Ref. 74. (B) The scheme of the putative pathway of scaffold assembly in flies: black arrows indicate recruitment, red arrows indicate phosphorylation, and the orange broken arrow indicates that Cnn helps to maintain the Spd-2 scaffold, but does not recruit Spd-2 into the scaffold. (C) The illustration on how ENS may form a positive feedback loop to drive the expansion of the mitotic PCM around the mother centriole (light green). (i) Interphase, Polo, Spd-2, and Cnn form a torus around the mother centriole: Polo inactive, Spd-2 and Cnn unphosphorylated, no scaffold. (ii) Mitosis, activated

Polo phosphorylates Spd-2, which forms the scaffold spreading away from the centriole (indicated by red broken arrows). The phosphorylated Spd-2 scaffold recruits Polo and Cnn, Polo phosphorylates Cnn, and Cnn forms a scaffold. (iii) The Cnn scaffold maintains the Spd-2 scaffold, allowing it to expand and to recruit more Polo and Cnn. (B,C) Adapted from Ref. 73. Copyright © 2019 by Elsevier Inc.

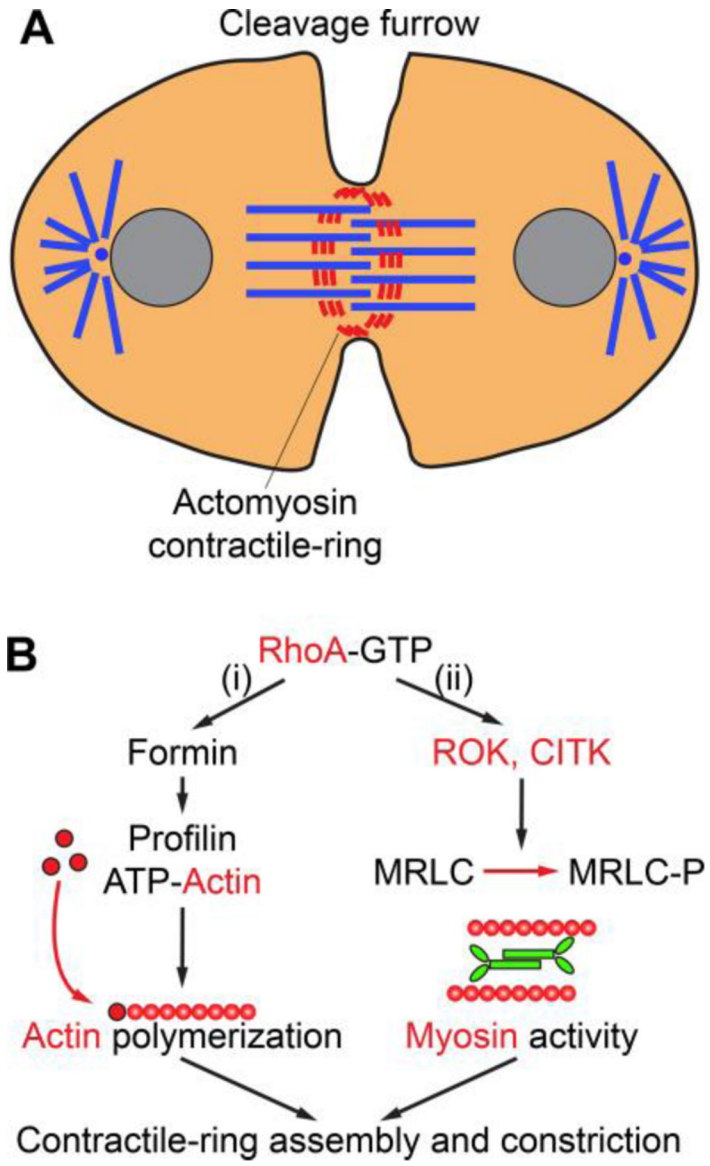

Figure 6.

(A) The illustration of cleavage furrow and actomyosin contractile-ring. (B) The ENS processes for the dynamics of contractile ring (red represent enzymes and enzymatic reactions): GTP-bound RhoA promotes (i) profilin-mediated actin polymerization through the formin; and (ii) phosphorylation of the myosin regulatory light chain (MRLC) by two kinases, Rho kinase (ROK) and citron kinase (CITK). Together, these events promote the sliding of myosin heads along actin filaments, and therefore the formation and ingression of the cleavage furrow. Adapted from Ref. 75. Copyright © 2009 by The Company of Biologists.

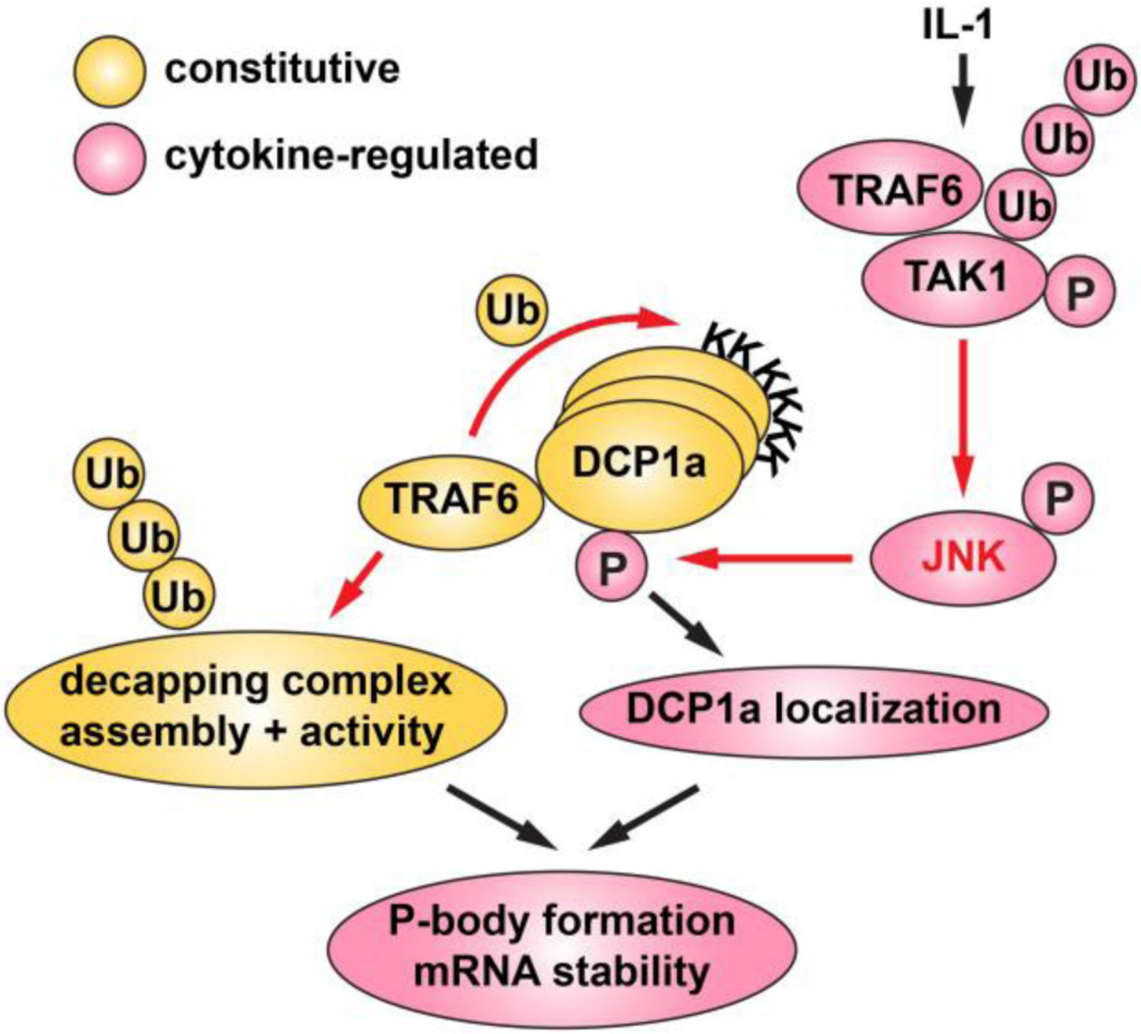

Figure 7.

An example of forming P-bodies by ENS. Trimerization of DCP1a triggers minimal P-body formation. TRAF6 ubiquitylates DCP1a at specific sites for recruiting more DCP1a to be phosphorylated by JNK (red indicates enzymes or enzymatic reaction). This process supports remodeling or "growing" of the P-body structure. Adapted from Ref. 87. Copyright © 2016 by Elsevier Inc.

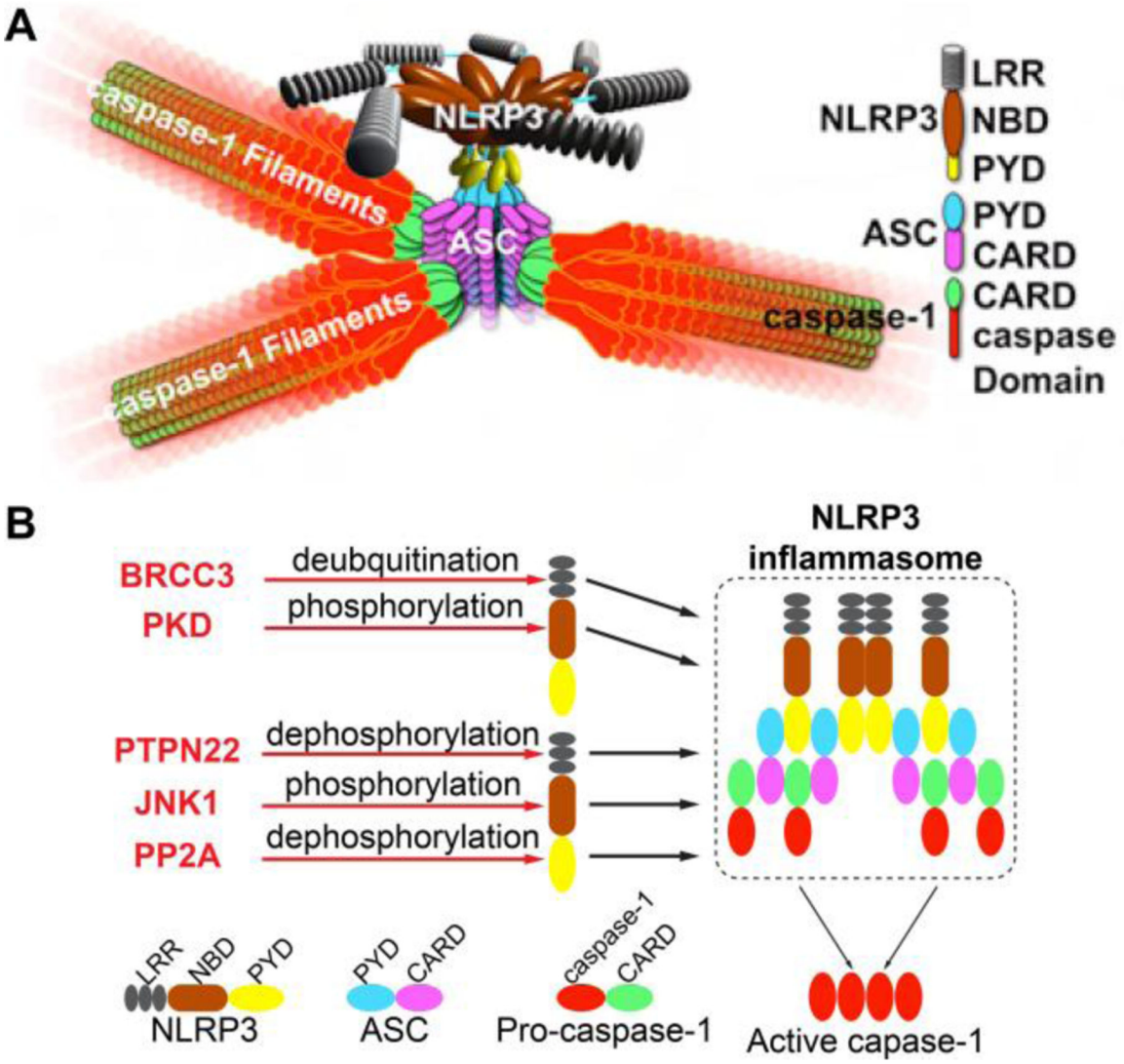

Figure 8.

(A) The model of the inflammasome assembly constituted by NLPR3, ASC, and Caspase-1. Multiple ASC-CARD molecules cluster to promote caspase-1 filament formation through CARD/CARD interactions. Adapted from Ref. 89. Copyright © 2014 by Elsevier Inc. (B) Schematic structure and PTM sites on different domains of NLRP3 (LRR, NBD, and PYD). BRCC3 and PTPN22 target the LRR domain of NLRP3 to promote NLRP3 inflammasome activation by deubiquitylation and dephosphorylation, respectively. Phosphorylation of NLRP3 by JNK1 and PKD, respectively, are key events for NLRP3 inflammasome activation. Dephosphorylation of NLRP3 PYD domain by PP2A promotes NLRP3–ASC as well as NLRP3 PYD–PYD interactions (red color representing enzymes or enzymatic reactions). Adapted from Ref. 42.

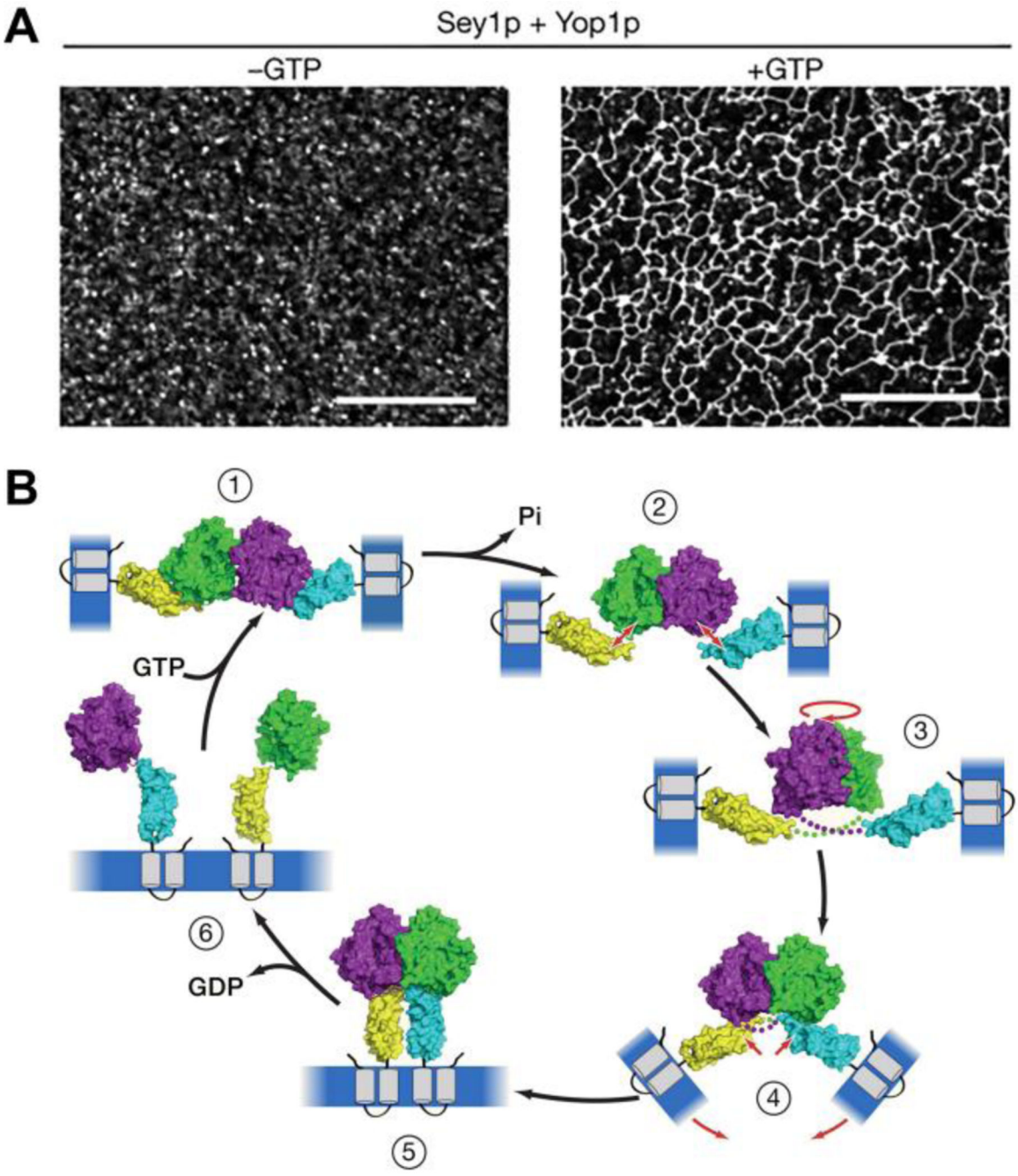

Figure 9.

(A) *S. cerevisiae* Sey1p and Yop1p were co-reconstituted into rhodamine-PE-labelled liposomes at protein:lipid ratios of 1:500 and 1:35, respectively, incubated without (left) or with (right) 2 mM GTP, and visualized by fluorescence microscopy. Scale bar 20 mm. Adapted from Ref. 103. Copyright © 2017 by Springer Nature. (B) The mechanism of membrane tethering and fusion is based on two crystal structures (state 1 and state 5) and biochemical experiments. The two ATL molecules dimerize and tether the membranes. Then, GTP hydrolysis causes conformational changes that pull the membranes together.

Finally, GDP is released to reset the fusion machinery. Adapted from Ref. 104. Copyright © 2011 by Elsevier Inc.

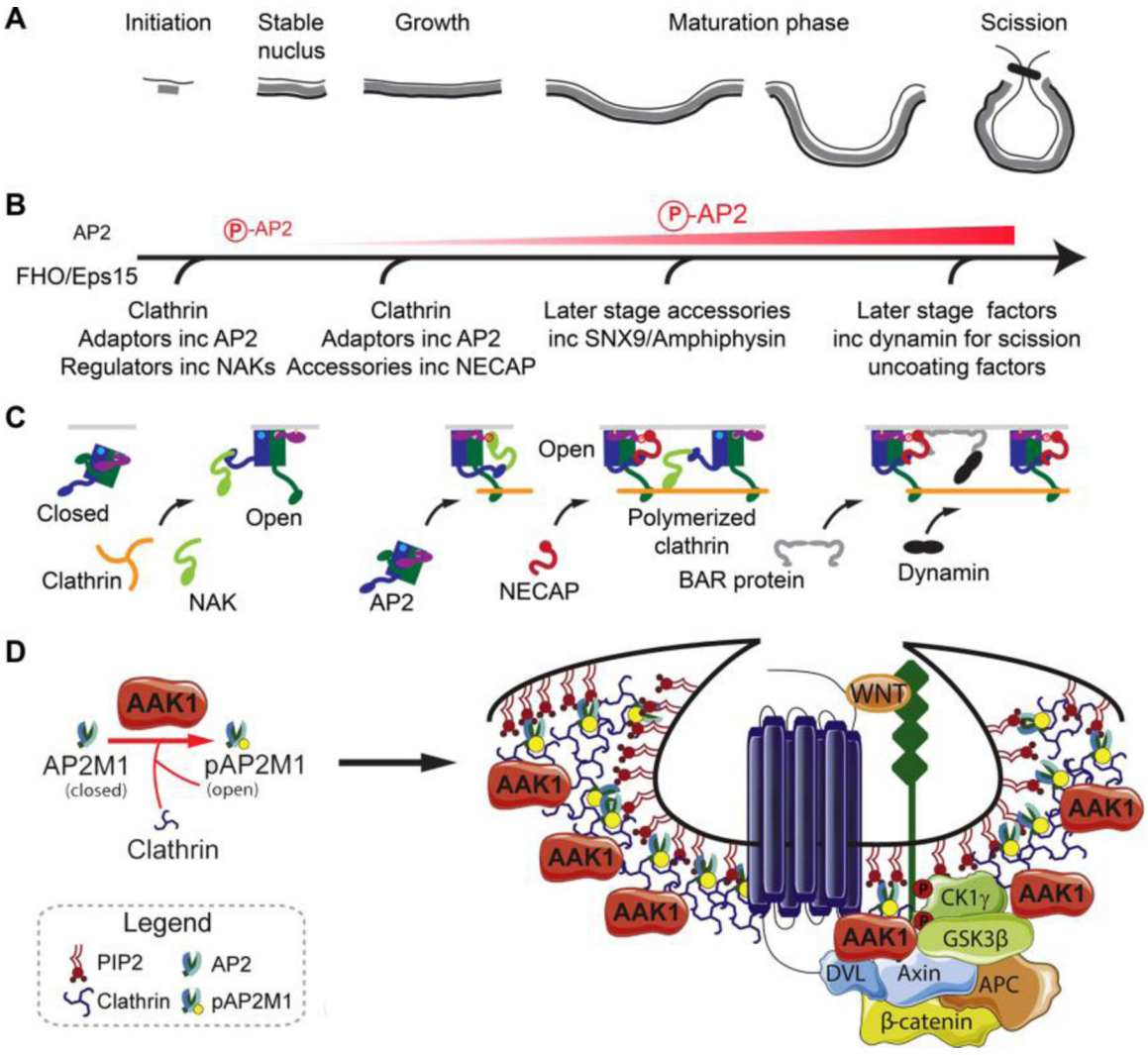

Figure 10.

(A, B, C) A schematic model of phosphorylation of AP2 for CCP maturation. Adapted from Ref. 105. Copyright © 2019 by Elsevier Inc. (A) The evolving CCP structure and the phases it passes through. (B) The degree of phosphorylation of μ2T156 of AP2. (C) The individual components and their recruitment. (D) Prolonged exposure to WNT ligand drives AAK1-dependent AP2M1 phosphorylation, CME, and ultimately removal of the WNT receptors from the plasma membrane. Adapted from Ref. 106.

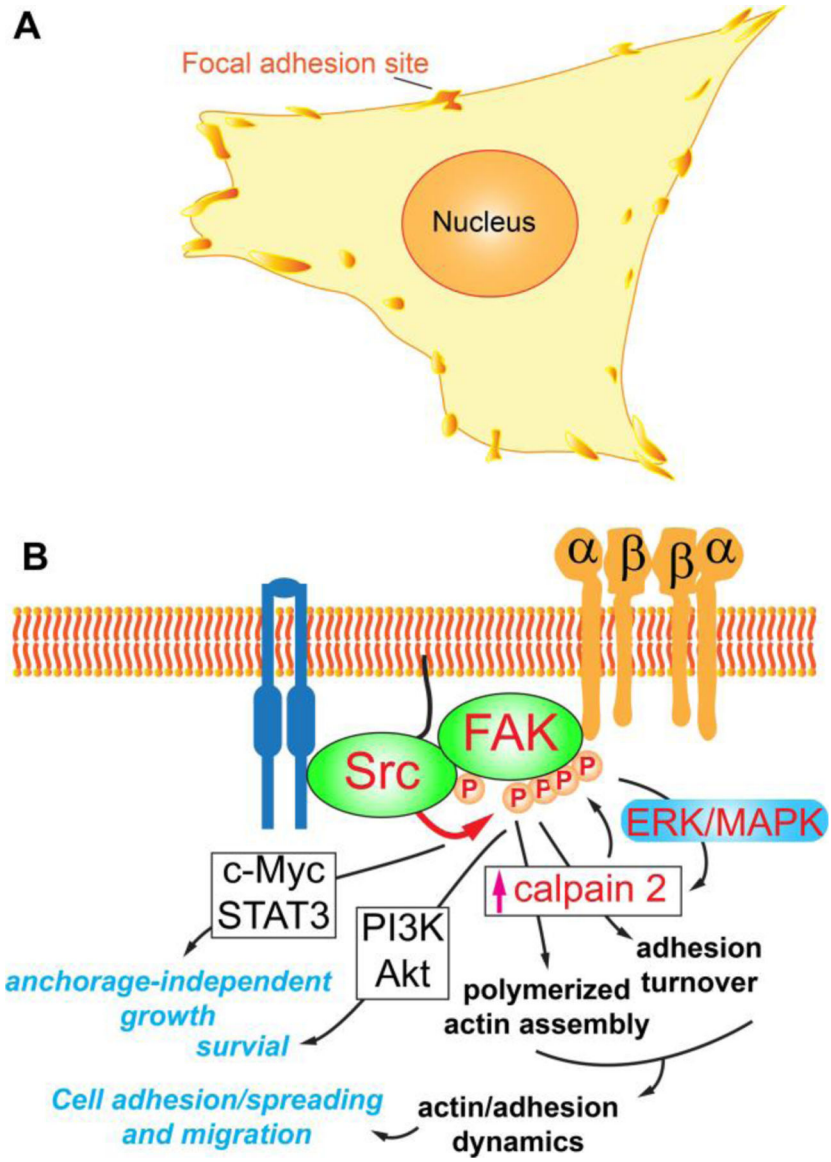

Figure 11.

(A) FA signaling is mediated by phosphorylation: the illustration of localization of pTyr in an attached human fibroblast highlights FAs around the cell periphery.[109] (B) Src-induced phosphorylation of FAK modulates adhesion dynamics, cell migration, survival, and anchorage-independent growth. Phosphorylated FAK results in actin stress fiber assembly and focal adhesion via activation of calpain, likely by linking calpain to the ERK/MAPK pathway. The Src-phosphorylated FAK also promotes cell survival and anchorage-independent growth of transformed cells. Adapted from Ref. 110. Copyright © 2004 by American Society for Microbiology.

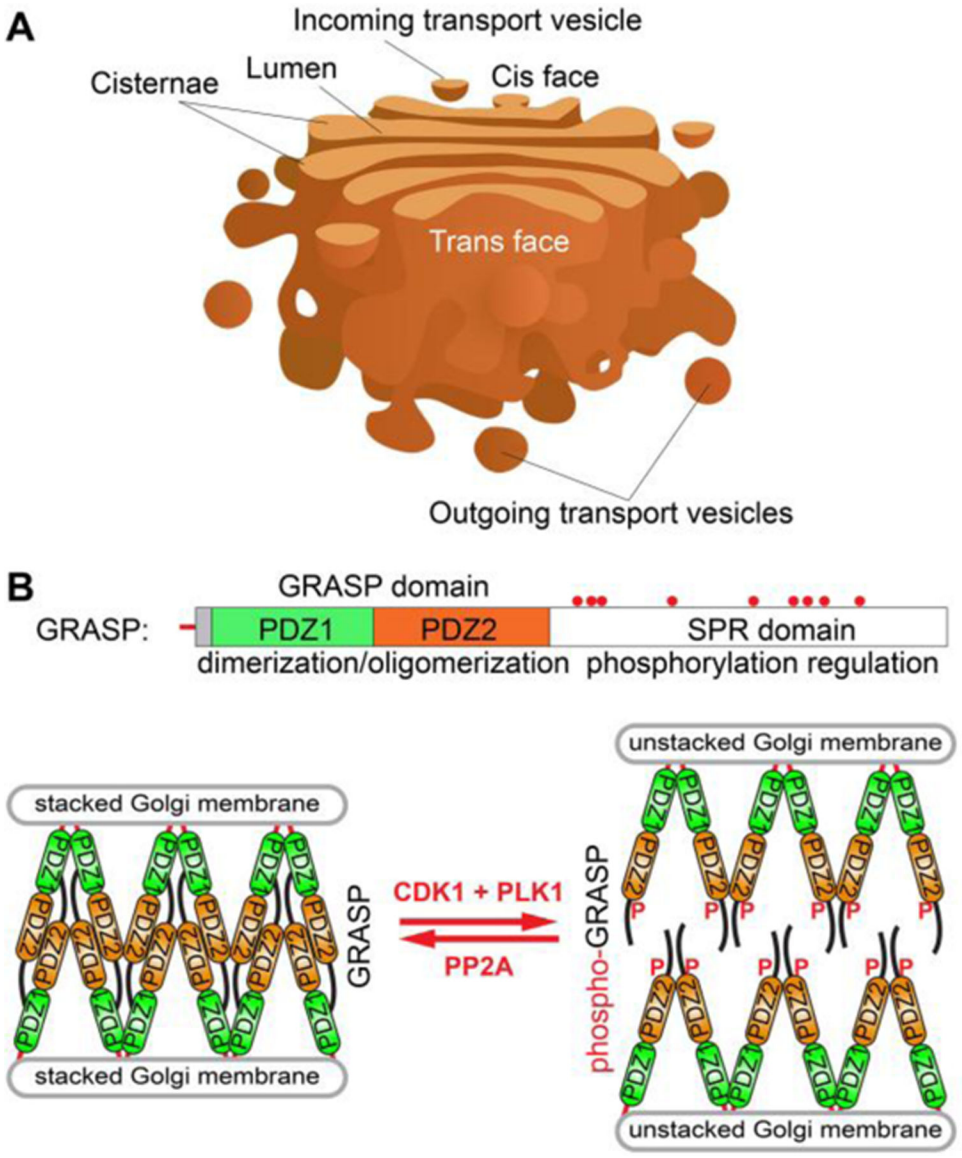

Figure 12.

(A) The illustration of Golgi apparatus. (B) GRASP oligomerization and Golgi stack formation. During interphase, GRASP65 homodimers self-assemble to form oligomers through the GRASP domain. During mitosis, phosphorylation of GRASP65 results in the disassembly of GRASP65 oligomers and Golgi stack. Adapted from Ref. 113.

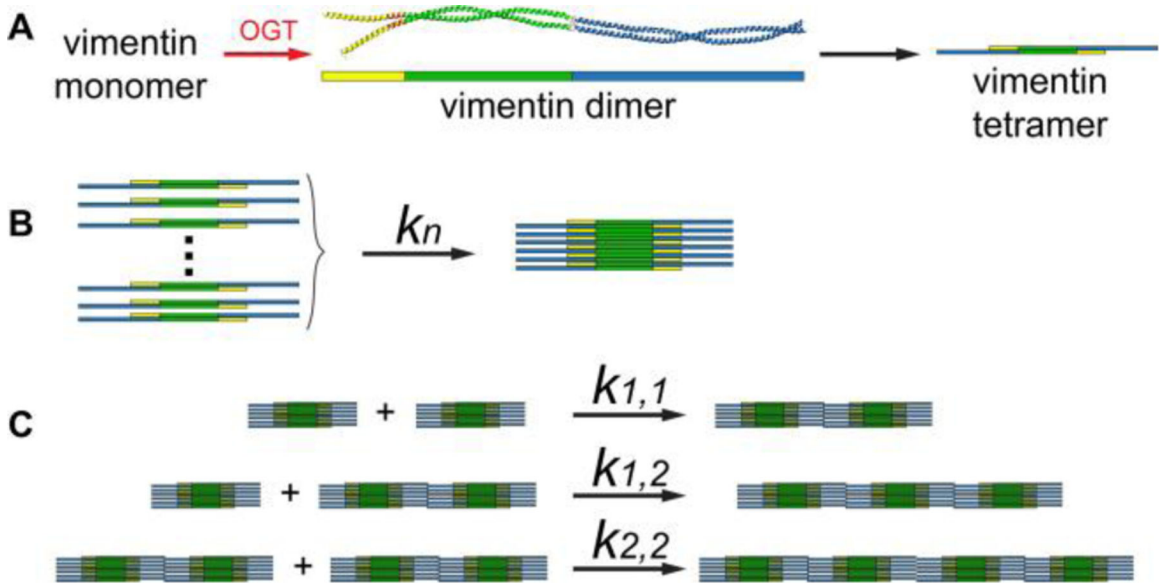

Figure 13.

Formation of IF of vimentin. (A) *O*-GlcNAc transferase (OGT) glycosylates vimentin monomers to form vimentin dimer (structure with the central α-helical rod domain, green boxes). (B) Lateral assembly step: tetramers associate to form a unit length filament (ULF). (C) Elongation reaction of ULF. Adapted from Ref. 120. Copyright © 2016 by National Academy of Sciences.

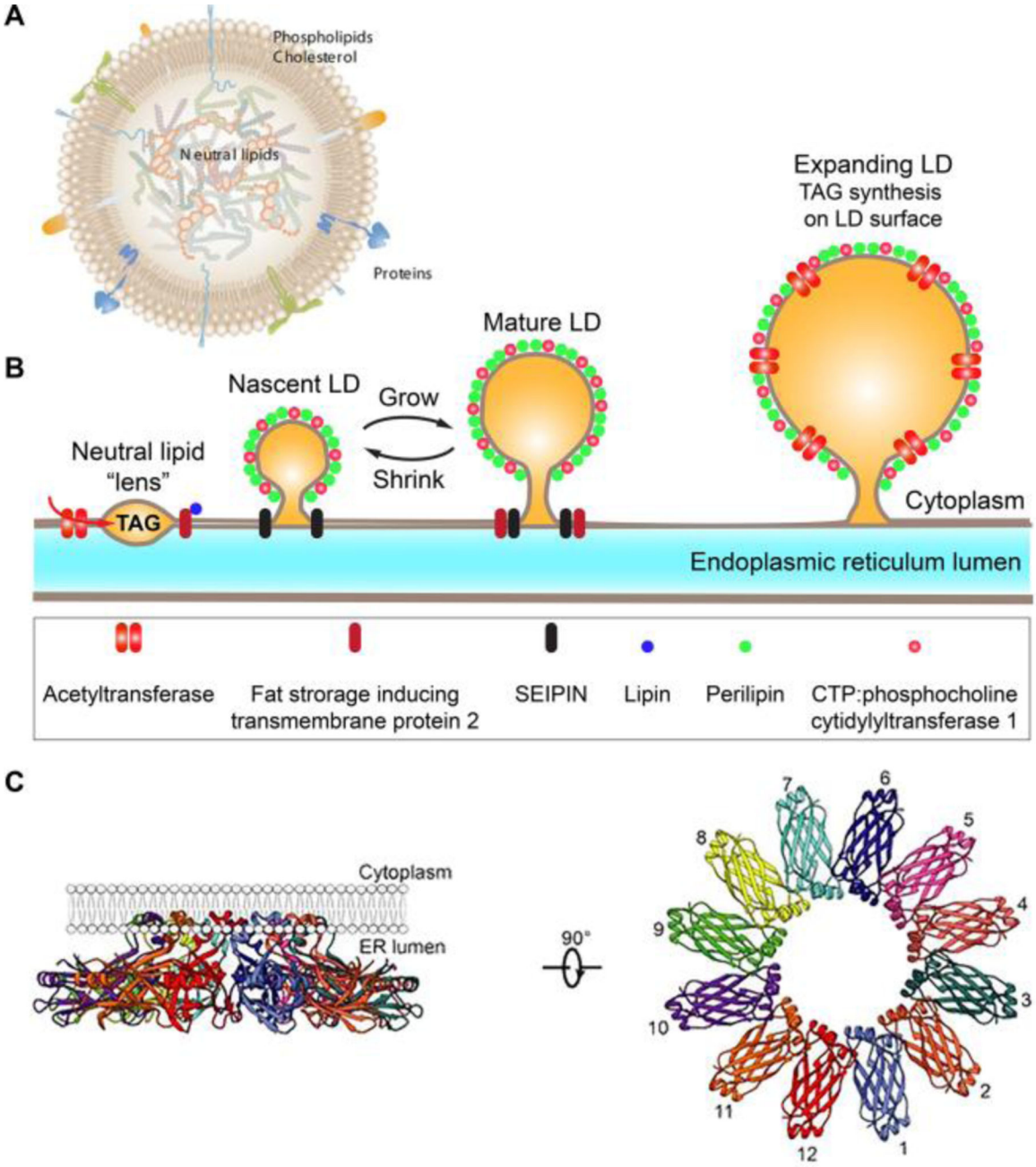

Figure 14.

(A) The illustration of lipid droplet (LD). Adapted from Ref. 121. Copyright © 2013 by The Association for the Publication of the Journal of Internal Medicine. (B) Model of LD biogenesis. Adapted from Ref. 126. Copyright © 2017 by Elsevier Inc. (C) A Cryo-EM structure of seipin: ribbon diagram side (left) and top (right) views of the luminal domains of seipin. Adapted from Ref. 125. Copyright © 2018 by Sui et al.

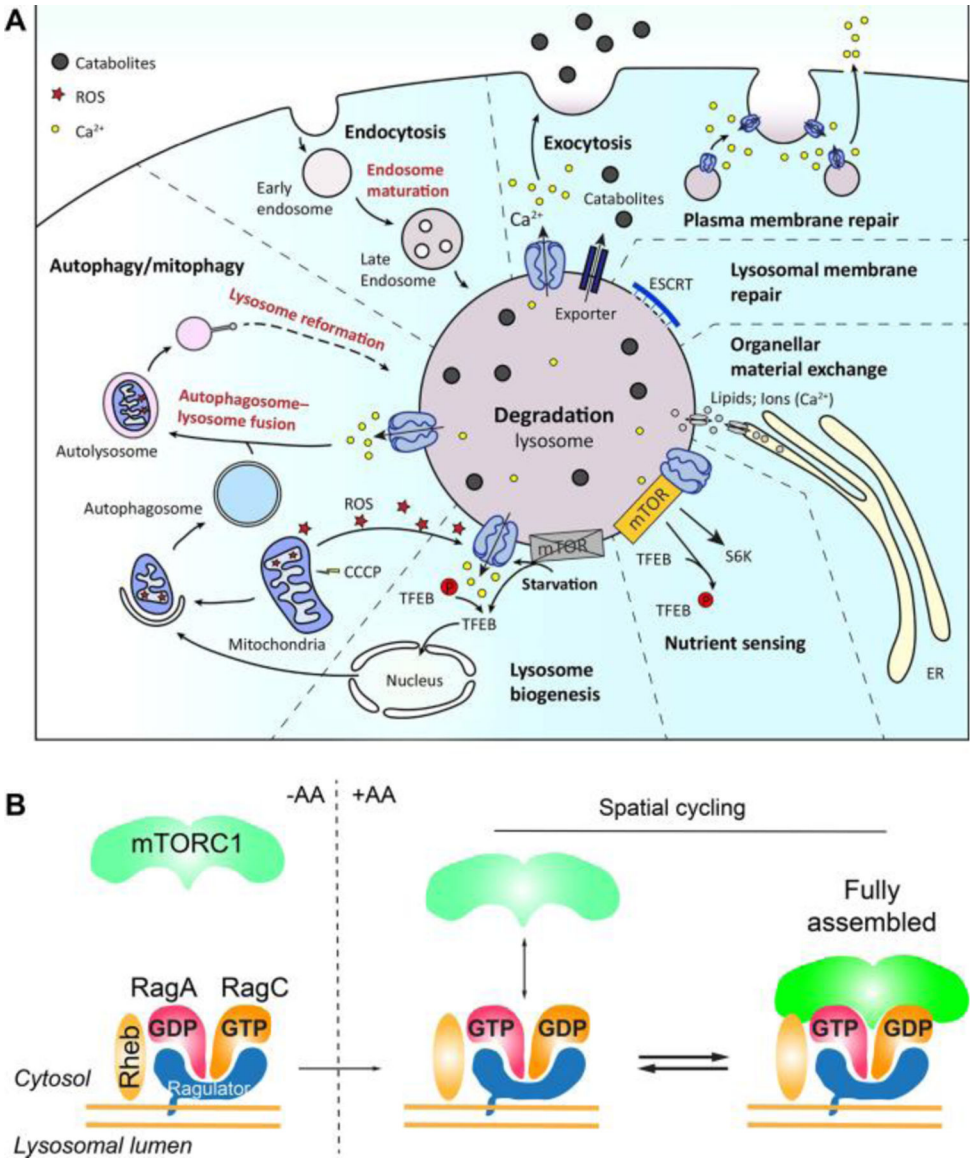

Figure 15.

(A) Function and regulation of lysosomes. Adapted from Ref. 132. Copyright © 2009 by Springer Nature. (B) Rag GTPase controls the capture of nutrient-induced mTORC1 on lysosome for nutrient sensing. Adapted from Ref. 131. Copyright © 2018 by Springer Nature.

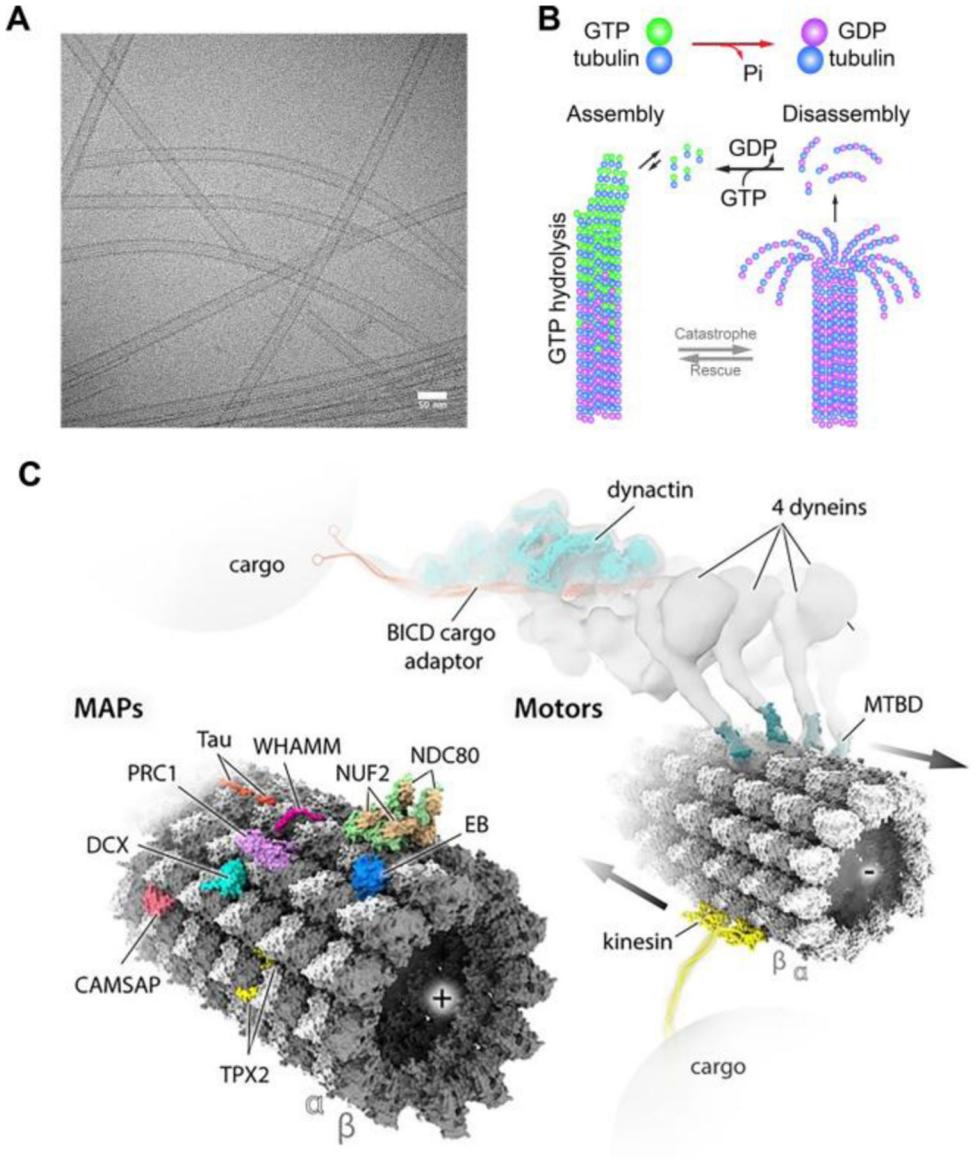

Figure 16.

(A) Electron cryo-micrograph of straight and curved microtubules with a uniform diameter (scale bar = 50 nm). Some microtubules are bundled, flattened or otherwise disrupted. (B) Conformational change of αβ-tubulin accompanying GTP hydrolysis. In the GTP state (β-tubulin in green), α and β tubulin monomer interfaces result in a 'straight' tubulin dimer. In the GDP state, the αβ-tubulin dimer interface is curved by 5° (arrow), leading to a 'bent' tubulin dimer. During microtubule assembly, the plus ends form a sheet-like group of straight protofilaments. GTP-tubulin dimers (green) assemble on the ends, forming a cap of GTP-tubulin. GTP hydrolysis over time converts GTP-tubulin in the lattice to GDP-tubulin. During the microtubule disassembly phase, GDP-tubulin protofilaments curl and peel off the microtube plus ends. The transitions between growth and shrinkage states are termed catastrophe and rescue. Adapted from Ref. 133. Copyright © 2011 by Elsevier Inc. (C) MAPs and cargo interact with microtubules. (A, C) Adapted from Ref. 134.

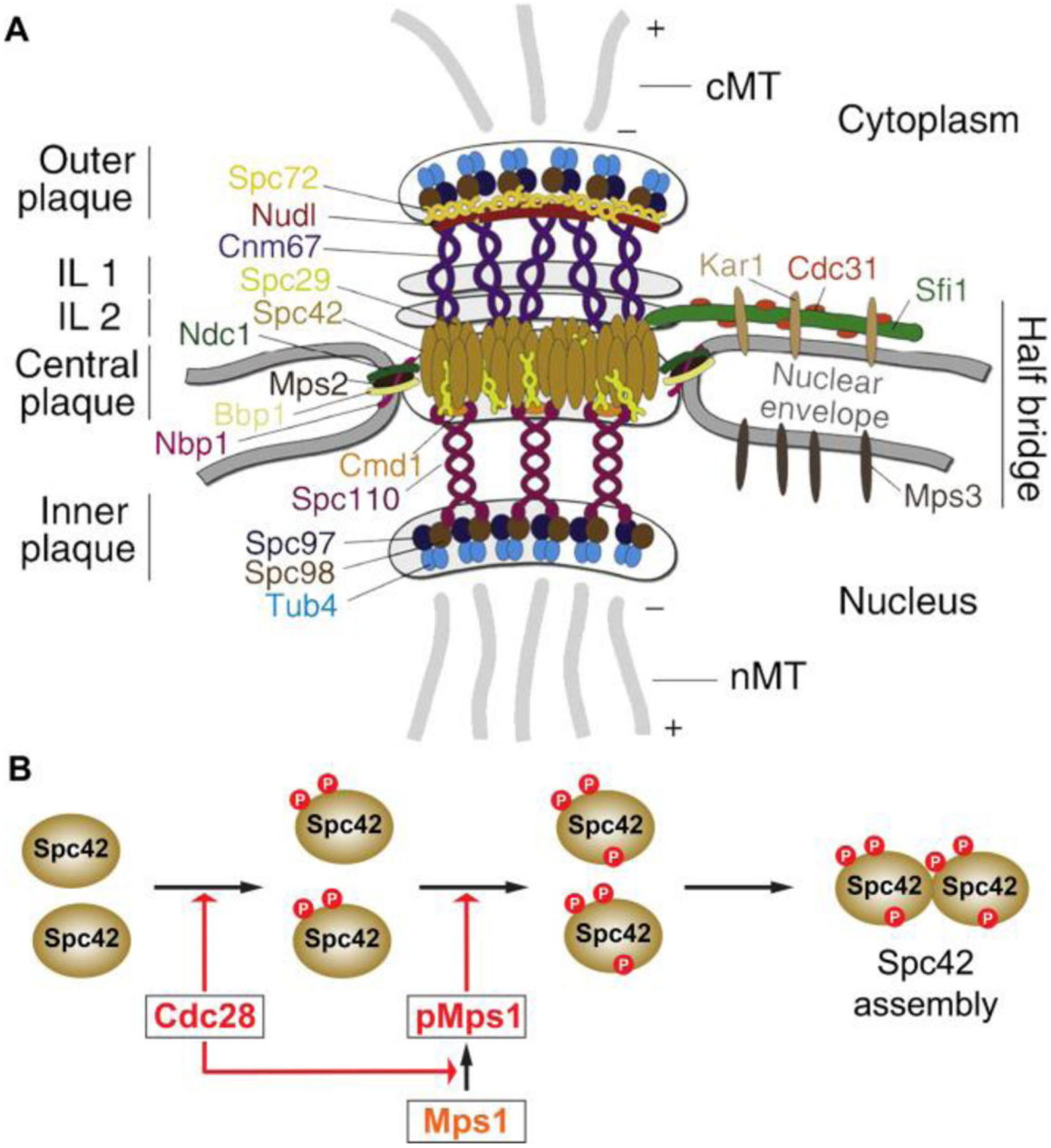

Figure 17.

(A) A schematic representation of the SPB proteins and their location within the organelle. Nuclear and cytoplasmic microtubules are illustrated and the distribution of their plus (+) and minus (–) ends is specified. IL 1, intermediate layer 1; IL 2, intermediate layer 2; cMT, cytoplasmic microtubules; nMT, nuclear microtubules. Adapted from Ref. 137. Copyright © 2013 by Elsevier Inc (B) Cdc28 regulates Spc42 assembly through multiple mechanisms (red color indicating enzymes or enzymatic reactions). Adapted from Ref. 138. Copyright © 2004 by Elsevier Inc.

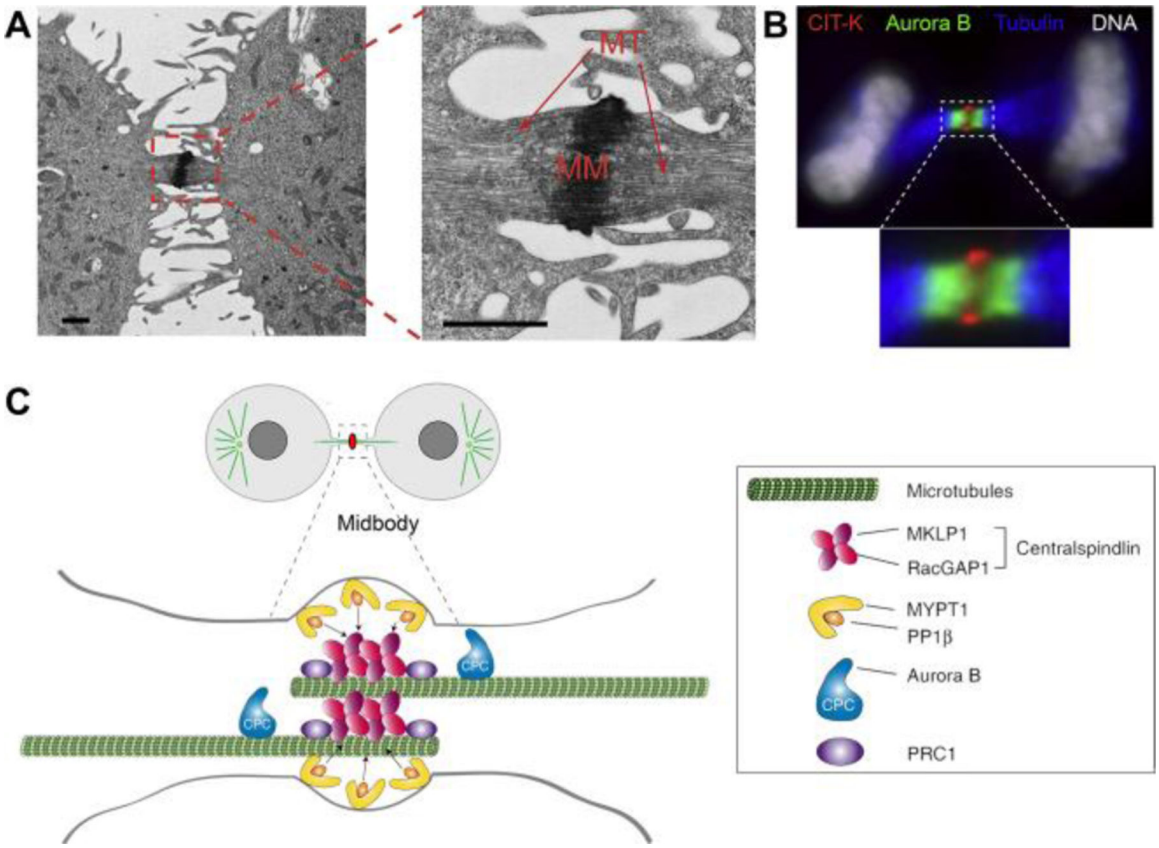

Figure 18.

(A) TEM image of a HeLa cell in cytokinesis. A magnification of the midbody is shown on the right. MM, midbody matrix; MT, microtubules. Scale bar = 1 μm. (B) HeLa cells were fixed and stained to detect CITK, aurora B, tubulin and DNA. The bottom panel shows a 3× magnification of the midbody. (A, B) Adapted from Ref. 142. Copyright © 2016 by Elsevier Inc. (C) PP1β dephosphorylates MKLP1 to strengthen the association of centralspindlin with PRC1. Adapted from Ref. 143.

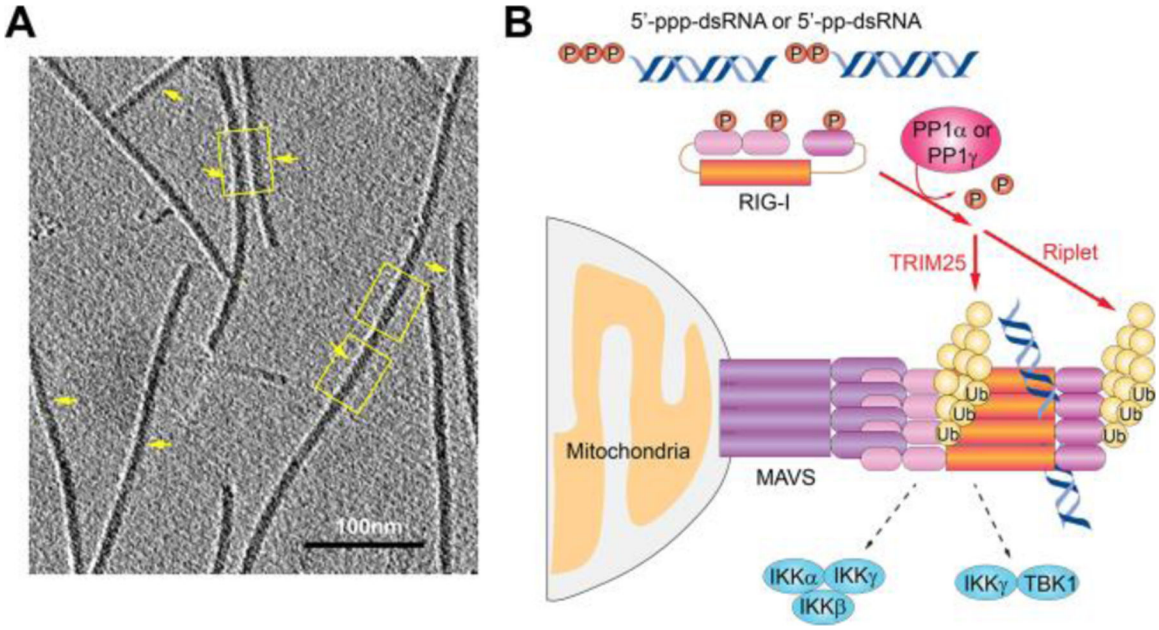

Figure 19.

(A) The projection image of MAVS filaments calculated from a 2.7 nm slice out of the cryo-ET reconstruction as viewed from the outer surface of the filaments. Yellow arrows point to portions of multiple filaments where apparent helical stripes were resolved. Adapted from Ref. 161. (B) The inactive retinoic acid-inducible gene-I protein (RIG-I) has phosphorylation at its caspase activation and recruitment domains (CARDs) and carboxy-terminal domains (CTDs) and adopts a 'closed' auto-inhibited conformation. Following the binding of RNA, an enzymatic reaction cascade results in the self-assembly of MAVS. The MAVS filaments activate TBK1 or IκB kinase-ε (IKKε) as well as the IKKα–IKKβ–IKKγ complex. Adapted from Ref. 160.

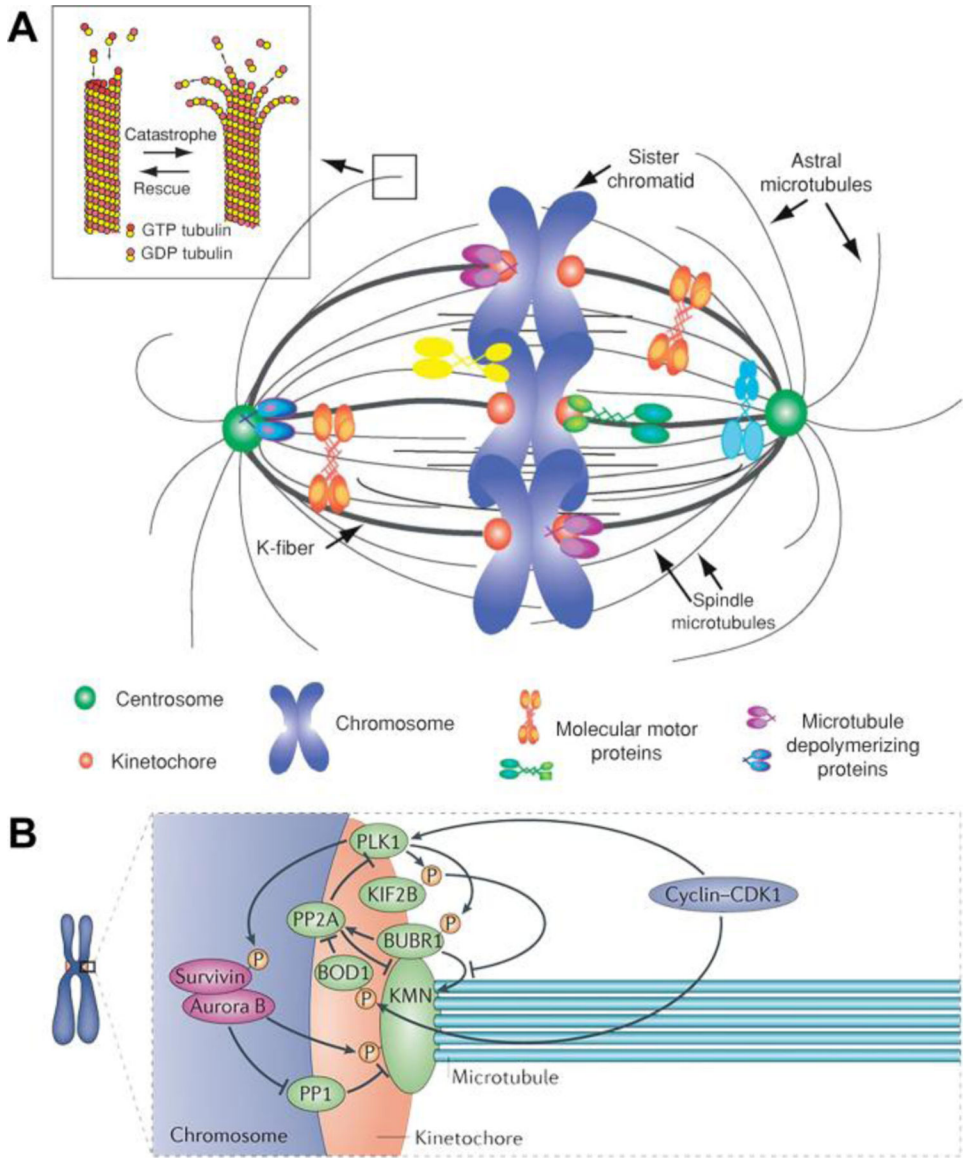

Figure 20.

(A) The key proteins involved in the assembly of mitotic spindles. Adapted from Ref. 163. Copyright © 2008 by Elsevier Inc. (B) The attachment of kinetochores to microtubules is regulated by enzymes. Adapted from[164]. Copyright © 2014 by Springer Nature.

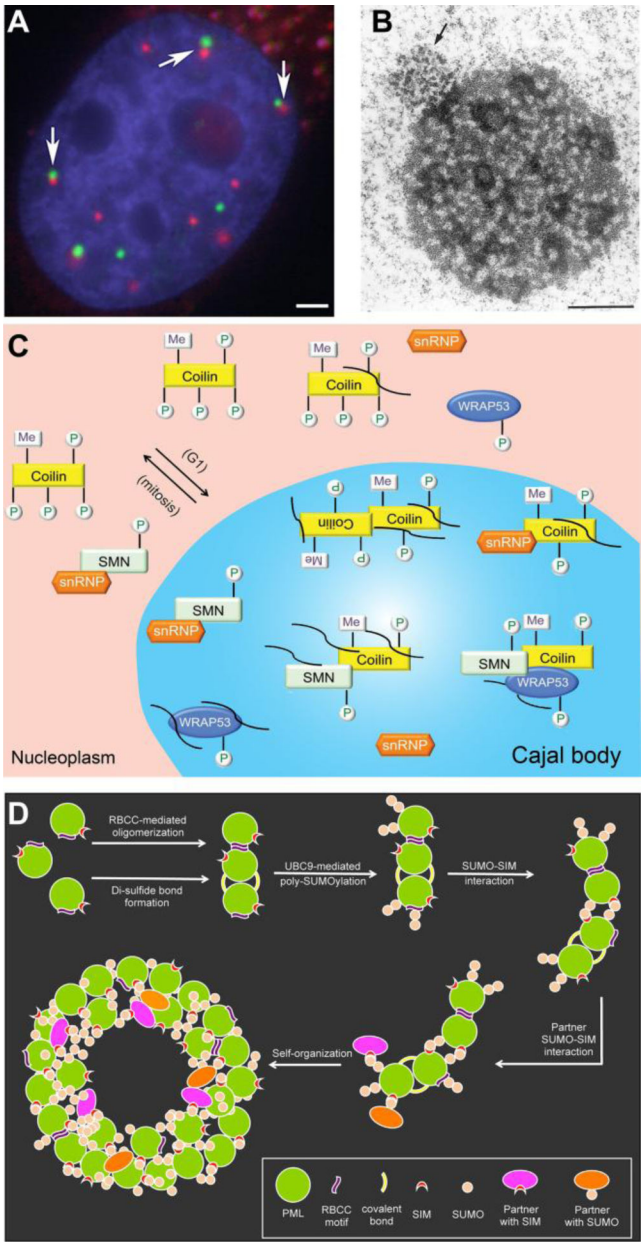

Figure 21.

(A) Cajal bodies (green) and promyelocytic leukemia protein (PML) bodies (red) in human cells. DNA is stained with DAPI. Scale bar: 2 μm. Adapted from Ref. 173. Copyright © 2005 by Annual Reviews. (B) The dense coiled threads of this CB (arrow) are in direct continuity with the dense fibrillar component at the nucleolar surface. Scale bar = 1 μm. Adapted from Ref. 174. Copyright © 2005 by Wiley Inc. (C) A hypothetical model of the impact of PTMs on the interactions and localizations of SMN and coilin. During mitosis, CBs disassemble and coilin is hyperphosphorylated. CBs reform at G1 phase, in which mitotic coilin is paired in the CB. Less phosphorylated coilin interacts with SMN, Sm proteins, sRNPs and WRAP53. Methylation of coilin (and certain SM proteins) increases it interaction with SMN. Differential phosphorylation results in the differential interaction of

coilin with SMN and Sm proteins to allow for subsequent snRNP biogenesis steps. Thus, many non-coding RNAs (curved lines) are enriched in the CB and coilin complex. Adapted from Ref. 166. Copyright © 2017 by Taylor & Francis. (D) Assembly of promyelocytic leukemia (PML) nuclear bodies controlled by SUMO ligases. Adapted from Ref. 172.

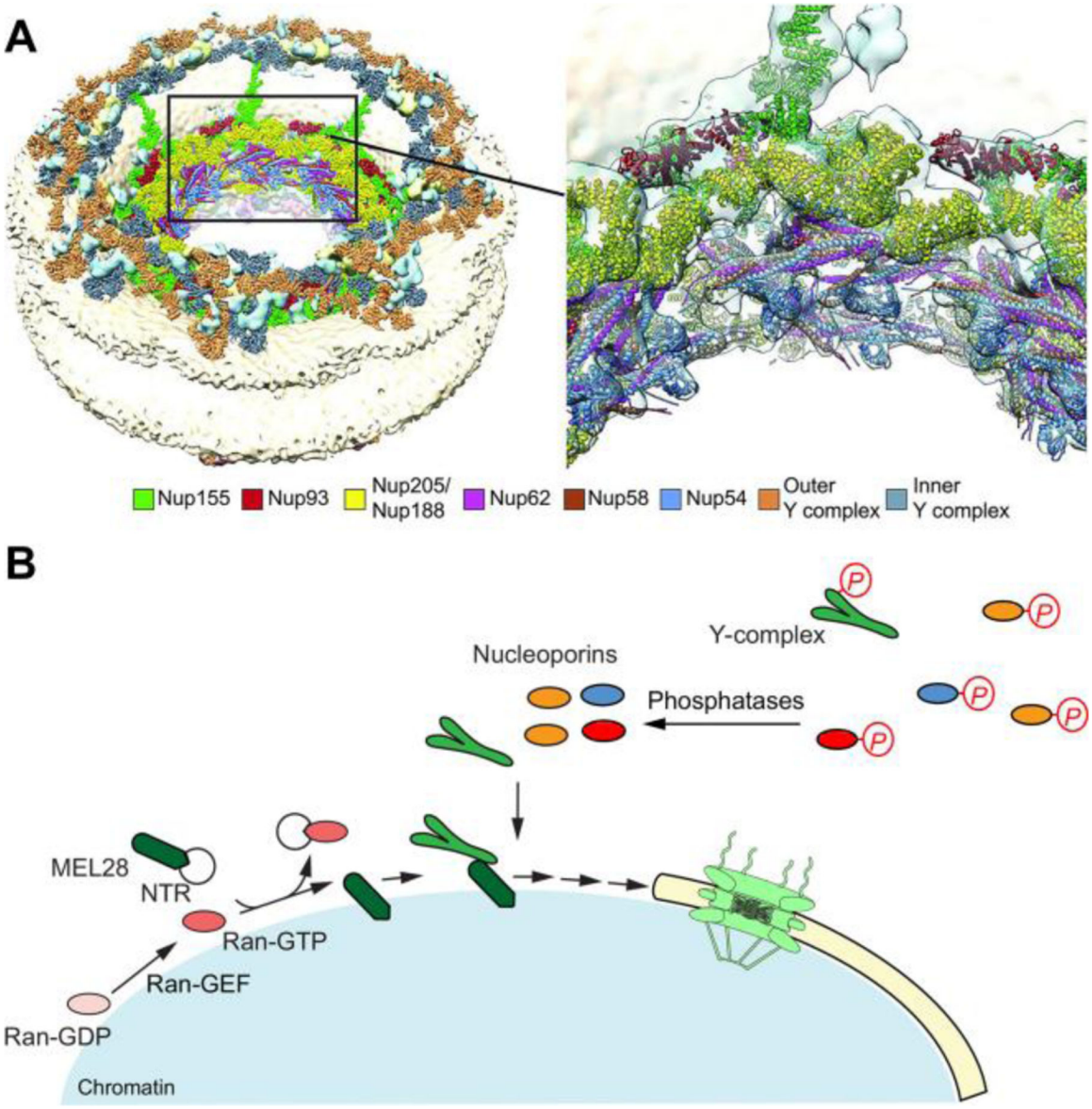

Figure 22.

(A) Right: overview of the composite structure of the entire NPC, unassigned density is shown in cyan; the nuclear ring is facing up. Right: Zoomed-in view of the inner ring region framed in right. High-resolution structures (colored ribbons) are shown in the context of the tomographic map (transparent isosurface). Adapted from Ref. 176. Copyright © 2017 by AAAS. (B) Mitotic NPC assembly is regulated by Ran and phosphatases. The local generation of Ran-GTP on the chromatin allows release of inhibitory NTRs from nucleoporins (exemplified for MEL28). MEL28 binds to the decondensing chromatin and recruits the Y-complex. Dephosphorylation of nucleoporins enables their interaction and allows NPC assembly. Adapted from Ref. 182. Copyright © 2016 by The Company of Biologists.

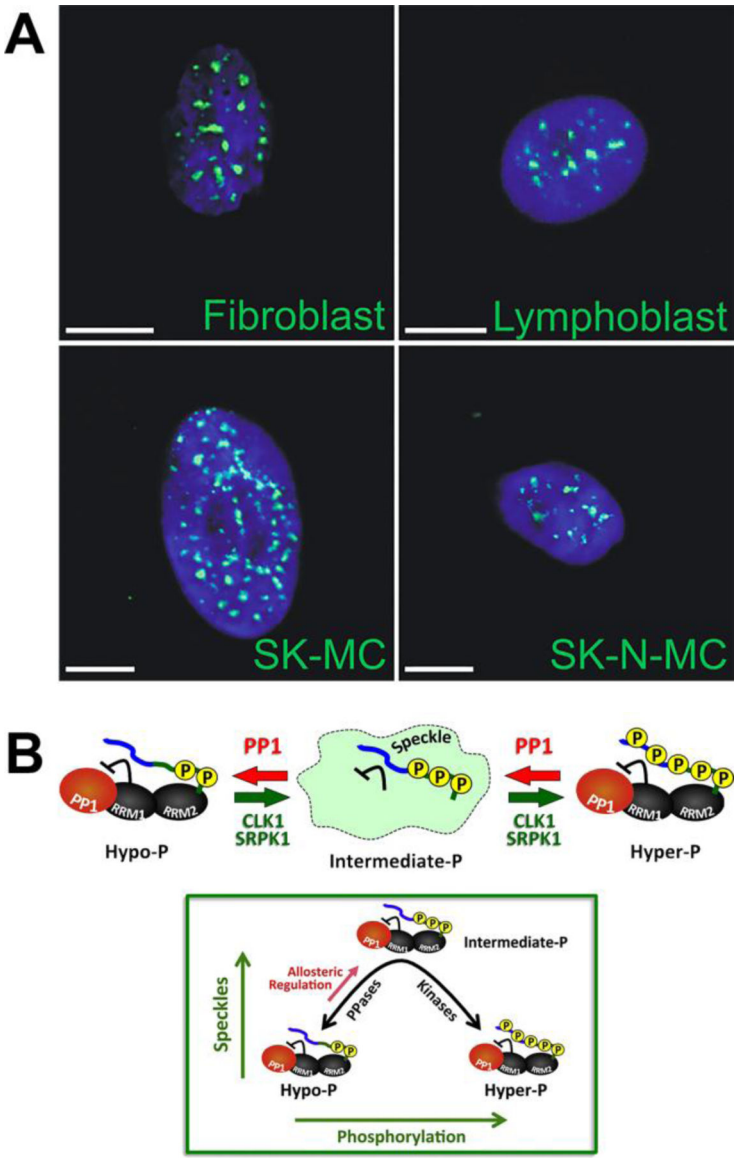

Figure 23.

(A) Representative microscopy images of NSs in cells (labeled for SRSF2). Bars = 10 μm (for the fibroblast, SK-MC and SK-N-MC) and 5 μm (for the lymphoblast). Adapted from Ref. 184. (B) Speckle localization is regulated by the balanced actions of kinases (e.g., SRPK1 and CLK1) and phosphatases (e.g., PP1). Adapted from Ref. 187. Copyright © 2017 by Elsevier Inc.

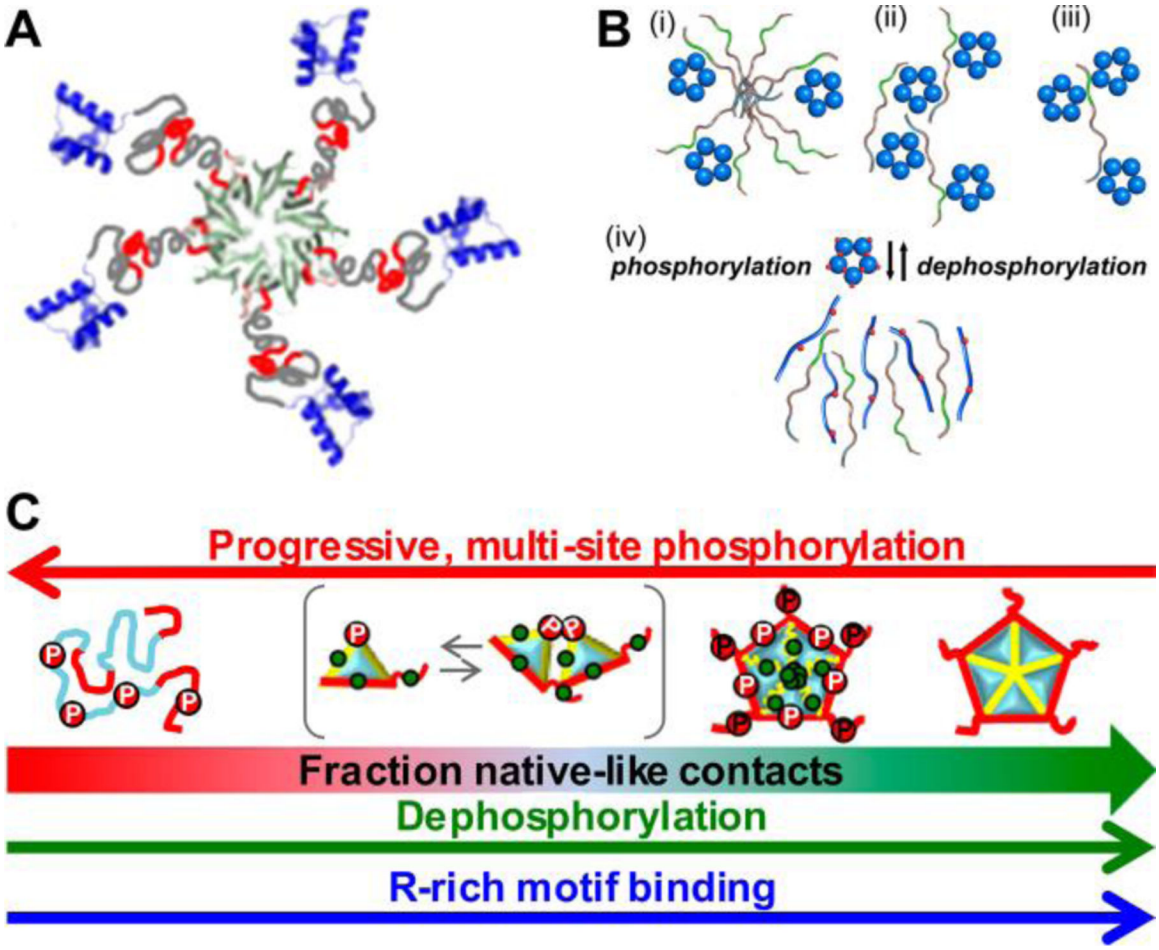

Figure 24.

(A) Pentamer of NPM. Adapt from Ref. 189. (B) The illustration of p14arf-NPM-N heteropolymerization. (i) p14arf may form homo-oligomers to interact with different NPM-N pentamers (blue spheres or ribbons). (ii) Both the N-terminal end and the central regions of p14arf may interact with different NPM-N pentamers. (iii) The central region of p14arf interacts with two different NPM-N pentamers at the same time with its two arginine clusters, leaving the N-terminal ends free to interact with another NPM-N pentamers. (iv) Upon sequential phosphorylation of different exposed and buried Ser/Thr sites played by several kinases, NPM-N monomerizes and unfolds thus releasing active p14arf in the nucleoplasm. Red dots represent phosphorylation sites in NPM-N. Adapted from Ref. 190. (C) Enzymatic control of the conformation and assembly of NPM. Adapted from Ref. 188.

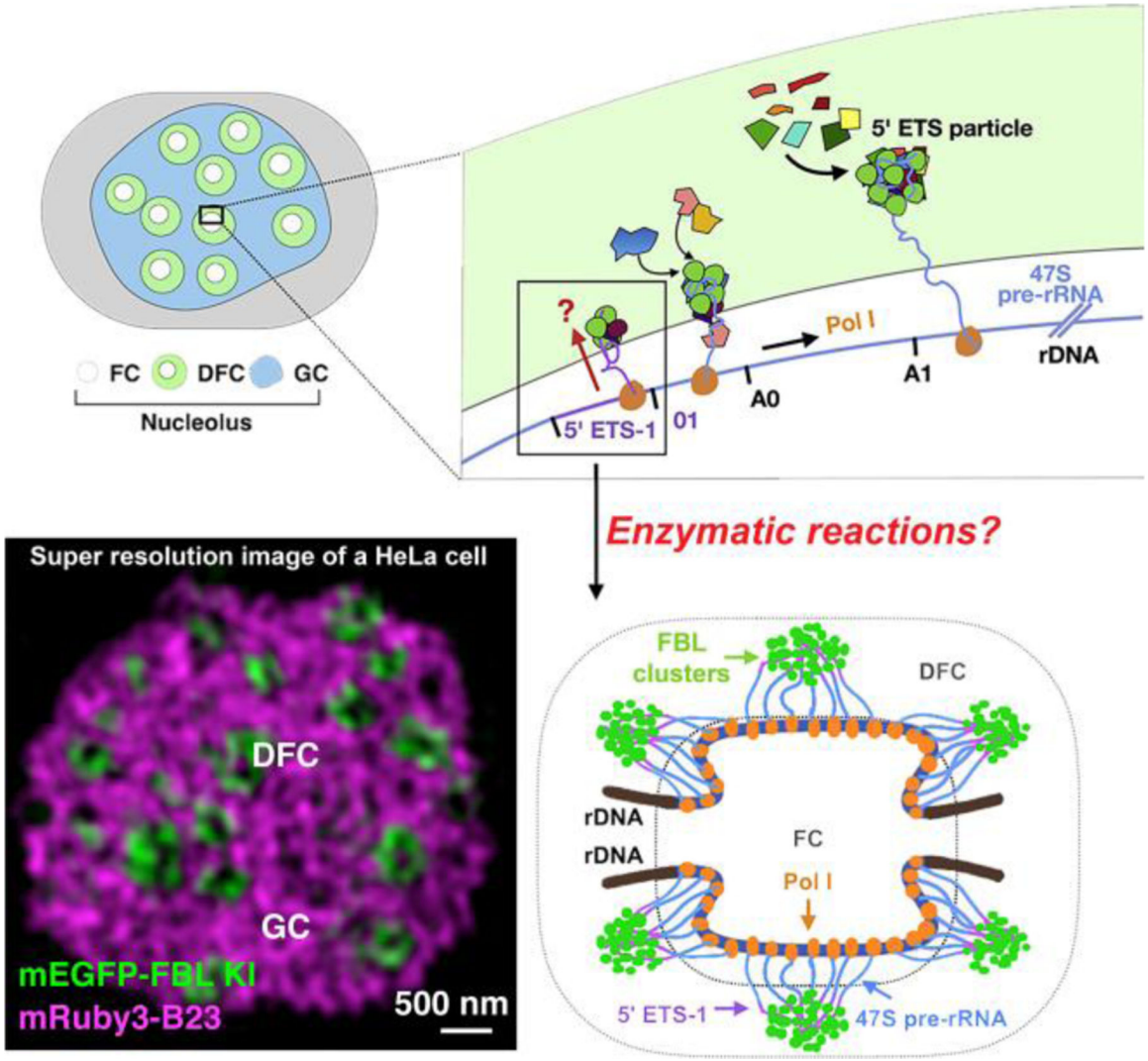

Figure 25.

Sorting of pre-rRNA at the interface of FC and DFC. Adapted from Ref. 192. Copyright © 2019 by Elsevier Inc.

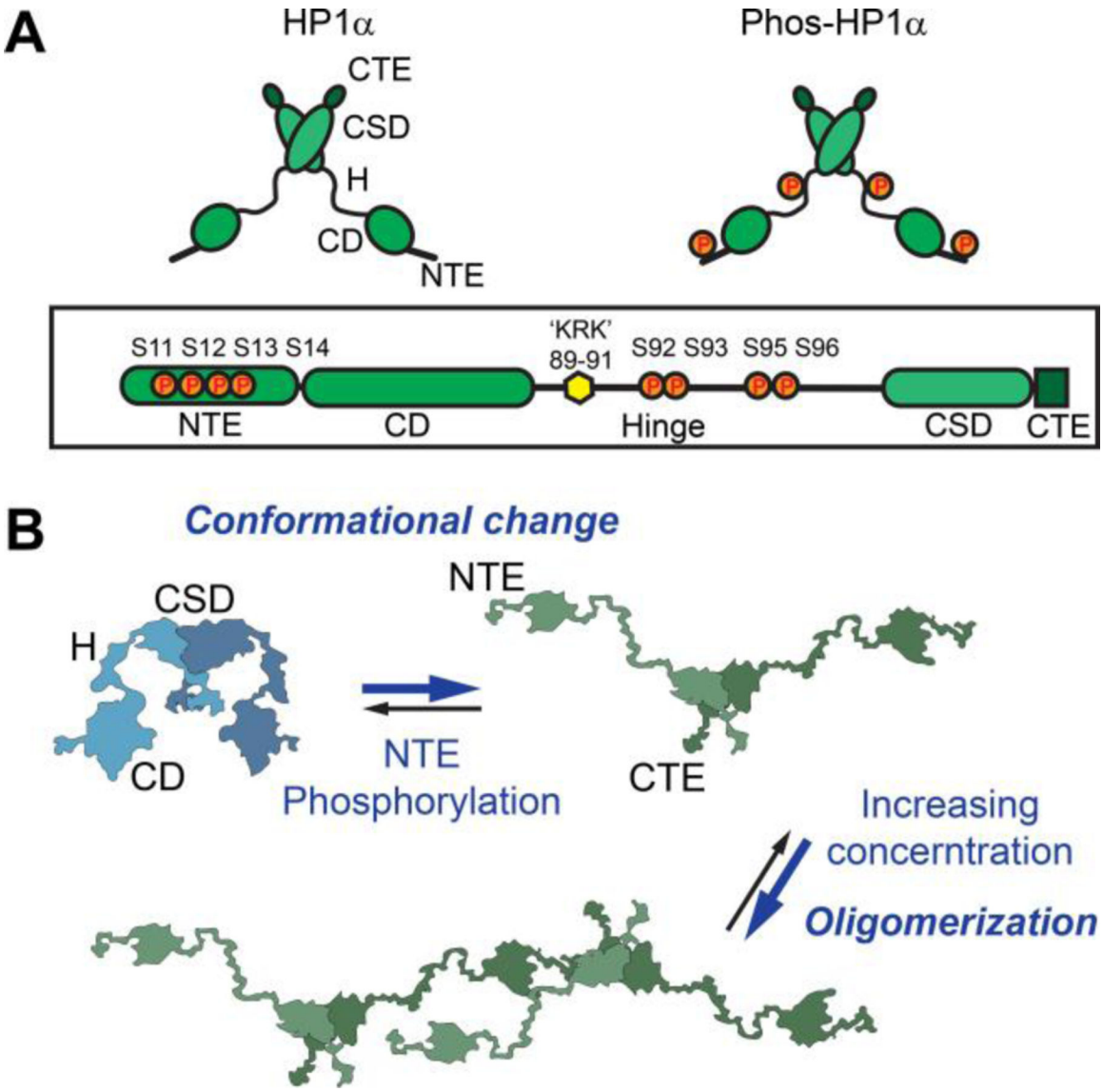

Figure 26.

(A) Schematics of HP1α phosphorylation. CD, chromodomain; CSD, chromoshadowdomain; CTE, C-terminal extension; H, hinge; NTE, N-terminal extension. (B) Model for how HP1α switches between a compact and extended state: the N-terminal phosphates interact with basic hinge residues to stabilize inter-dimer contacts in the extended state and promote higher-order oligomerization. Adapted from Ref. 193. Copyright © 2017 by Springer Nature.

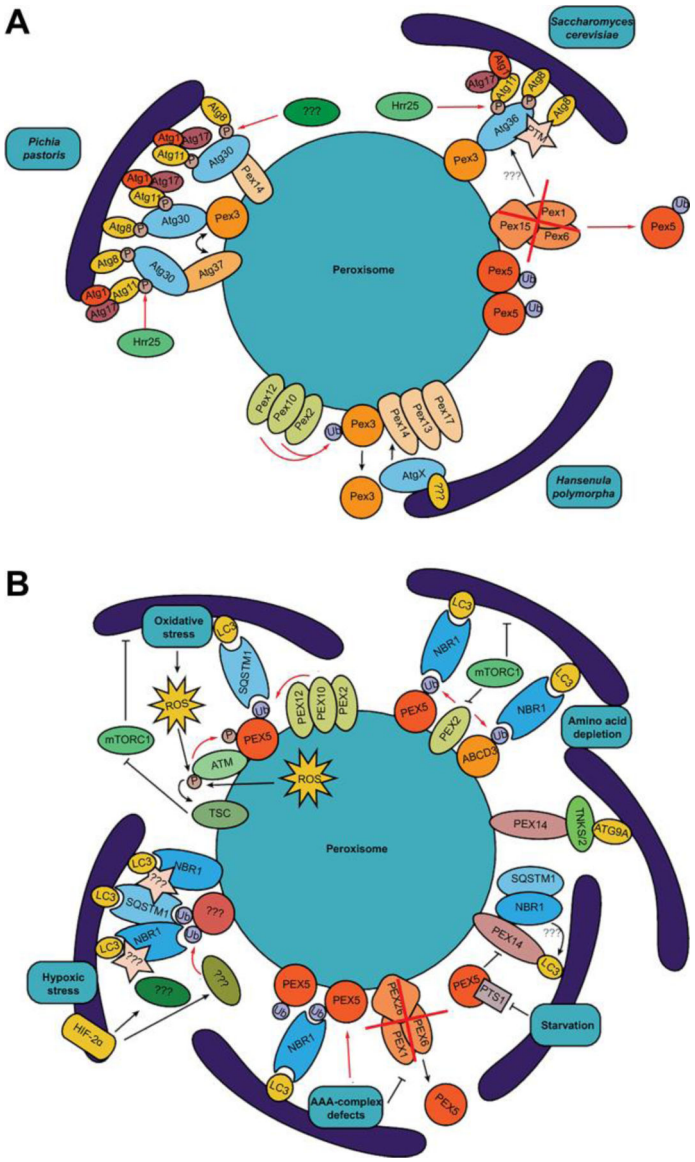

Figure 27.

Mechanisms of pexophagy in (A) yeast and (B) mammalian cells. (A) Hrr25 phosphorylates Atg30 and Atg36 to allow recruitment of the autophagic scaffold protein Atg11. Recognition of the peroxisome by the autophagic machinery requires Pex14. (B) Several stress conditions (e.g., hypoxia in mammalian cells) leads to ubiquitination of PEX5 and ABCD3 and the recruitment of ubiquitin-binding autophagy receptors NBR1 and SQSTM1 for tethering peroxisomes to the phagophore. Adapted from Ref. 196. Copyright © 2018 by Springer Nature.

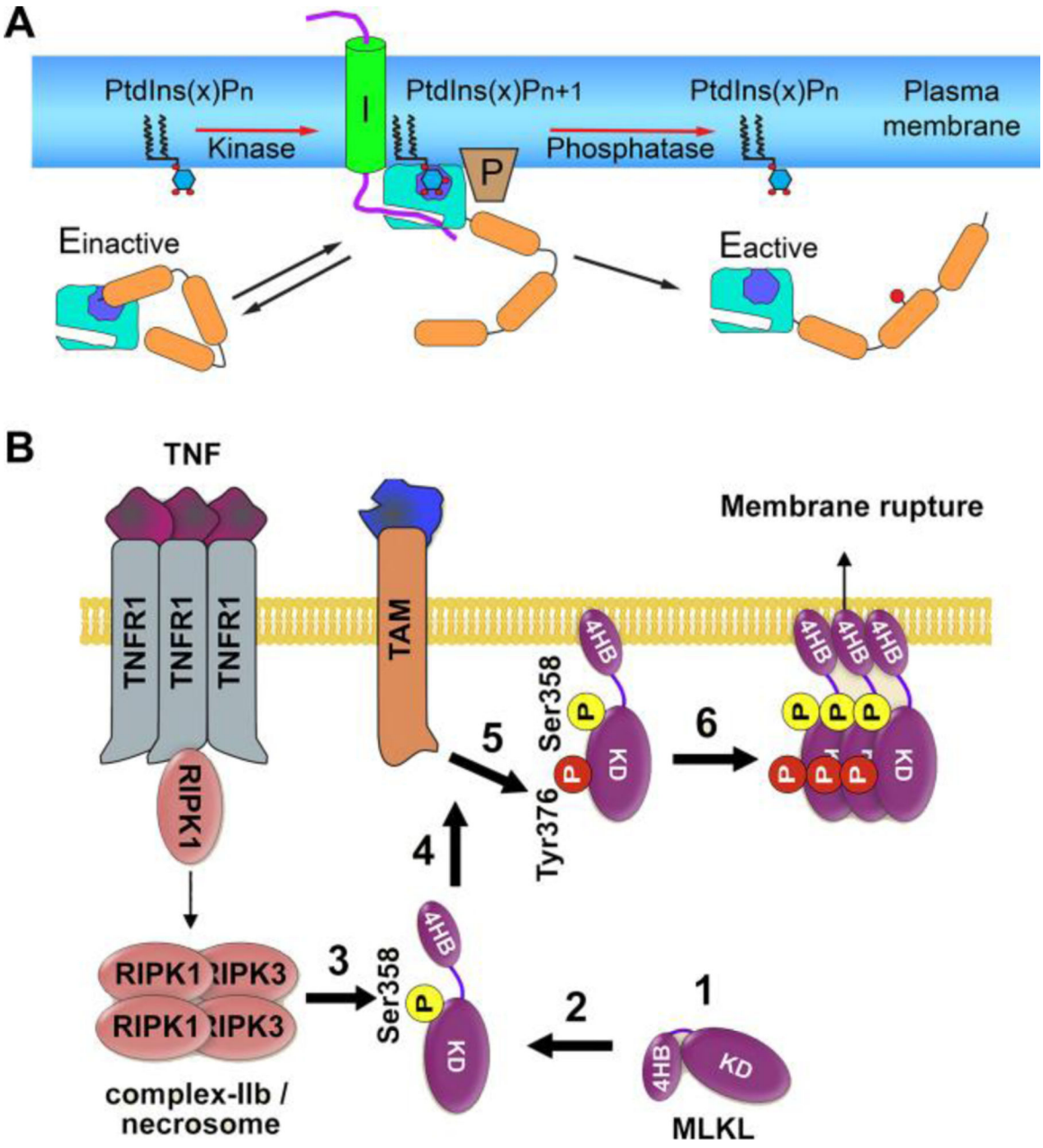

Figure 28.

(A) Enzymatic reaction of phosphoinositides PtdIns(x,y)Pn control several kinds of signaling processes. $E_{inactive}$: proteins contain phosphoinositide-recognition domains and assume an inactive conformation. Phosphorylated phosphoinositide (PtdIns(x,y)Pn+1) recruits the protein to the membrane, and to interact with integral (I) or peripheral (P) membrane proteins. The complex can remain active at the membrane and recruit additional proteins. The protein can return to the cytosol in an activated (i.e. phosphorylated) form (E_{active}). Adapted from Ref. 197. Copyright © 2005 by The Company of Biologists. (B) Diagram of the mechanistic findings for the TAM-MLKL input into the necroptosis

pathway, which involves enzymatic phosphorylation and assembly. Adapted from Ref. 198.

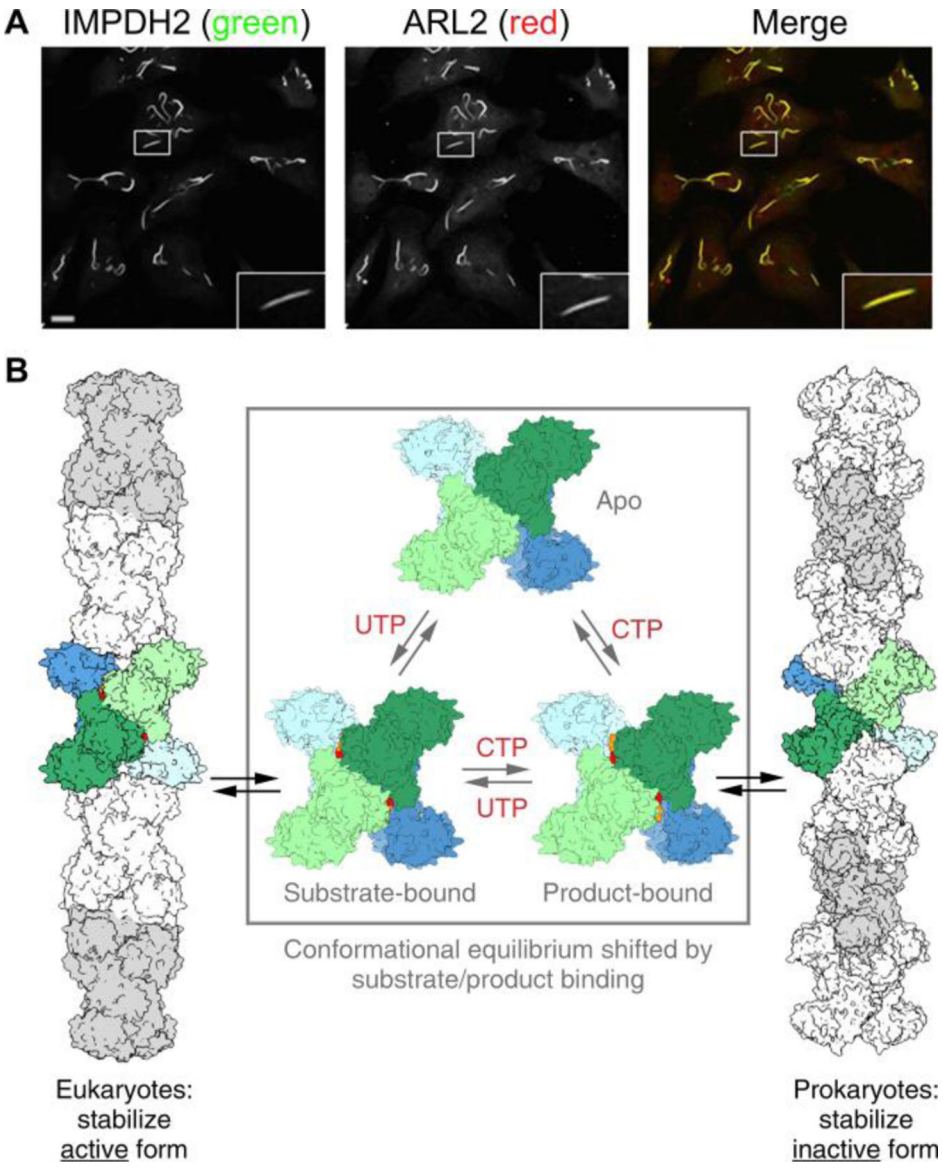

Figure 29.

(A) ARL2 localizes to IMPDH2-positive structures that are inducible with MPA in HeLa cells. Scale bar in bottom left panel = 10 μm and is the same for each image. Adapted from Ref. 202. (B) The model for the allosteric regulation of CTPS filament assembly. ecCTPS and hCTPS1 undergo a conserved conformation cycle but have opposite determinants for filament assembly. Adapted from Ref. 203. Copyright © 2017 by Springer Nature.

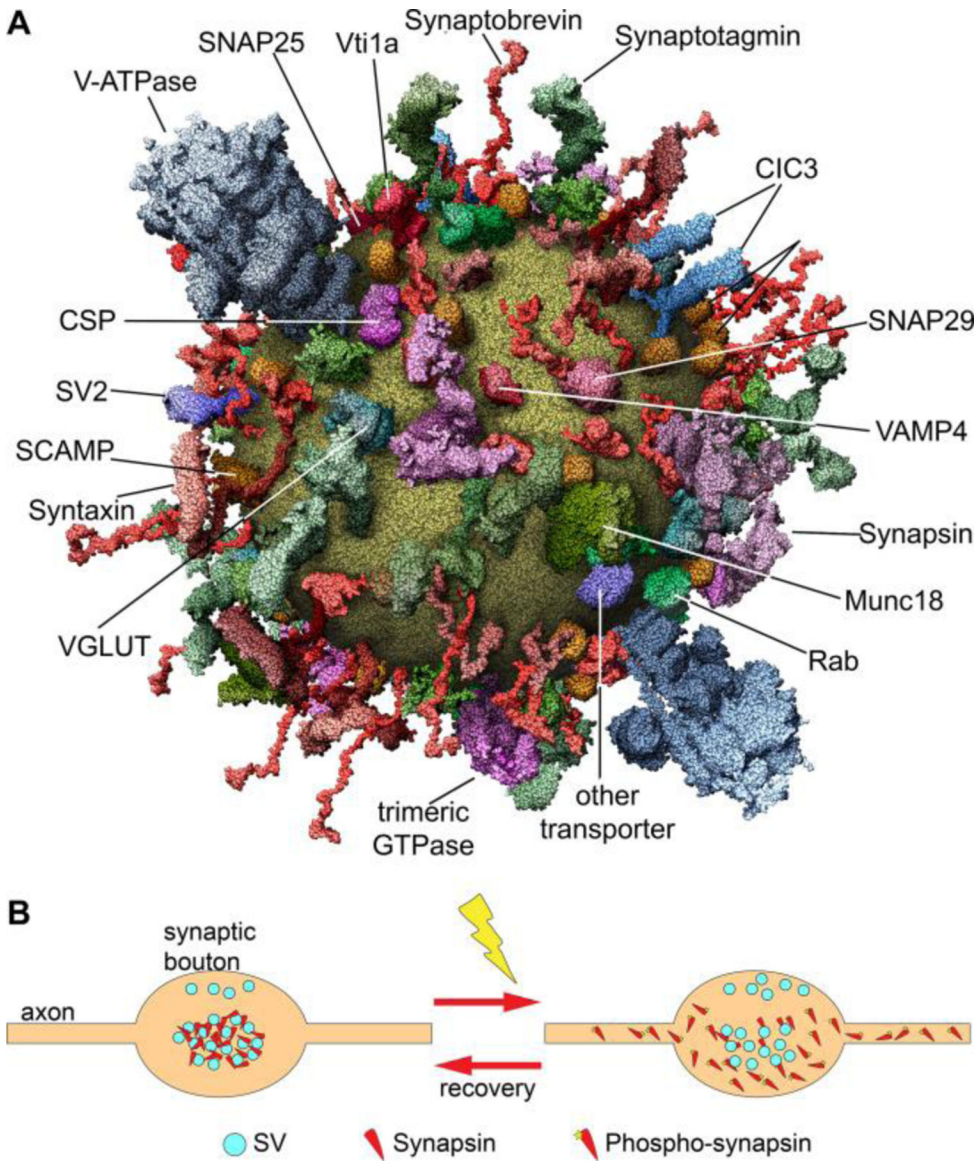

Figure 30.

(A) The composition of synaptic vesicles. Adapted from Ref. 207. Copyright © 2006 by Elsevier Inc. (B) Synapsin dispersion and recovery in pre-synaptic terminals. That is, synapsin dispersion and recovery in synaptic boutons: phosphorylated synapsin diffusing in the bouton and into the axonal compartment; after the stimulus, synapsin molecules are dephosphorylated and re-cluster on SVs in the bouton. Adapted from Ref. 206. Copyright © 2010 by Elsevier Inc.

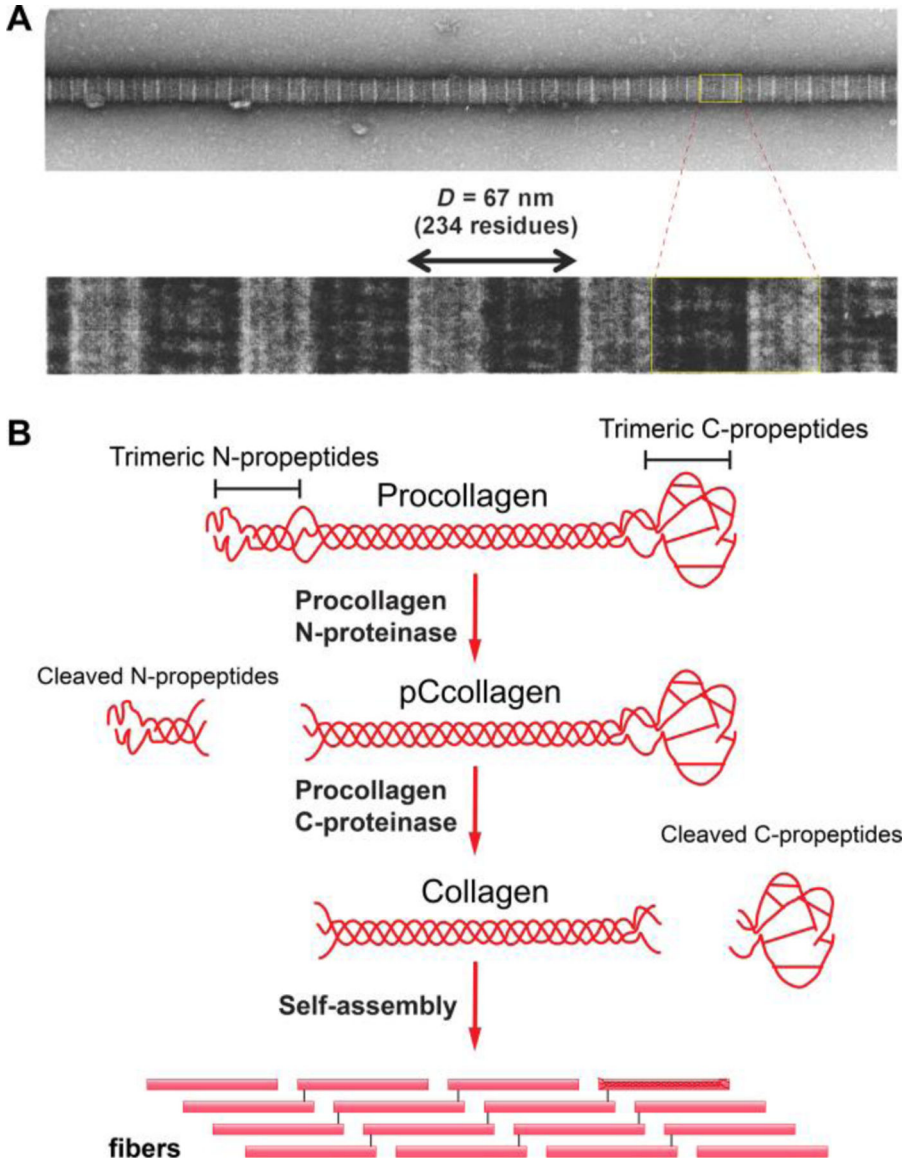

Figure 31.

(A) Negatively stained unipolar collagen fibril isolated from embryonic chick metatarsal tendon. Enlargement shows the axial periodicity. (B) Schematic representation of collagen fibril formation by cleavage of procollagen. Sequential cleavage of the N-propeptides (by procollagen N-proteinase, which are ADAM 2, 3, 14) and the C-propeptides (by procollagen C-proteinase, which are the BMP-1/tolloid family) of procollagen generates collagen that self-assembles into unipolar collagen fibrils. Adapted from Ref. 211.

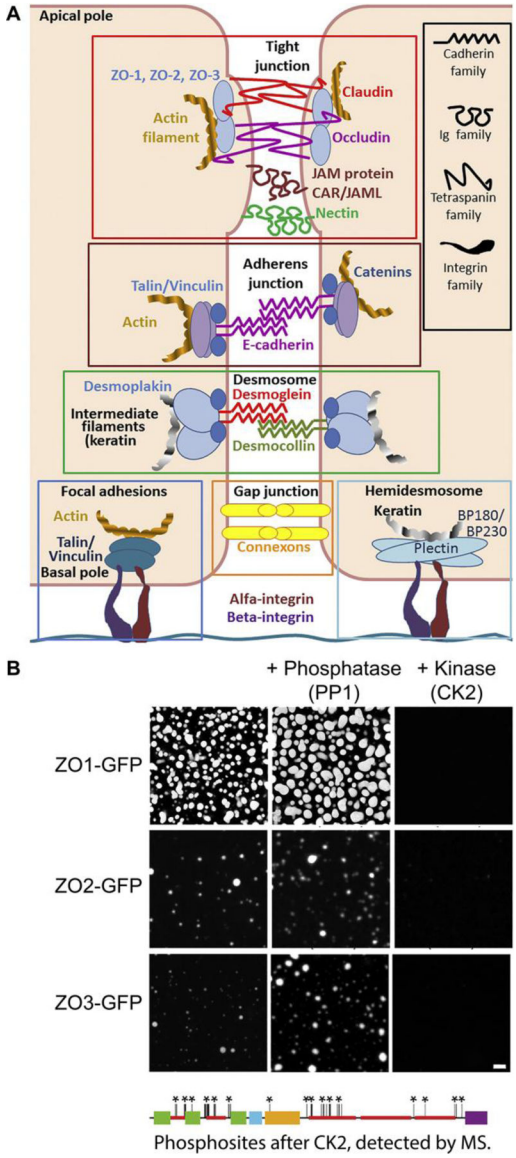

Figure 32.

(A) Cell junctions typical for normal epithelial and endothelial cells and the relevant major proteins of junctions. Adapted from Ref. 212. Copyright © 2018 by Elsevier Inc. (B) De-/Phosphorylation controls phase separation of ZO proteins. Scale bar = 5 μm. Adapted from Ref. 218. Copyright © 2019 by Elsevier Inc.

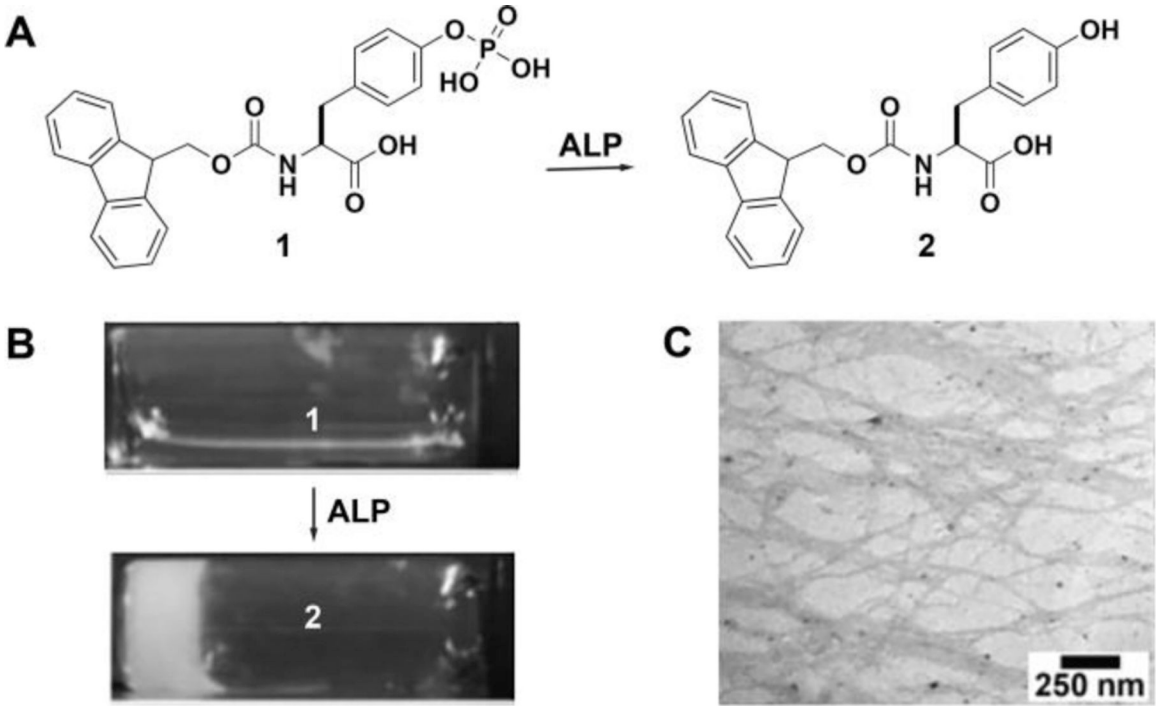

Figure 33.

(A) ALP catalyzes the dephosphorylation of **1** to form **2**. (B) The sol-gel transition after adding ALP to the solution of **1**. (C) The TEM image of the hydrogel formed by **2**. Adapted from Ref. 37. Copyright © 2004 by Wiley Inc.

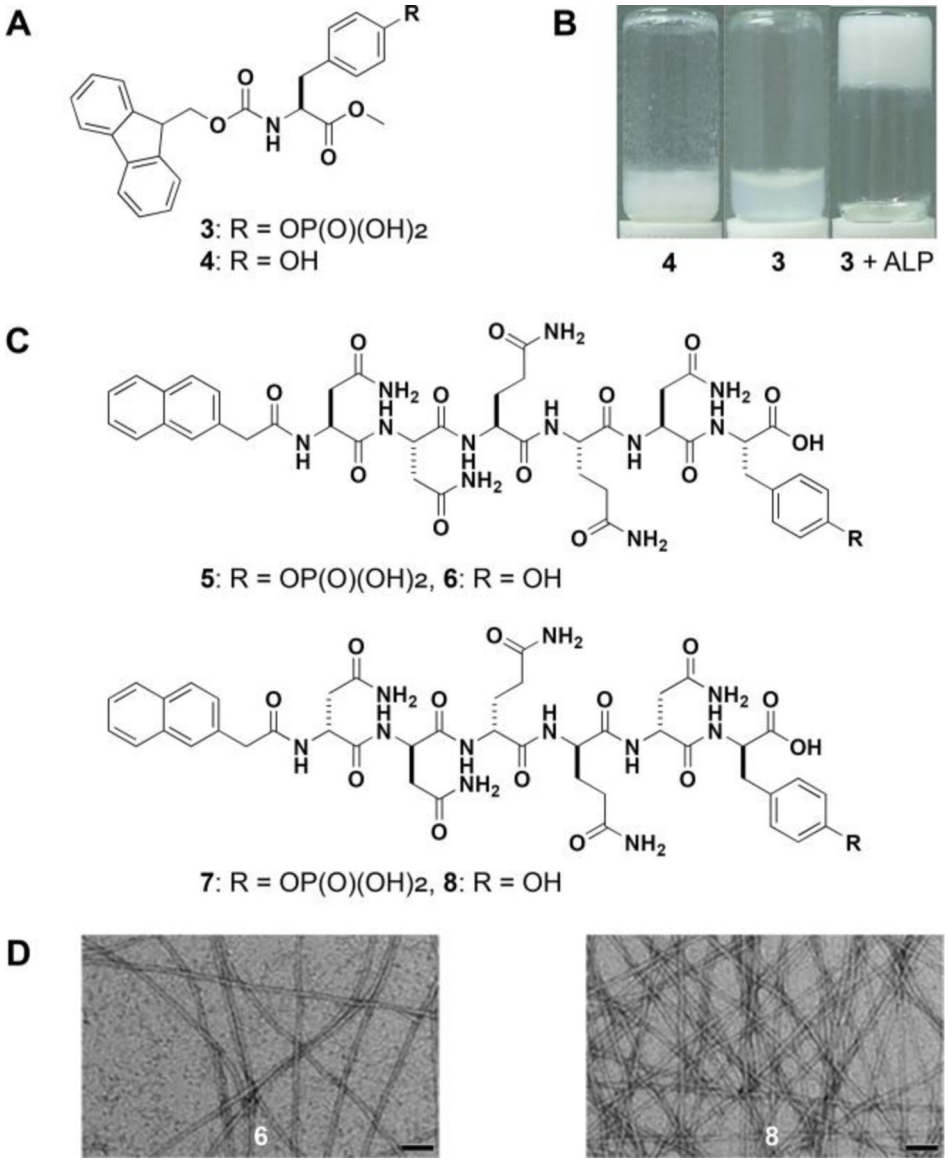

Figure 34.

(A) The structures of **3** and **4**. (B) Optical images of the suspension of **4** (1.0 wt%, PBS, pH 8.0), the solution of **3**, and the gel formed 10 minutes after adding ALP (16 U/mL) to the solution of **3** (1.0 wt%, PBS, pH 8.0). Adapted from Ref. 240. Copyright © 2009 by American Chemical Society. (C) The structure of **5**/**6** and **7**/**8**. (D) TEM images of the nanofibers in the gels formed by **6** and **8**. Scale bar = 100 nm. Adapted from Ref. 302. Copyright © 2016 by Royal Chemical Society.

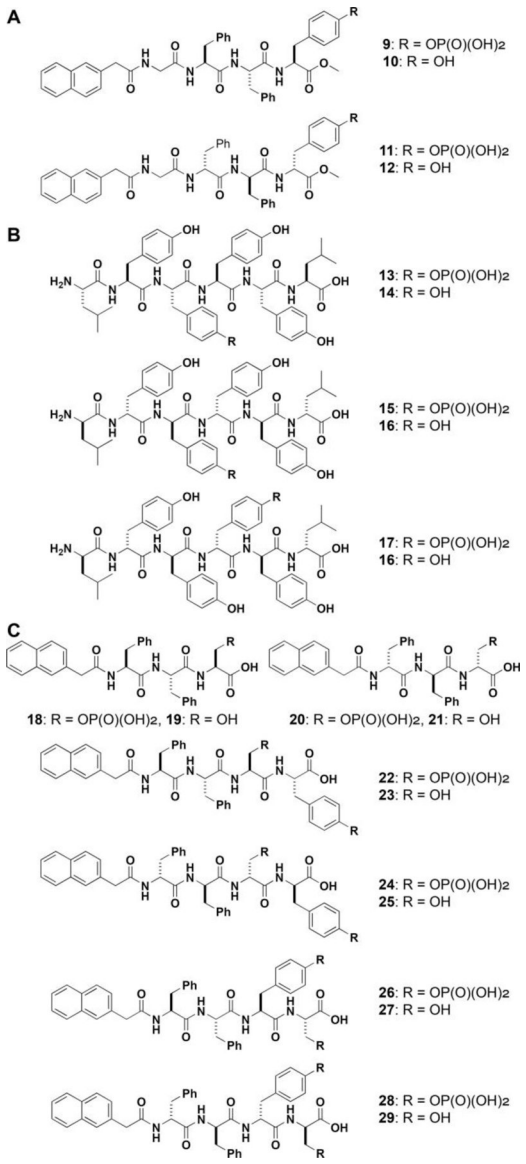

Figure 35.

(A) The structures of **9**/**10** and **11**/**12**. (B) The structures of the hexapeptide (**14**) in an ITIM, and its enantiomer (**16**) and the corresponding phosphorylated precursors (**13**, **15**, and **17**). (C) The structure of the phosphoserine containing peptides (**22**, **24**, **26**, and **28**) and their corresponding dephosphorylated products (**23**, **25**, **27**, and **29**).

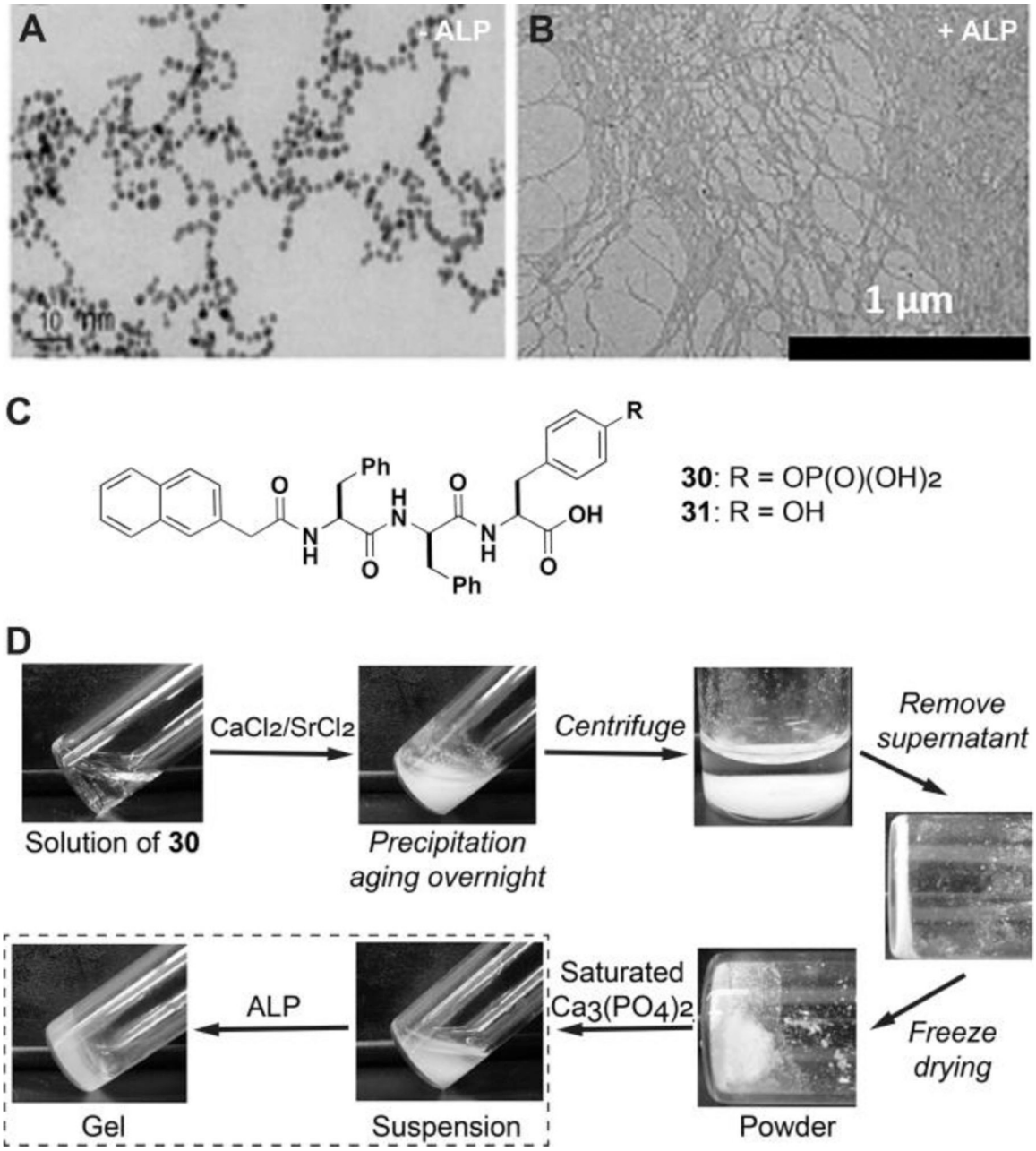

Figure 36.

(A) TEM images of the $GGFF_pY$ decorated QDs in the absence and (B) presence of ALP. Adapted from Ref. 318. Copyright © 2018 by Royal Chemical Society. (C) The structures of **30** and **31**. (D) A typical procedure for preparation of the hydrogels via the enzymatic solid-gel transition: **30** dissolves in 7.4 tris-HCl buffer at initial concentration of 0.6 wt% (8.29 mM), the concentration of saturated $Ca_3(PO_4)_2$ is around 3.87 μM, and $[\mathbf{30}]_0$:$[Ca^{2+}$ or $Sr^{2+}]_0$ is 1:2. Adapted from Ref. 319. Copyright © 2015 by Wiley Inc.

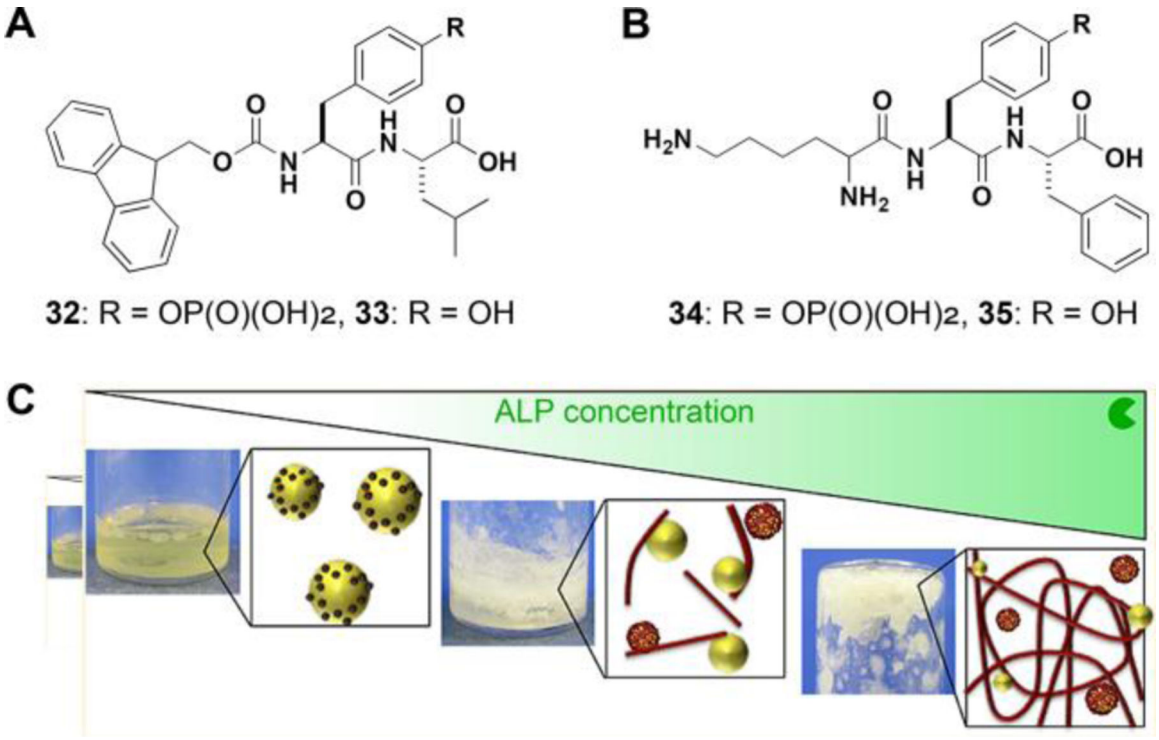

Figure 37.

(A) The structures of **32** and **33**. (B) The structures of **34** and **35**. (C) In a biphasic system, ALP addition converts a two-phase system with some micelles of **34** at the interface of oil droplets into a more established oil-in-water emulsion by the formation of nanofibers at the interface and surrounding oil droplets, with the emulsifying ability controlled by the specific amount of enzyme used. Adapted from Ref. 322. Copyright © 2017 by American Chemical Society.

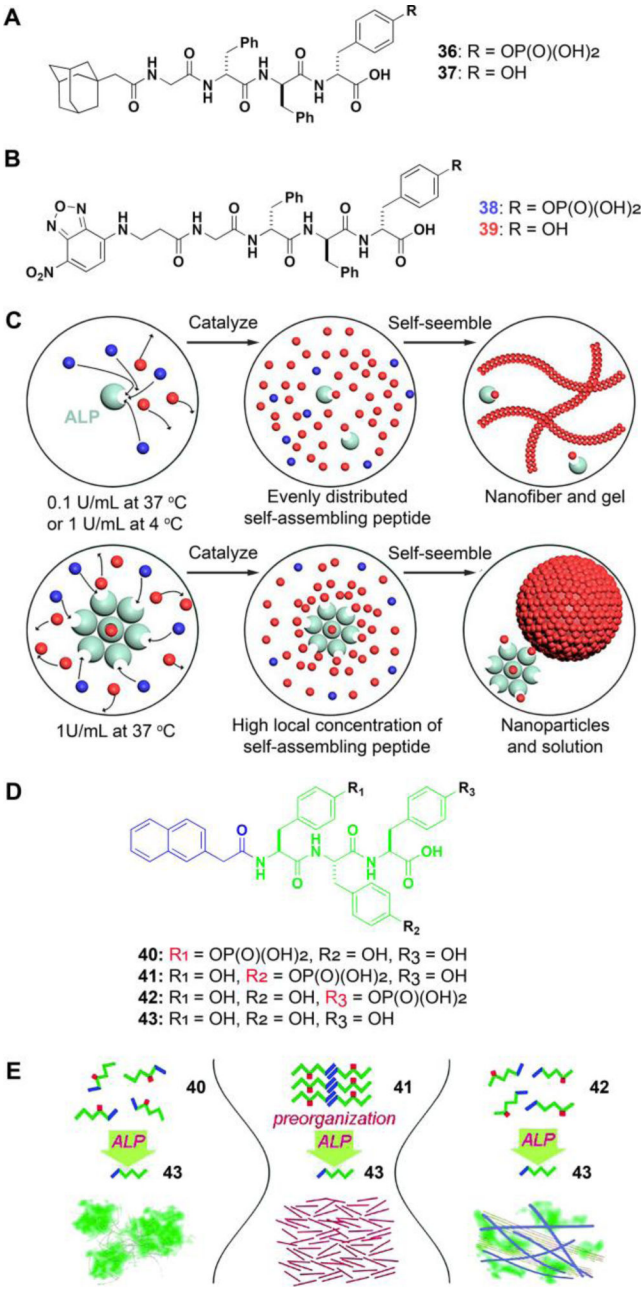

Figure 38.

(A) The structures of Ada-Gff$_p$y (**36**) and Ada-Gffy (**37**). (B) The structures of NBDgff$_p$y (**38**) and NBDgffy (**39**). (C) ENS spatiotemporally controlled by temperature and the concentration of ALP. Adapted from Ref. 324. Copyright © 2017 by American Chemical Society. (D) The structures of Nap-YYY (**40**), Nap-$_p$YYY (**41**), Nap-Y$_p$YY (**42**), and Nap-YY$_p$Y (**43**). (E) Schematic illustration of different self-assemble behaviors of three precursors. Adapted from Ref. 325. Copyright © 2018 by Royal Chemical Society.

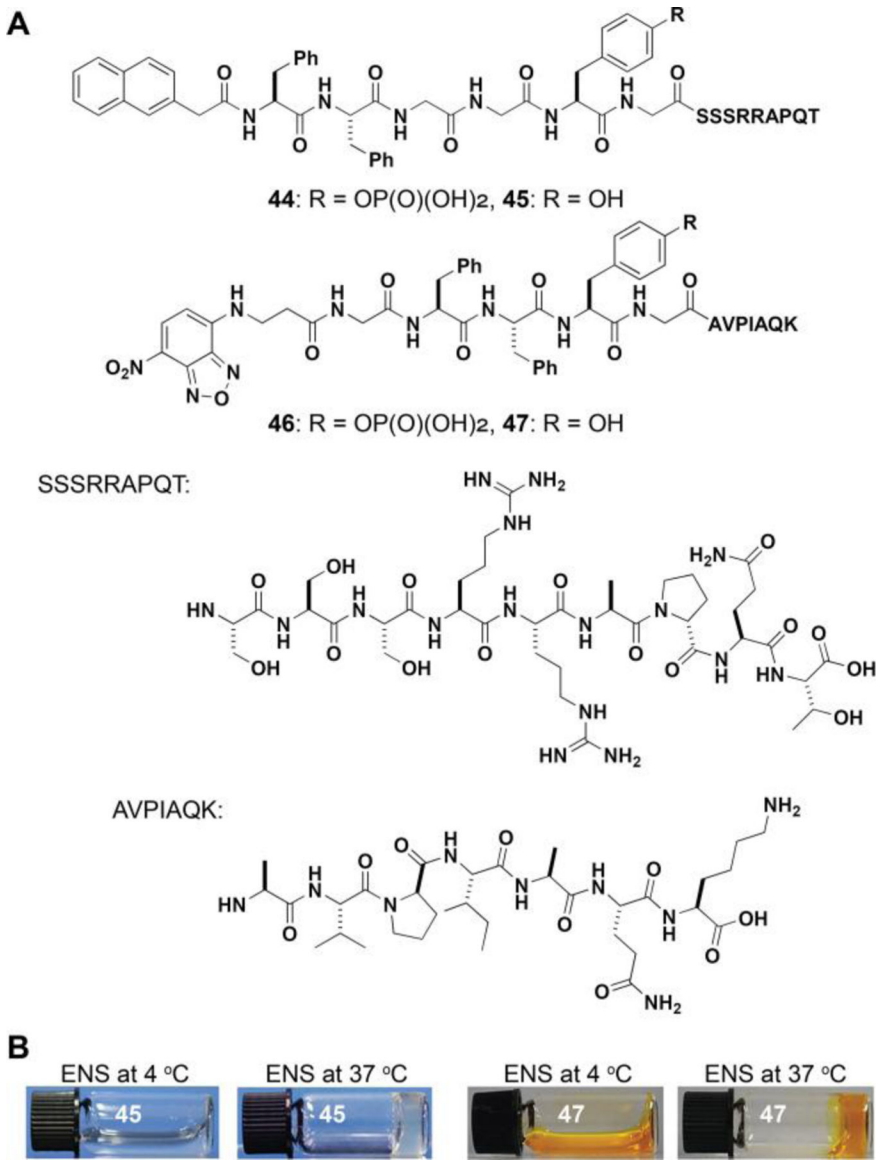

Figure 39.

(A) The structures of Nap-FFGG$_p$YGSSSRRAPQT (**44**) and NBD-GFF$_p$YGAVPIAQK (**46**). (B) Optical images of the solutions of **45** and **47** formed by ALP catalyzed ENS at 4 °C, and the corresponding hydrogels formed raising the temperature 37 °C. Adapted from Ref.[327]. Copyright © 2019 by Royal Chemical Society.

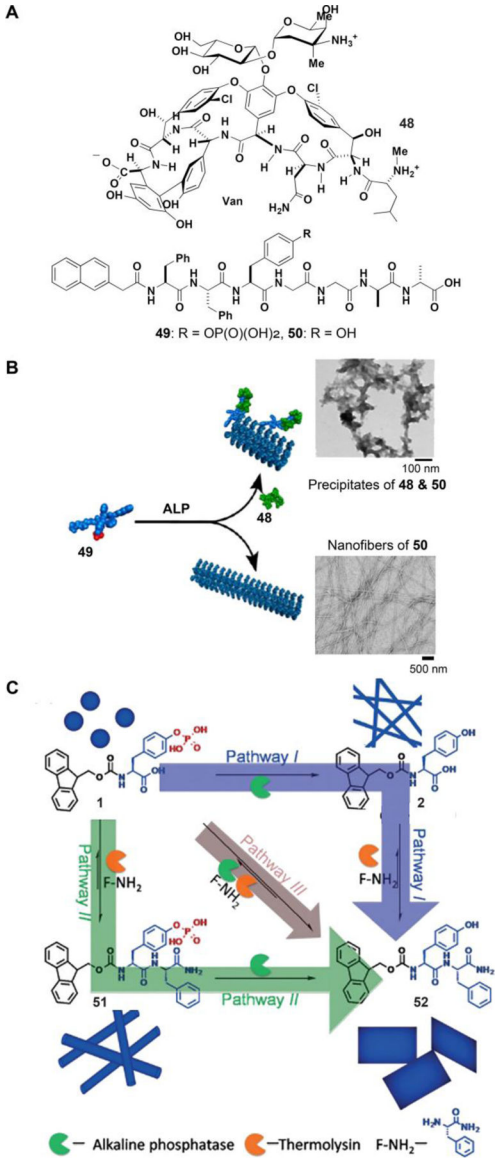

Figure 40.

(A) The structures of vancomycin (**48**) and the peptides, **49** and **50**. (B) The illustration of ligand–receptor interaction of small molecules dictating the pathways of ENS. Adapted from[328]. Copyright © 2016 by American Chemical Society. (C) Schematic representation of sequential (blue and green arrows, Pathways I and II) and competing (brown arrow, Pathway III) biocatalytic pathways from precursors **1** and F-NH_2 for generating assemblies with different morphologies. Adapted from Ref.[336]. Copyright © 2017 by Wiley Inc.

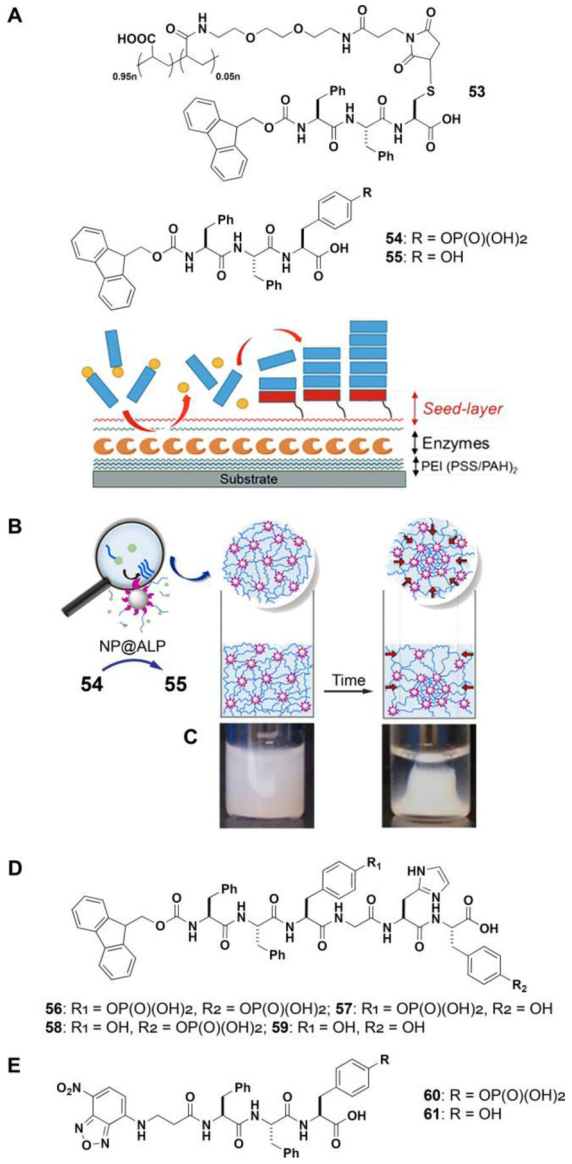

Figure 41.

(A) The structures of polyelectrolytes (**53**) and the peptides (**54** and **55**) and the illustration of the surface-localized ENS. Adapted from Ref.[338]. Copyright © 2015 by Wiley Inc. (B) ALP on silica nanoparticles dephosphorylates **54** to form **55**, leading to hydrogelation, and the nanofibers of **55** (in blue) self-assembled from NP@ALP by dephosphorylation of **54** leading to a hybrid supramolecular hydrogel undergoing a phase separation over time. (C) Optical images of the gel of **55** before and after phase separation. Adapted from Ref.[339]. Copyright © 2019 by American Chemical Society. (D) The structure of Fmoc-GFF$_p$YGH$_p$Y (**56**) and its dephosphorylated products. (E) The structures of NBD-FF$_p$Y (**60**) and NBD-FFY (**61**).

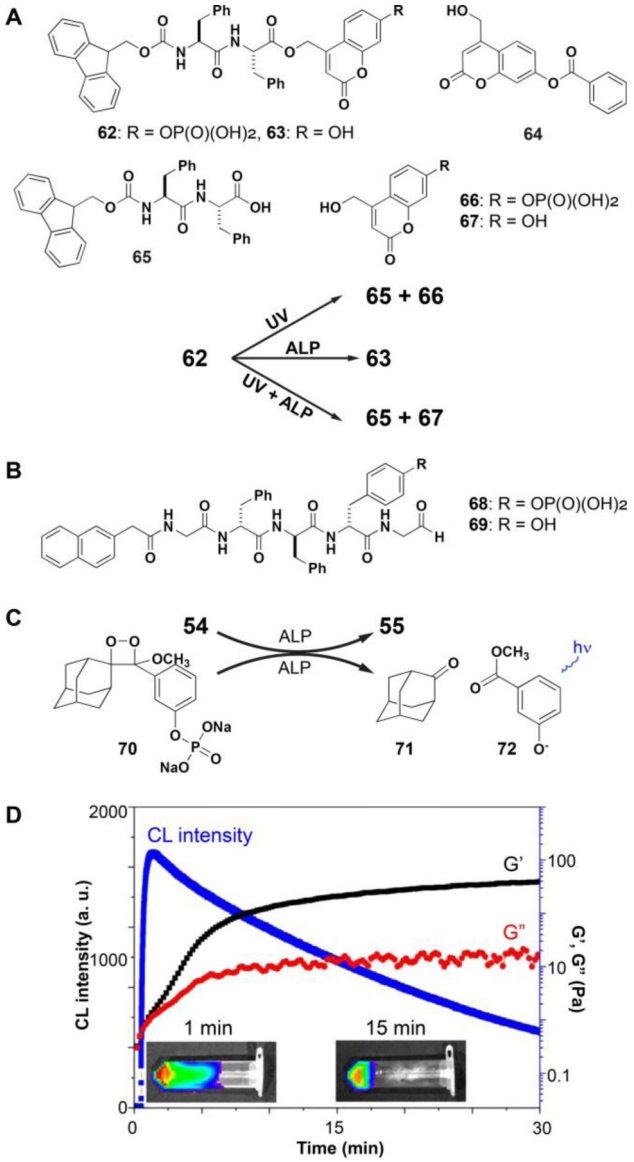

Figure 42.

(A) The structures of the gelators (**63** and **64**) and the corresponding precursor (**62**) and photochemical products (**65**, **66**, and **67**) and their enzymatic or photochemical conversion. (B) The structures of Nap-gff$_p$y-CHO (**68**) and Nap-gffy-CHO (**69**). (C) The illustration of ALP-triggered simultaneous hydrogelation of **55** and chemiluminescence of **72** (D) CL kinetic curve and time sweep of 12.9 mM **54** and 1.25 mM **70** incubated with 2 μM ALP at 25 °C. Insets: time-course CL images of **54** and **70** incubated with ALP at 25 °C. Adapted from Ref.[347]. Copyright © 2017 by American Chemical Society.

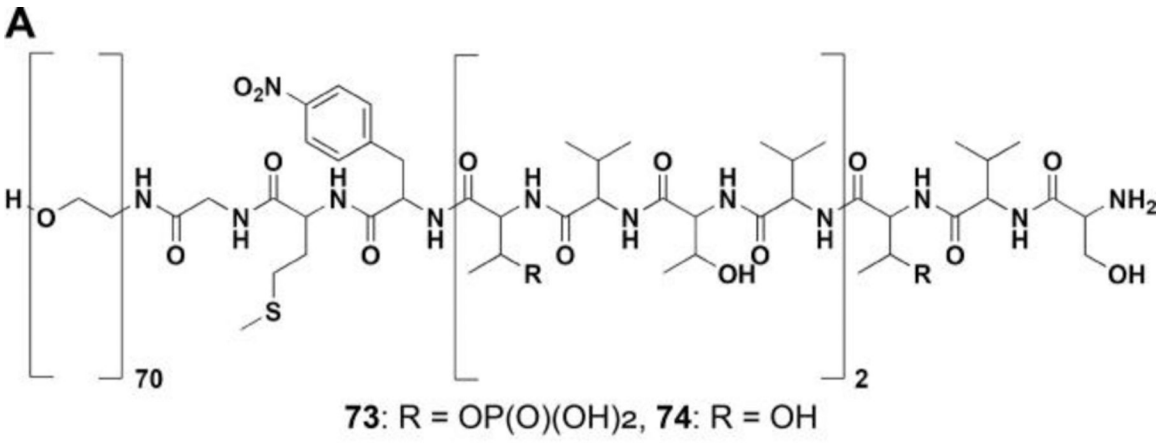

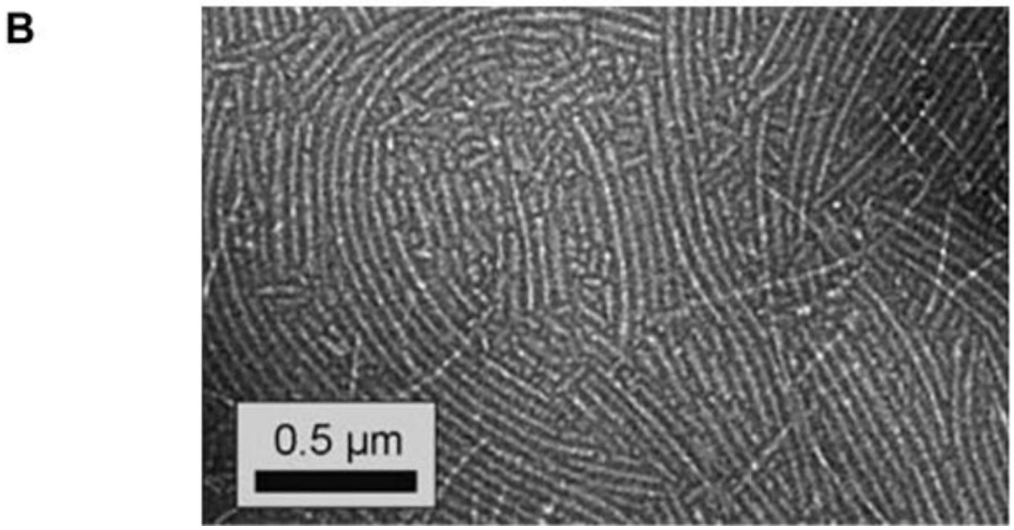

Figure 43.

(A) The structures of the polymer substrate (**73**) of acid phosphatase and the dephosphorylated product (**74**). (B). Microstructures formed by ACP triggered self-assembly of **74** visualized by TEM. Adapted from Ref.[348]. Copyright © 2009 by Wiley Inc.

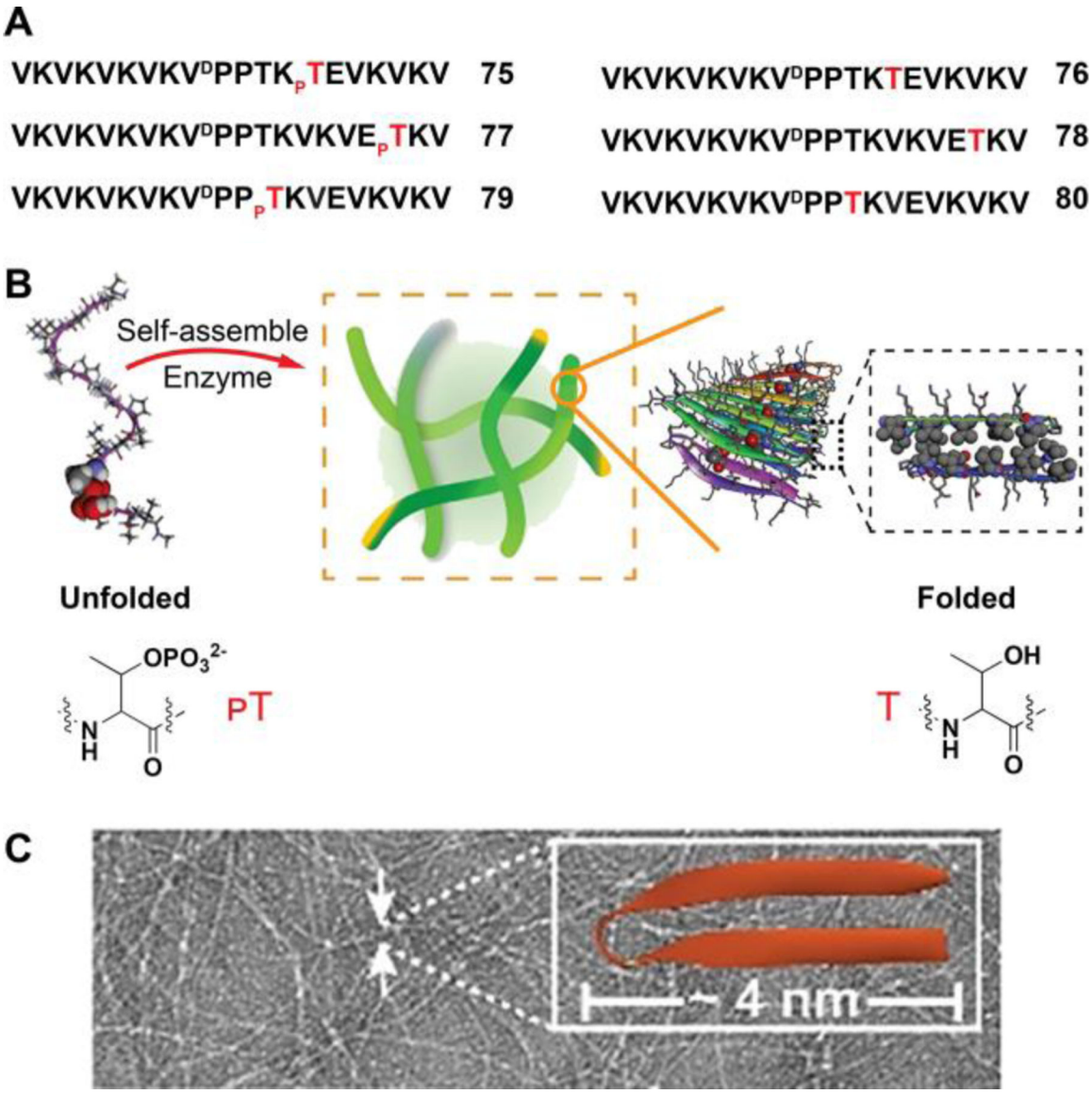

Figure 44.

(A) The sequences of the phosphopeptides and the corresponding peptides. (B) Enzymatic dephosphorylation shifts the conformational equilibrium favoring folded hairpin in the self-assembled state. (B) Enzymatic dephosphorylation shifts the conformational equilibrium to favor folded hairpin in the self-assembled state. (C) The TEM of the nanofibers formed by the self-assembly of **76**. Adapted from Ref.[349]. Copyright © 2018 by Wiley Inc.

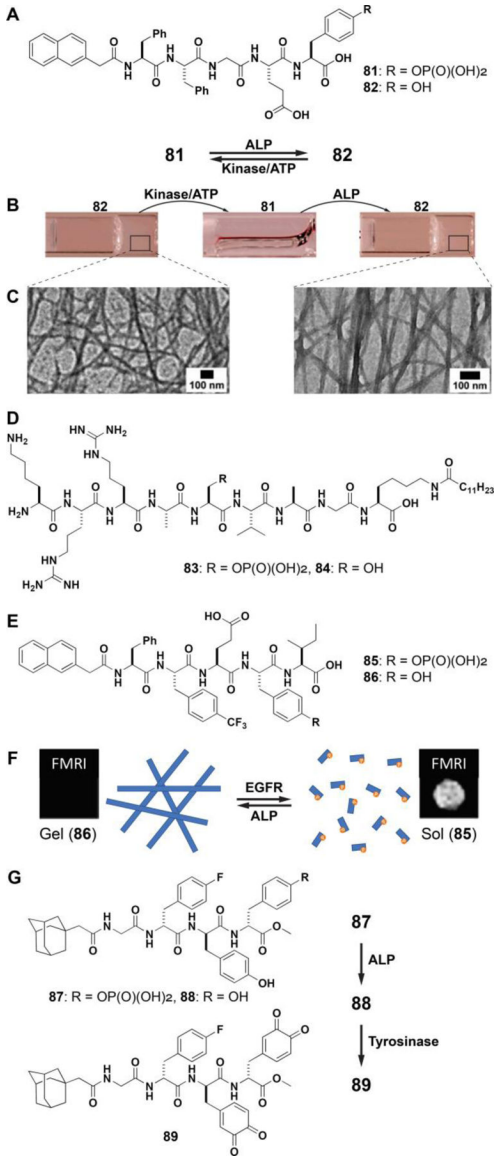

Figure 45.

(A) The structures of **81** and **82**, which are the substrates of phosphatase and kinase, respectively. (B) The kinase/phosphatase enzyme switch controls phase transition. (C) TEM shows the nanofibers in the hydrogel formed by ENS is more ordered (Right). Adapted from Ref. 226. Copyright © 2006 by American Chemical Society. (D) The structures of a pair of peptide amphiphiles (**83**/**84**) that is able to undergo phase transition controlled by protein kinase A (PKA)/ALP. (E) The structures of hydrogelator **86** and the phosphorylate precursor (**85**). (F) The illustration of the ^{19}F-fluorinated hydrogelator that undergoes ALP-instructed self-assembly and EGFR-guided disassembly. Hydrogel leads to the "OFF" signal and solution results in the "ON" signal of ^{19}F NMR/MRI. Adapted from Ref.[355]. Copyright © 2006 by American Chemical Society. (G) The structures of the molecules, **87**, **88**, **89**, which that exhibit OFF mode and ON mode of NMR by enzymatic reactions.[274]

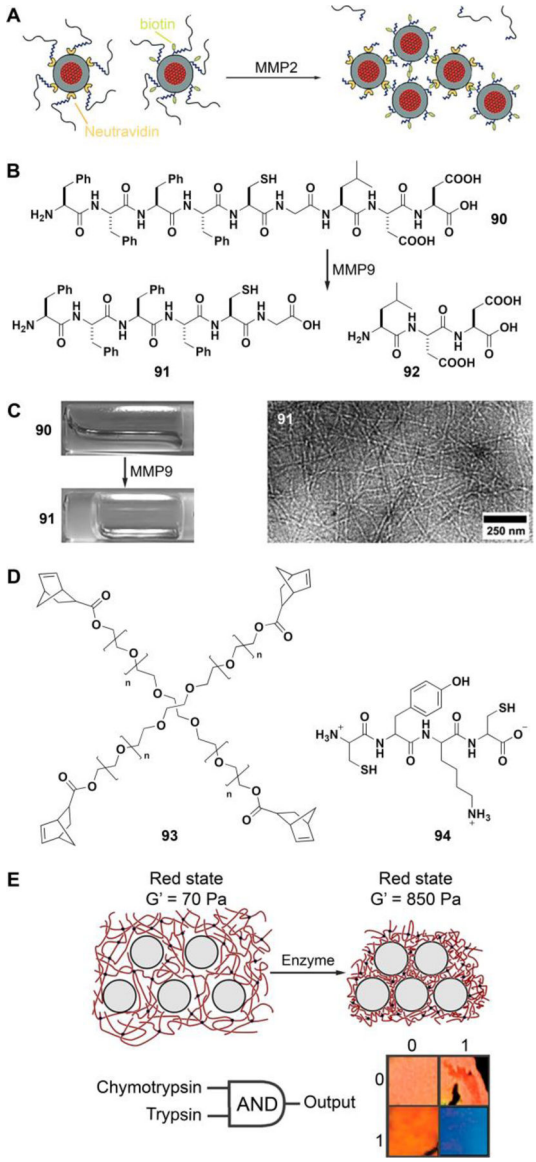

Figure 46.

(A) The illustration of a proteolytic actuation of self-assembly of neutravidin- and biotin-functionalized superparamagnetic iron oxide nanoparticles by MMP-2 cleaving peptide substrates (GPLGVRGC). Adapted from Ref.[359]. Copyright © 2006 by Wiley Inc. (B) The structure of **90**, a substrate of MMP-9, and the enzymatic hydrolysis process. (C) Optical images of the sol-gel transition and the TEM images of the nanofibers in the gel. Adapted from Ref. 238. Copyright © 2009 by Royal Chemical Society. (D) The structures of **93** and **94**. (E) Schematic depicting the enzyme induced stiffening of nanoparticle-hydrogel composites with a structural color. Adapted from Ref.[362]. Copyright © 2015 by American Chemical Society.

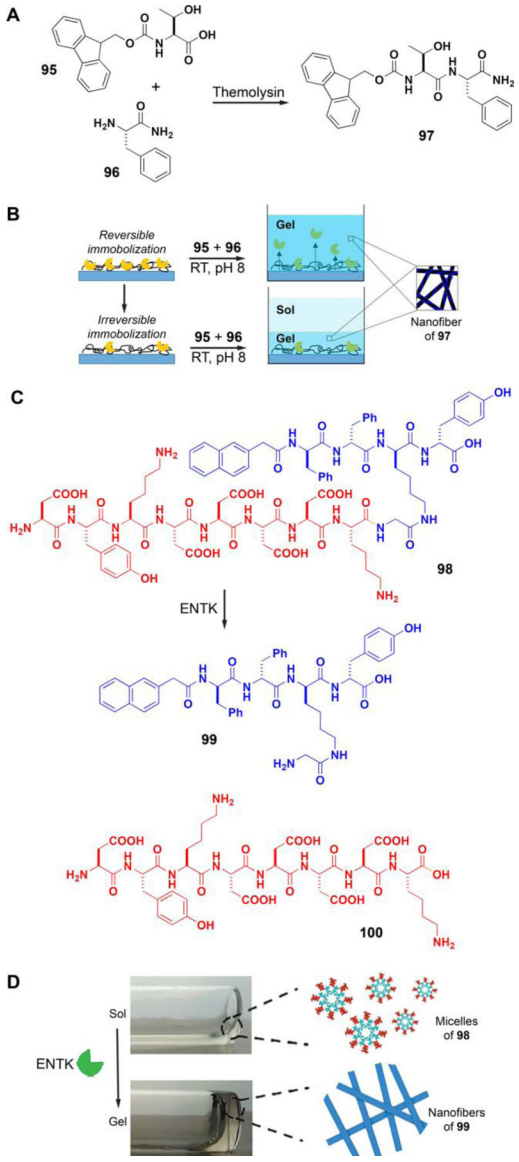

Figure 47.

(A) Conversion of the **95** and **96** to the gelator **97**, catalyzed by thermolysin. (B) Reversible and irreversible enzyme immobilization on modified surfaces for biocatalytic self-assembly. Adapted from Ref.[365]. Copyright © 2017 by American Chemical Society. (C) The structure of the branched peptide (**98**) that is a substrate of ENTK. (D) Optical image of the solution of **98** (2.5 wt%, PBS, pH 7.4) and the hydrogel of **99** formed after adding ENTK to the solution for 24 h and the schematic illustration of ENTK-catalyzed transformation of micelles to nanofibers. Adapted from Ref.[368]. Copyright © 2017 by American Chemical Society.

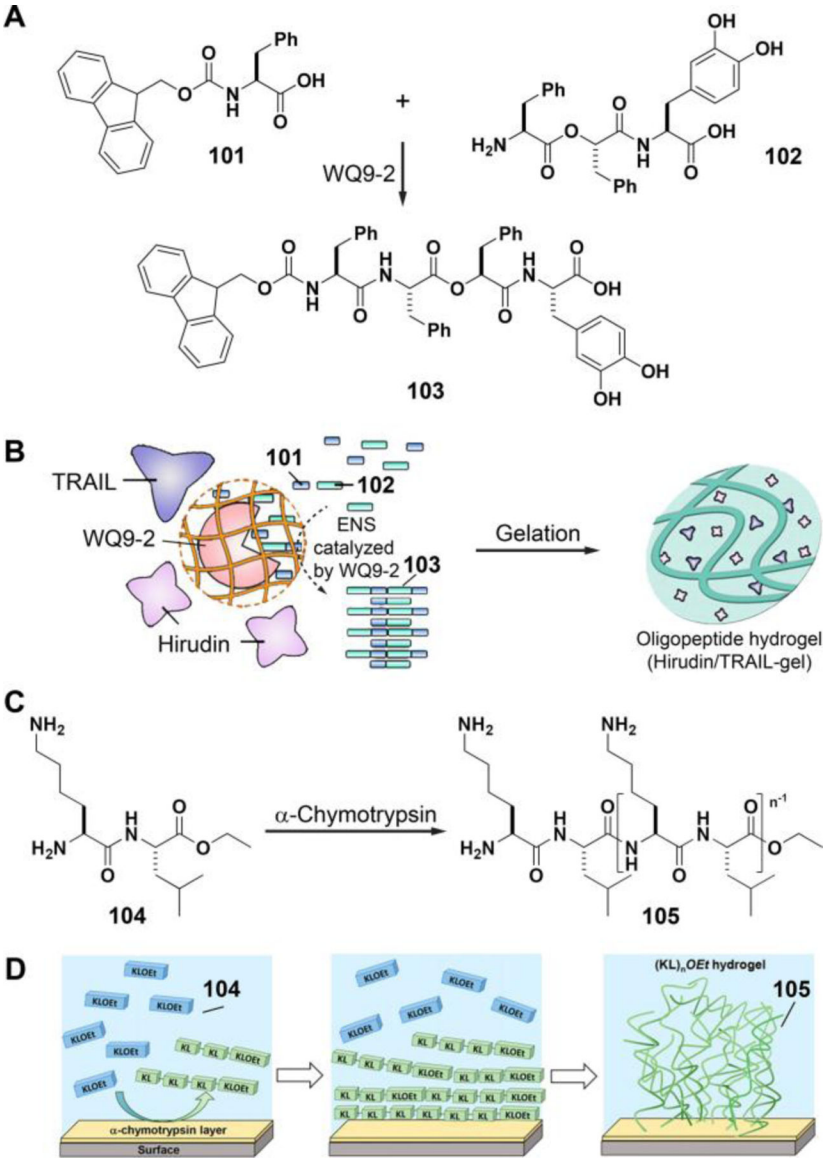

Figure 48.

(A) Reverse hydrolysis that generates **103** from **101** and **102**. (B) The illustration of substrate-selective protease-catalyzed self-assembly of the oligopeptide hydrogel for efficient encapsulation of hirudin and TRAIL (Hirudin/TRAIL Gel). Adapted from Ref.[372]. Copyright © 2017 by American Chemical Society. (C) Enzymatic conversion of the lysine-leucine ehyl ester dipeptides, KLOEt (104), to $(KL)_nOEt$ oligomers (**105**). (D) Schematic representation of the ENS of **105** formed near the surface adsorbed an α-chymotrypsin layer. Adapted from Ref.[375]. Copyright © 2017 by American Chemical Society.

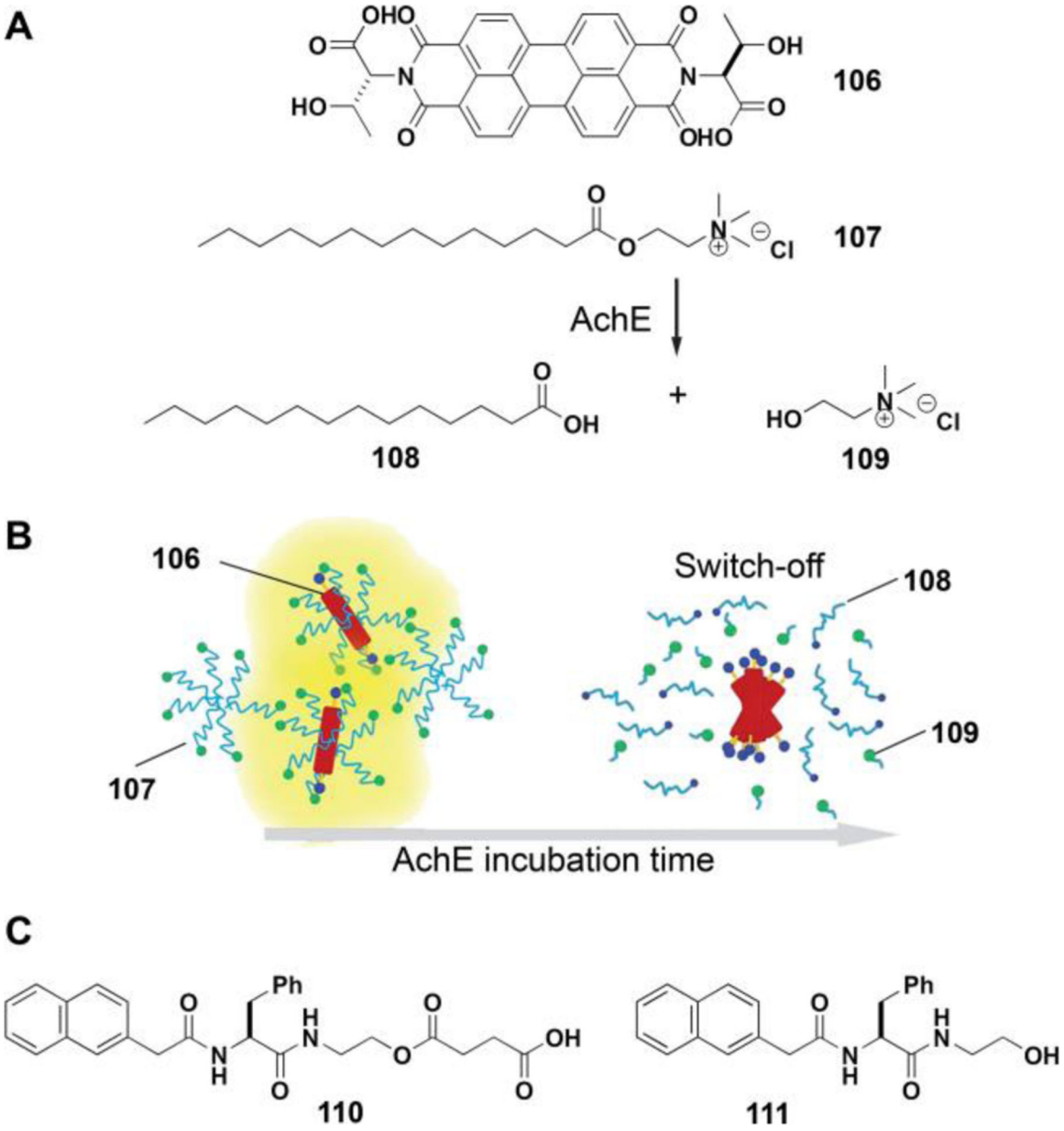

Figure 49.

(A) The structure of PDI-Thr (**106**) and AChE catalyzed hydrolysis of **107**. (B) Illustration of AchE catalyzed indirect ENS of the assembly of **106**. Adapted from Ref.[379]. Copyright © 2016 by Royal Chemical Society. (C) The structures of **110** and **111**.

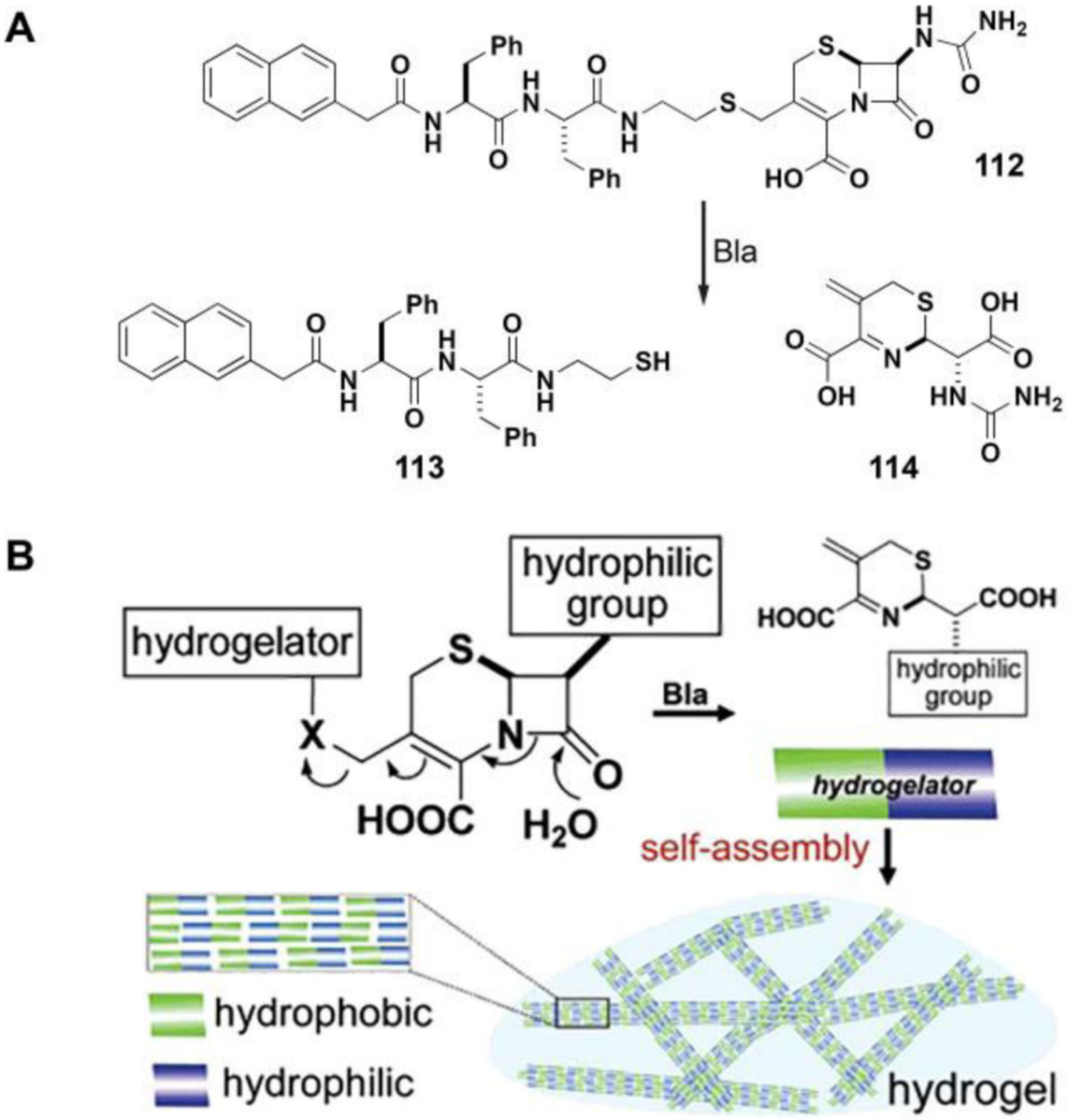

Figure 50.

(A) The structure of the substrate of β-lactamase (Bla) and its degradation catalyzed by Bla. (B) The illustration of the ENS catalyzed by Bla. Adapted from Ref. 228. Copyright © 2007 by American Chemical Society.

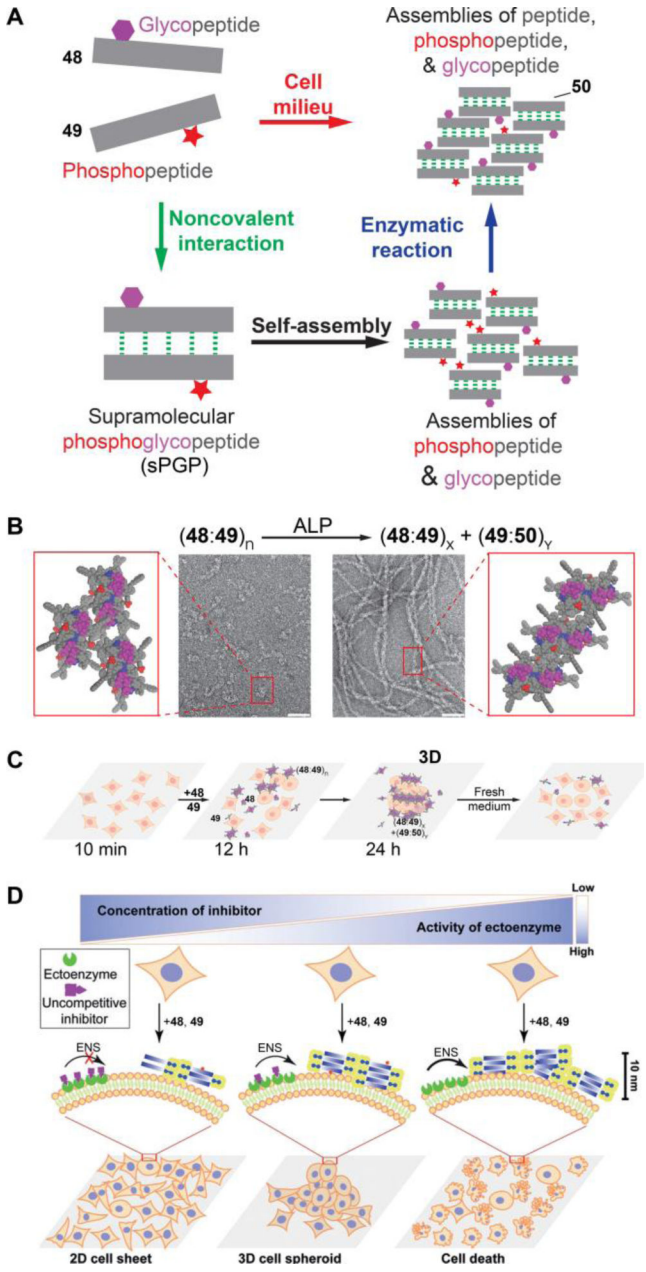

Figure 51.

(A) The illustration of sPGP, formed by non-covalent interactions, as a dynamic continuum in the cell milieu. (B) TEM images of **48**:**49** (300 μM) before (left) and after (right) being treated by a phosphatase (ALP, 1 U/mL, 24h). Inset structures show CPK models of molecular assemblies. Scale bar is 20 nm. (C) The illustration of forming 3D spheroids from a 2D cell sheet upon the addition of **48**:**49** and the reversibility of the process. (D) Context-dependent dynamic continuum of molecular assemblies for controlling cell fate. By controlling the activity of the ectophosphatase (e.g., ALPL) on cancer cells with a corresponding enzyme inhibitor, the sPGP (**48**:**49**) assemblies can result in a 2D cell sheet, 3D cell spheroids, or cell death. Adapted from Refs.[331,332]. Copyright © 2017, 2018 by Wiley Inc.

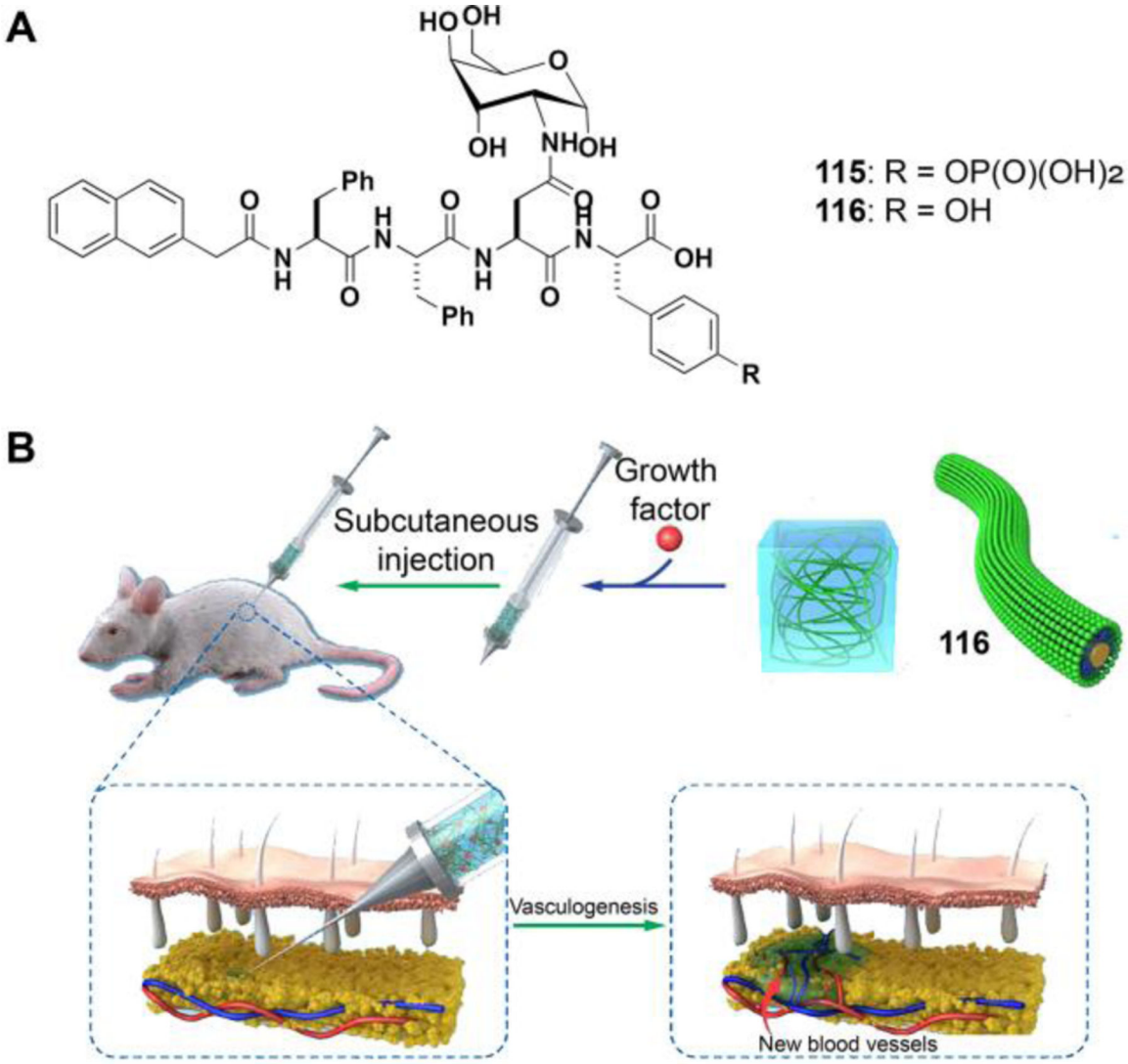

Figure 52.

(A) The structures of a glycopeptide hydrogelator (**116**) and its precursor (**115**). (B) ENS of **116** to for a hydrogel, which encapsulates DFO for inducing angiogenesis in vivo. Adapted from Ref.[395]. Copyright © 2018 by American Chemical Society.

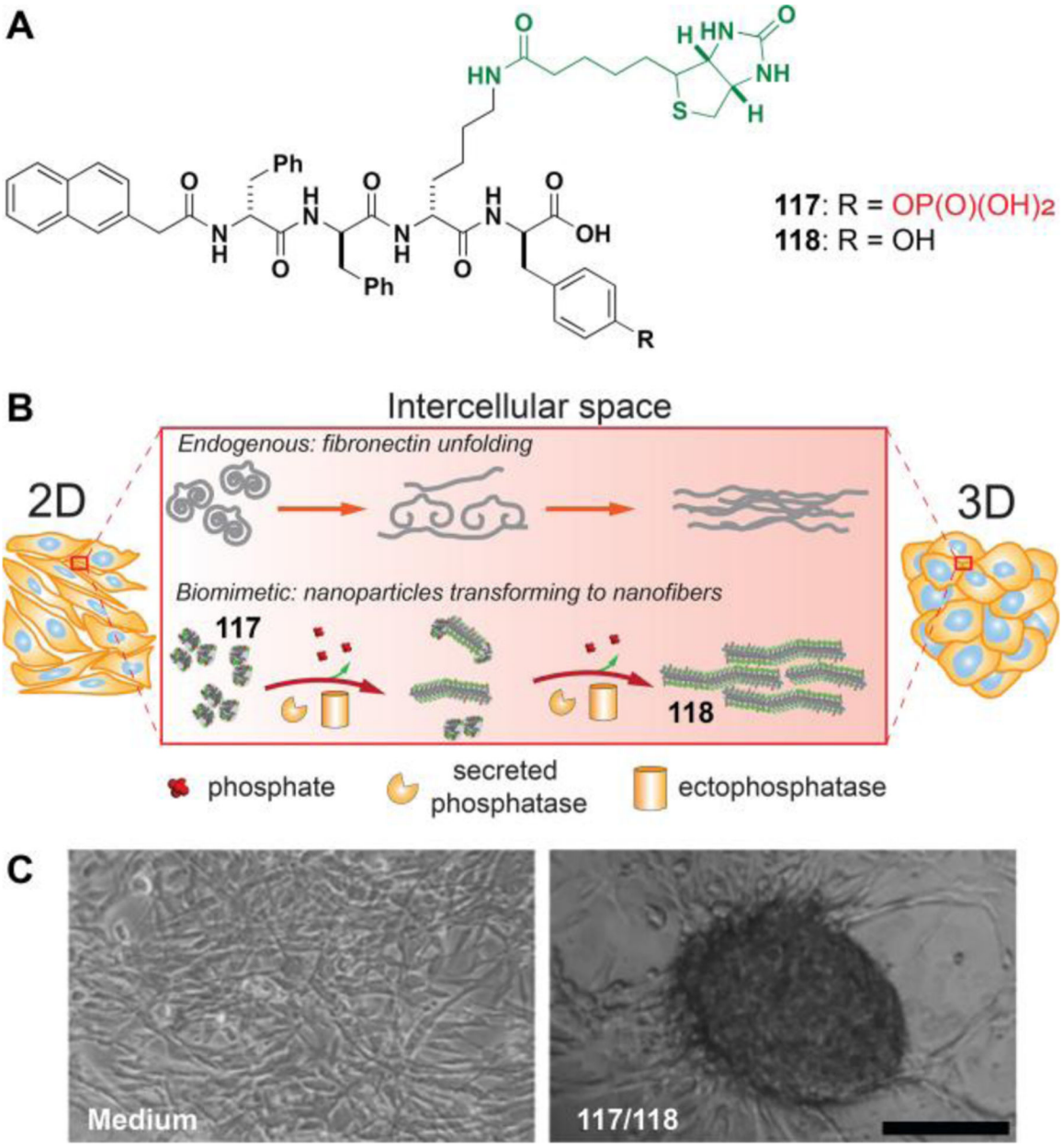

Figure 53.

(A) The structure of a single component molecule precursor (**117**) for intercellular ENS. (B) Intercellular instructed assembly to mimic the essence of the dynamic of an ECM protein. (C) Optical images of HS-5 cells in culture medium (left) and coincubation with **117** (right). Scale bar = 150 μm. Adapted from Ref.[396]. Copyright © 2019 by American Chemical Society.

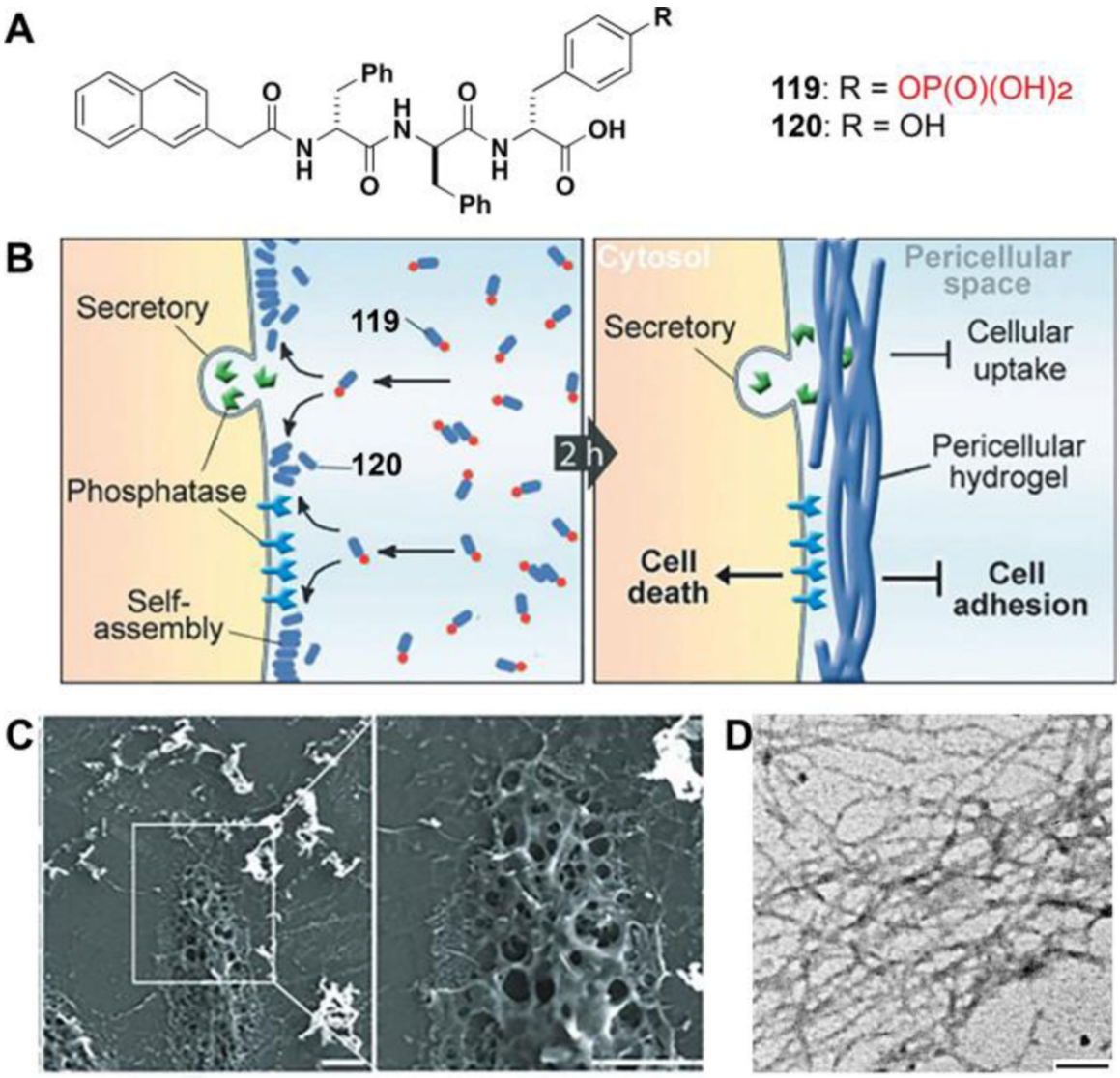

Figure 54.

(A) The structures of the precursor (**119**) and the hydrogelator (**120**) for pericellular ENS. (B) The illustration of ENS of pericellular hydrogel/nanonets to induce cell death. (C) SEM images of freeze-dried HeLa cells treated with **119** (560 μM) for 2 h. Scale bar = 10 mm. (D) Negative stained TEM images of the pericellular hydrogels on the HeLa cells treated by **119** at 280 μM. Adapted from Ref. 267. Copyright © 2014 by Wiley Inc.

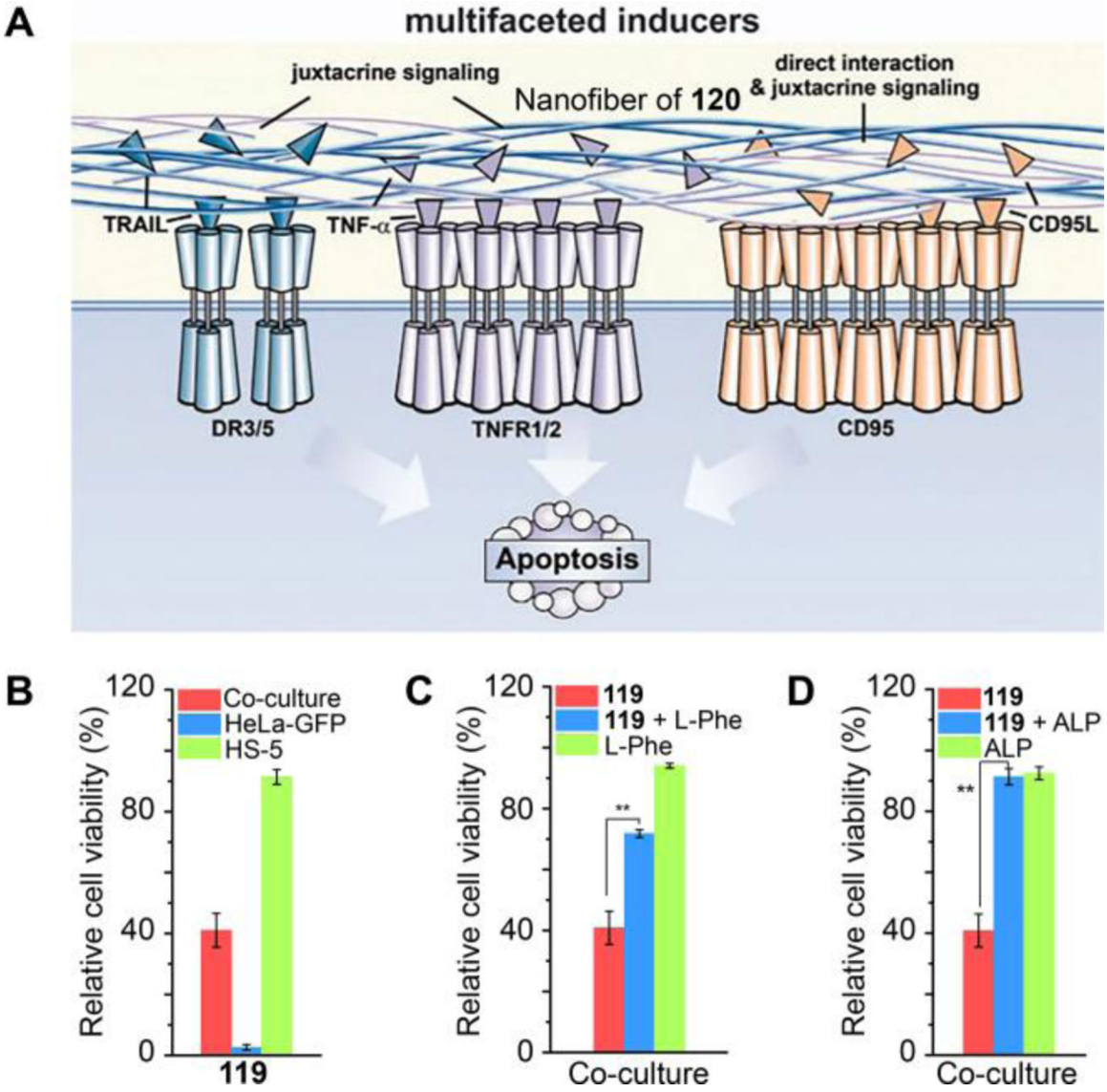

Figure 55.

(A) The illustration of pericellular fibrils of **120** formed by ENS to selectively inhibit cancer cells in co-culture via promiscuously activating cell death signaling. (B) The co-cultured cells (HS-5 and HeLa-GFP cells), HeLa-GFP, or HS-5 incubated with **119**. (C) The co-cultured HS-5 and HeLa-GFP cells incubated with **119**, **119**+L-Phe, or L-Phe. (D) The co-cultured HS-5 and HeLa-GFP cells incubated with **119**, **119**+ALP, or ALP in DMEM for 48 hrs. (B, C,D) The initial number of cells is 1.0×10^4/well (e.g., 1.0×10^4 HeLa-GFP or HS-5 cells, or mixture of 5.0×10^3 HeLa-GFP cells and 5.0×10^3 HS-5 cells) and [**119**] = 216 μg/mL, [L-Phe] = 1.0 mM, [AP] = 0.1 U/mL. n = 3. Data are shown as mean ± SD. *p < 0.05, **p < 0.01 by Student's t test. Adapted from Ref.[402]. Copyright © 2017 by Springer Nature.

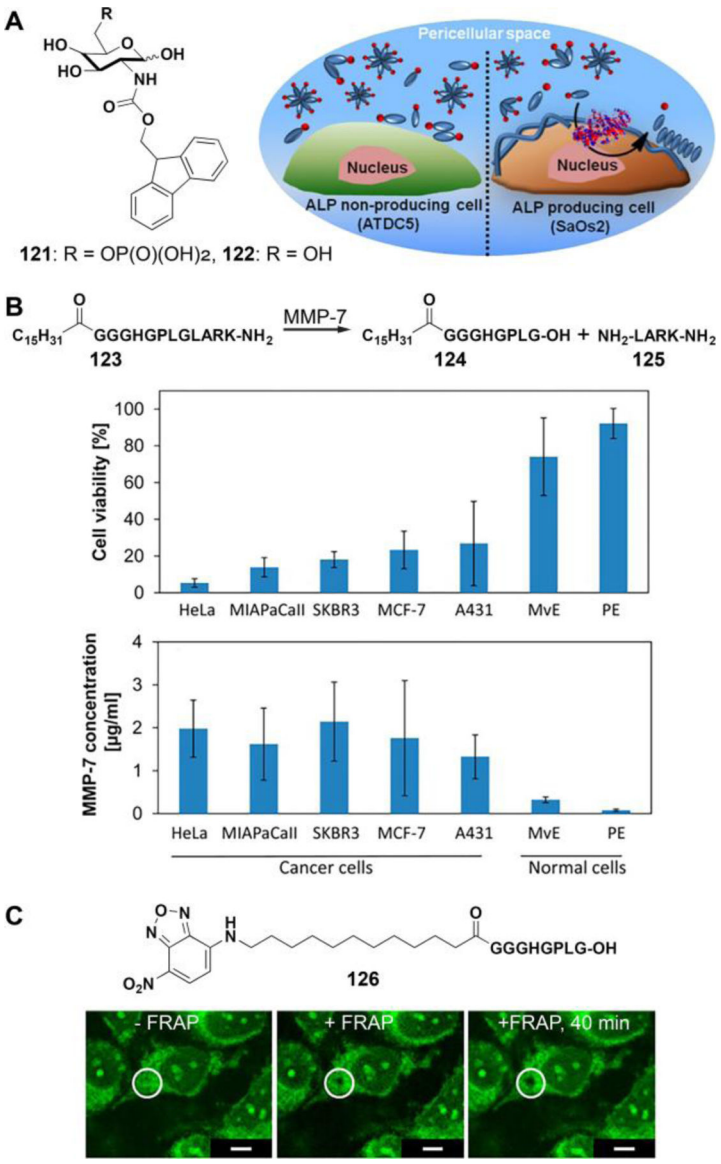

Figure 56.

(A) The structures of **121** and **122** and the illustration of enzymatic transformation of **121** to 1**22** upon enzymatic activity of ALP for in situ self-assembly. Adapted from Ref. 275. Copyright © 2015 by American Chemical Society. (B) The structures of **123**, **124**, and **125** and the viability assays of cancer cells and normal human cells after incubation with **123** (0.025 wt %) and the MMP-7 concentration in the culture media after culturing the cells. PE represents primary human pancreatic epithelial cells. (C) The structure of **126** and fluorescence recovery after photobleaching of HeLa cells observed using CLSM. Adapted from Ref.[405]. Copyright © 2015 by American Chemical Society.

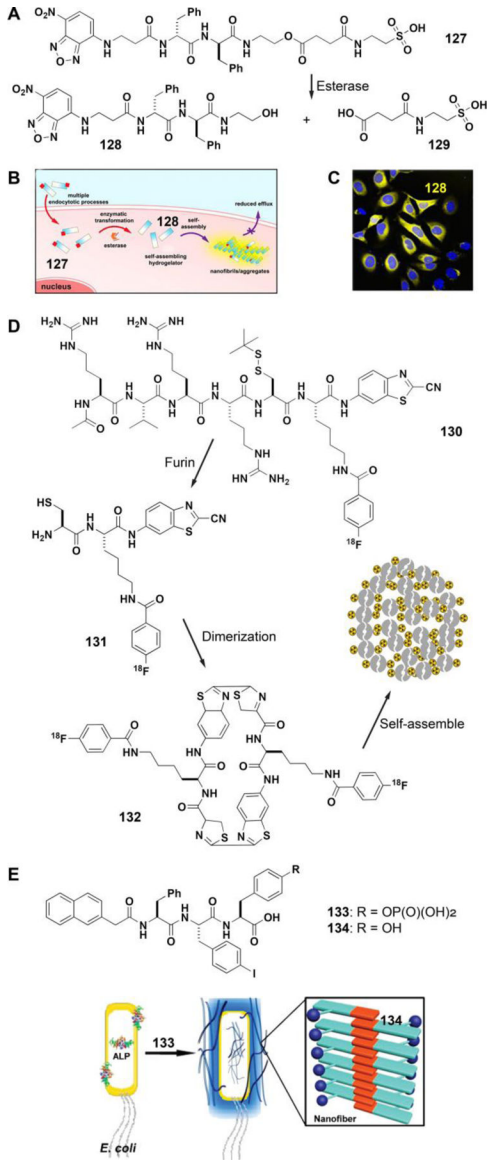

Figure 57.

(A) The structures of precursor **127** and the corresponding hydrogelators **128** and the esterase catalyzed enzymatic transformation. (B) Taurine conjugation and intracellular ENS boosts cellular uptake of the D-peptide precursors and subsequent accumulation of nanofibers inside cells. (C) Fluorescent confocal microscope images showing the fluorescence emission in HeLa cells with the treatment of **127** at 200 μM concentration in culture medium for 24 h and co-stained with Hoechst 33342 (nuclei). Adapted from[411]. Copyright © 2015 by American Chemical Society. (D) Schematic illustration of a furin-catalyzed condensation of **131** to form the dimer of **132**, followed by self-assembly to form nanoparticles for PET imaging. Adapted from Ref.[413]. (E) The structures of **133** and **134** and the illustration of bacterial ALP-catalytically dephosphorylating **133** to form nanofibers. Adapted from Ref.[414]. Copyright © 2016 by American Chemical Society.

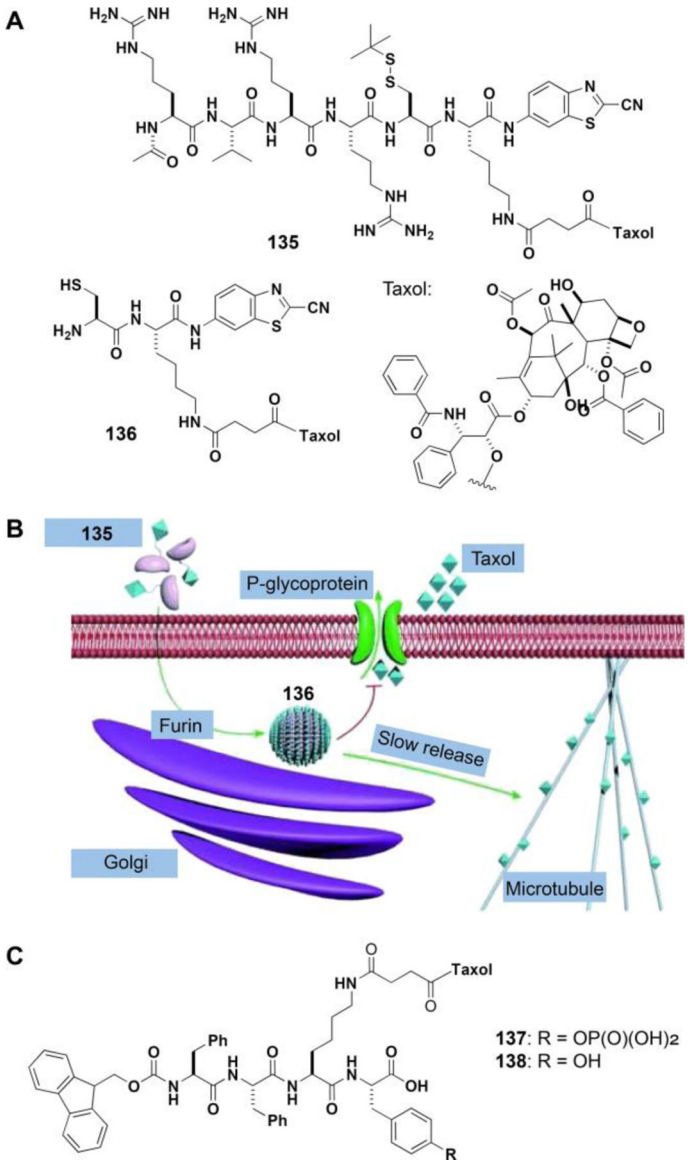

Figure 58.

(A) The structures of **135** and **136**. (B) The illustration of intracellular furin controlled self-assembly of **136** for anti-MDR. Adapted from Ref.[415]. (C) The structures of **137** and **138**.

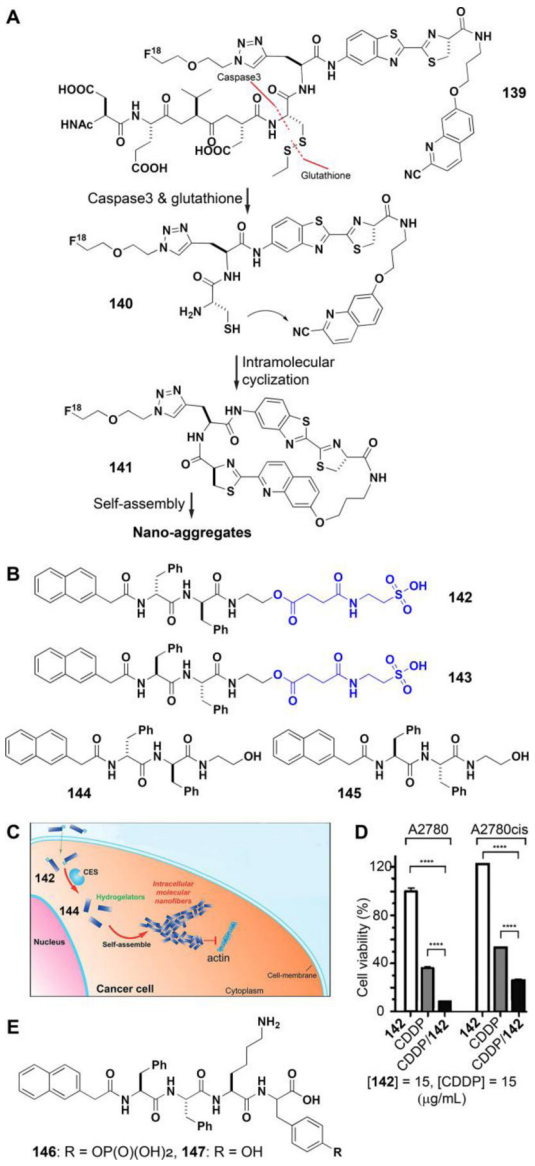

Figure 59.

(A) The structures of **139** and its products after caspase cleavage and glutathione reduction. (B) The structures of the precursors (**142** and **143**) as substrates of carboxylesterase (CES) to the corresponding hydrogelators (**144** and **145**). (C) The illustration of intracellular ENS for disrupting actin dynamics. (D) The cell viability of A2780 cells and A2780cis cells incubated with the precursors **142** alone, or in combination with cisplatin (CDDP) for 72 h. Adapted from Ref.[422]. Copyright © 2015 by Wiley Inc. (E) The structures of **147** and **148**.

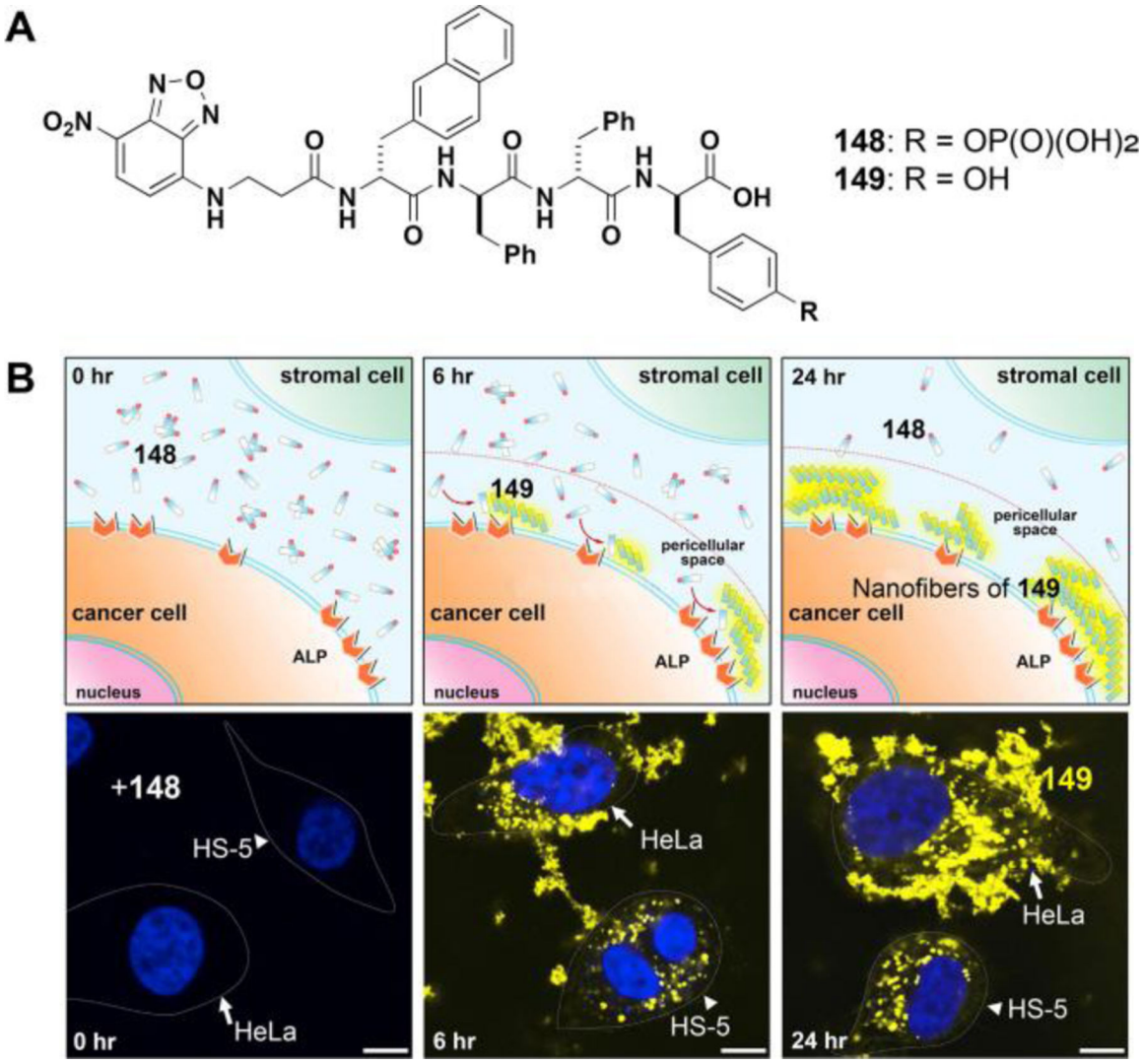

Figure 60.

(A) The structures of **148** and **149**. (B) The illustration of the ENS to form fluorescent pericellular nanofibers of **149** in co-culture and the fluorescent imaging of the fluorescent nanofibers of **149** selectively formed on HeLa cells (the cancer cell, white arrows) and in HS-5 cells (the stromal cell, white arrowheads) in the co-culture of HeLa and HS-5 cells ([**148**] = 500 mM). Adapted from Ref.[426]. Copyright © 2016 by Elsevier Inc.

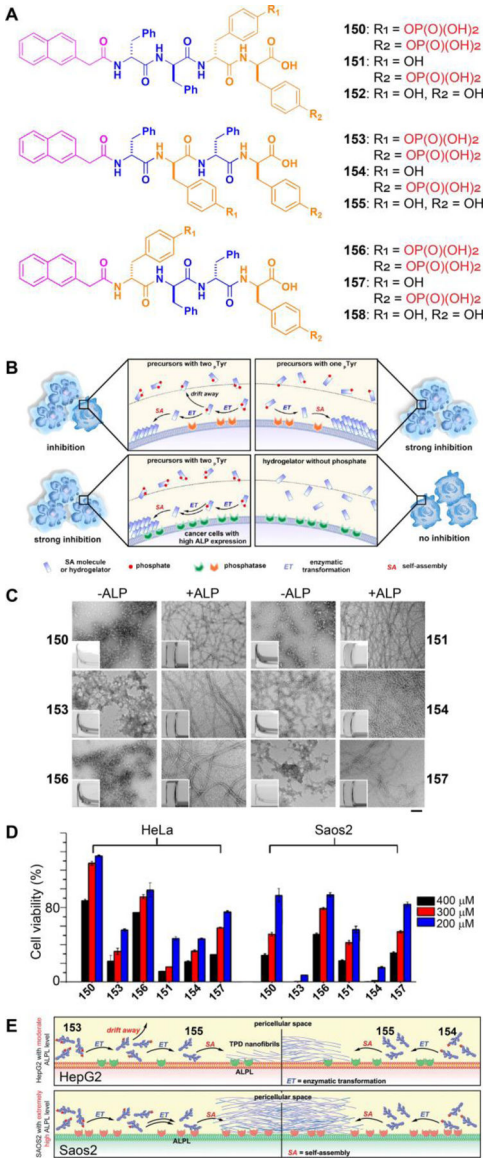

Figure 61.

(A) The structures of the precursors that have one or two phosphotyrosine residues and the corresponding self-assembling D-peptides. (B) ENS of the tetrapeptides to inhibit cancer cells that express different levels of ALPs. (C) TEM images of aggregates/nanofibers in the solutions of different precursors or nanofibers in the hydrogels (inset: optical images) formed by treating the solutions of the precursors with ALP. (D) 48-h cell viability (determined by MTT assay) of HeLa and Saos2 cells incubated with different precursors at the concentrations of 200, 300, and 400 μM in culture medium. Adapted from Ref.[428]. Copyright © 2016 by American Chemical Society. (E) The illustration of the use of the rate of ENS (controlled by the number of enzymatic sites) to amplify the difference of the expression level of ALPL in different cell lines (HepG2 and Saos2). Adapted from Ref.[429]. Copyright © 2016 by Wiley Inc.

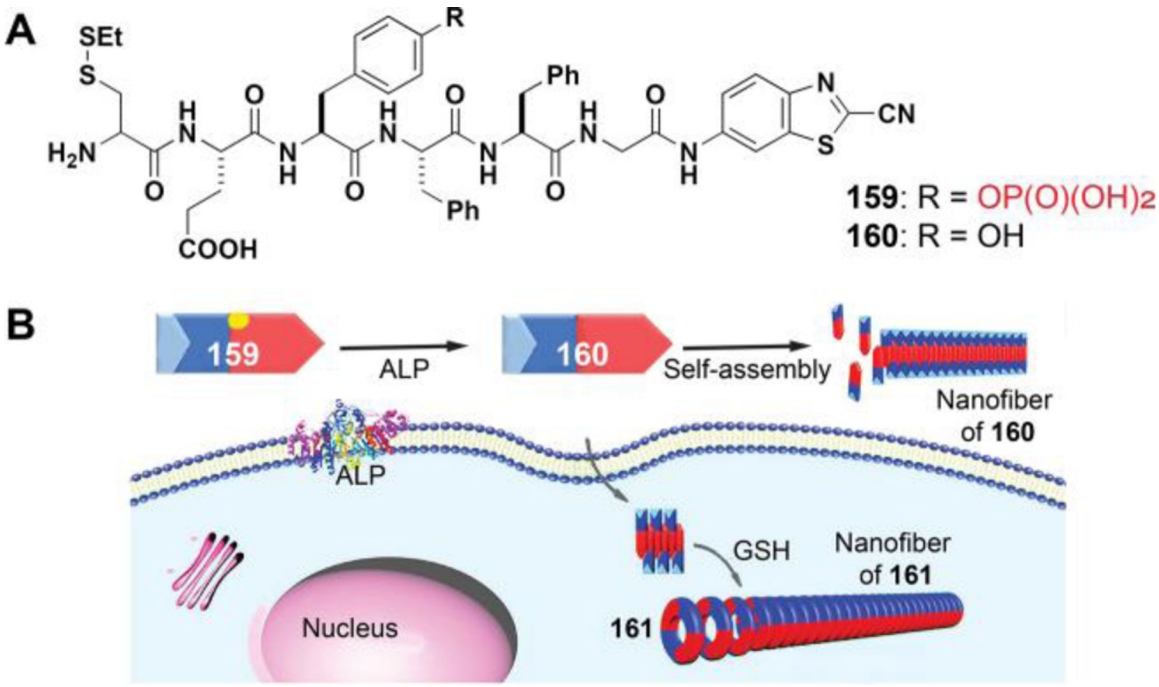

Figure 62.

(A) The structures of **159** and **160**. (B) Proposed mechanism of hydrogelator precursor **159** that undergoes ALP-based ENS to form nanofibers of **160**, followed by GSH-associated intracellular condensation and self-assembly to form nanofibers of **161**. Adapted from Ref. [430]. Copyright © 2016 by American Chemical Society.

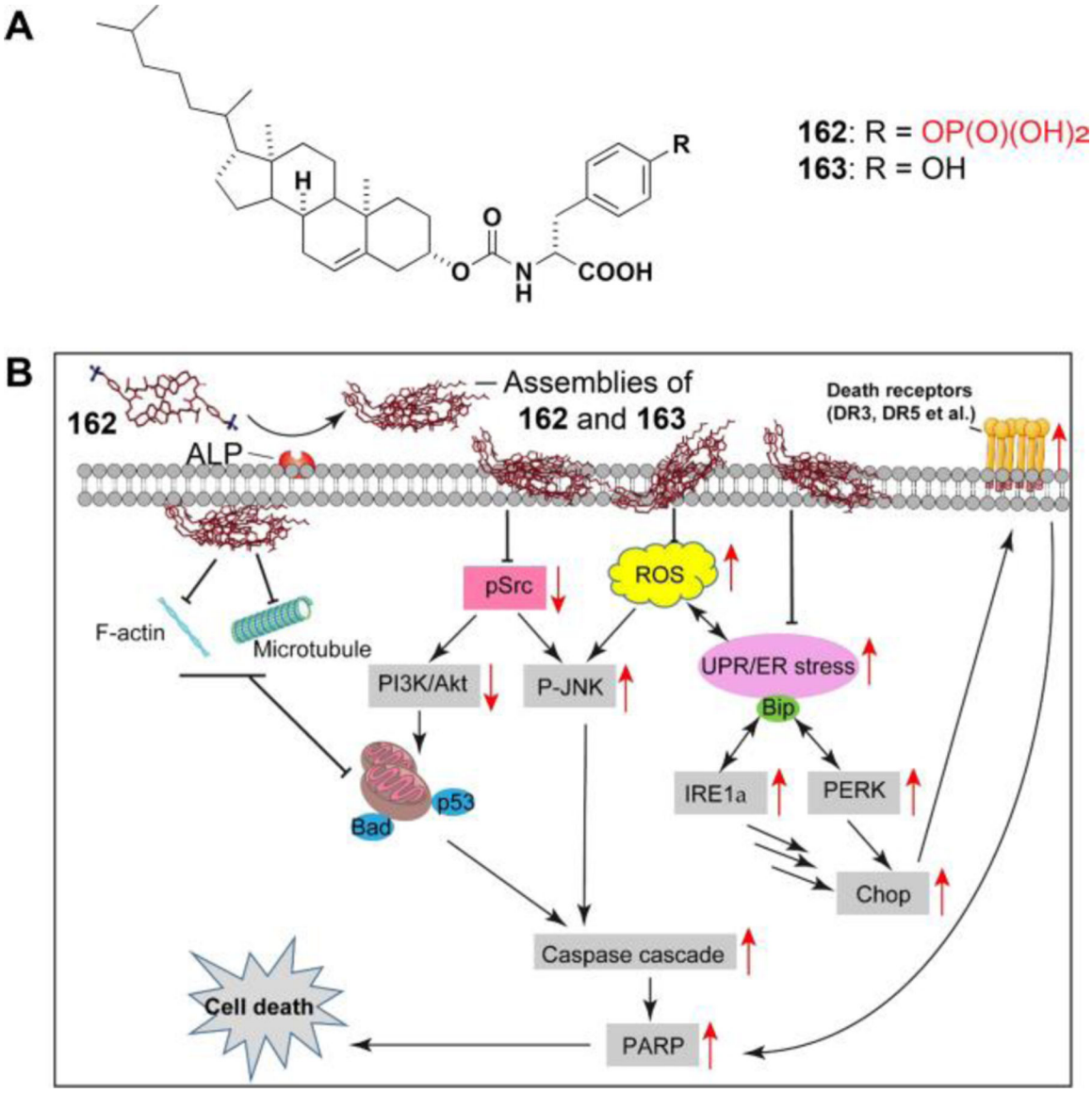

Figure 63.

(A) The structures **162** and **163**. (B) ENS forms the assemblies of **162**/**163** to activate multiple cell death signaling pathways, thus minimizing the acquired drug resistance of the cancer cells. Adapted from Ref.[433]. Copyright © 2019 by American Association for Cancer Research.

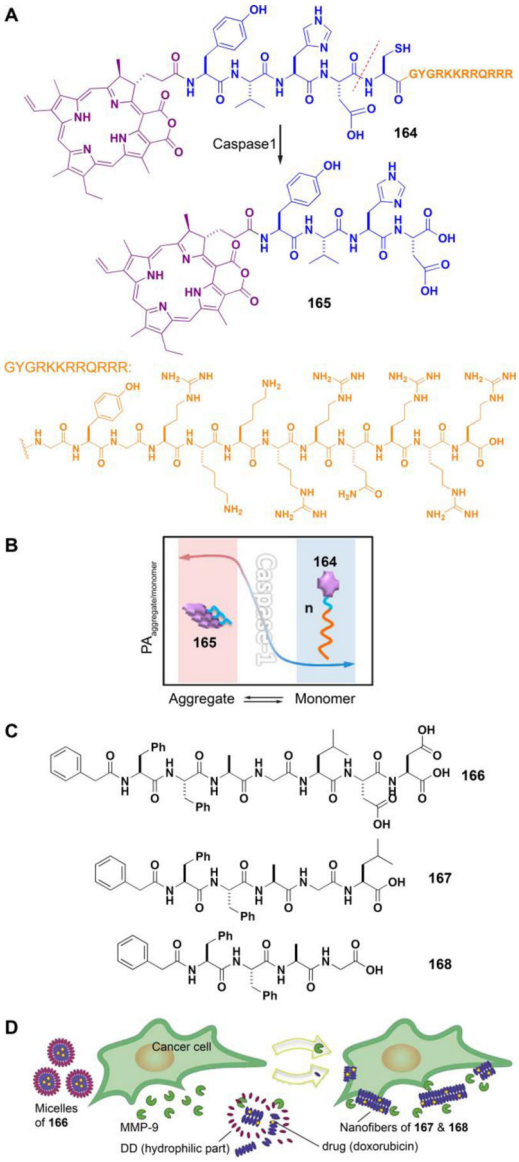

Figure 64.

(A) The structures of **164** and **165**. (B) The illustration of enzyme-induced dynamic equilibrium of nano-assemblies for modulating ratiometric photoacoustic signal in living cells. Adapted from Ref.[437]. Copyright © 2016 by American Chemical Society. (C) The structure of a substrate (**166**) of MMP-9 and the corresponding proteolysis products (**167** and **168**). (D) Schematic representation of micelle-to-fiber transition in the presence of cancer cells due to MMP-9 secretion, followed by entrapment of doxorubicin in fibrillar structures, which act as the less mobile depots of the anticancer drug. Adapted from Ref.[438]. Copyright © 2016 by Elsevier Inc.

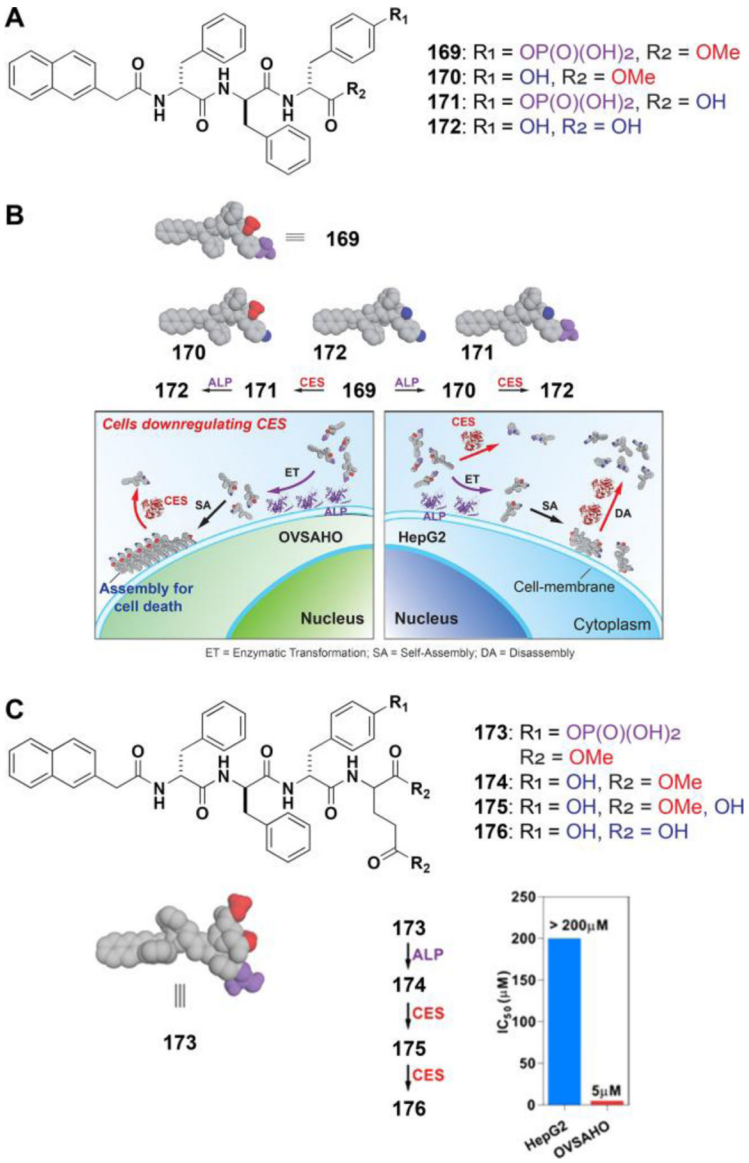

Figure 65.

(A) The structures of the precursor and its hydrolysis products. (B) The concept of targeting the cells that downregulate CES while expressing ALP. (C) The structure and enzymatic conversion of the precursor **173**, and the IC_{50} values (at 72 h) of **173** against HepG2 or OVSAHO cells. Adapted from Ref.[439]. Copyright © 2017 by American Chemical Society.

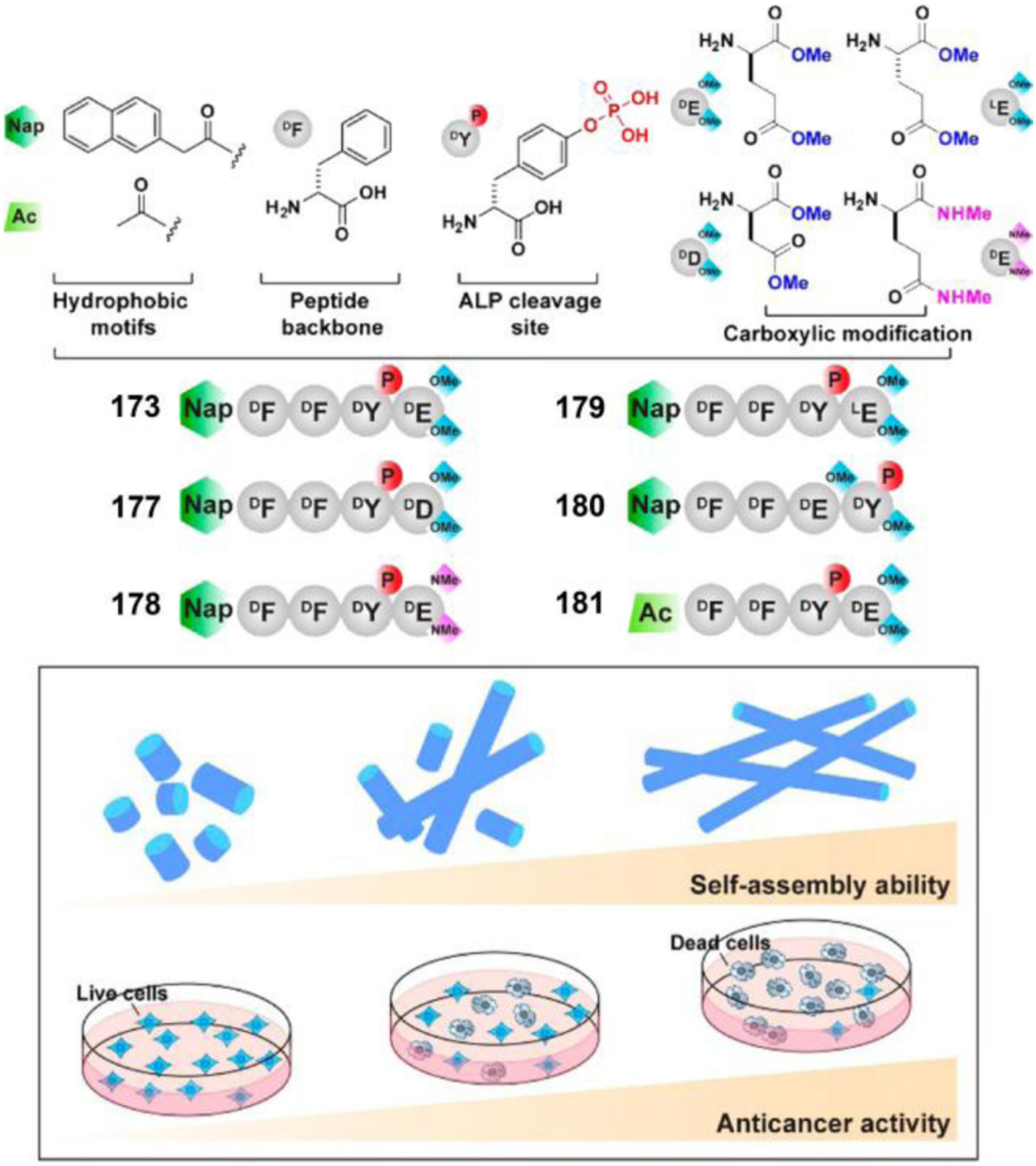

Figure 66.

Molecular structures of the precursors and the correlation between the ability for self-assembly of small molecules and anticancer activity. Adapted from Ref.[441]. Copyright © 2017 by American Chemical Society.

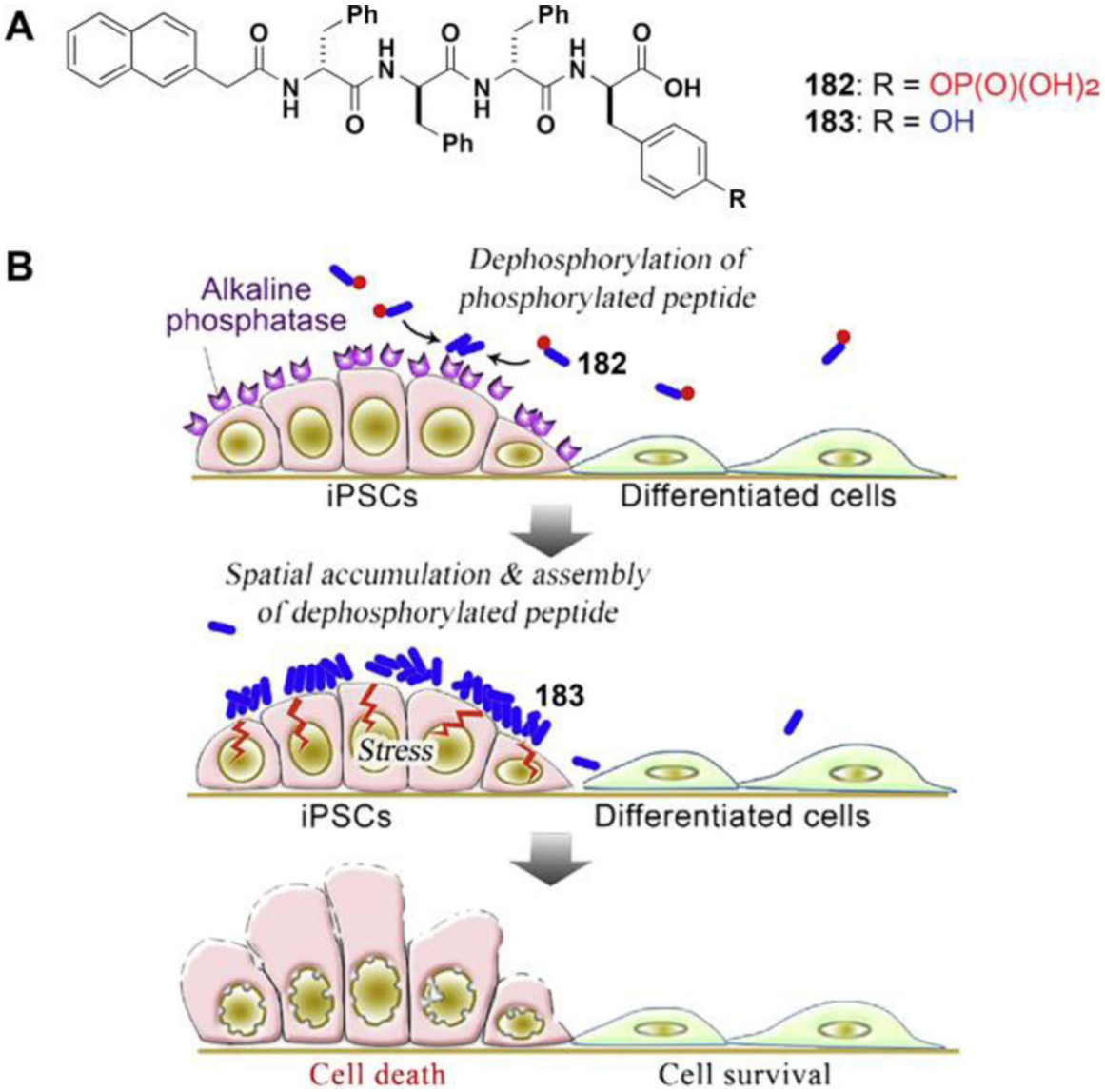

Figure 67.

(A) The structures of the phospho-D-peptide derivative. (B) The illustration of the possible mechanism by which phospho-D-peptides induce iPSC-selective cell death. Adapted from Ref.[442]. Copyright © 2017 by Elsevier Inc.

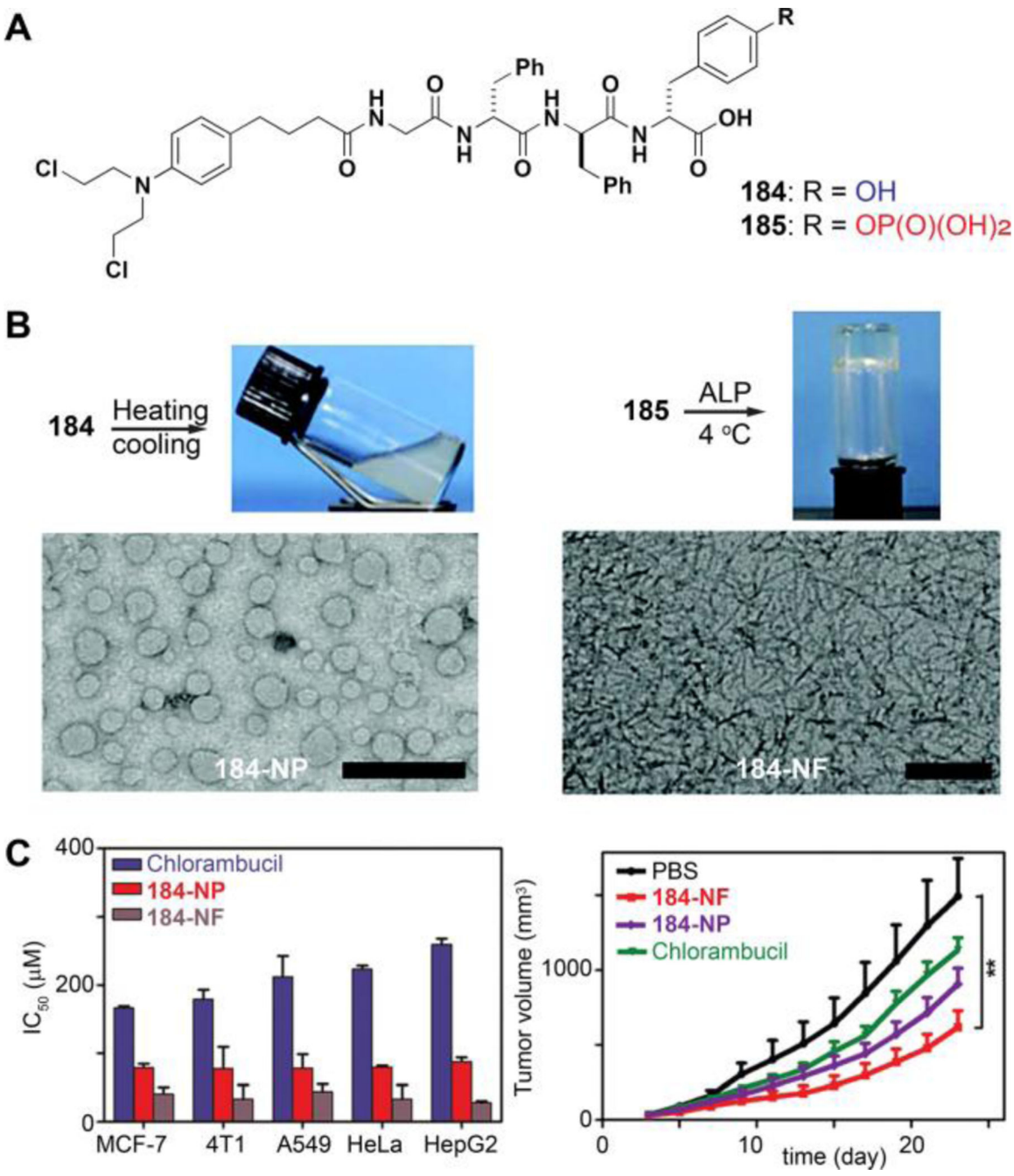

Figure 68.

(A) The structures of chlorambucil-Gffy (**184**) and chlorambucil-Gff$_p$y (**185**) (B) The optical images of the suspension of **184** formed by a heating-cooling process and the hydrogel of **184** formed by ALP enzymatic reaction at 4 °C and the TEM images of the nanostructures in the suspension and the hydrogel (scale bars = 500 nm). (C) the IC_{50} values of CRB, the nanofibers of **184**, and the nanoparticles of **184** against different cancer cells, and the in vivo anti-cancer efficiency of CRB, the nanofibers of **184**, and the nanoparticles of **184** against a 4T1 tumor model (the data are shown as mean ± SEM (n = 5); ** represents $P < 0.05$). Adapted from Ref.[443]. Copyright © 2017 by Royal Chemical Society.

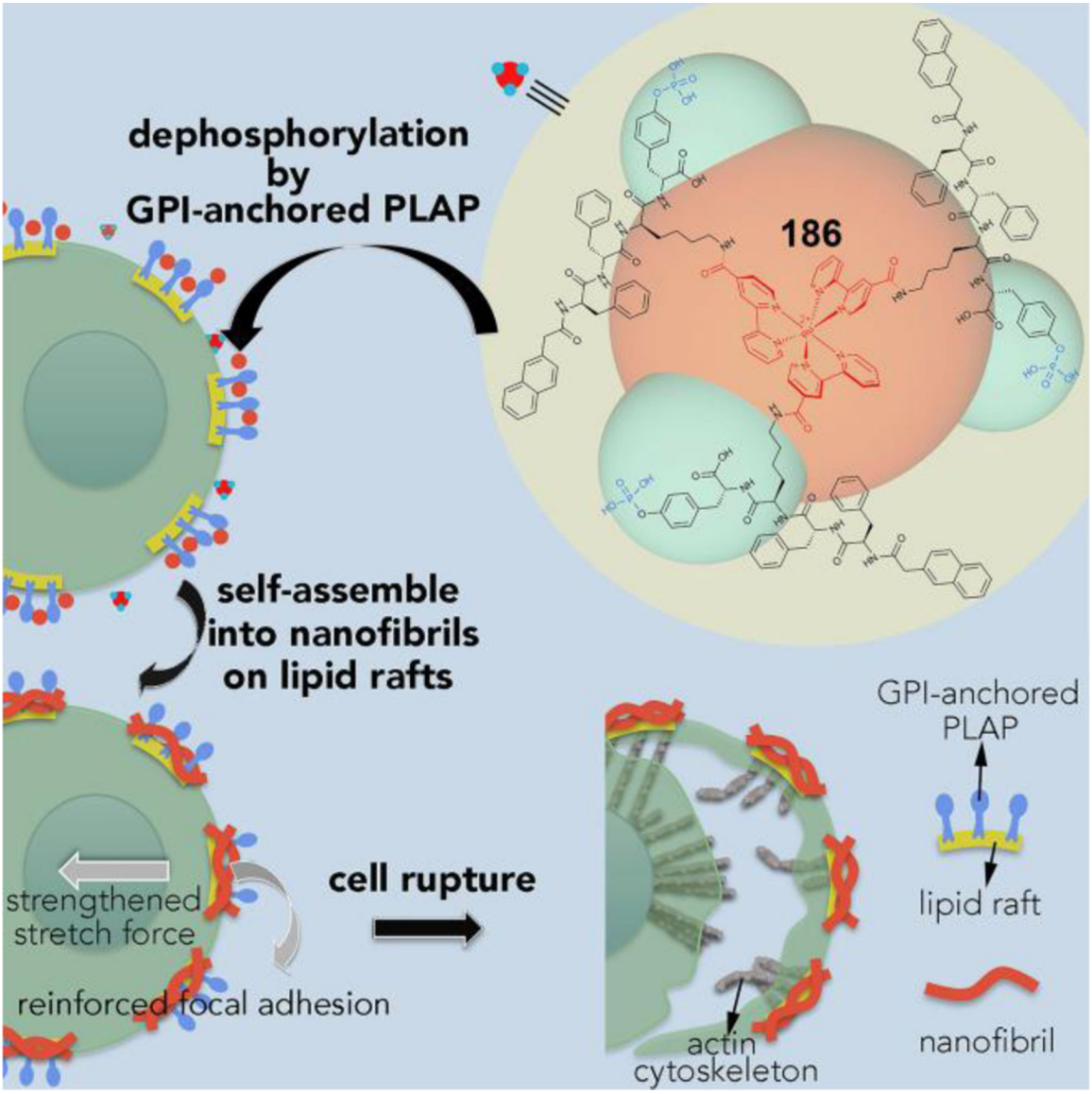

Figure 69.

The ruthenium complex (**186**) with octahedral geometry serves as a core building block of peptidic molecule construction for protein-guided molecular self-assembly with enhanced sensitivity. The self-assembled nanofibrils selectively capture the lipid rafts of cervical cancer cells and exert mechanical stimuli on raft-associated receptors, leading to inhibition of cancer cell migration and cellular physical damage. Adapted from Ref.[444]. Copyright © 2017 by Elsevier Inc.

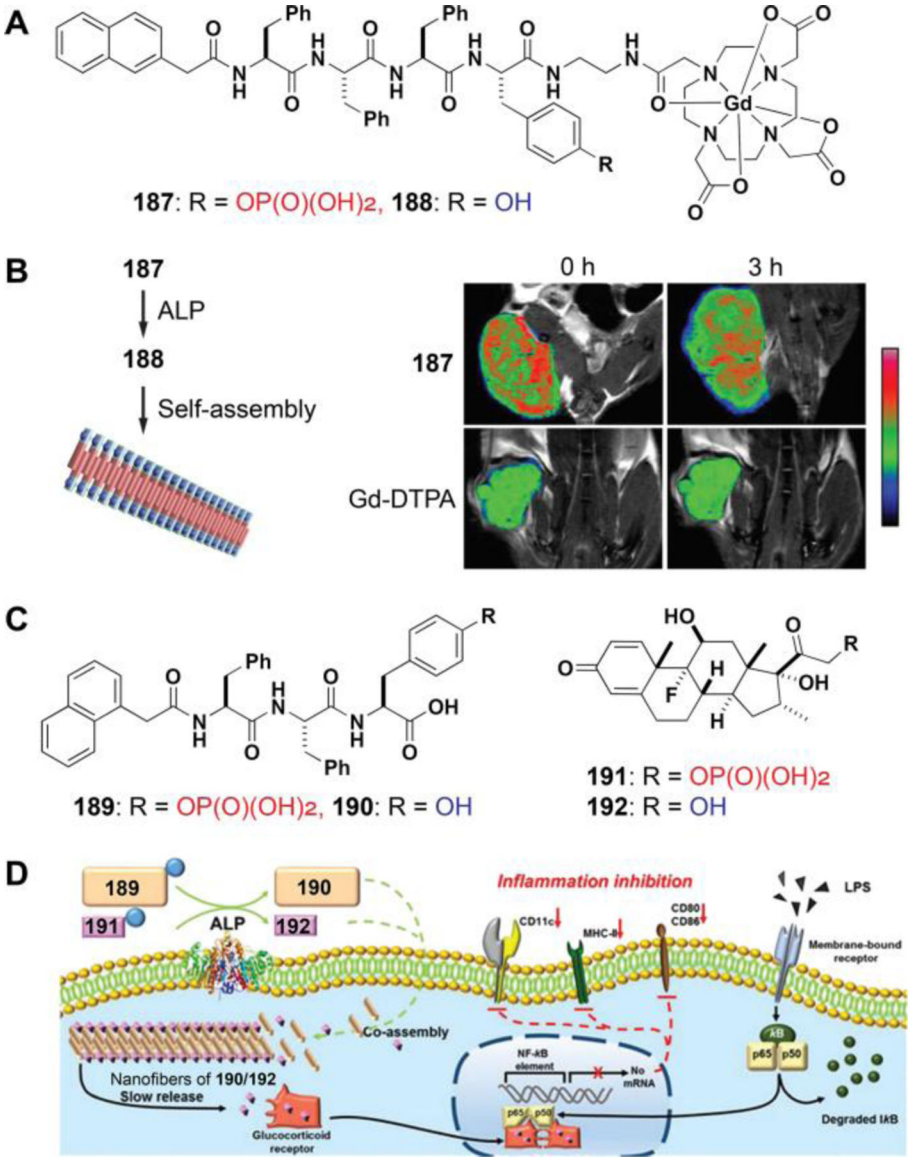

Figure 70.

(A) The structures of **187** and **188**. (B) The illustration of ALP-based ENS of gadolinium nanofibers and *in vivo* T_2-weighted coronal MR images of **187**-injected mice (top row) and Gd-DTPA-injected mice (bottom row) at 0 h and 3 h post injection. Adapted from Ref.[448]. Copyright © 2017 by American Chemical Society. (C) The structures of the precursors for ALP-catalyzed assembly. (D) The illustration of intracellular ENS resulted in co-assembly to form nanofibers made of **190** and **192**. Adapted from Ref.[445]. Copyright © 2017 by Royal Chemical Society.

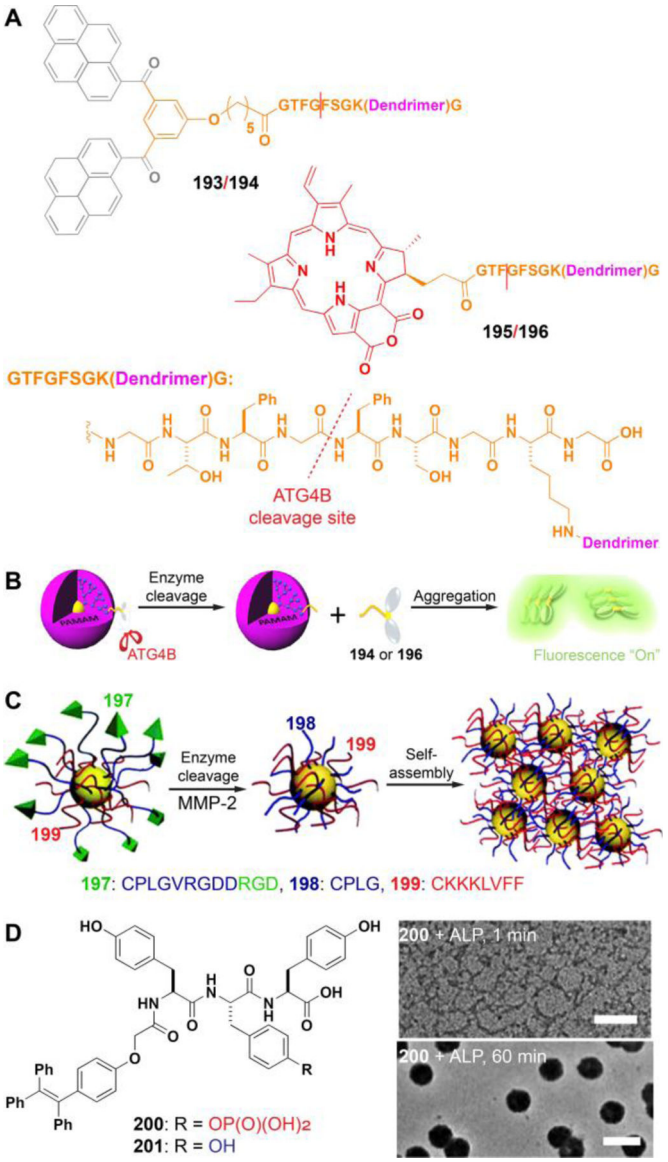

Figure 71.

(A) The structure of dendrimers connected to bis(pyrene) or purpurin 18 by peptide linker. (B) The illustration of the probe for autophagy detection. Adapted from Ref.[450]. Copyright © 2017 by American Chemical Society. (C) Schematic illustration of MMP-2-triggered self-assembly of AuNPs@**197**/**199**. Adapted from Ref.[454]. Copyright © 2017 by Royal Chemical Society. (D) The structures of **200** and **201** and the TEM images of **200** treated with ALP for 1 min and for 60 min. Adapted from Ref.[455]. Copyright © 2017 by Wiley Inc.

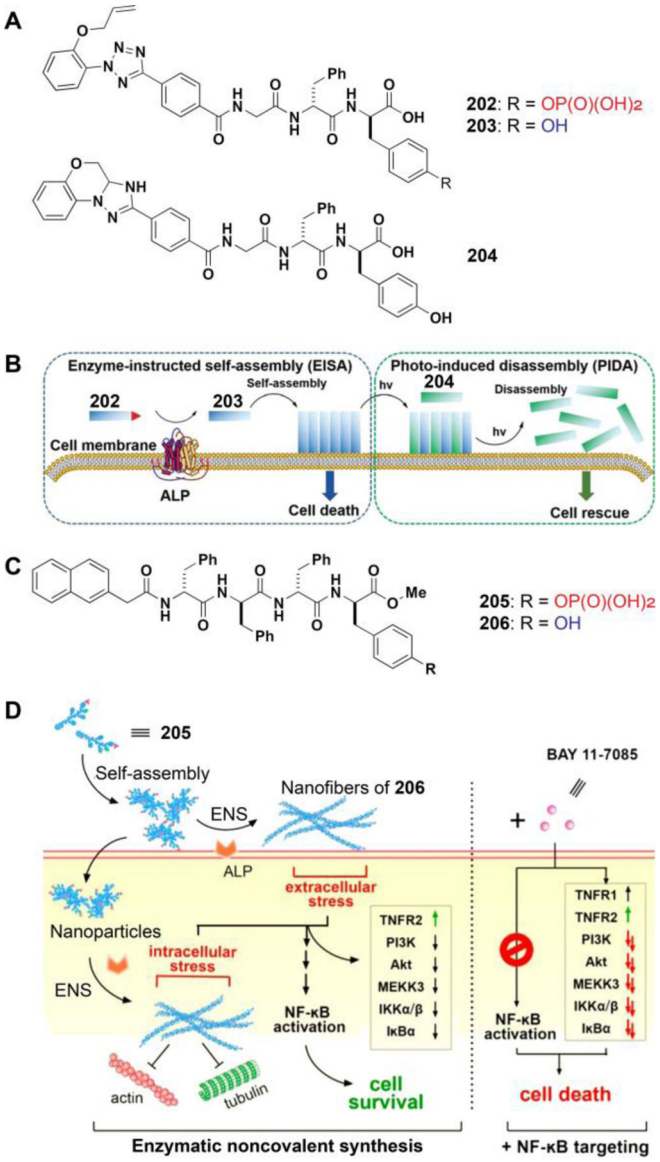

Figure 72.

(A) The structures and transformations of **202** upon treatment with ALP followed by photoirradiation. (B) The illustration of using **202** for monitoring EISA–PIDA processes and the photo-regulation of the cancer cells. Adapted from Ref.[456]. Copyright © 2017 by Royal Chemical Society. **(C)** The structures of the C-terminal methylated phosphotetrapeptide (**205**) and the corresponding tetrapeptide (**206**). (D) The illustration of ENS in cellular milieu causes cell stress to activate NF-κB signaling for cell survival and the combination of ENS and NF-κB targeting effectively inhibits cancer cells. Adapted from Ref.[457]. Copyright © 2018 by American Chemical Society.

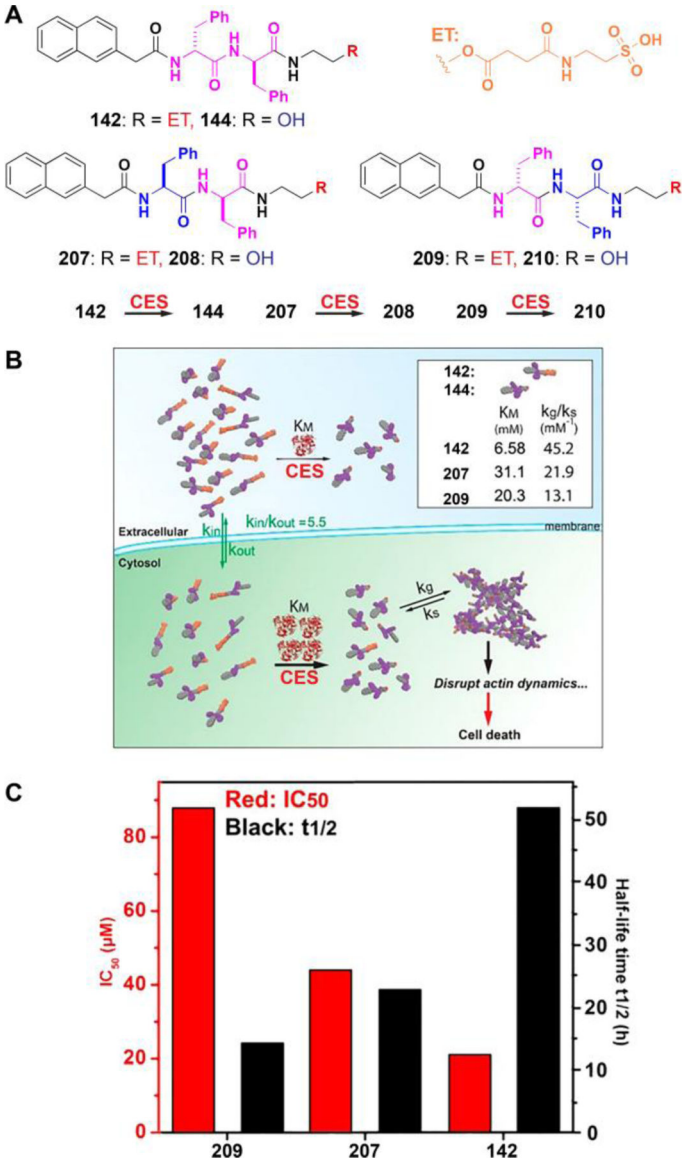

Figure 73.

(A) The structures of the precursors and the corresponding hydrogelators. (B) Extracellular hydrolysis and cancer cell death caused by intracellular ENS. (C) IC_{50} values (against JHOS-4) and $t_{1/2}$ values of **209**, **207**, and **142**. Adapted from Ref.[465]. Copyright © 2018 by American Chemical Society.

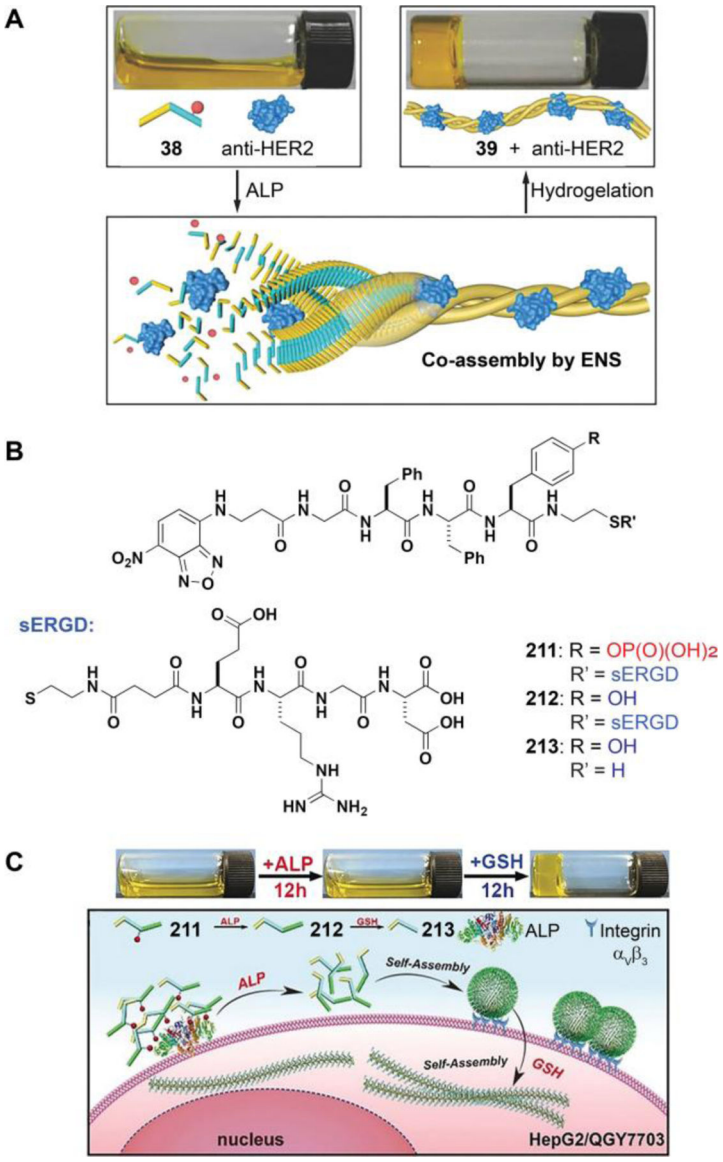

Figure 74.

(A) Optical images of a PBS solution containing NBD-Gff$_p$y (**38**, 0.2 wt%) and antiHER2 affibody (0.03 wt%) and hydrogel formed by the addition of ALP, and the illustration of the co-assembly process triggered by ALP. Adapted from Ref.[466]. Copyright © 2018 by Wiley Inc. (B) The structures of NBD-GFF$_p$Y-ss-ERGD (**211**) and the corresponding dephosphorylation and reduction products. (C) Optical images of a PBS solution of **211** (200 μM, 0.03 wt%), PBS solution of **213** formed by adding ALP (1 U/mL) to the solution of **211**, and hydrogel formed of **213** by adding GSH (4 equiv.) to the solution of **212**, and the proposed mode of the molecular self-assembly extra- and intra-cellular environment of HepG2 and QGY7703 liver cancer cell lines. Adapted from Ref.[467]. Copyright © 2018 by Wiley Inc.

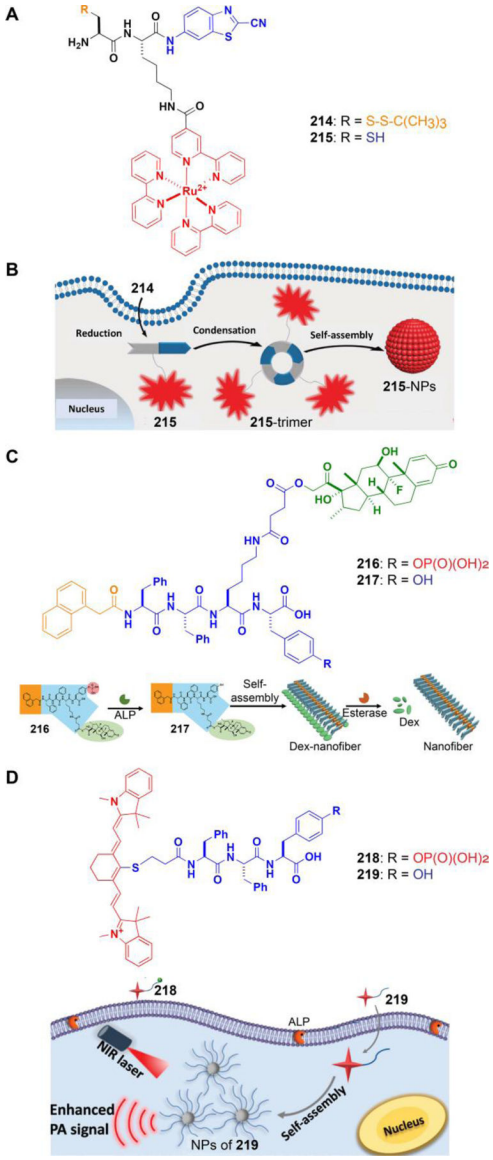

Figure 75.

(A) The structure of **214**. (B) The illustration of intracellular condensation-controlled transition of **214** to **215**-NPs for tumor imaging. Adapted from Ref.[469]. Copyright © 2018 by Royal Chemical Society. (C) The illustration of ALP-catalyzed ENS of **217** to form Dex-nanofibers followed by esterase-controlled slow release of Dex from the nanofiber. Adapted from[470]. Copyright © 2018 by American Chemical Society. (D) The illustration of ALP-catalyzed ENS to form **219**-NPs, from **218**, for enhanced photoacoustic imaging of tumors. Adapted from Ref.[471]. Copyright © 2018 by American Chemical Society.

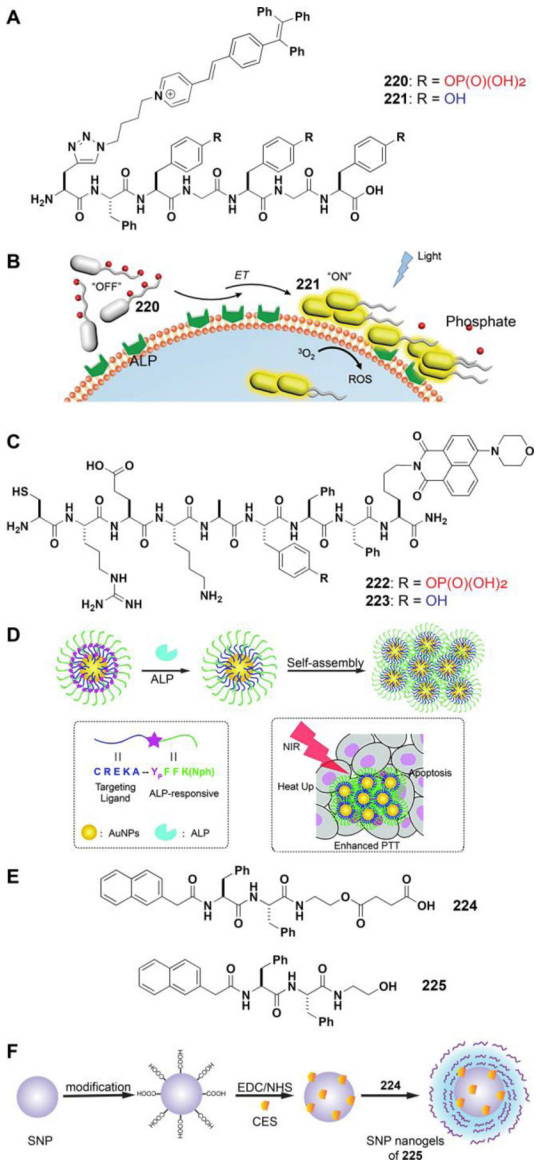

Figure 76.

(A) The structure of TPE-Py-$F_pYG_pYG_pY$ (**220**). (B) The illustration of the self-assembly of TPE-Py-FYGYGY (**221**) generated by the action of ALP that is overexpressed on the cancer cell surface, which significantly activates the fluorescence and ROS generation capability. Adapted from Ref.[472]. Copyright © 2018 by Royal Chemical Society. (C) The structures of **222** and **223**. (D) Enzymatic transformation of the precursor as a substrate of ALP to the corresponding aggregates for intracellular self-assembly. Adapted from Ref.[473]. Copyright © 2018 by Royal Chemical Society. (E) The structures of **224** and **225**. (F) The scheme of the preparation of the core–shell nanogels by ENS.

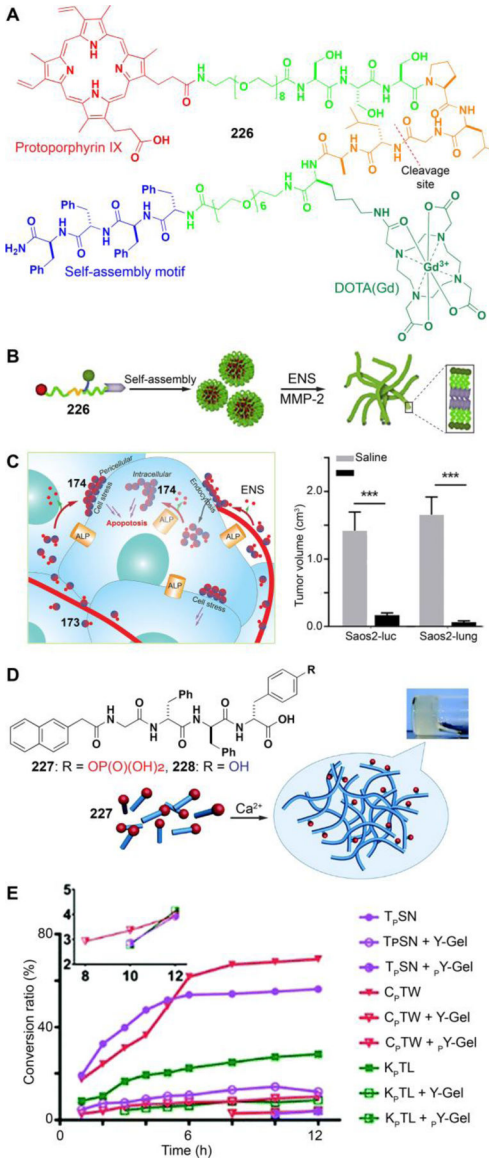

Figure 77.

(A) The structure of **226**. (B) The illustration of MMP-2-triggered transformation of Ppdf-Gd from spherical nanoparticles to nanofibers for amplified MRI and PDT. Adapted from Ref.[475]. Copyright © 2018 by Elsevier Inc. (C) The illustration of ALP-based ENS of the assembly of peptides which inhibit metastatic osteosarcoma in an orthotopic mouse model and the tumor volumes of orthotopic osteosarcoma model established by Saos2-luc and Saos2-lung cells after tail intravenous injection of compound **173** or saline for 4 weeks. Adapted from Ref.[479]. Copyright © 2019 by Elsevier Inc. (D) The structure of Nap-Gff$_p$y (**227**), the illustration of self-assembly of **227** induced by Ca^{2+}, and the optical image of the formed $_p$Y-Gel; (E) Conversion ratios of phosphorylated peptides in PBS, $_p$Y-Gel and Y-Gel. Adapted from Ref. 304. Copyright © 2018 by Royal Chemical Society.

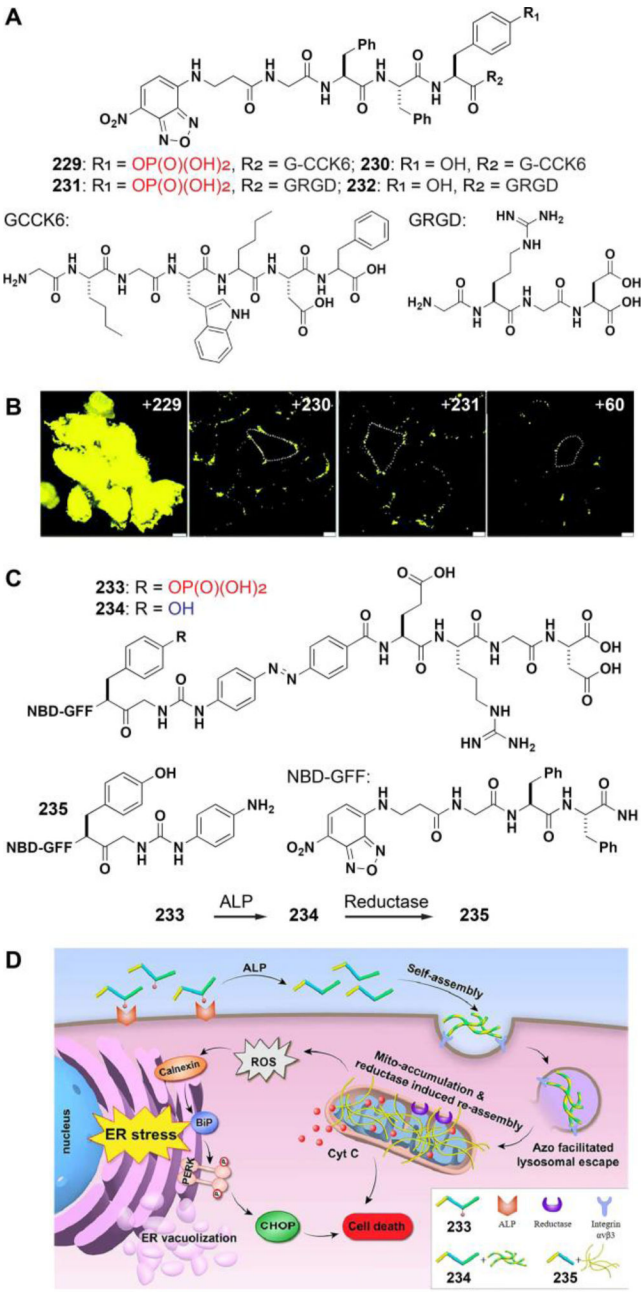

Figure 78.

(A) The structures of NBDGFF$_p$Y-G-CCK6 (**229**); (B) CLSM images of HeLa cells incubated with **229**, **230**, **231**, and **66** (from left to right) for 8 h. Adapted from Ref.[480]. Copyright © 2019 by Royal Chemical Society. (C) The structures of **233**, **234**, and **235** and the enzymatic reactions from **233** to **234** by ALP and from **234** to **235** by reductase. (D) The illustration of the induction of ER stress by the self-assembly of **233**; Adapted from Ref.[481].

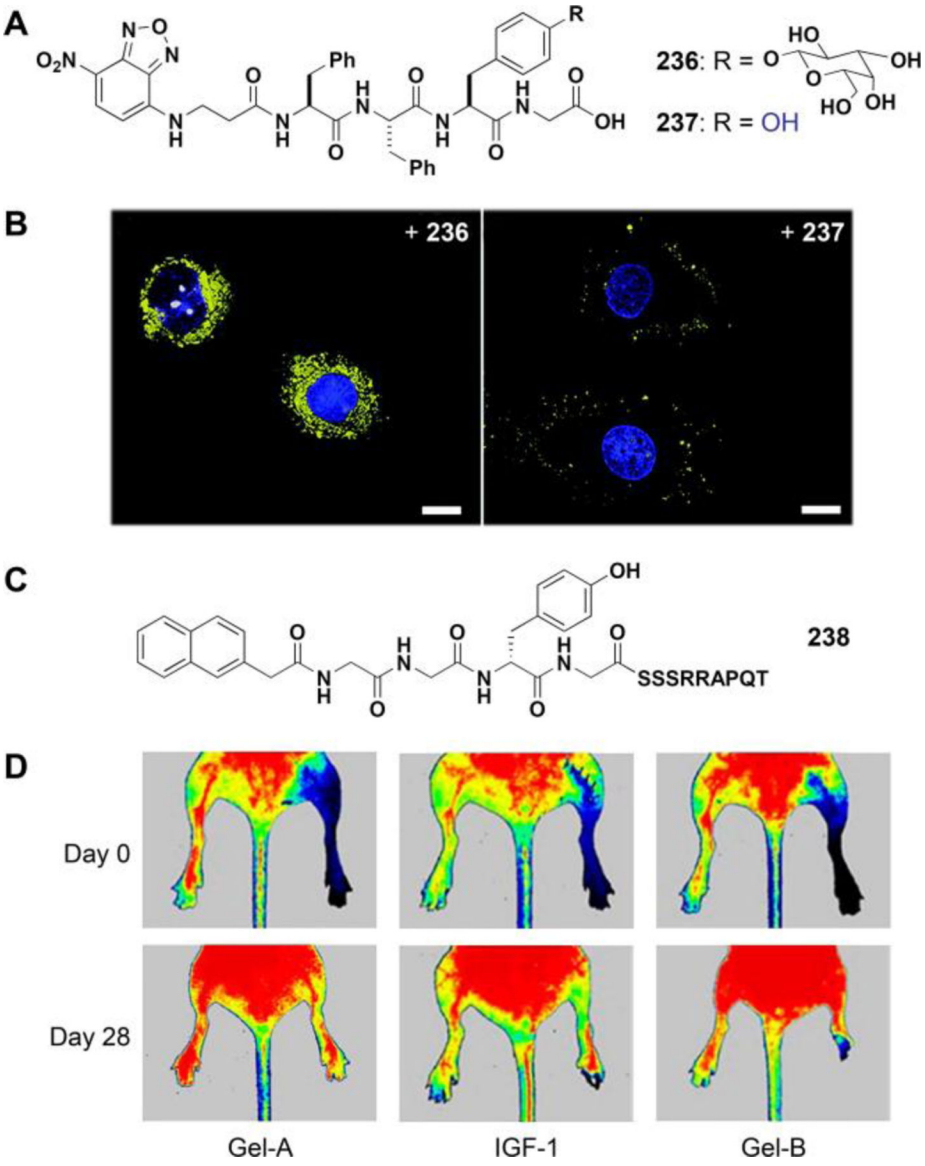

Figure 79.

(A) The structures of NBD-FFY(gal)G (**236**) and NBD-FFYG (**237**). (B) CLSM image of HeLa cells incubated with **236** or **237** (200 μM) for 12 h. Adapted from Ref.[482]. Copyright © 2019 by Royal Chemical Society. (C) The structure of Nap-GGYGSSSRRAPQT (**238**). (D) Representative laser Doppler perfusion images of mice subjected to limb ischemia at Day 0 and Day 28 after injection of Gel-A, IGF-1, ad Gel-B. Adapted from Ref.[485]. Copyright © 2019 by American Chemical Society.

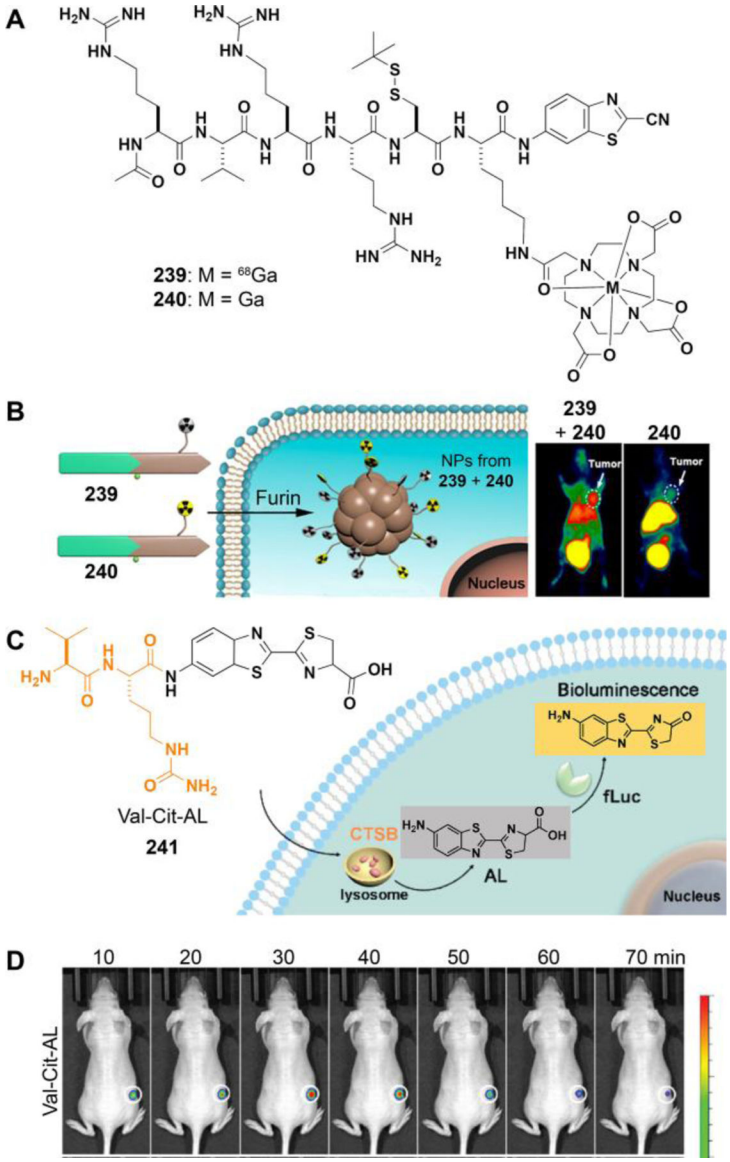

Figure 80.

(A) The structures of the **239** or **240**. (B) The illustration of furin-instructed formation of CBT-^{68}Ga nanoparticles and microPET images of MDA-MB-468 tumor-bearing mice injected with either CBT-^{68}Ga alone or the mixture of CBT-^{68}Ga and CBT-Ga. Adapted from Ref.[486]. Copyright © 2019 by American Chemical Society. (C) The illustration of the CTSB-specific bioluminescence "turn-on" after cellular internalization. (D) Time-dependent images of tumors in a murine model. Adapted from Ref.[488]. Copyright © 2019 by American Chemical Society.

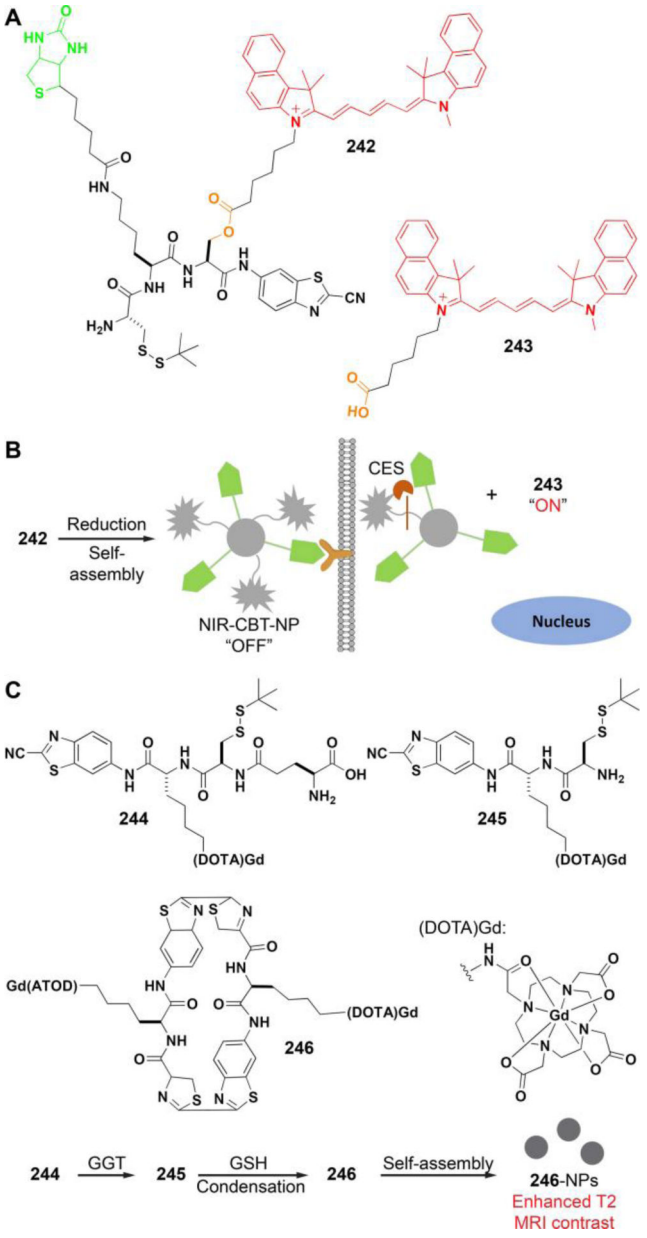

Figure 81.

(A) The structures of **242** and **243**. (B) The illustration of biotinylated NIR-CBT probe for tumor-targeted imaging. Adapted from Ref.[490]. (C) The illustration of GGT-triggered cleavage and GSH-instructed condensation to form **246**-Dimers which self-assemble to form **246**-NPs with enhanced T_2 MRI contrast. Adapted from Ref.[491]. Copyright © 2019 by American Chemical Society.

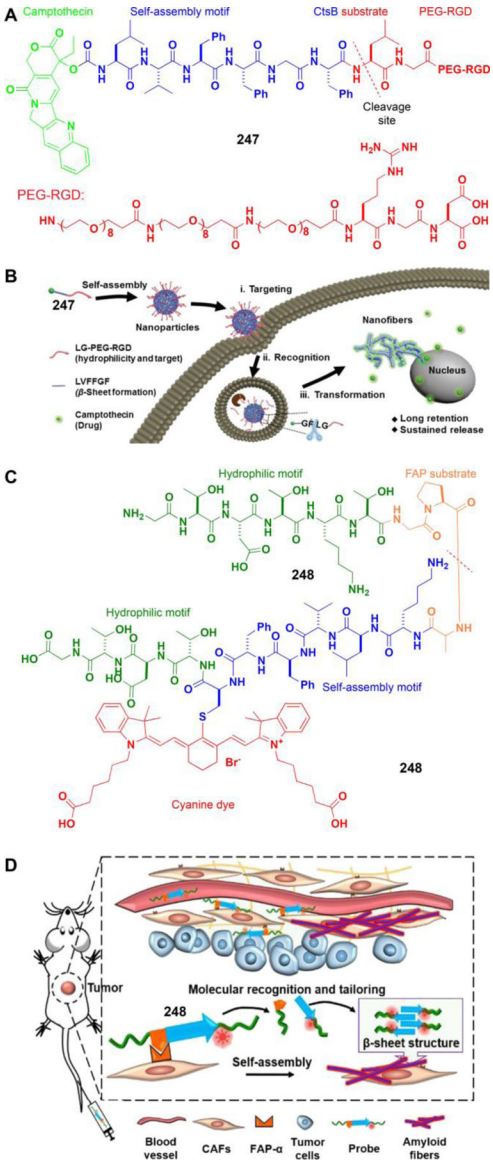

Figure 82.

(A) The structure of **247**. (B) The illustration of self-assembly behavior of **247** and construction of fibrous drug depots in cells. Adapted from Ref.[492]. Copyright © 2019 by Wiley Inc. (C) The structure of **248** with four motifs. (D) The illustration of CAF instructed nanofibers self-assembly in situ for enhanced tumor imaging. Adapted from Ref.[495]. Copyright © 2019 by Wiley Inc.

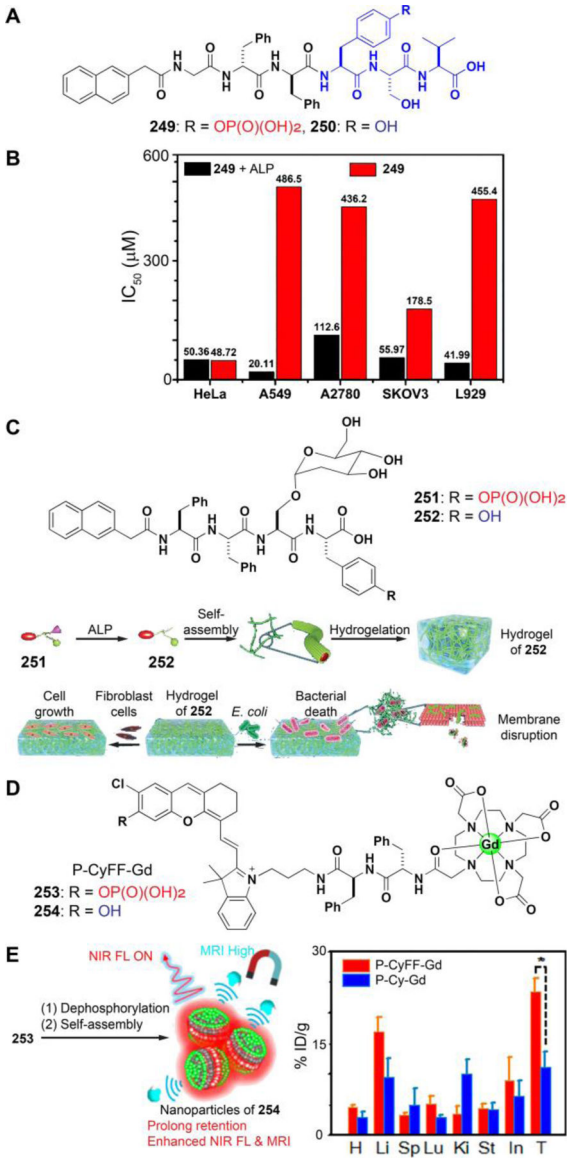

Figure 83.

(A) The structures of Nap-G^{D}F^{D}FpYSV (**249**) and Nap-G^{D}F^{D}FYSV (**250**). (B) IC_{50} values of **249** and the pre-treated **249** by ALP catalysis in vitro against different cells after incubation for 48 h. Adapted from Ref.[496]. Copyright © 2019 by Royal Chemical Society. (C) The structures of **251** and **252** and the ENS process generating supramolecular nanofibers and hydrogels with mannose decoration for cultured fibroblast cells and inhibiting *E. coli*. Adapted from Ref.[497]. Copyright © 2019 by Wiley Inc. (D) The structures of **253** and **254**. (E) Illustration showing an ALP-activatable NIR fluorescence (FL)/MR bimodal probe for in vivo imaging and the biodistribution (% ID/g) of P-CyFF-Gd (red) or P-Cy-Gd (blue) in HeLa tumors and main organs (H: heart, Li: liver including gallbladder, Lu: lung, Sp: spleen, Ki: kidneys, St: stomach, In: intestines, T: tumor) at 4 h after i.p. injection into mice (0.015 mmol kg^{-1} Gd^{3+}). Adapted from Ref.[498]. Copyright © 2019 by American Chemical Society.

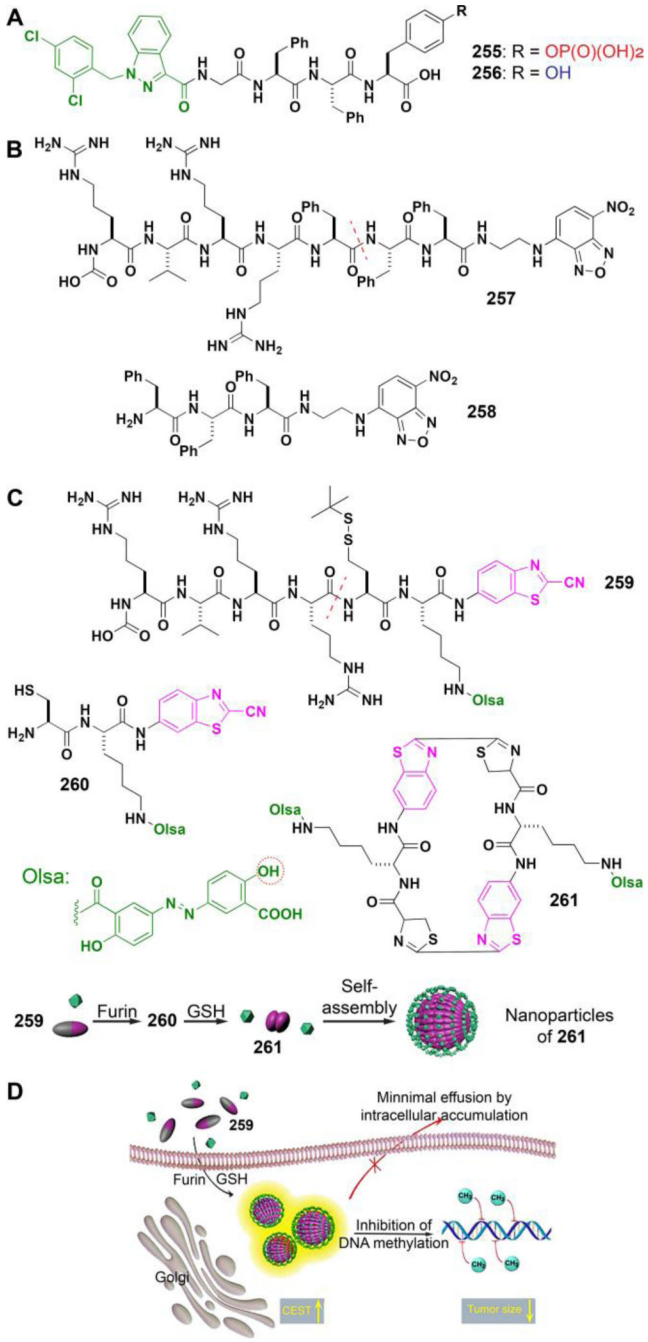

Figure 84.

(A) The structures of **255** and **256**. (B) The structures of **257** and **258**. (C) Self-assembly of Olsa-RVRR (**259**) into Olsa-NPs (i.e., nanoparticles of **261**) through a series of steps. Red line indicates the site of furin cleavage, and the circled hydroxyl group indicates the exchangeable hydroxyl proton that provides OlsaCEST signal at 9.8 ppm from the water frequency. (D) After **259** enters the cytoplasm of high furin-expressing cells (HCT116 cells in this study), it undergoes reduction by GSH and cleavage of the peptide by furin near the Golgi complex where **260** is generated. Amphiphilic oligomers (mostly dimers) are then

formed from the click reaction between two **260** molecules, followed by self-assembly into **261**-NPs as a result of intermolecular **π-π** stacking. The intracellular accumulation of **261**-NPs then serves as a reservoir of Olsa molecule-enhancing CEST contrast and can inhibit DNA methylation for tumor therapy. Adapted from Ref.[502]. Copyright © 2019 by Springer Nature.

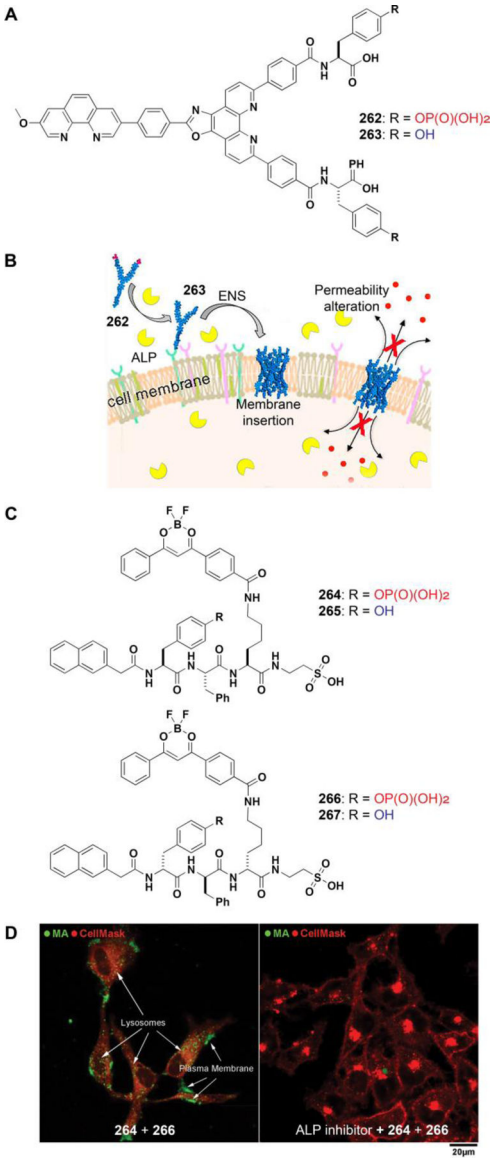

Figure 85.

(A) The structures of **262** and **263**. (B) The illustration of ENS-directed membrane insertion of a long and rigid synthetic analogue causing permeability alteration. Adapted from Ref. [504]. Copyright © 2019 by American Chemical Society. (C) The structures of **264** and **266** and their dephosphorylated products. (D) The fluorescence image of HeLa cells incubated with a mixture of **264** and **266** (1 : 1, total concentration 100 μM, 12 h) without and with ALP inhibition, and co-stained with CellMask Red. Adapted from Ref.[506]. Copyright © 2019 by Royal Chemical Society.

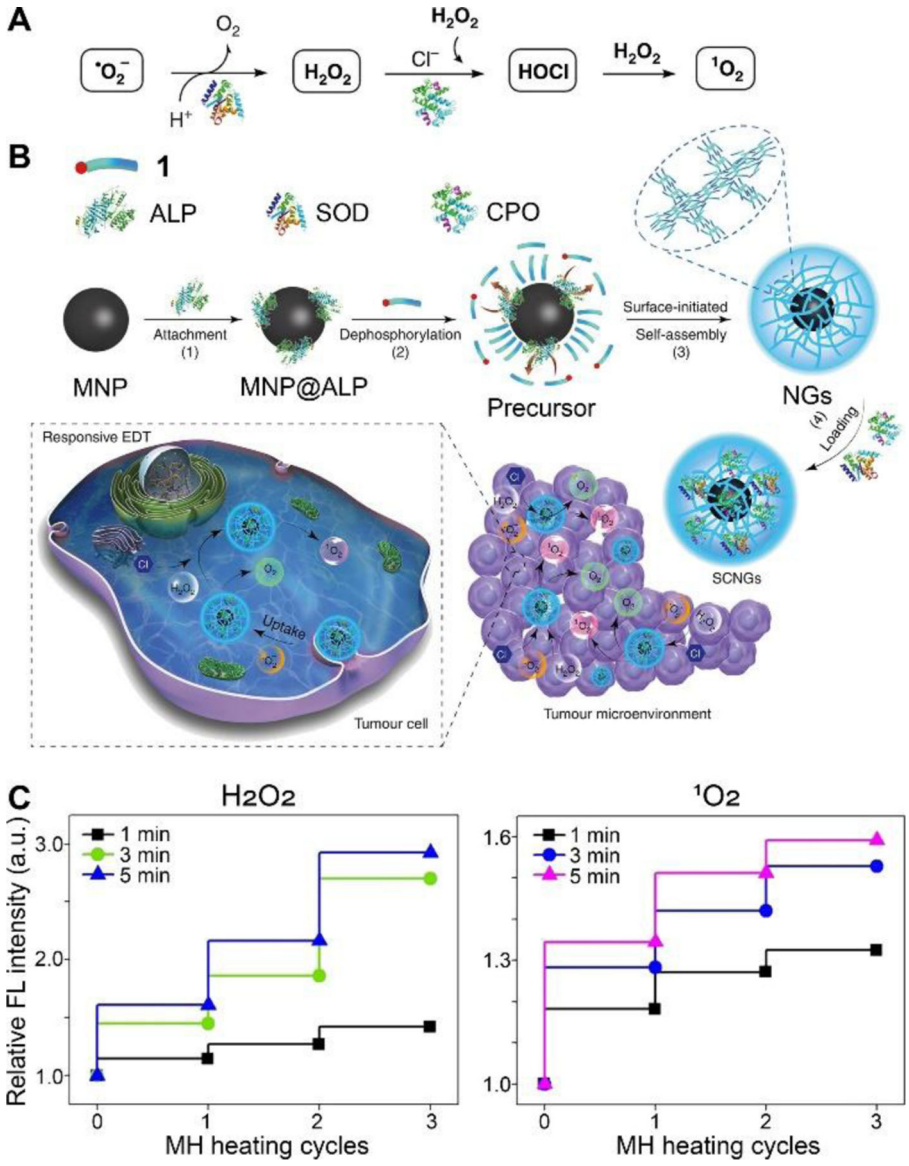

Figure 86.

The scheme of the responsive EDT mechanism and preparation of SCNGs. (A) The cascade SOD/CPO-mediated therapy includes the catalysis of $^{\cdot}O_2^-$ into H_2O_2 by SOD, conversion of both as-obtained H_2O_2 and endogenous H_2O_2 species into final $^1O_2$ species with CPO. (B) The fabrication process of SCNGs involves (1) modification of MNPs for attaching the ALP trigger, (2) dephosphorylation of hydrophilic peptide precursors to hydrophobic hydrogelators by the ALP on the MNPs, (3) ALP-triggered self-assembling between the hydrophobic portions and hydrophilic parts of hydrogelators through **π–π** stacking and electrostatic interactions around MNP, (4) immobilization of cascade SOD and CPO and further a safe and effective EDT in tumor microenvironment. The responsive SCNGs can effectively convert the endogenous ROS ($^{\cdot}O_2^-$ and H_2O_2) into highly reactive $^1O_2$ by the cascade reactions of SOD and CPO in tumor region, which subsequently cause cancer cell death. Adapted from Ref.[507]. (C) Relative fluorescence intensity of correlated with the levels

of H_2O_2 and $^1O_2$ in U87 cells exposed to MNP@Nanogels and MNP-CPO@Nanogels, respectively, with programmed MH. Adapted from Ref.[508]. Copyright © 2019 by Wiley Inc.

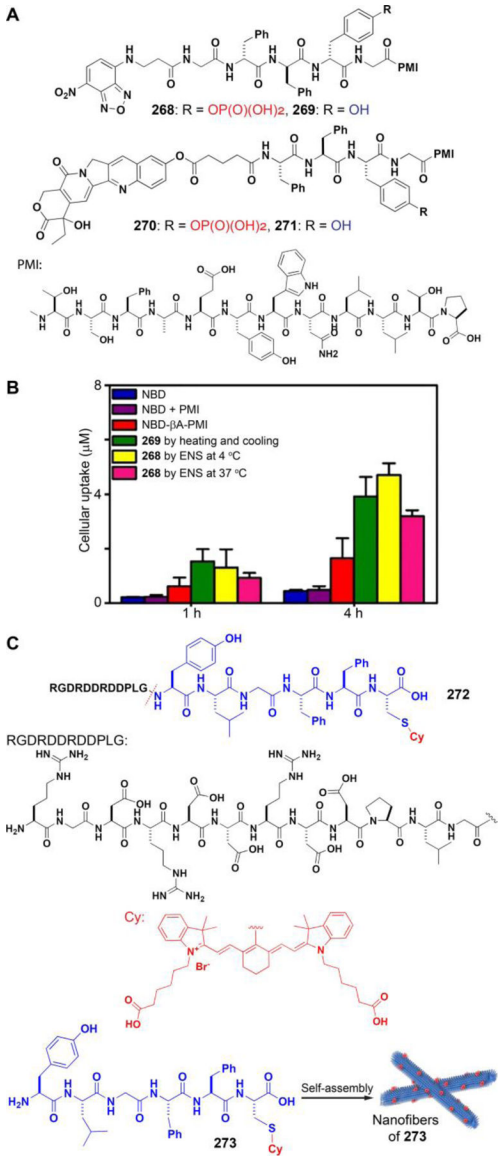

Figure 87.

(A) The structures of **268**, **269**, **270**, and **271**. (B) Cellular uptake of the different assemblies into HepG2 cells at 1 h and 4 h (concentration of peptide = 200 μM). Adapted from Ref.[509]. Copyright © 2020 by Elsevier Inc. (C) The structures of **272** and its ENS product **273**. Adapted from Ref.[510]. Copyright © 2020 by American Chemical Society.

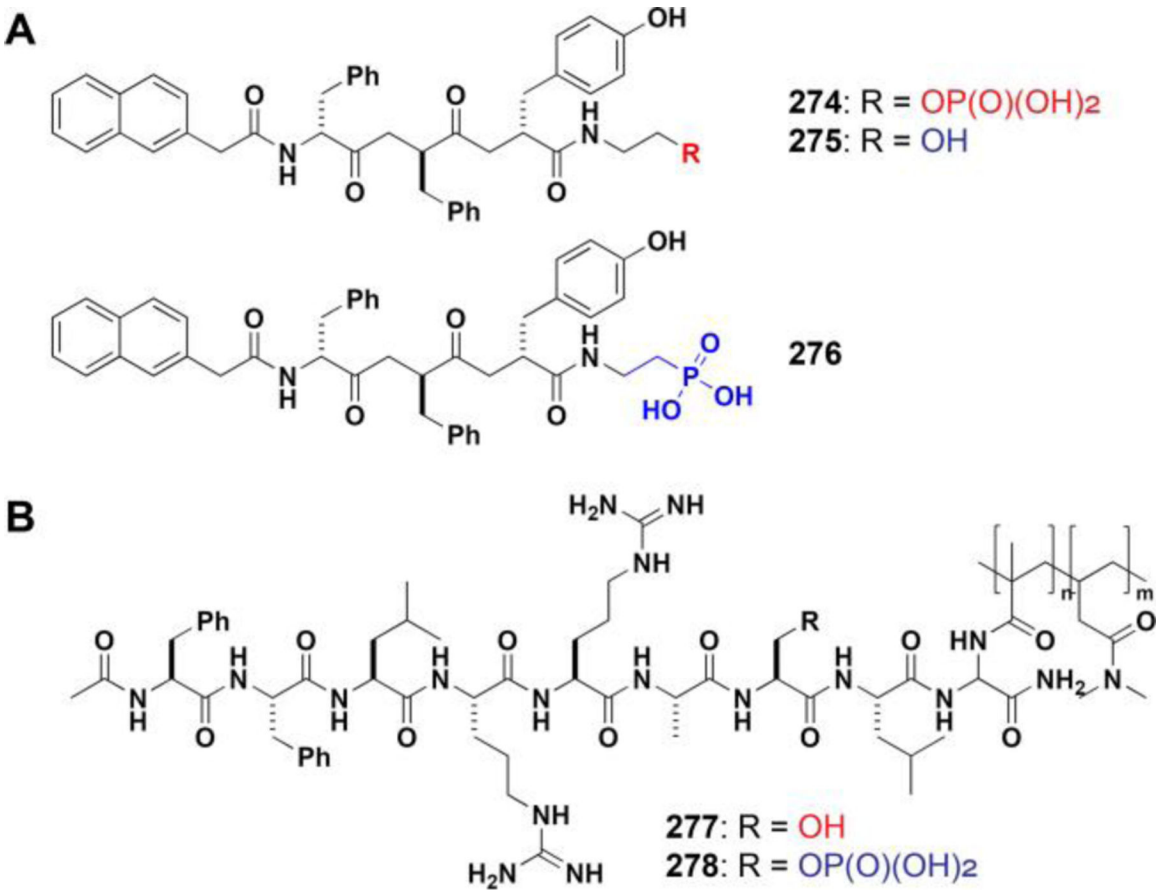

Figure 88.
The structures of (A) **274**, **275**, and **276** and (B) **277** and **278**.

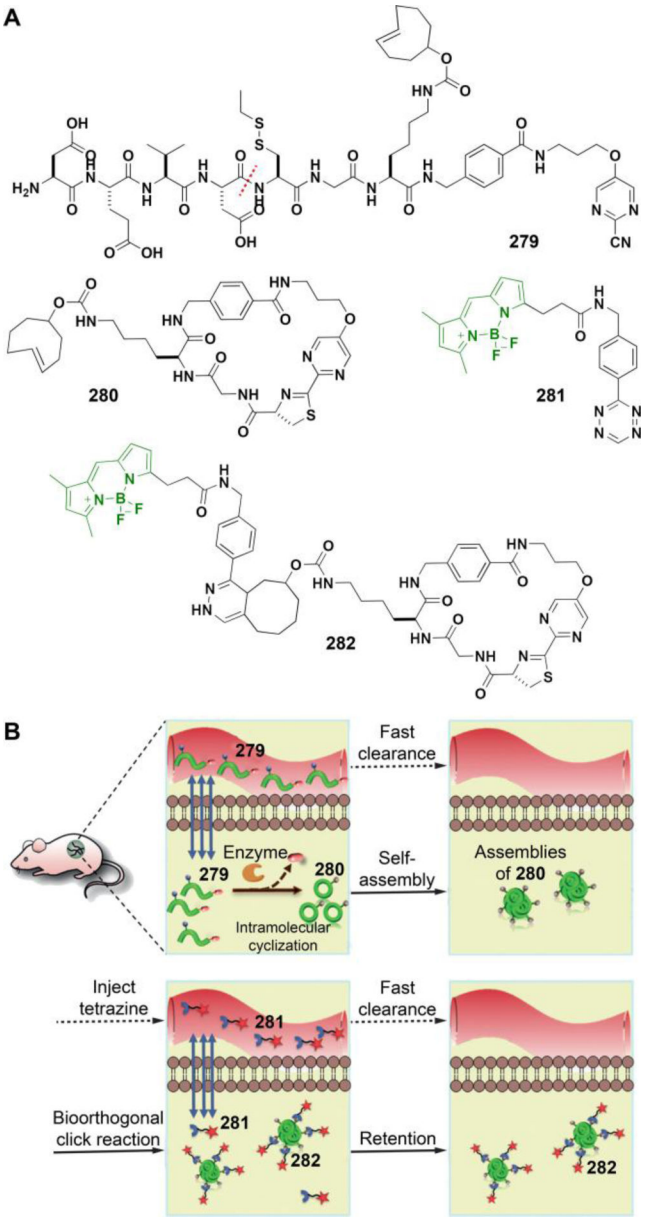

Figure 89.

(A) The structures of the substrate of caspase-3/7 and the oxidant of GSH (**279**, the cleavage site shown by a red dotted line), the intramolecular cyclization product (**280**), the tetrazine (**281**), and the product (**282**) of the click reaction. (B) The illustration of pre-targeted imaging of enzyme activity based on target-enabled in situ ligand aggregation. Adapted from Ref.[514]. Copyright © 2020 by Wiley Inc.

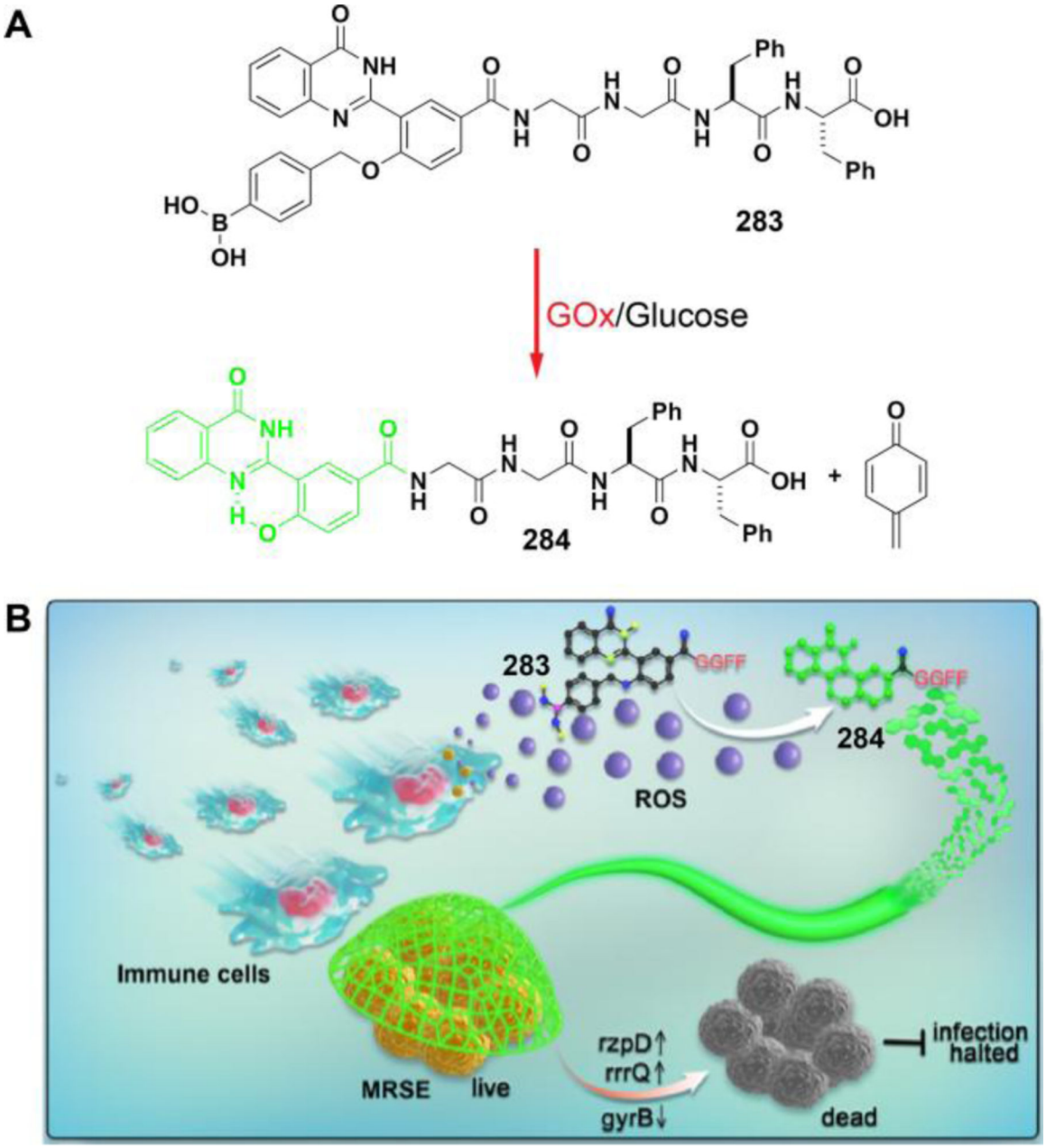

Figure 90.

(A) The structure of **283** and the indirect enzymatic oxidation, by glucose oxidase, to generate the self-assembling molecule, **284**. (B) The use of the indirect ENS to form in situ artificial NETs to halt MRSE infection. Adapted from Ref.[516]. Copyright © 2020 by Elsevier Inc.

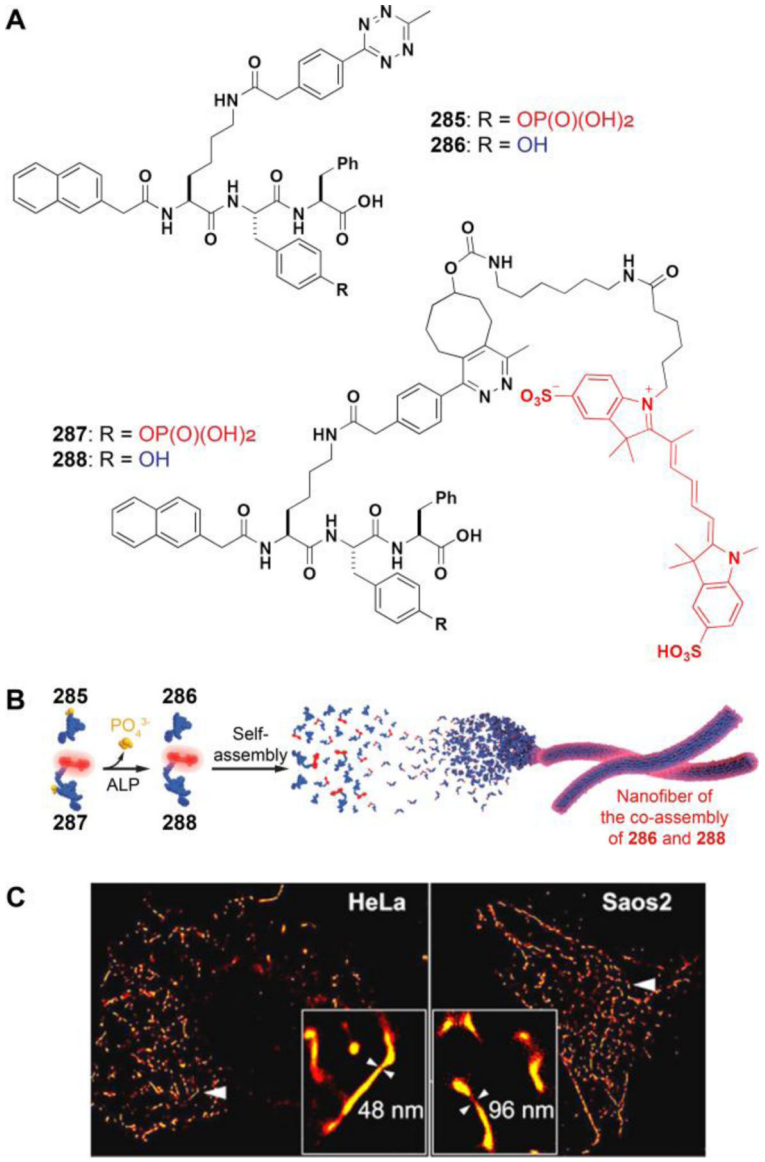

Figure 91.

(A) The structures of the substrates (**285** and **287**) of ALP and the corresponding dephosphorylation products (**286** and **288**). (B) The illustration of the co-assembly of **286** and **288** to form fluorescent nanofibers after ALP catalyzed ENS. (C) dSTORM images of the assemblies in fixed HeLa and Saos2 cells pre-incubated with 500 μM of **285** and 0.05 μM of **287**. Adapted from Ref.[519]. Copyright © 2020 by American Chemical Society.

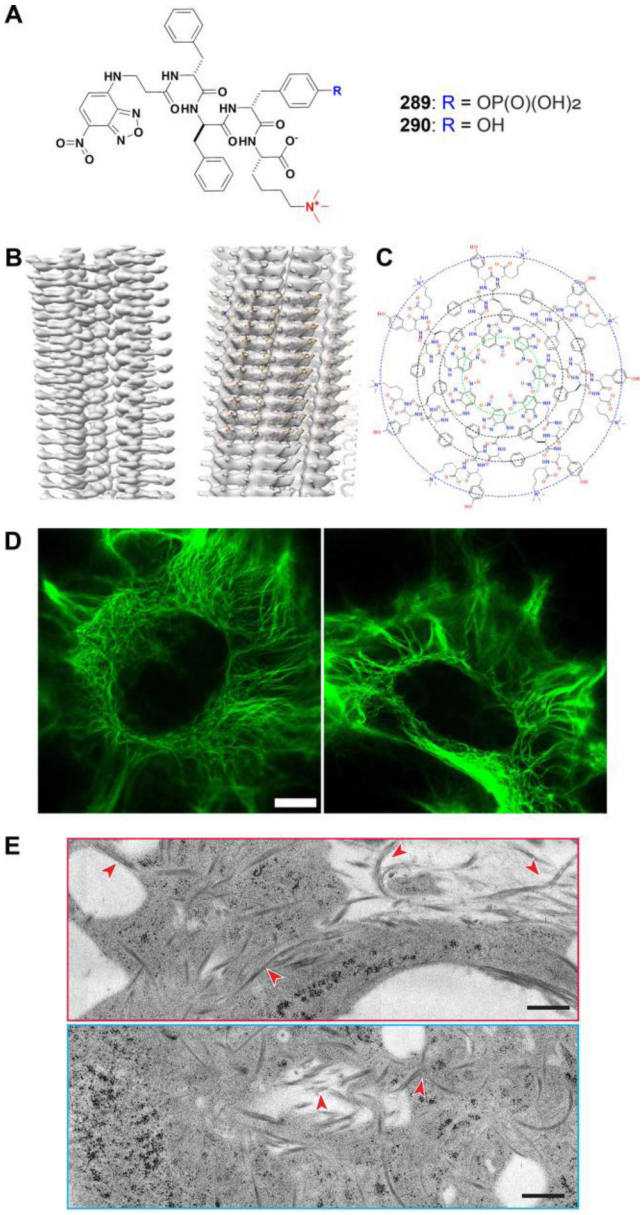

Figure 92.

(A) The molecular structures of a phosphorylated and trimethylated tetrapeptide (**289**) and its dephosphorylated product (**290**). (B) 3D reconstruction of type 1 filaments of **290** from cryo-EM images and the atomic model of the type 1 filaments with cross-β structure. (C) The chemical structures of one layer of the filament at the cross section of (B). (D) CLSM images of Saos2 cells treated with **289** (200 μM) for 24 h. Scale bars = 10 μm. (E) TEM image of a treated Saos2 cell (**289**, 200 μM, 24h) at two regions of the cells. Scale bar = 500 nm. Adapted from Ref.[528].

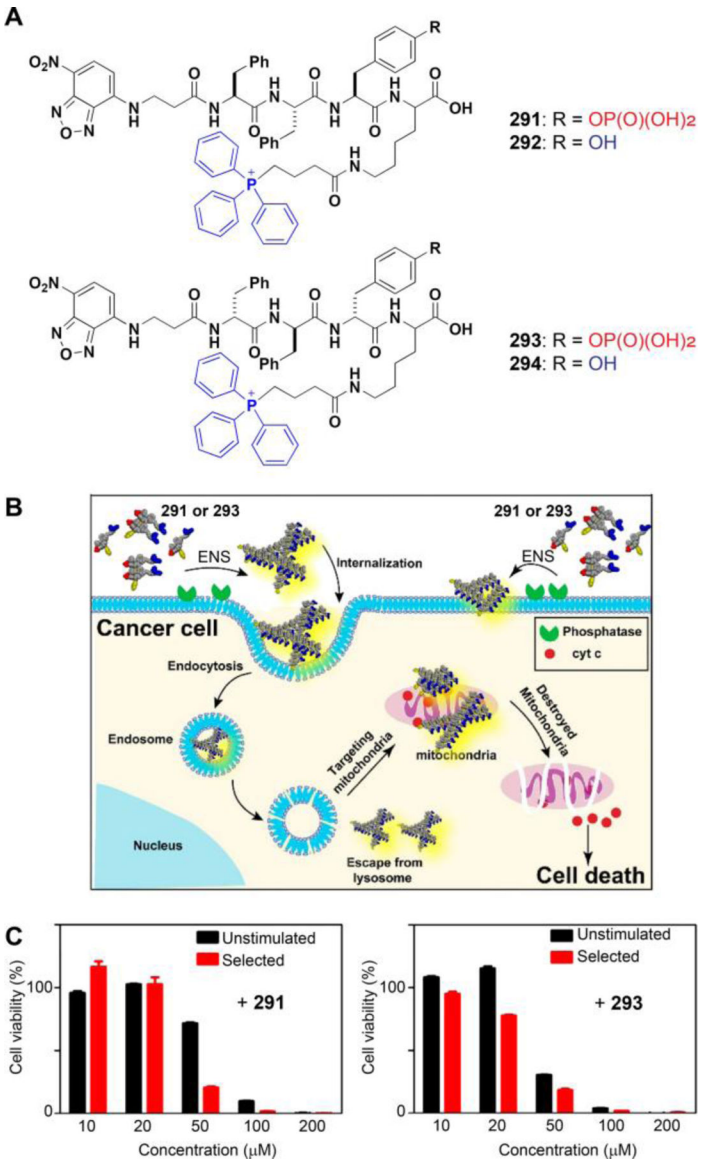

Figure 93.

(A) The structures of **291**, **293**, and their dephosphorylated products. (B) The illustration of ENS for targeting mitochondria and inducing death of cancer cells. (C) Cell viability of unstimulated Saos2 cell line or selected Saos2 cell line (after 5 weeks treatment of the precursors with gradually increasing concentrations) incubated with **291** or **293** at different concentrations for 48 h. Adapted from Ref.[529]. Copyright © 2016 by American Chemical Society.

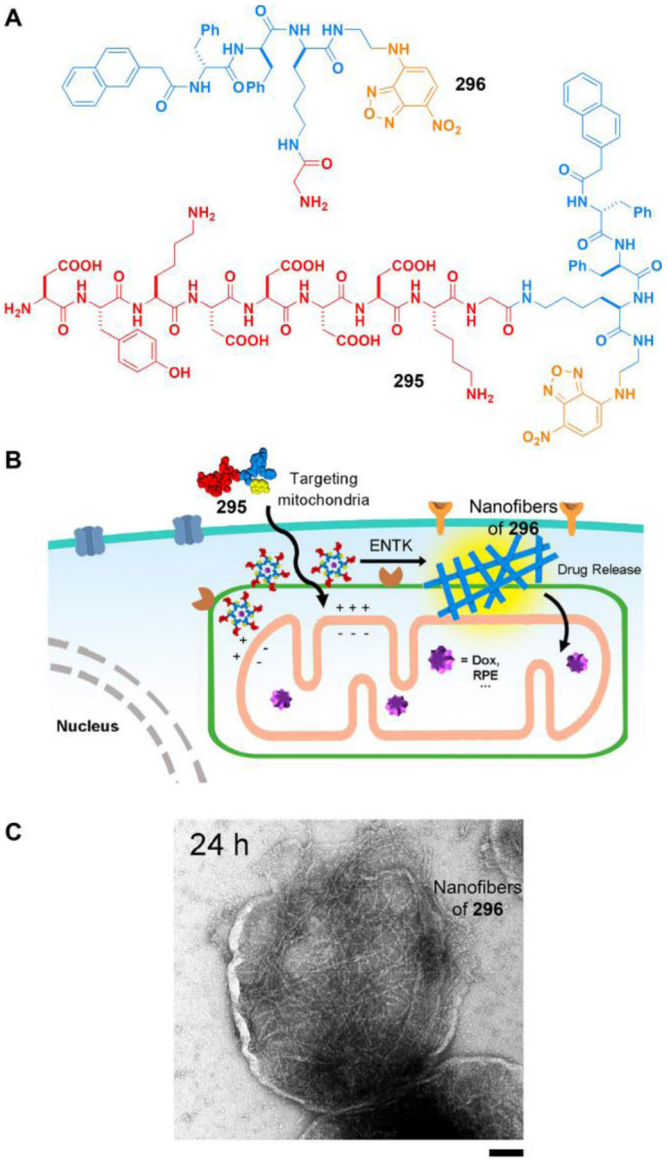

Figure 94.

(A) The structures of the branched peptide **295** and its ENTK-cleaved product **296**. (B) ENTK cleaving the branch to convert the micelles to nanofibers on mitochondria for targeting mitochondria. (C) TEM images of mitochondria isolated from HeLa cells being incubated with **295** (200 μM) for 24 h. Scale bar equals 100 nm. Adapted from Ref.[367]. Copyright © 2018 by American Chemical Society.

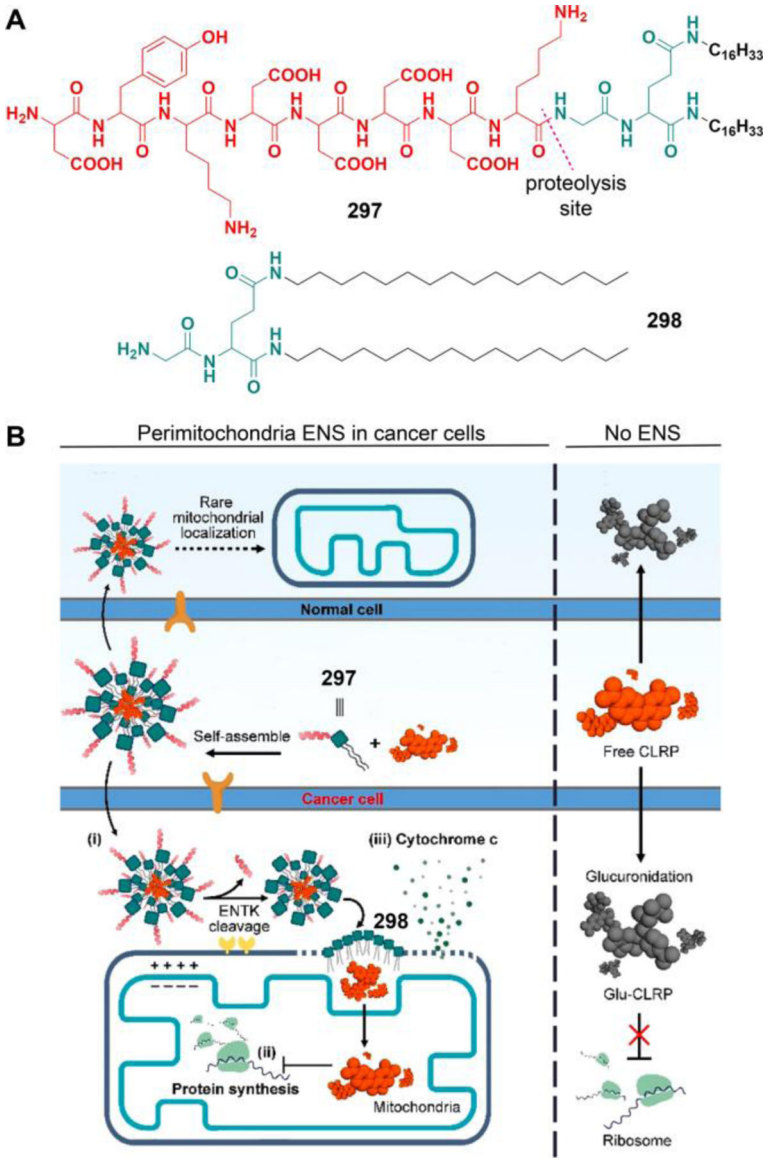

Figure 95.

The multiple functions of the ENS of **297** in cancer cells for delivering chloroamphenicol (CLRP) into mitochondria to inhibit protein synthesis and for changing permeability of mitochondria membrane: (i) perimitochondrial accumulation, (ii) mitochondria-targeting drug delivery, and (iii) mitochondrial outer membrane permeabilization (MOMP). Adapted from Ref.[535]. Copyright © 2020 by American Chemical Society.

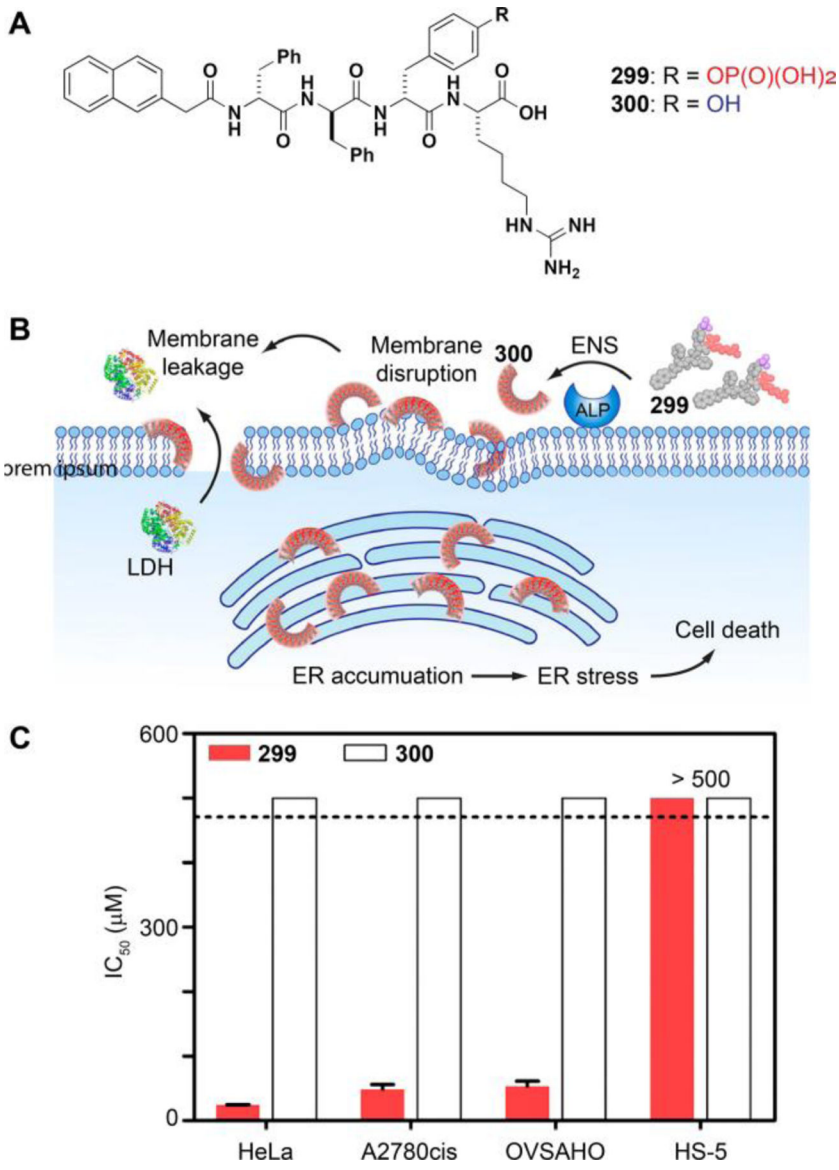

Figure 96.

(A) The structures of **299** and **300**. (B) The illustration of ENS of peptide assemblies to disrupt the cell membrane and to target the ER to cause cell death. (B) IC_{50} (24 h) of **299** or **300** against HeLa cells, A2780cis cells, OVSAHO cells, and HS-5 cells. Adapted from Ref. [543]. Copyright © 2018 by American Chemical Society.

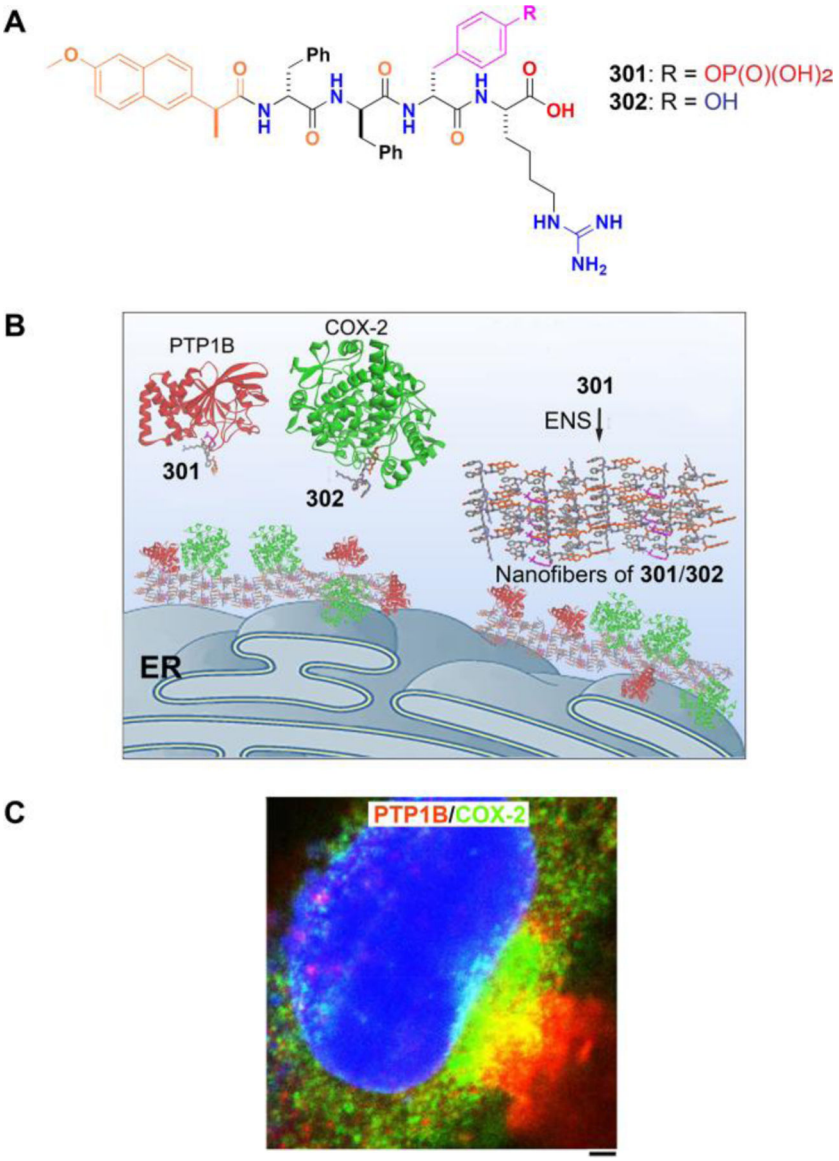

Figure 97.

(A) The structures of **301** and **302**. (B) The illustration of ENS for intracellular sequestration of PTP1B and COX-2. (C) CLSM images of Saos2 cells treated with **301** (12.5 μM) for 1 h and then stained with antibodies of PTP1B (red) and COX-2 (green) (scale bar = 10 μm). Adapted from Ref.[527]. Copyright © 2018 by American Chemical Society.

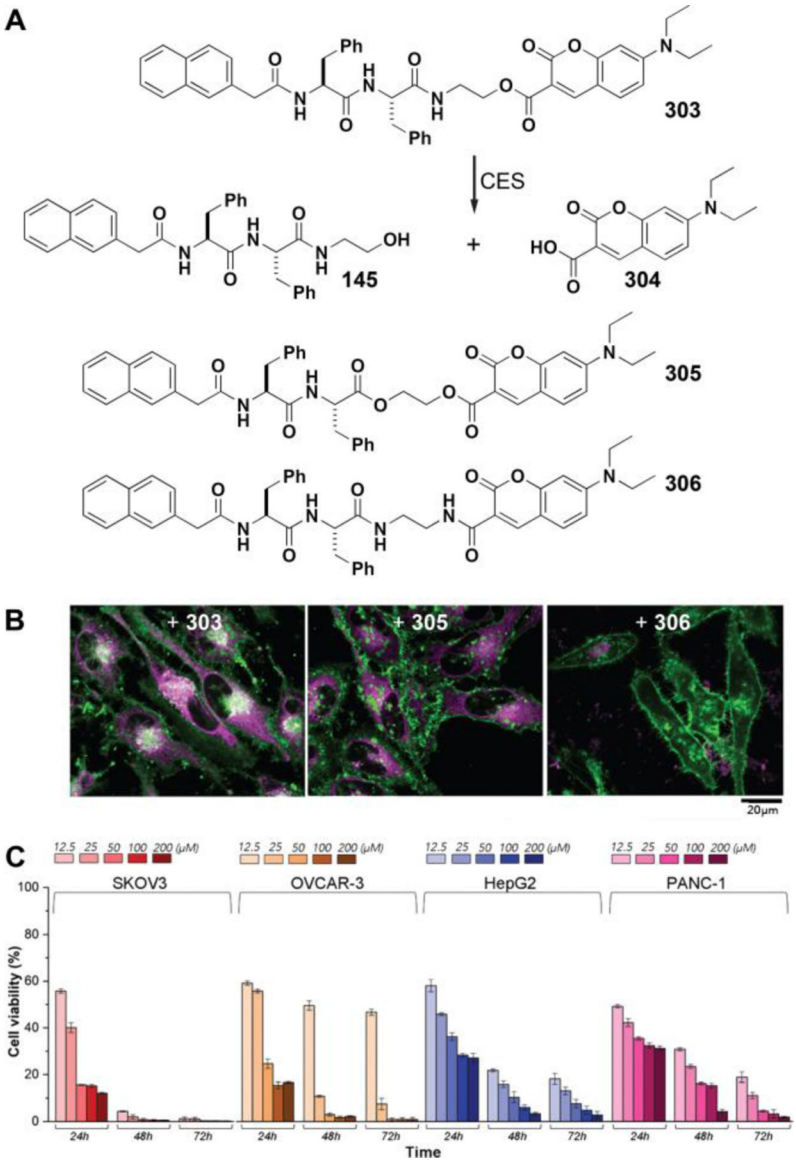

Figure 98.

(A) The structures of **303**, **304**, **305**, and **306**. (B) The fluorescent images of HeLa cells incubated with **303**, **305**, or **306** at a concentration of 10 μM for 4 hours and stained with CellMask Green (plasma membrane). Violet represents the emissions of coumarin derivatives. The scale bar represents 20 μm. (C) SKOV-3, OVCAR-3, HepG2 and PANC-1 cell viability under treatment with **303** at various concentrations. Adapted from Ref.[544].

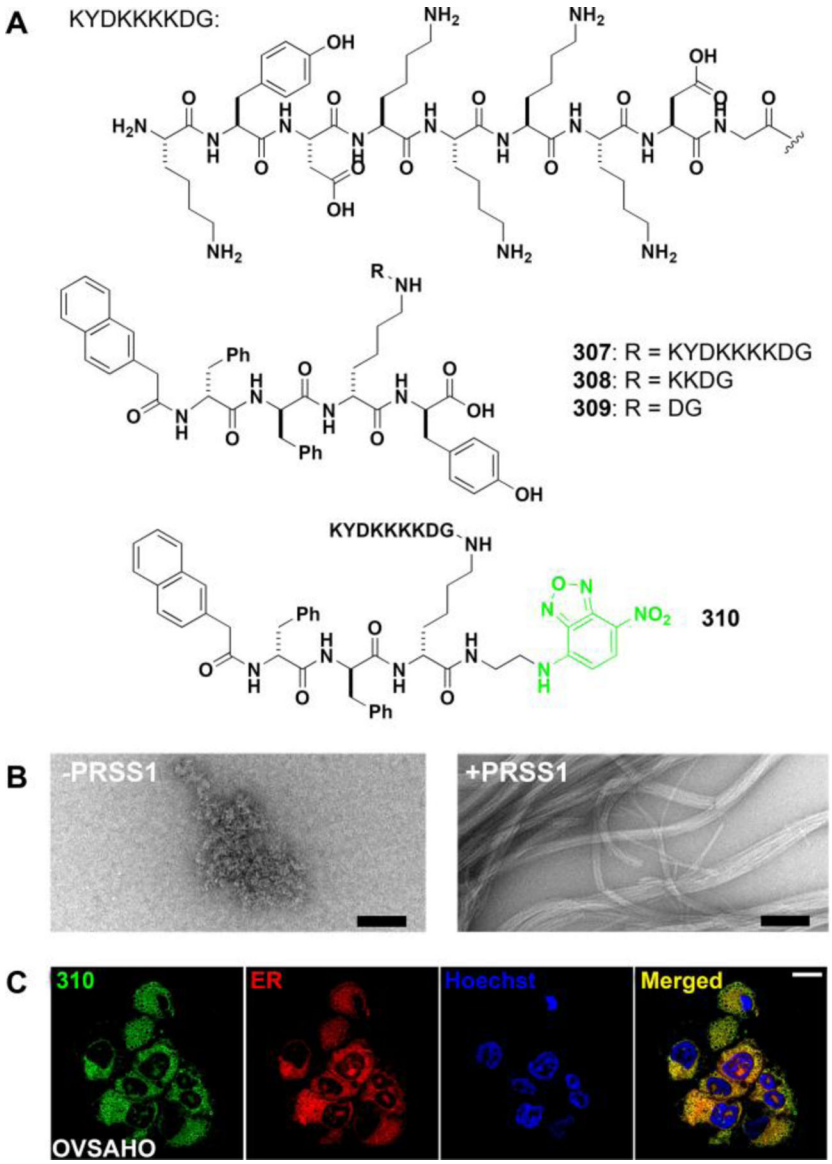

Figure 99.

(A) The structures of the branched peptide (**307**), its proteolysis products (**308** and **309**), and its fluorescent analog (**310**). (B) TEM images of **307** (200 μM) before and after the addition of PRSS1. Scale bars = 100 nm. (C) Fluorescent images of OVSAHO cells treated with **310** (400 μM) for 2 hours. Cells were stained with ER-Tracker™ red (for ER) and Hoechst 33342 (for nucleus). Scale bars: 10 μm. (B, C) Adapted from Ref.[545]. Copyright © 2020 by Wiley Inc.

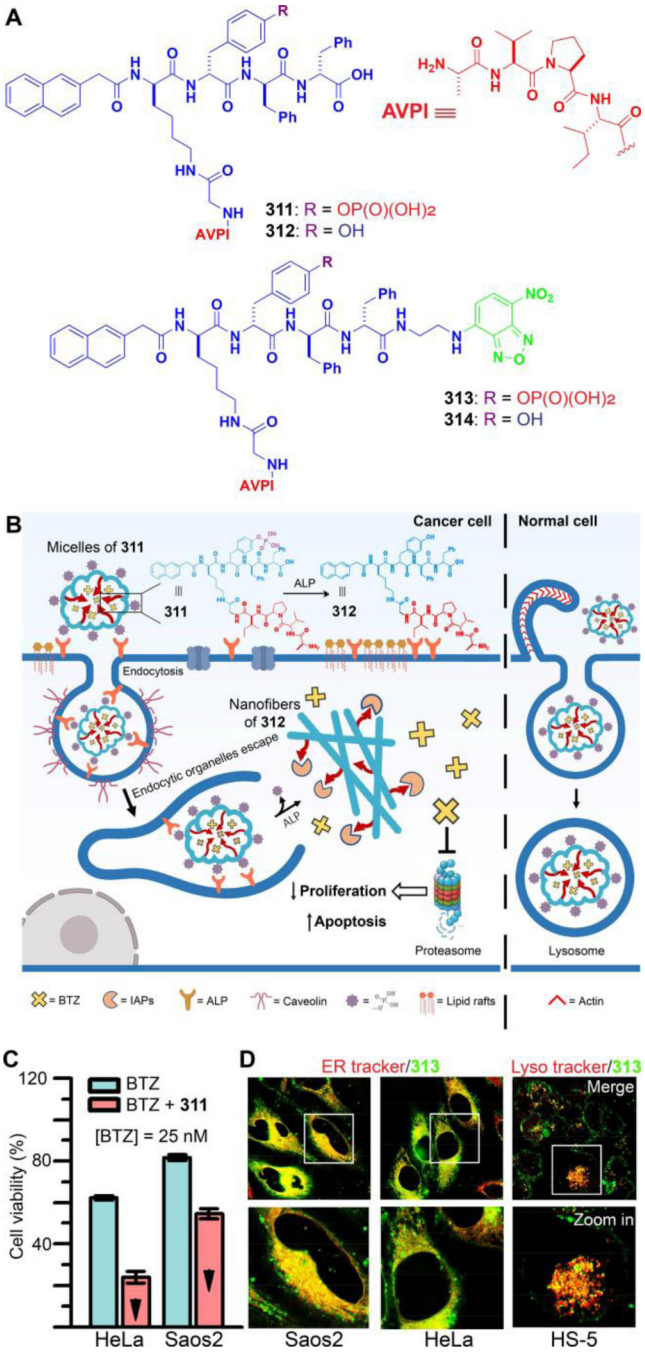

Figure 100.

(A) The molecular structures of the AVPI-bearing phosphopeptides (**311** and **313**) and the corresponding peptides (**312** and **314**). (B) The illustration of enzymatically-forming peptide assemblies to sequestrate IAPs for selectively killing cancer cells. (C) Sequestration of AVPI boosting the activity of BTZ for inhibiting cancer cells. (D) Fluorescent images of Saos2, HeLa, and HS-5 cells incubated with **313** (50 μM, 4 h). For Saos2 and HeLa cells, the ER

was stained by ER tracker; for HS-5 cells, the lysosome was stained by Lyso tracker. Adapted from Ref.[546]. Copyright © 2020 by Wiley Inc.